

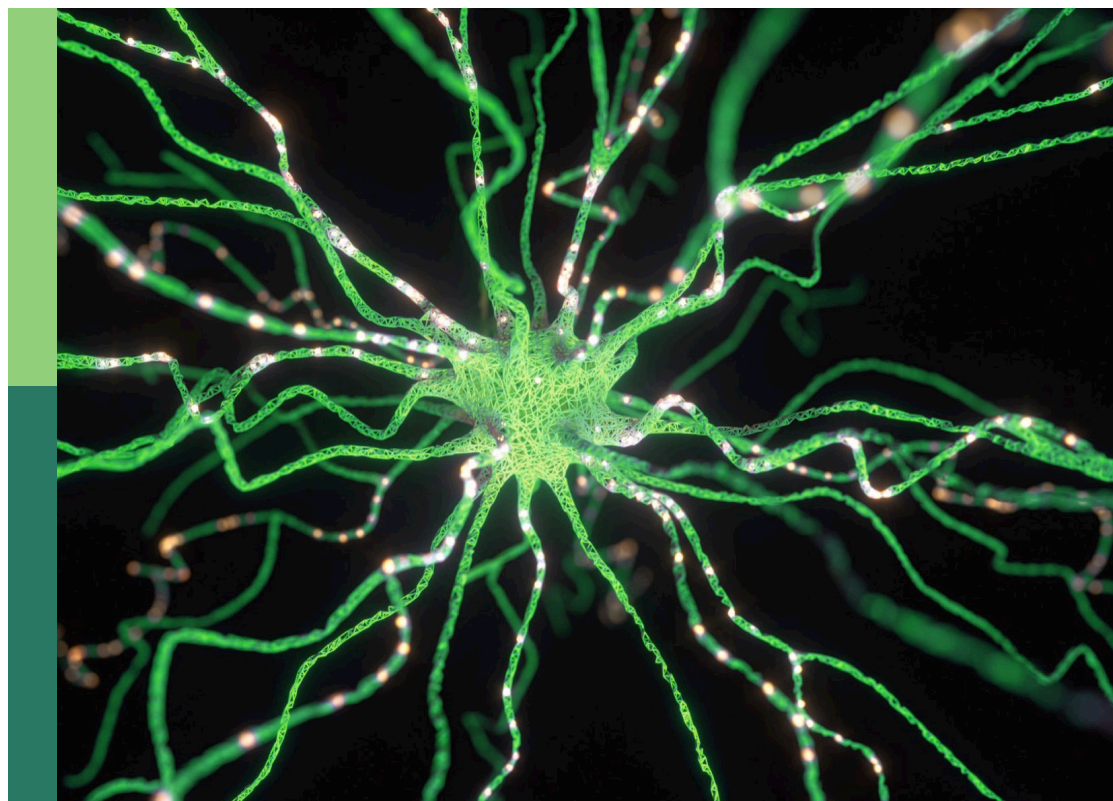
Wearable robotics in the rehabilitation continuum of care: Assessment, treatment and home assistance

Edited by

Emilio Trigili and Sandra Hirche

Published in

Frontiers in Neurorobotics



FRONTIERS EBOOK COPYRIGHT STATEMENT

The copyright in the text of individual articles in this ebook is the property of their respective authors or their respective institutions or funders. The copyright in graphics and images within each article may be subject to copyright of other parties. In both cases this is subject to a license granted to Frontiers.

The compilation of articles constituting this ebook is the property of Frontiers.

Each article within this ebook, and the ebook itself, are published under the most recent version of the Creative Commons CC-BY licence. The version current at the date of publication of this ebook is CC-BY 4.0. If the CC-BY licence is updated, the licence granted by Frontiers is automatically updated to the new version.

When exercising any right under the CC-BY licence, Frontiers must be attributed as the original publisher of the article or ebook, as applicable.

Authors have the responsibility of ensuring that any graphics or other materials which are the property of others may be included in the CC-BY licence, but this should be checked before relying on the CC-BY licence to reproduce those materials. Any copyright notices relating to those materials must be complied with.

Copyright and source acknowledgement notices may not be removed and must be displayed in any copy, derivative work or partial copy which includes the elements in question.

All copyright, and all rights therein, are protected by national and international copyright laws. The above represents a summary only. For further information please read Frontiers' Conditions for Website Use and Copyright Statement, and the applicable CC-BY licence.

ISSN 1664-8714
ISBN 978-2-8325-3869-2
DOI 10.3389/978-2-8325-3869-2

About Frontiers

Frontiers is more than just an open access publisher of scholarly articles: it is a pioneering approach to the world of academia, radically improving the way scholarly research is managed. The grand vision of Frontiers is a world where all people have an equal opportunity to seek, share and generate knowledge. Frontiers provides immediate and permanent online open access to all its publications, but this alone is not enough to realize our grand goals.

Frontiers journal series

The Frontiers journal series is a multi-tier and interdisciplinary set of open-access, online journals, promising a paradigm shift from the current review, selection and dissemination processes in academic publishing. All Frontiers journals are driven by researchers for researchers; therefore, they constitute a service to the scholarly community. At the same time, the *Frontiers journal series* operates on a revolutionary invention, the tiered publishing system, initially addressing specific communities of scholars, and gradually climbing up to broader public understanding, thus serving the interests of the lay society, too.

Dedication to quality

Each Frontiers article is a landmark of the highest quality, thanks to genuinely collaborative interactions between authors and review editors, who include some of the world's best academicians. Research must be certified by peers before entering a stream of knowledge that may eventually reach the public - and shape society; therefore, Frontiers only applies the most rigorous and unbiased reviews. Frontiers revolutionizes research publishing by freely delivering the most outstanding research, evaluated with no bias from both the academic and social point of view. By applying the most advanced information technologies, Frontiers is catapulting scholarly publishing into a new generation.

What are Frontiers Research Topics?

Frontiers Research Topics are very popular trademarks of the *Frontiers journals series*: they are collections of at least ten articles, all centered on a particular subject. With their unique mix of varied contributions from Original Research to Review Articles, Frontiers Research Topics unify the most influential researchers, the latest key findings and historical advances in a hot research area.

Find out more on how to host your own Frontiers Research Topic or contribute to one as an author by contacting the Frontiers editorial office: frontiersin.org/about/contact

Wearable robotics in the rehabilitation continuum of care: Assessment, treatment and home assistance

Topic editors

Emilio Trigili — Institute of BioRobotics, Sant'Anna School of Advanced Studies, Italy
Sandra Hirche — Technische Universitaet Muenchen, Germany

Citation

Trigili, E., Hirche, S., eds. (2023). *Wearable robotics in the rehabilitation continuum of care: Assessment, treatment and home assistance*. Lausanne: Frontiers Media SA. doi: 10.3389/978-2-8325-3869-2

Table of contents

- 04 **Editorial: Wearable robotics in the rehabilitation continuum of care: assessment, treatment and home assistance**
Emilio Trigili and Sandra Hirche
- 07 **Upper limb home-based robotic rehabilitation in chronic stroke patients: A pilot study**
Federica Bressi, Benedetta Campagnola, Laura Cricenti, Fabio Santacaterina, Sandra Miccinilli, Giovanni Di Pino, Francesca Fiori, Marco D'Alonzo, Vincenzo Di Lazzaro, Lorenzo Ricci, Fioravante Capone, Alessandra Pacilli, Silvia Sterzi and Marco Bravi
- 18 **Adaptive cueing strategy for gait modification: A case study using auditory cues**
Tina L. Y. Wu, Anna Murphy, Chao Chen and Dana Kulić
- 29 **Hybrid FES-exoskeleton control: Using MPC to distribute actuation for elbow and wrist movements**
Nathan Dunkelberger, Jeffrey Berning, Eric M. Scheerer and Marcia K. O'Malley
- 46 **Quasi-passive lower limbs exosuit: an in-depth assessment of fatigue, kinematic and muscular patterns while comparing assistive strategies on an expert subject's gait analysis**
Christian Di Natali, Jesus Ortiz and Darwin G. Caldwell
- 62 **Contralaterally EMG-triggered functional electrical stimulation during serious gaming for upper limb stroke rehabilitation: a feasibility study**
Chiara Höhler, Laura Wild, Alexandra de Crignis, Klaus Jahn and Carmen Krewer
- 75 **A fabric-based soft hand exoskeleton for assistance: the ExHand Exoskeleton**
Juan C. Maldonado-Mejía, Marcela Múnera, Camilo A. R. Diaz, Helge Wurdemann, Mehran Moazen, Maria José Pontes, Marcelo Eduardo Vieira Segatto, Maxwell E. Monteiro and Carlos A. Cifuentes
- 90 **Spasticity evaluation with the Amadeo Tyromotion device in patients with hemispheric stroke**
Rocío Urrutia, Ane Miren Gutiérrez-Muto, Clara B. Sanz-Morère, Arantxa Gómez, Angela M. Politi, Francesca Lunardini, Marco Baccini, Francesca Cecchi, Natacha León, Antonio Oliviero and Jesús Tornero
- 101 **Online detection of compensatory strategies in human movement with supervised classification: a pilot study**
Neha Das, Satoshi Endo, Sabrina Patel, Carmen Krewer and Sandra Hirche
- 118 **Uncertainty-aware automated assessment of the arm impedance with upper-limb exoskeletons**
Samuel Tesfazgi, Ronan Sangouard, Satoshi Endo and Sandra Hirche



OPEN ACCESS

EDITED AND REVIEWED BY
Florian Röhrbein,
Technische Universität Chemnitz, Germany

*CORRESPONDENCE

Emilio Trigili
✉ emilio.trigili@santannapisa.it

RECEIVED 02 October 2023

ACCEPTED 05 October 2023

PUBLISHED 20 October 2023

CITATION

Trigili E and Hirche S (2023) Editorial: Wearable robotics in the rehabilitation continuum of care: assessment, treatment and home assistance. *Front. Neurobot.* 17:1305786. doi: 10.3389/fnbot.2023.1305786

COPYRIGHT

© 2023 Trigili and Hirche. This is an open-access article distributed under the terms of the [Creative Commons Attribution License \(CC BY\)](https://creativecommons.org/licenses/by/4.0/). The use, distribution or reproduction in other forums is permitted, provided the original author(s) and the copyright owner(s) are credited and that the original publication in this journal is cited, in accordance with accepted academic practice. No use, distribution or reproduction is permitted which does not comply with these terms.

Editorial: Wearable robotics in the rehabilitation continuum of care: assessment, treatment and home assistance

Emilio Trigili^{1,2*} and Sandra Hirche³

¹The BioRobotics Institute, Scuola Superiore Sant'Anna, Pisa, Italy, ²Department of Excellence in Robotics and AI, Scuola Superiore Sant'Anna, Pisa, Italy, ³Chair of Information-Oriented Control, Department of Electrical and Computer Engineering, Technical University of Munich, Munich, Germany

KEYWORDS

wearable robotics, rehabilitation robotics, robotic assessment, functional electric stimulation (FES), exoskeletons

Editorial on the Research Topic

Wearable robotics in the rehabilitation continuum of care: assessment, treatment, and home assistance

Global population aging is posing long-term challenges to societal welfare and sustainability. The prevalence of age-associated chronic diseases is causing a growing demand for physical and cognitive rehabilitation. Healthcare providers are faced with the challenge of guaranteeing a continuum of care after hospital discharge, and the management and delivery of outpatient and home rehabilitation has become critical ([Gonzaga et al., 2023](#)).

Wearable robotics can support people affected by neurological conditions in recovering their motor functions by aiding therapists in providing customized, task-specific rehabilitation training, or by augmenting human movement capabilities in activities of daily living (ADLs). The number of commercially available wearable robotics is rising across different application domains, predominantly in the healthcare and industry sectors. Nevertheless, several open challenges remain regarding actuation, sensing, and control, which limit the wide adoption of these devices outside the controlled laboratory environment ([Babič et al., 2021](#)).

Exoskeletons made of physically compliant structures, usually referred to as *soft* exoskeletons or *exosuits*, are promising for their capability to assist users with mild to moderate impairments while maintaining a lightweight and compact structure. [Maldonado-Mejía et al.](#) presented a fabric-based hand exoskeleton with pneumatic actuation (ExHand), designed for assisting grasping tasks in ADLs. The capability of the device to maintain stable contact with different objects was verified on 10 participants without any hand impairments. [Di Natali et al.](#) developed a modular lower-limb exosuit for walking assistance (XoSoft). The exosuit uses soft pneumatic *quasi-passive* actuators, which can modulate the forces generated by the deformation of an elastic tendon via a variable stiffness textile-based clutch. This approach mimics the behavior of the human muscle and tendons and allows the injection of positive energy into the gait cycle without requiring powerful actuators.

Over the last few years, hybrid neuroprostheses combining low-power robotic actuation with functional electrical stimulation (FES) have also been proposed. Such hybrid systems provide biomimetic assistance by distributing the power resources between the user's muscles and the robotic actuator. A recent review paper analyzed the efficacy of hybrid neuroprostheses employed in randomized controlled trials for upper-limb impairment after stroke, showing their positive effects in the recovery of upper-limb motor function (Höhler et al., 2023). Still, most of the current hybrid devices use both actuation types to address separate functions for each (e.g., distal or proximal joint actuation). Dunkelberger et al. presented a controller based on model predictive control for a hybrid upper-limb powered exoskeleton to assist individuals with spinal cord injuries. The controller was designed to provide an optimal distribution of power at the same joint, favoring FES over robotic actuation to assist in tracking movements.

Physical training, either via FES or via robotic devices, can also be combined with cognitive training by means of serious games based on virtual or augmented reality. Such hybrid combinations are suggested to increase patients' engagement, motivation, and adherence to the treatment. Höhler et al. recruited 18 patients after stroke in a randomized crossover trial to investigate the feasibility and benefits of combining serious games with contralaterally electromyography-triggered FES. The results of this study also provide valuable insight into the potential translation of such systems to the home environment.

To ensure a continuum of care from hospital to home rehabilitation, it is paramount to develop devices that are intuitive, portable, and easy to use. These devices should be designed in a way that allows them to be worn and used without the supervision of the therapist, gathering at the same time quantitative measures to monitor the progress of the therapy. Bressi et al. investigated the use of a robotic end-effector type device (iCONE, Heaxel, Italy) for the home-based rehabilitation of chronic stroke patients. The study encourages the exploration of possible correlations between the clinical evaluation scales and the metrics obtained via the robot sensors, with the inclusion of a larger pool of participants. Urrutia et al. investigated the correlation between the scores of the Modified Ashworth Scale and the measurements obtained with the Amadeo[®] (Tyromotion, Austria) finger-hand rehabilitation device for the assessment of joint spasticity. Making a reliable and standardized robotic assessment of joint spasticity is still an open challenge due to the need to capture an intricate interaction of neurophysiological mechanisms (Pilla et al., 2020).

Longitudinal assessment protocols merging clinical evaluations with the quantitative measurement of physiological and biomechanical parameters are crucial for achieving more efficient and cost-effective rehabilitation programs. Such assessments would be extremely valuable for the stratification of patients into groups with similar characteristics to identify the most appropriate and customized treatment plan for each individual. Tesfazgi et al. analyzed the sources of uncertainty in the estimation of the human arm impedance using upper-limb wearable robotics. These uncertainties arise from the physical human-robot interaction, and their identification plays a pivotal role in the reliable and

automated estimation of the user's neuromechanical state. This, in turn, can open new possibilities for true customization of rehabilitation treatments. Das et al. proposed a method for the online classification of compensatory movement strategies based on kinematic information. The automatic detection of compensatory motion could be exploited to inform the patient about the correct execution of the task, e.g., during home training without the therapist's supervision. In addition, such information could be used to adjust the assistance profiles of robotic devices to enforce the proper movement kinematics. Finally, Wu et al. demonstrated the benefits of closed-loop cueing training for people with Parkinson's disease. This strategy can provide patients with adaptive, optimized cues to improve their gait performance by learning a personalized model of the user's responsiveness to the cues.

Overall, the articles in this Research Topic provide different insights for the further development of wearable technologies across the rehabilitation continuum of care. These insights revolve around three main pillars: the need for customization of the rehabilitation treatment, the importance of an objective quantification and characterization of the patient's conditions, and the value of smart mechatronic designs to guarantee the seamless and intuitive use of wearable robotics. Further advancements in each of these three pillars will be paramount to ultimately enable the translation of wearable robotics into our daily lives.

Author contributions

ET: Writing—original draft. SH: Writing—review and editing.

Funding

The author(s) declare that no financial support was received for the research, authorship, and/or publication of this article.

Acknowledgments

The authors would like to acknowledge the H2020 ReHyb project (Rehabilitation based on hybrid neuroprosthesis, Grant Agreement: 871767) funded by the EU Commission for their collaboration on this Research Topic.

Conflict of interest

The authors declare that the research was conducted in the absence of any commercial or financial relationships that could be construed as a potential conflict of interest.

Publisher's note

All claims expressed in this article are solely those of the authors and do not necessarily represent those of their affiliated organizations, or those of the publisher, the editors and the reviewers. Any product that may be evaluated in this article, or claim that may be made by its manufacturer, is not guaranteed or endorsed by the publisher.

References

- Babič, J., Laffranchi, M., Tessari, F., Verstraten, T., Novak, D., Šarabon, N., et al. (2021). Challenges and solutions for application and wider adoption of wearable robots. *Wearab. Technol.* 2, e14. doi: 10.1017/wtc.2021.13
- Gonzaga, S., Jedlanek, E., Kim, G., and Raghavan, P. (2023). Addressing the operational challenges for outpatient stroke rehabilitation. *Am. J. Phys. Med. Rehab.* 102, S61–S67. doi: 10.1097/PHM.00000000000002145
- Höhler, C., Trigili, E., Astarita, D., Hermsdörfer, J., Jahn, K., and Krewer, C. (2023). The efficacy of hybrid neuroprostheses in the rehabilitation of upper limb impairment after stroke, a narrative and systematic review with a meta-analysis. *Artif. Organs.* 1–22. doi: 10.1111/aor.14618
- Pilla, A., Trigili, E., McKinney, Z., Fanciullacci, C., Malasoma, C., Posteraro, F., et al. (2020). Robotic rehabilitation and multimodal instrumented assessment of post-stroke elbow motor functions—A randomized controlled trial protocol. *Front. Neurol.* 11, 587293. doi: 10.3389/fneur.2020.587293



OPEN ACCESS

EDITED BY

Emilio Trigili,
Sant'Anna School of Advanced Studies, Italy

REVIEWED BY

Jose Maria Catalan Orts,
Miguel Hernández University of Elche, Spain
Giovanni Pellegrino,
McGill University Health Centre, Canada

*CORRESPONDENCE

Laura Cricenti
✉ l.cricenti@unicampus.it

RECEIVED 23 December 2022

ACCEPTED 27 February 2023

PUBLISHED 16 March 2023

CITATION

Bressi F, Campagnola B, Cricenti L,
Santacaterina F, Miccinilli S, Di Pino G, Fiori F,
D'Alonzo M, Di Lazzaro V, Ricci L, Capone F,
Pacilli A, Sterzi S and Bravi M (2023) Upper limb
home-based robotic rehabilitation in chronic
stroke patients: A pilot study.
Front. Neurobot. 17:1130770.
doi: 10.3389/fnbot.2023.1130770

COPYRIGHT

© 2023 Bressi, Campagnola, Cricenti,
Santacaterina, Miccinilli, Di Pino, Fiori,
D'Alonzo, Di Lazzaro, Ricci, Capone, Pacilli,
Sterzi and Bravi. This is an open-access article
distributed under the terms of the [Creative
Commons Attribution License \(CC BY\)](#). The use,
distribution or reproduction in other forums is
permitted, provided the original author(s) and
the copyright owner(s) are credited and that
the original publication in this journal is cited, in
accordance with accepted academic practice.
No use, distribution or reproduction is
permitted which does not comply with these
terms.

Upper limb home-based robotic rehabilitation in chronic stroke patients: A pilot study

Federica Bressi¹, Benedetta Campagnola¹, Laura Cricenti^{1*},
Fabio Santacaterina¹, Sandra Miccinilli¹, Giovanni Di Pino²,
Francesca Fiori², Marco D'Alonzo², Vincenzo Di Lazzaro³,
Lorenzo Ricci³, Fioravante Capone³, Alessandra Pacilli⁴,
Silvia Sterzi¹ and Marco Bravi¹

¹Physical Medicine and Rehabilitation Unit, Campus Bio-Medico University of Rome, Rome, Italy,

²Research Unit of Neurology, Neurophysiology and Neurobiology and Biomedical Robotics and Biomicrosystems, Campus Bio-Medico University of Rome, Rome, Italy, ³Unit of Neurology, Neurophysiology and Neurobiology, Department of Medicine, Campus Bio-Medico University of Rome, Rome, Italy, ⁴Heaxel, Milan, Italy

Introduction: Robotic therapy allow to propose sessions of controlled and identical exercises, customizing settings, and characteristics on the individual patient. The effectiveness of robotic assisted therapy is still under study and the use of robots in clinical practice is still limited. Moreover, the possibility of treatment at home allows to reduce the economic costs and time to be borne by the patient and the caregiver and is a valid tool during periods of pandemic such as covid. The aim of this study is to assess whether a robotic home-based treatment rehabilitation using the iCONE robotic device has effects on a stroke population, despite the chronic condition of patients involved and the absence of a therapist next to the patient while performing the exercises.

Materials and methods: All patients underwent an initial (T0) and final (T1) assessment with the iCONE robotic device and clinical scales. After T0 evaluation, the robot was delivered to the patient's home for 10 days of at-home treatment (5 days a week for 2 weeks).

Results: Comparison between T0 and T1 evaluations revealed some significant improvements in robot-evaluated indices such as Independence and Size for the Circle Drawing exercise and Movement Duration for Point-to-Point exercise, but also in the MAS of the elbow. From the analysis of the acceptability questionnaire, a general appreciation of the robot emerged: patients spontaneously asked for the addition of further sessions and to continue therapy.

Discussion: Telerehabilitation of patients suffering from a chronic stroke is an area that is still little explored. From our experience, this is one of the first studies to carry out a telerehabilitation with these characteristics. The use of robots can become a method to reduce the rehabilitation health costs, to ensure continuity of care, and to arrive in more distant places or where the availability of resources is limited.

Conclusion: From the data obtained, this rehabilitation seems to be promising for this population. Moreover, promoting the recovery of the upper limb, iCONE can improve patient's quality of life. It would be interesting to conduct RCT studies to compare a conventional treatment in structure with a robotic telematics treatment.

KEYWORDS

home-based, stroke, robotic device, upper limb, rehabilitation, technologies

Introduction

Stroke is the second leading cause of death and a major cause of disability worldwide. Currently it is estimated that every year about 33 million people suffer a stroke, but this incidence is expected to increase due to the progressive aging of the population (Wang et al., 2016; Soriano et al., 2017; Katan and Luft, 2018). Typically, 1 year after stroke 65% of these patients remain severely impaired and the degree of disability is correlated with the severity of stroke (McConnell et al., 2017); this translates into an increase in assistance for carrying out the activities of daily living (ADL). Motor impairment is the most common consequence of stroke, which can be regarded as loss or limitation of function in muscle control or movement in an arm and a leg on one side of the body (Pollock et al., 2014). Upper limb weakness is a common condition, affecting about the 85% of survivors. Therefore, one of the main aims of rehabilitation is to improve upper limb functions.

Evidence in the literature underlined how motor training can positively influence the recovery by enhancing brain plasticity after stroke, especially, when a multisensory rehabilitation is proposed (Poli et al., 2013) and when repetitive and task-oriented exercises, with a high number of repetitions, are delivered. This type of rehabilitation requires great commitment for both patients and physiotherapists, resulting in high costs for the health care system (Jenkins and Merzenich, 1987; Masiero and Carraro, 2008; Poli et al., 2013). Robotic devices can help overcome these obstacles indeed, the use of these devices has been proposed since the 90s to help therapists increase the intensity of sessions, provide multisensory stimulation, and reduce costs (Poli et al., 2013; McConnell et al., 2017). Furthermore, robotic devices allow to propose sessions of controlled and identical exercises, tailored on the characteristics of the individual patient (Li et al., 2022). Moreover, through the use of screens and visual feedback, robotic devices provide sensory input, encouraging learning thanks to the increased involvement given by the interactivity of the technological device (Maciejasz et al., 2014).

The effectiveness of robotic assisted therapy is still under study and the use of robots in clinical practice is still limited. One of the reasons may be related to the logistics of using these devices. In fact, the patients for whom the use of the robot is indicated are generally severely disabled, requiring the assistance of a caregiver to get to visits and therapeutic sessions (Li et al., 2022). The solution to this problem could be the use of robotic devices for home rehabilitation: most of the recent robotic rehabilitation devices are designed and built to be transported to the patient's home, so that the patient can perform the exercises several times a day. Home treatments can also be provided using devices such as smartphones and tablets or through the use of webcams. A recent review reported that in motor recovery after stroke, telerehabilitation appears to have similar results to clinical rehabilitation. According to this review, both for sub-acute and chronic patients, technological rehabilitation programs should be integrated into conventional therapy (Maciejasz et al., 2014). These results are also supported by a recent Cochrane review by Laver et al., in which 22 Randomized Controlled Trials were analyzed, for a total of 1,937 patients. This review shows that there is no difference in daily life activities between people who at discharge have received telerehabilitation and those who have received regular care (Laver et al., 2020).

However, the few studies in the literature show conflicting results, so the aim of this pilot study is to evaluate the effectiveness of a robotic home treatment rehabilitation on patients suffering from chronic stroke. This study also allows to analyze another important aspect: the effectiveness of robotic therapy in the absence of a physiotherapist alongside the patient. In addition, an acceptability questionnaire was administered to assess patients and caregivers' satisfaction of the robot and whether robotic therapy increases the workload of the caregiver. In fact, although the commitment related to the transport of the patient to the rehabilitation site is eliminated, the involvement of the caregiver cannot be eliminated, but the workload can be reduced by ensuring the maximum flexibility of the therapy.

Materials and methods

Study design

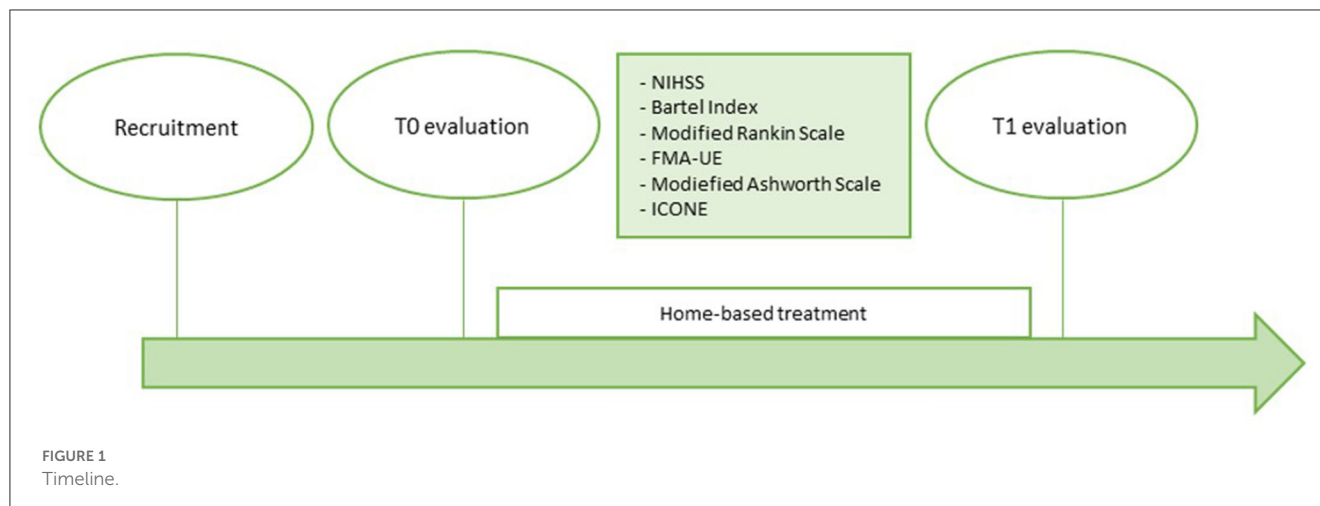
The present study is a monocentric pilot study on the use of the iCONE robotic device (Heaxel srl, Milan, Italy) for home rehabilitation of patients with chronic stroke outcome approved by the ethics committee of the Fondazione Policlinico Universitario Campus Bio-Medico (protocol number 29/19).

This study aims to assess whether a robotic home-based treatment rehabilitation delivered by the use of the iCONE robotic device for two consecutive weeks has effects on this population, despite the chronic condition of patients involved and the absence of a therapist next to the patient while performing the exercises. Two evaluations were provided in order to assess the effectiveness of treatment: before the start of treatment and at the end of treatment. The evaluations included the administration of clinical scales by medical staff and physiotherapists and the execution of exercises provided by the robot. The exercises administered for the evaluation with the robot were the same for all patients and for both evaluations.

Participants

The study involved patients recruited in the period between March 2021 and April 2022 by the Complex Operative Unit (COU) of Physical Medicine and Rehabilitation, the COU of Neurology, and the Research Unit of Neurology, Neurophysiology and Neurobiology and Biomedical Robotics and Biomicrosystems of the Campus Bio-Medico University Hospital Foundation of Rome. Enrolled patients underwent clinical examination before the initial assessment.

Inclusion criteria for this study included patients aged between 18 and 80 years, with chronic stroke outcome (stroke onset at least 6 months before treatment) and residual upper limb deficiency evaluated with an Upper Limb Fugl-Meyer Assessment ≥ 3 . Patients also had to be able to understand the indications given by the therapist and the ability to sign the informed consent. Moreover, no patients who had criteria contrary to the conditions required by the use of the robot were recruited. These criteria were: a positive history of epilepsy, presence of severe cognitive deficits and/or psychiatric disorders, severe flaccidity of the upper limb, lack of



balance of the trunk in sitting position, and orthopedic pathologies of the upper limb that made it difficult to use the robot.

General intervention description

After recruitment, patients underwent an initial assessment (T0) through a series of clinical scales to assess the degree of cognitive and functional disability of the patient, autonomy in ADL, motor skills, and the degree of spasticity. In particular, the NIHSS, the Barthel Index, the Modified Ranking Scale, the Fugl-Meyer Assessment for the upper limb, and the Modified Ashworth Scale were administered. The detailed description of the scales is given below. Patients were then subjected to a motor and performance assessment using the robotic device iCONE, in order to evaluate parameters such as coordination and muscle synergy, precision, fluidity of movement, strength.

The home-rehabilitation included 10 sessions of exercises performed with the iCONE device with the supervision of a caregiver previously trained by the engineering team on robot management. At the end of the 2 weeks of home treatment a second evaluation (T1) was repeated in the same way as the T0. [Figure 1](#) shows the timeline of the study.

The exercises proposed in the evaluation do not coincide with those proposed in the exercises at home. This prevents the results obtained in the T1 assessment from being affected by the exercise training component.

The iCONE robotic device

iCONE (Heaxel, Milan, Italy) is a medical device for robot-assisted neurorehabilitation of the upper limb ([Figure 2](#)). It consists of a metal structure connected to a handle that allows the movement on the transverse plane of the upper limb and a monitor that shows the exercise to be carried out. The handle is interchangeable to adapt to the patient's grip. It requires the movement both of shoulder and elbow, while the hand is not involved and is anchored to the handle. The robot comes with a



table adjustable in height to adapt to the most comfortable seat of the patient.

At the moment of taking charge of the patient, the robot provides to create a user card in which the date of the event, the type, and the injured side can be recorded. iCONE has the authorization for use in both healthcare facilities and in non-hospital environment. For this reason, it can be used at the patient's home favoring the possibility of telerehabilitation.

The robot allows the administration of protocols based on the intensive repetition of therapeutic exercises and integrates a computer that indicate on the display the specific points that must be reached in the movement, requiring shoulder and elbow

coordination to perform tasks of reaching. The use of the screen also provides visual feedback for the patient.

The iCONE robotic device can perform two types of session: the evaluative session and the therapy session. The evaluative session involves performing six standard exercises and provides a complete report extrapolating quantitative indicators from the planned exercises. These indicators are shown both numerically and graphically and when a new evaluation is made, the data of the previous evaluations are reported alongside the new ones, facilitating comparison. For each indicator, or index, a description is given to define what it refers to. Moreover, the expected trend is reported.

The six exercises proposed for the evaluation and the respective indices are described below:

- **Circle drawings:** it requires to draw a total of twenty circles divided into four series of five repetitions for different directions: the circles must be drawn clockwise and counterclockwise, starting from the left and then from the right, so that there will be five circles from left to right passing from the top and five circles passing from the bottom, and five circles from right to left from the top and five from the bottom. The therapist gives the start and the stop for each circle. The robot is in a transparent mode, which means that it provides neither assistance nor resistance to the patient during the execution of the task. It provides two indexes: independence and size.
 - o *Independence:* it is the ratio of the minor axis to the main axis of the ellipse that adapts to the circles drawn by the patient. An increase is expected as therapy progresses (a perfect circle would have a ratio of 1.00). Higher values indicate better coordination and synergistic control of the elbow and shoulder.
 - o *Size:* it is the total area of the ellipse that best suits the circles drawn by the patient. An increase is expected as the therapy proceeds. Indicates improvements in the Range of Motion (ROM) of the paretic limb.
- **Point-to-point:** it consists in the classic round of the clock in which the patient must reach the eight targets arranged along the perimeter of a circle starting each time from the center. The exercise includes five clock turns. During the exercise the robot is in transparent mode. It provides seven indexes: init time, mean speed, movement duration, path error, reach error, smoothness, and peak speed.
 - o *Init time:* it indicates the time needed to start the movement independently. It is expected to decrease as therapy progresses. It is an indicator of the ability of planning movement.
 - o *Mean speed:* Average speed of the end-effector in the execution of the point-point movements. The average speed is expected to increase as therapy progresses.
 - o *Movement duration:* Average time needed to perform a point-to-point movement. It is a measure of temporal efficiency. It decreases as therapy progresses.
 - o *Path error:* Average distance of each point in the patient's trajectory from the theoretical path. It measures the accuracy of the entire reaching movement. Decreases as therapy progresses (ideally zero).
 - o *Reach error:* Indicates how close the patient is to the target, on average. It is a precision measurement. Lower result indicates better performance. A radar graph shows the value of the indicator along each direction of movement.
 - o *Smoothness (speed shape):* Ratio between average and maximum speed during point-to-point movements. It is an indicator of fluidity and ease of execution of the movement: the higher the value, the easier it is for the patient to complete the movement. It increases with the progress of therapy.
 - o *Peak speed:* Peak speed value of the patient. Indicates ease of movement. Increases as therapy progresses.
- **Playback static:** requires the patient to hold the handle of the robot in the center, while the robot moves toward the eight targets. This exercise provides one index: hold deviation.
 - o *Hold deviation:* It represents the average deviation from the center during the Playback Static exercise. A patient with a flaccid limb may show a star-shaped movement. The indicator tends to shrink as therapy proceeds.
- **Round dynamic:** it is the opposite of the previous exercise. Requires that the patient brings the robot's end-effector to the eight targets, while the robot applies a resistance to the center. It provides the index displacement.
 - o *Displacement:* Average distance covered against resistance from the central target during Round Dynamic exercise. The value increases with the progress of therapy.
- **Shoulder horizontal abduction:** the straps on the forearm are loosened and only the hand remains in contact to the end-effector. The patient is positioned with the elbow extended and the shoulder at 90°. The handle of the robot freezes in the middle of the screen and the patient is asked for a 5 s shoulder abduction. The exercise is repeated five times. It provides one index: shoulder horizontal abduction.
 - o *Shoulder horizontal abduction:* Maximum variation of force exerted by the patient during the 5 s of the five repetitions, while trying to remove the end-effector from its sagittal plane. It increases in the course of therapy.
- **Shoulder horizontal adduction:** the conditions are the same as the previous exercise, but the movement required is an adduction. It provides one index: shoulder horizontal adduction.
 - o *Shoulder horizontal adduction:* Maximum variation of force exerted by the patient during the 5 s of the five repetitions, while trying to bring the end-effector to its sagittal plane. Increases in the course of therapy.



FIGURE 3
Evaluation exercises: circle drawing, point to point e horizontal abduction/adduction.

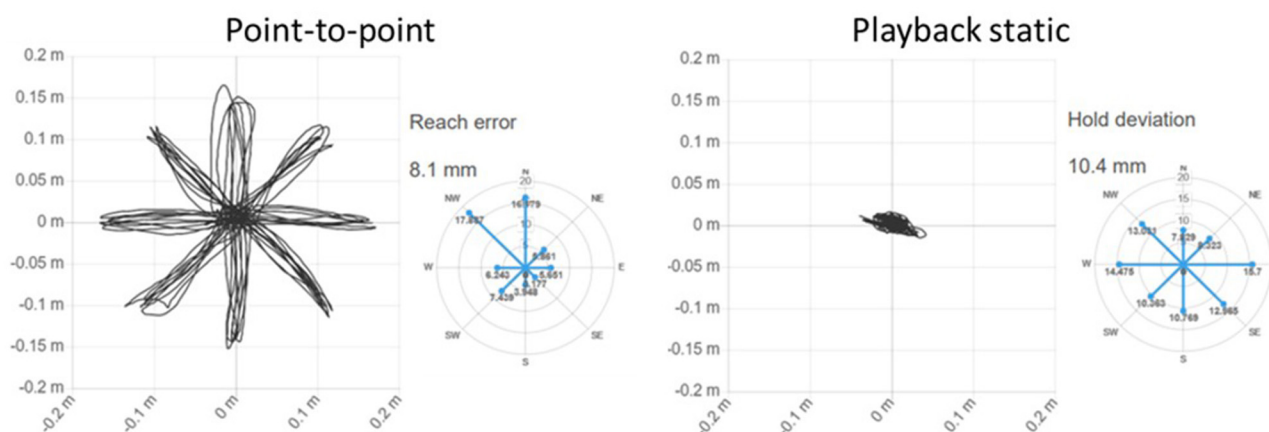


FIGURE 4
Example of trajectories and indices of two exercises.

Figure 3 shows the screen shown to the patient in the exercises Circle drawing, Point-to-point e Horizontal Abduction/Adduction, while Figure 4 shows the trajectories and two examples of indices for the exercises proposed in the evaluation.

While exercises for evaluation are standard, for therapy several parameters can be set. In particular, the width and stiffness of the haptic tunnel, the level of assistance and resistance, the number of repetitions for exercise, the accuracy of the target, the scenery can be changed. In addition, it can be customized the waiting time for the start of the movement before the robot activates to help the patient and the maximum assigned time to complete the movement before the robot passes to the next target. There are three modes of interaction to adapt to each degree of disability of the patient: assistive, resistive, or adaptive. The assistive mode requires the robot to help the patient perform tasks and allows a different degree of assistance to be set according to the patient's conditions. The resistive mode allows to set up a resistance training for patients who have achieved a good degree of movement control and who need muscle reinforcement. The adaptive mode requires the robot to help the patient only when the movement can't be completed.

This study has adopted the assistive modality in order to adapt to all the levels of impairment.

An important feature of this device is the ability to follow the patient remotely by the cloud. In fact, therapy progress and session execution data are constantly updated and stored in the cloud, so that the therapist can monitor and change the training sessions at any time by remotely accessing the device delivered to the patient thanks to the wi-fi connection. For this purpose, in case the patient was not provided with wi-fi, a router was provided with the device.

Intervention

All patients included in the study carried out an initial (T0) and final (T1) assessment administered at the CESA (Health Center of the Elderly) of Campus Bio-Medico University Polyclinic Foundation of Rome.

The two evaluations included the administration of the following clinical scales: National Institute of Health Stroke Scale (NIHSS), Modified Rankin Scale (MRS), and Barthel

Index (BI) submitted by neurologists; Fugl-Meyer Assessment for upper extremity (FMA-UE) and Modified Ashworth Scale (MAS) administered by physiotherapists.

In this study, NIHSS, MRS, and BI were administered with the aim to frame the degree of disability and severity of the included patients.

The NIHSS is used to measure stroke severity. It is composed of 15 items that investigate level of consciousness, eye movements, integrity of visual fields, facial movements, arm and leg muscle strength, sensation, coordination, language, speech, and neglect. For each domain, a score ranging from 0 to 2, 0 to 3, or 0 to 4 can be recorded. The total score ranging from 0 to 42 is calculated as the sum of individual item scores. The higher the score, the more severe the stroke (Kwah and Diong, 2014).

The MRS was developed to measure the disability or dependence in the daily activities of people with stroke outcomes or other neurological disorders (Haggag and Hodgson, 2022). It is composed of a single item ranging from 0 to 6, where 0 means no symptoms, 1 no significant disability, 2 slight disability, 3 moderate disability, 4 moderately severe disability, 5 severe disability, and 6 refer to death (Broderick et al., 2017).

The BI measures 10 basic aspects of activity related to self-care and mobility. It investigates 10 items (feeding, grooming, bowel and bladder management, toilet use, dressing, bathing, transfer, mobility, and stairs) with a score ranging from 0 to 10 or 0 to 15. The normal score for this scale is 100 points and lower scores indicate greater dependency (Kasner, 2006).

The FMA-UE has different domains: it evaluates the motor aspects, the sensitivity, the passive ROM and the pain. The Motor function has a maximum score of 66 points. The evaluation investigates voluntary movement, speed, coordination, and reflex activity. For each item a score ranging from 0 to 2 can be assigned depending on the ability to perform and complete the task: 0 = cannot be performed, 1 = partially performed, 2 = performed completely. The total score allows to classify the motor impairment as severe (<32 points), moderate (between 32 and 47), or mild (>47 points) (Barbosa et al., 2019; Rech et al., 2020). Sensitivity is evaluated both as light touch and proprioception and it has a maximum score of 12. Passive ROM and joint pain are evaluated for all districts. The passive ROM has a maximum score of 24, the pain has a maximum score of 12. As for the motor function, for these domains the scores for each item ranges from 0 to 2.

MAS is used to evaluate passive movement resistance. This scale allows to obtain an indirect assessment of spasticity. The score ranges from 0 (no tonus increase) to 4 (stiffness). Patients are evaluated in a lying position, and they are asked to remain relaxed during the test (Maciejasz et al., 2014; Rech et al., 2020).

In addition, patients also performed an evaluation session with the robot consisting of a series of six exercises as described previously. The exercises provided by the robot for evaluation are standardized to always be the same for all patients. At the end of the evaluation, the robot provides a report with numerical indexes comparable between the two evaluation times and graphs with the trajectories followed by the patient during the exercises.

At the final evaluation, an acceptability questionnaire was administered consisting of a question for the patient about the difficulty of using the robot and the possibility to integrate it in the daily activities, and one for the caregiver to assess how much the

required workload in patient care has increased. It was also required to quantify this feature giving a score ranging from 0 to 10. The acceptability questionnaire is available in the Italian version and in an English translation in the [Supplementary material](#).

After initial evaluation, the robot was delivered to the patient's home. The rehabilitation protocol provided 10 days of at-home treatment (5 days a week for 2 weeks).

The robot allows to plan therapies with customizable sessions. Each session consisted in point to point reaching exercises for a total of 1,024 reaching movements. For each session we adapted the number of consecutive repetitions, depending on the patient's need to make breaks with greater or lesser frequency.

For this protocol, a typical session was as follows: four exercises of 16 repetitions and six exercises of 160 repetitions according to the following scheme: 16-160-160-16-160-160-16-160-160-16.

For patients with increased motor impairment, it was necessary to further divide the session, to allow the patient to intersperse the exercises with more frequent breaks. For these patients each of the exercises of 160 repetitions was divided into five exercises of 32. This distinction was based on the difficulties reported by the individual patient. In the first days of therapy the physiotherapist assessed the need to divide the session.

The total number of repetitions for each session to be performed throughout the day was fixed at 1,024 movements for each patient.

Despite the customization of the rehabilitation, some patients had difficulty to complete all the required tasks, while others exceeded in the sessions for which it was necessary to add some more to complete the 10 days of therapy.

During the home treatment the patients were followed exclusively by a caregiver (usually a family member of the patient) designated by the therapist at the initial evaluation or by the engineer at the time of delivery of the robot at home. The caregiver did not have an active role in the therapy, but his presence is required for the use of the robot and his purpose is to intervene in case of need or adverse events.

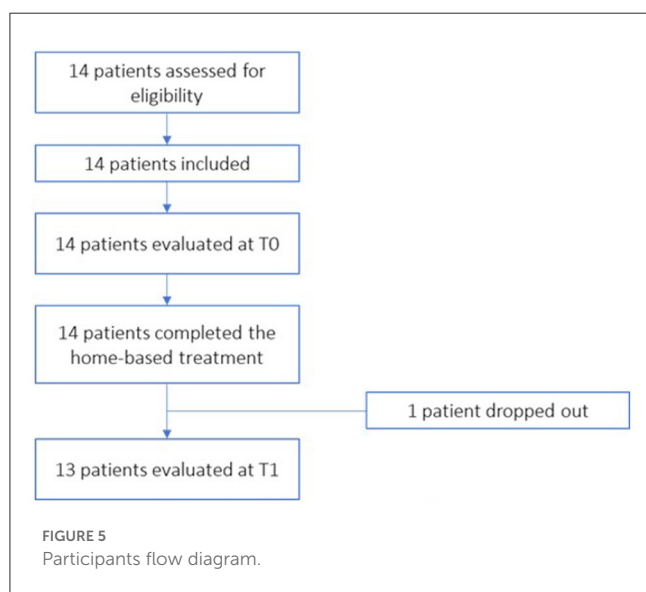
It is not possible to establish the overall commitment of the treatment as this varies greatly from patient to patient: for some patients it took an hour a day to complete all the exercises, while others took up to 3 h.

Physiotherapist had the ability to follow the patient remotely via cloud, so that it was possible to add a new session wherever the patient exceeded daily therapy or reduce the number of tasks per exercises if the patient required more breaks. When many incomplete exercises appeared or abnormalities were found, the therapist contacted the patient by phone to make sure the therapy was adequate.

Data analysis

Normality assumptions were tested by means of the Shapiro-Wilk test ($p > 0.05$) and data were then analyzed with the appropriate statistical test. Technical failure caused a lack of data in some conditions, in fact, in some cases the robot has not recorded the full values of the indices, especially when patients made incomplete movements or were not able to complete the

assessment exercise. Thus, data were analyzed with generalized linear mixed models (GLMM) and, when necessary, scaled with a (min–max) + 1 normalization to obtain positive numbers > 1. This has made it possible to carry out a more complete analysis, since unlike other methods, the GLMM allow to analyze the data albeit partial, avoiding data loss. Moreover, for the same reason also allows to use data of the drop out patient. We chose the most appropriate family and link function as the model with the lowest Akaike information criterion (AIC).



All the reported results were corrected, when appropriate, with Holm correction for multiple comparisons. Statistical significance was set at p -values < 0.05.

Results

All the patients recruited were evaluated and considered suitable for treatment as regards the eligibility criteria. A total of 14 patients were included in the treatment. Figure 5 shows the flow diagram of patient recruitment.

The patients recruited were all adults, with an average age of 59.29 years (between 32 and 79 years) suffering from chronic, ischemic or hemorrhagic stroke (respectively, 11 vs. 3 cases). They had residual upper limb disabilities due to a first ever stroke and the minimum time away from the cerebrovascular event was at least 6 months from the start of the study. They were predominantly women (8F/6M) and the affected side was equally distinct among the participants: seven patients had a right hemisphere injury and seven had a left hemisphere injury.

Data regarding demographic information of the included patients are reported in Table 1.

During the study a voluntary drop-out was recorded related to problems of the patient's family (patient 5): it was not possible for family members to bring the patient to the T1 evaluation. Then, of the 14 patients recruited, 13 completed all evaluations.

Data obtained from the NIHSS, BI, and MRS were reported to describe the clinical status of the sample analyzed. Table 1 shows the values recorded for each patient and the average and standard deviation for the total of the patients.

Table 2 show the results obtained in the Fugl-Meyer Assessment divided for the different domain and the Ashworth scale evaluation

TABLE 1 Characteristics of the patients.

Participants (no. 14)	Age	Sex	Type of stroke	Affected limb	Time from stroke (months)	NIHSS	BI	MRS
Patient 1	73	M	I	L	177.97	2	75	3
Patient 2	55	F	I	L	188.39	4	75	4
Patient 3	64	M	H	R	32.49	2	75	3
Patient 4	52	M	H	L	113.97	4	80	2
Patient 5*	59	M	I	R	28.98	8	85	2
Patient 6	32	F	I	R	192.00	3	95	1
Patient 7	69	M	I	R	6.74	5	61	3
Patient 8	78	F	I	L	8.25	3	90	1
Patient 9	46	F	I	R	22.21	3	98	1
Patient 10	63	F	I	R	6.12	7	85	3
Patient 11	58	F	I	L	701.04	3	95	1
Patient 12	79	F	I	L	14.06	10	30	4
Patient 13	53	M	H	R	343.46	6	89	3
Patient 14	49	F	I	L	37.72	2	90	2
Mean \pm sd	59.29 \pm 13.0	6M/8F	11I/3E	7L/7R	133.8 \pm 192.1	4.43 \pm 2.47	80.21 \pm 17.63	2.36 \pm 1.08

M, male; F, female; I, ischemic; H, hemorrhagic; NIHSS, National Institutes of Health Stroke Scale; BI, Barthel Index; MRS, Modified Ranking Scale.

*Patient 5 dropped out after treatment.

for shoulder, elbow, and wrist districts. Data were analyzed with GLMM method. Average and standard deviation are reported for each data for both T0 and T1. Moreover, statistical significance is reported for the comparison between T0 and T1.

The comparison of the results obtained in the FMA-UE between T0 and T1 highlights a substantial stability at T1 for all the domains analyzed, with a slight but not significant improvement in motor function.

The MAS for the elbow district reported a statistically significant result in the comparison between T0 and T1.

In the analysis of robot indices data were analyzed with GLMM and, when necessary, scaled with a (min-max) + 1 normalization to obtain positive numbers > 1. We chose the most appropriate family and link function as the model with the lowest AIC. Table 3 summarize mean, standard deviation, and *p*-values related to the comparison between the two times T0 and T1 for all the variables.

TABLE 2 FMA-UE and MAS comparison between T0 and T1.

	T0 (mean ± sd)	T1 (mean ± sd)	<i>p</i> -value
FMA motor function	33.21 ± 14.87	35.69 ± 15.92	0.882
FMA sensibility	10.36 ± 2.71	10.92 ± 2.25	0.952
FMA passive ROM	18.71 ± 3.07	18.92 ± 3.09	0.985
FMA pain	21.21 ± 2.78	21.69 ± 2.69	0.296
MAS shoulder	1.07 ± 0.73	0.92 ± 0.95	0.113
MAS elbow	1.86 ± 0.95	1.46 ± 1.2	0.017*
MAS wrist	1.36 ± 0.93	1.46 ± 1.13	0.955

FMA, Fugl-Meyer Assessment; MAS, Modified Ashworth Scale.
The * symbol indicates values that reach statistical significance.

TABLE 3 Comparison between T0 and T1 for iCONE indices.

Index	T0 (mean ± sd)	T1 (mean ± sd)	<i>p</i> -value
Independence	0.59 ± 0.39	0.76 ± 0.25	0.040*
Size	0.04 ± 0.03	0.05 ± 0.02	0.019*
Init time	0.14 ± 0.23	0.12 ± 0.28	0.916
Mean speed	0.07 ± 0.03	0.08 ± 0.05	0.073
Movement duration	3.53 ± 1.46	2.66 ± 1.52	0.002**
Path error	13.02 ± 5.17	11.12 ± 4.49	0.218
Reach error	20.46 ± 14.81	18.72 ± 17.59	0.993
Smoothness	0.54 ± 0.09	0.57 ± 0.12	0.514
Peak speed	0.12 ± 0.04	0.14 ± 0.07	0.168
Hold deviation	26.78 ± 21.1	24.97 ± 16.89	0.448
Displacement	58.65 ± 22.71	64.07 ± 15.59	0.068
Shoulder horizontal abduction	20.84 ± 9.36	23.24 ± 5.89	0.273
Shoulder horizontal adduction	21.72 ± 12.12	23.9 ± 6.5	0.444

The * and ** symbols indicate values that reach statistical significance. A single asterisk for *p*-values ≤ 0.05; two asterisks for *p*-values ≤ 0.01.

As reported in Table 3, statistically significant results have been recorded for three indices: Independence significantly increased between T0 and T1 (*p* = 0.040), Size significantly increased between T0 and T1 (*p* = 0.019), and Movement Duration significantly decreased between T0 and T1 (*p* = 0.002). The distribution of the variables at the two evaluations are shown in Figure 6.

Figure 6 shows box and whisker plot of MAS for the elbow district, Independence, Size, and Movement Duration represented in A, B, C, D, respectively. The thick horizontal gray line within the boxplot represents the median value. Asterisks indicate significant differences (**p* < 0.05, ***p* < 0.01).

Two variables have achieved interesting results although not statistically significant: Mean Speed (*p* = 0.073) and Displacement (*p* = 0.068). Both variables are increased between T0 and T1.

From the results obtained in the acceptability questionnaire, all the patient (100%) stated that the treatment proposed at home was compatible with daily life activities. The average score given to the liking of the robot was 9.23 points on a scale from 0 to 10. Ten caregivers (76.92%) reported that their care load did not increase during the home-based treatment, with a score of 0 on a scale from 0 to 10, while three of them (23.08%) reported that their workload increased with an average score of 7.3.

No adverse events were recorded during the evaluations or the home-based treatment.

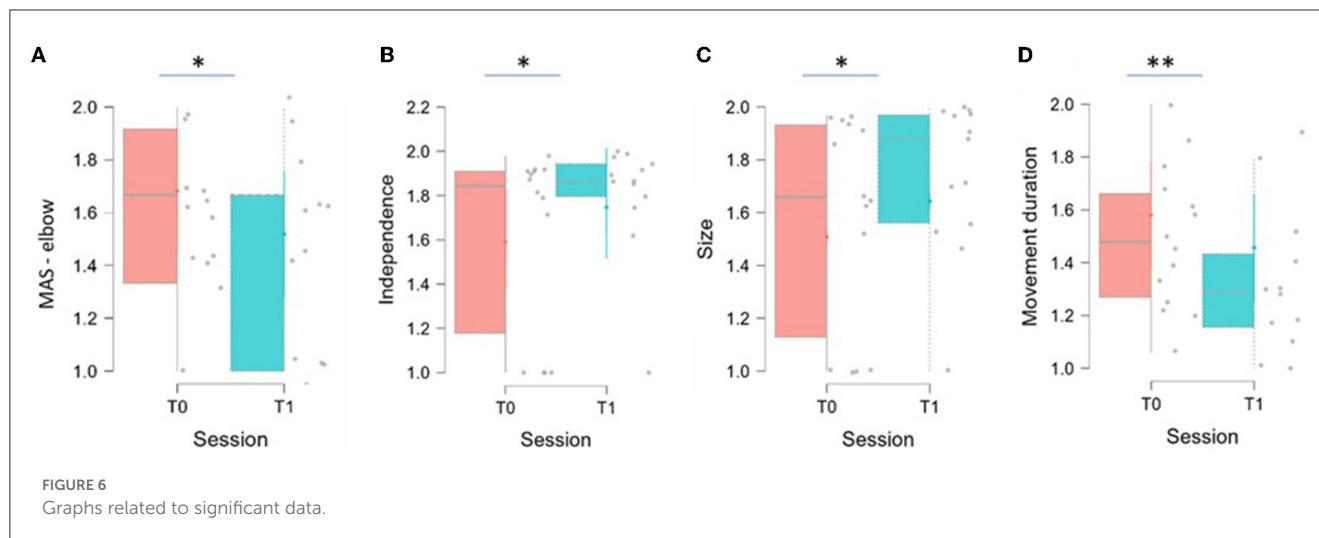
Discussion

The purpose of the present study was to assess whether a rehabilitation treatment delivered at home using a robotic device could have a positive effect on patients with chronic stroke outcome, even when the therapist is not next to the patient while performing the exercises. The results obtained from our study seem to support the hypothesis of the usefulness of this type of rehabilitation.

The significant data obtained in the Independence, Size, and Movement Duration relate to the synergy of movement, the ROM, and the duration of movement, indicating an improvement of the patient in performing wider movements, with better control, greater fluidity, and shorter time. This could result in improved functionality of the paretic limb, which has been reported by many of the patients, even if it has not been found in the clinical scales administered. This result is in line with the results obtained in the evaluation with MAS. In fact, the significant decrease in tone at the elbow of the examined limb may have contributed to the greater fluidity of the movement, indicating that this device is suitable for use in these patients, avoiding causing an increase in spasticity.

The two indices Mean Speed and Displacement reached very interesting even if not significant values. These variables refer, respectively, to the speed and to the distance covered against resistance in the execution of the reaching movement. The increase of these two parameters could be a next step in the improvement of the movement management, as it provides for a good control by the patient even during the application of a force.

Moreover, the results obtained in the robotic evaluation cannot be linked to the learning in the use of the device by the patient, in fact the exercises proposed in the treatment are different to those proposed in the evaluation. Consequently, it was not possible to find a clear response and support to our results, although these



seem favorable not only for the outcomes obtained by patients, but also for the management of therapy.

As reported by Chen et al. in their systematic review, the results obtained from home treatment with these devices are very discordant. Several studies reported that patients treated with robotic devices can achieve improvements comparable to those treated with conventional therapies. Alongside these studies, however, there are numerous studies that report no statistically significant results in the same comparison (Chen et al., 2019).

Although the robotic indices reported several significant data, the scales of evaluation of the functionality did not show major changes, in particular the FMA-UE. This could be explained by a higher sensitivity of indices compared to clinical scales that require greater variation to record changes in scores.

For the duration of treatment, as already mentioned, it was not possible to make a direct comparison with studies involving the use of the same robot, so it was compared with robots having similar structure and the same degrees of freedom, for example the MIT-Manus device (Massachusetts Institute of Technology, Cambridge, MA, USA). The analyzed studies took into consideration the treatment in structure and not at home. This analysis showed that treatment times vary from 4 to 6 weeks for this type of devices, with a frequency of 5 days a week (Volpe et al., 2000, 2008; Ang et al., 2014; Sale et al., 2014). Therefore, it would be interesting to increase the treatment period to assess whether this produces an improvement in the results or an abandonment of the therapy.

According to the questionnaires administered at T1, patients were satisfied with robotic therapy, showing that the device was found to be well-tolerated by the patients. Therefore, caregivers reported that their workload is not increased during the home-based treatment, not affecting the organization of daily activities.

The purpose of post-stroke rehabilitation is to promote the recovery of lost functions to allow the patient to achieve independence and reintegration into social life. To date there are no studies in the literature carried out with this robotic device and there are still few studies about the use of robots at the patient's home. Even if they are not yet widespread, robotic systems offering home rehabilitation for patients with neurological diseases are becoming increasingly known and accepted (Guillén-Climent et al., 2021). Robotic devices for the therapy of the upper limb enabled to

operate at the patient's home present several advantages. In fact, patients can perform the established therapy at any time of the day, without the need to reach a rehabilitation facility with consequent less impact on the caregiver's load. Moreover, the costs relative to the attainment of the structure and the times of employment demanded to the caregiver are significantly reduced.

An important factor in favor of home robotic therapy is the possibility of providing high-dose rehabilitation therapy even to those patients with chronic outcomes, for whom the journey within hospital facilities has ended. This type of rehabilitation at home could therefore represent a valid alternative to the management of chronic diseases, guaranteeing this category of patients an adequate treatment to maintain longer the autonomy achieved in the acute phase. Moreover, the interactivity of telerehabilitation and the possibility of modulating the intensity of treatment are useful to adapt the therapy to the progress of the patient (Cramer et al., 2019) and possibility to vary the proposed games and actions enable these devices to always being stimulating (Nijenhuis et al., 2015). The proposal of exercises in the form of play, can increase the patient's involvement and consequently his adherence to therapy (Popović et al., 2014; Rodríguez-De-Pablo et al., 2016).

Home robotic rehabilitation also has disadvantages: using robotic devices at home concerns the need for ample space for placement. This can be a problem for subjects living in apartments with little spaces. In addition, in some cases robots produce forces that can affect the safety of the treatment (Chen et al., 2019). For this reason, the iCONE provides the presence of a caregiver during treatment trained to stop the robot in the event of problems or risks to the patient.

Therefore, it could be interesting for the future to introduce in the proposals of the robotic devices also functional activities and exercises aimed at the recovery of common activities in everyday life (Poli et al., 2013; World Health Organization, 2022).

Limitations and future implications

The limitations that we have found in the conduct of this study are linked to a poor sensitivity of the scales administered, which have not allowed to make a more specific comparison with the

indices obtained by the robot. It would be interesting to introduce a more complete evaluation of the fluidity and precision of the movement together with a functional evaluation of the upper limb in daily life activities. In fact, the evaluation of the ADL was carried out only with the administration of the BI, which is not specific enough to assess the impairment related to the functionality of the arm.

A second limitation concerns the low number of patients included and the absence of randomization. It would be interesting to evaluate the difference between a group that carries out the treatment in a facility with the possibility for the physiotherapist to intervene in the correction of the task, and the summation of the same therapy at home, with the assistance of the caregiver.

A third limit concerns the treatment time, which is shorter than the robotic home rehabilitation studies found in the literature. This time in fact varies between 6 and 12 weeks, while our study has provided a treatment time of only 2 weeks.

Finally, it was not possible to find in the literature a questionnaire validated in Italian that would consider items related to the use of the robot at home and that would evaluate both patients' and caregivers' acceptability. The questionnaire adopted in this study is not sufficiently structured to detect all the problematics that may occur during rehabilitation at home but was intended to assess in a simple and fast way the degree of acceptability of the patient and the caregiver toward the robot at home. It would be interesting to include a more structured questionnaire with more specific questions about the robot and compatibility in home use to assess whether there is a category of patients more suitable for this type of treatment.

In the future it would be interesting to include an economic feasibility study, considering the aspects related to the transport of the device, the need for internet connection, and aspects related to patient insurance at home.

Conclusions

The presented study assessed the feasibility and the effectiveness of a home robotic rehabilitation program. Despite the small sample recruited, it was possible to record interesting and significant results, which support the use of robotic devices at home for the treatment of patients suffering from chronic stroke, even long after the acute event. These results are promising for this type of rehabilitation, so it would be interesting to continue the study on a larger sample, providing a longer therapy time and inserting a control group. The study presented is in fact a pilot study, without control group, so the results obtained should be considered as preliminary data and should be confirmed with better structured studies, such as Randomized Controlled Trials. It would also be useful to re-evaluate the patient to follow-up, to

see if the results obtained are kept even at time from the use of the robot.

Data availability statement

The original contributions presented in the study are included in the article/[Supplementary material](#), further inquiries can be directed to the corresponding author.

Ethics statement

The studies involving human participants were reviewed and approved by Campus Bio-Medico Ethical Committee. The patients/participants provided their written informed consent to participate in this study.

Author contributions

LC, BC, FS, FF, MD'A, LR, and AP: data collection. FB, BC, LC, and MB: handwritten. GD, SM, VD, FC, and SS: revision. All authors contributed to the article and approved the submitted version.

Conflict of interest

AP was employed by Heaxel, the company that supplied the robot, and was involved in the management of the robot at home, so she had direct contact with patients.

The remaining authors declare that the research was conducted in the absence of any commercial or financial relationships that could be construed as a potential conflict of interest.

Publisher's note

All claims expressed in this article are solely those of the authors and do not necessarily represent those of their affiliated organizations, or those of the publisher, the editors and the reviewers. Any product that may be evaluated in this article, or claim that may be made by its manufacturer, is not guaranteed or endorsed by the publisher.

Supplementary material

The Supplementary Material for this article can be found online at: <https://www.frontiersin.org/articles/10.3389/fnbot.2023.1130770/full#supplementary-material>

References

- Ang, K. K., Chua, K. S. G., Phua, K. S., Wang, C., Chin, Z. Y., Kuah, C. W. K., et al. (2014). A randomized controlled trial of EEG-based motor imagery brain-computer interface robotic rehabilitation for stroke. *Clin. EEG Neurosci.* 46, 310–320. doi: 10.1177/1550059414522229
- Barbosa, N. E., Forero, S. M., Galeano, C. P., Hernández, E. D., Landinez, N. S., Sunnerhagen, K. S., et al. (2019). Translation and cultural validation of clinical observational scales - the Fugl-Meyer assessment for post stroke sensorimotor function in Colombian Spanish. *Disabil. Rehabil.* 41, 2317–2323. doi: 10.1080/09638288.2018.1464604

- Broderick, J. P., Adeoye, O., and Elm, J. (2017). Evolution of the modified rankin scale and its use in future stroke trials. *Stroke* 48, 2007–2012. doi: 10.1161/STROKEAHA.117.017866
- Chen, Y., Abel, K. T., Janecsek, J. T., Chen, Y., Zheng, K., and Cramer, S. C. (2019). Home-based technologies for stroke rehabilitation: a systematic review. *Int. J. Med. Inform.* 123, 11–22. doi: 10.1016/j.ijmedinf.2018.12.001
- Cramer, S. C., Dodakian, L., Le, V., See, J., Augsburg, R., McKenzie, A., et al. (2019). Efficacy of home-based telerehabilitation vs in-clinic therapy for adults after stroke: a randomized clinical trial. *JAMA Neurol.* 76, 1079–1087. doi: 10.1001/JAMANEUROL.2019.1604
- Guillén-Climent, S., Garzo, A., Muñoz-Alcaraz, M. N., Casado-Adam, P., Arcas-Ruiz-Ruano, J., Mejías-Ruiz, M., et al. (2021). A usability study in patients with stroke using MERLIN, a robotic system based on serious games for upper limb rehabilitation in the home setting. *J. Neuroeng. Rehabil.* 18, 41. doi: 10.1186/S12984-021-00837-Z
- Haggag, H., and Hodgson, C. (2022). Clinimetrics: Modified Rankin Scale (mRS). *J. Physiother.* 68, 281. doi: 10.1016/j.jphys.2022.05.017
- Jenkins, W. M., and Merzenich, M. M. (1987). Reorganization of neocortical representations after brain injury: a neurophysiological model of the bases of recovery from stroke. *Prog. Brain Res.* 71, 249–266. doi: 10.1016/S0079-6123(08)61829-4
- Kasner, S. E. (2006). Clinical interpretation and use of stroke scales. *Lancet Neurol.* 5, 603–612. doi: 10.1016/S1474-4422(06)70495-1
- Katan, M., and Luft, A. (2018). Global burden of stroke. *Semin. Neurol.* 38, 208–211. doi: 10.1055/S-0038-1649503
- Kwah, L. K., and Diong, J. (2014). National Institutes of Health Stroke Scale (NIHSS). *J. Physiother.* 60, 61. doi: 10.1016/j.jphys.2013.12.012
- Laver, K. E., Aday-Wakeling, Z., Crotty, M., Lannin, N. A., George, S., and Sherrington, C. (2020). Telerehabilitation services for stroke. *Cochrane Database Syst. Rev.* 1, CD010255. doi: 10.1002/14651858.CD010255.PUB3
- Li, L., Fu, Q., Tyson, S., Preston, N., and Weightman, A. (2022). A scoping review of design requirements for a home-based upper limb rehabilitation robot for stroke. *Top. Stroke Rehabil.* 29, 449–463. doi: 10.1080/10749357.2021.1943797/FORMAT/EPUB
- Maciejasz, P., Eschweiler, J., Gerlach-Hahn, K., Jansen-Troy, A., and Leonhardt, S. (2014). A survey on robotic devices for upper limb rehabilitation. *J. Neuroeng. Rehabil.* 11, 3. doi: 10.1186/1743-0003-11-3
- Masiero, S., and Carraro, E. (2008). Upper limb movements and cerebral plasticity in post-stroke rehabilitation. *Aging Clin. Exp. Res.* 20, 103–108. doi: 10.1007/BF03324755
- McConnell, A. C., Moiola, R. C., Brasil, F. L., Vallejo, M., Corne, D. W., Vargas, P. A., et al. (2017). Robotic devices and brain-machine interfaces for hand rehabilitation post-stroke. *J. Rehabil. Med.* 49, 449–460. doi: 10.2340/16501977-2229
- Nijenhuis, S. M., Prange, G. B., Amirabdollahian, F., Sale, P., Infarinato, F., Nasr, N., et al. (2015). Feasibility study into self-administered training at home using an arm and hand device with motivational gaming environment in chronic stroke. *J. Neuroeng. Rehabil.* 12, 89. doi: 10.1186/S12984-015-0080-Y
- Poli, P., Morone, G., Rosati, G., and Masiero, S. (2013). Robotic technologies and rehabilitation: new tools for stroke patients' therapy. *Biomed Res. Int.* 2013, 153872. doi: 10.1155/2013/153872
- Pollock, A., Baer, G., Campbell, P., Choo, P. L., Forster, A., Morris, J., et al. (2014). Physical rehabilitation approaches for the recovery of function and mobility following stroke. *Cochrane Database Syst. Rev.* 2014, CD001920. doi: 10.1002/14651858.CD001920.PUB3
- Popović, M. D., Kostić, M. D., Rodić, S. Z., and Konstantinović, L. M. (2014). Feedback-mediated upper extremities exercise: increasing patient motivation in poststroke rehabilitation. *Biomed. Res. Int.* 2014, 520374. doi: 10.1155/2014/520374
- Rech, K. D., Salazar, A. P., Marchese, R. R., Schifino, G., Cimolin, V., and Pagnussat, A. S. (2020). Fugl-Meyer assessment scores are related with kinematic measures in people with chronic hemiparesis after stroke. *J. Stroke Cerebrovasc. Dis.* 29, 104463. doi: 10.1016/j.jstrokecerebrovasdis.2019.104463
- Rodríguez-De-Pablo, C., Popović, M., Savić, A., Perry, J. C., Bellosa, A., Tomić, T. D., et al. (2016). Post-stroke robotic upper-limb telerehabilitation using serious games to increase patient motivation: First results from armassist system clinical trial. *Biorobot.* 12, 63–78. doi: 10.1007/978-3-319-26242-0_5/COVER
- Sale, P., Franceschini, M., Mazzoleni, S., Palma, E., Agosti, M., and Posteraro, F. (2014). Effects of upper limb robot-assisted therapy on motor recovery in subacute stroke patients. *J. Neuroeng. Rehabil.* 11, 104. doi: 10.1186/1743-0003-11-104
- Soriano, J. B., Abajobir, A. A., Abate, K. H., Abera, S. F., Agrawal, A., Ahmed, M. B., et al. (2017). Global, regional, and national deaths, prevalence, disability-adjusted life years, and years lived with disability for chronic obstructive pulmonary disease and asthma, 1990–2015: a systematic analysis for the Global Burden of Disease Study 2015. *Lancet Respir. Med.* 5, 691–706. doi: 10.1016/S2213-2600(17)30293-X
- Volpe, B. T., Krebs, H. I., Hogan, N., Edelstein, L., Diels, C., and Aisen, M. (2000). A novel approach to stroke rehabilitation: robot-aided sensorimotor stimulation. *Neurology* 54, 1938–1944. doi: 10.1212/WNL.54.10.1938
- Volpe, B. T., Lynch, D., Rykman-Berland, A., Ferraro, M., Galgano, M., Hogan, N., et al. (2008). Intensive sensorimotor arm training mediated by therapist or robot improves hemiparesis in patients with chronic stroke. *Neurorehabil. Neural Repair* 22, 305–310. doi: 10.1177/1545968307311102
- Wang, H., Naghavi, M., Allen, C., Barber, R. M., Carter, A., Casey, D. C., et al. (2016). Global, regional, and national life expectancy, all-cause mortality, and cause-specific mortality for 249 causes of death, 1980–2015: a systematic analysis for the Global Burden of Disease Study 2015. *Lancet* 388, 1459–1544. doi: 10.1016/S0140-6736(16)31012-1
- World Health Organization. (2022). *World Health Statistics 2022*. Available online at: <https://www.who.int/data/gho/publications/world-health-statistics> (accessed December 20, 2022).



OPEN ACCESS

EDITED BY

Emilio Trigili,
Sant'Anna School of Advanced Studies, Italy

REVIEWED BY

Federico Villagra,
Aberystwyth University, United Kingdom
Joana Figueiredo,
University of Minho, Portugal

*CORRESPONDENCE

Tina L. Y. Wu
✉ lee.wu@monash.edu
Dana Kulić
✉ dana.kulic@monash.edu

RECEIVED 19 December 2022

ACCEPTED 28 February 2023

PUBLISHED 23 March 2023

CITATION

Wu TLY, Murphy A, Chen C and Kulić D (2023)
Adaptive cueing strategy for gait modification:
A case study using auditory cues.
Front. Neurobot. 17:1127033.
doi: 10.3389/fnbot.2023.1127033

COPYRIGHT

© 2023 Wu, Murphy, Chen and Kulić. This is an open-access article distributed under the terms of the [Creative Commons Attribution License \(CC BY\)](#). The use, distribution or reproduction in other forums is permitted, provided the original author(s) and the copyright owner(s) are credited and that the original publication in this journal is cited, in accordance with accepted academic practice. No use, distribution or reproduction is permitted which does not comply with these terms.

Adaptive cueing strategy for gait modification: A case study using auditory cues

Tina L. Y. Wu^{1*}, Anna Murphy², Chao Chen³ and Dana Kulić^{1,3*}

¹Department of Electrical and Computer Systems Engineering, Monash University, Clayton, VIC, Australia, ²Clinical Research Centre for Movement Disorders and Gait, Monash Health, Cheltenham, VIC, Australia, ³Department of Mechanical and Aerospace Engineering, Monash University, Clayton, VIC, Australia

People with Parkinson's (PwP) experience gait impairments that can be improved through cue training, where visual, auditory, or haptic cues are provided to guide the walker's cadence or step length. There are two types of cueing strategies: open and closed-loop. Closed-loop cueing may be more effective in addressing habituation and cue dependency, but has to date been rarely validated with PwP. In this study, we adapt a human-in-the-loop framework to conduct preliminary analysis with four PwP. The closed-loop framework learns an individualized model of the walker's responsiveness to cues and generates an optimized cue based on the model. In this feasibility study, we determine whether participants in early stages of Parkinson's can respond to the novel cueing framework, and compare the performance of the framework to two alternative cueing strategies (fixed/proportional approaches) in changing the participant's cadence to two target cadences (speed up/slow down). The preliminary results show that the selection of the target cadence has an impact on the participant's gait performance. With the appropriate target, the framework and the fixed approaches perform similarly in slowing the participants' cadence. However, the proposed framework demonstrates better efficiency, explainability, and robustness across participants. Participants also have the highest retention rate in the absence of cues with the proposed framework. Finally, there is no clear benefit of using the proportional approach.

KEYWORDS

continuum care, wearable robotics, rehabilitation robotics, human-in-the-loop, Parkinson's disease

1. Introduction

Parkinson's Disease (PD) is a progressive neurological disorder that causes a decline in motor capabilities. In advanced stages of PD, a key symptom known as Freezing of Gait (FoG) impairs people's ability to initiate, sustain, and control gait patterns, which reduces their quality of life (Sweeney et al., 2019). Cueing training can be helpful in improving gait performance, where people can use visual, auditory, or haptic cues to guide them on where/when to step (Ginis et al., 2018; Sweeney et al., 2019), thereby reducing the frequency of freezing and improving the temporal and spatial gait parameters such as speed, step length, and cadence (Nieuwboer et al., 2007).

Two types of cueing strategies have been identified: open or closed-loop (Muthukrishnan et al., 2019). The open loop strategy provides cues in a fixed manner that do not change regardless of the person's response. The fixed nature of the cue can be the constancy (e.g., visual cues at fixed distance, auditory/haptic cues at fixed pace) or its presence (i.e., always

on). The effectiveness of open-loop strategy has been validated extensively in a variety of settings with PwP [e.g., home (Nieuwboer et al., 2007)/clinic (McCandless et al., 2016), short/long term (Lirani-Silva et al., 2019)], showing that open-loop strategies can be effective in improving gait parameters in PwP. However, key weaknesses of open-loop cueing include cue-dependency, where participants start to rely on cues, or habituation, where cues become less salient (and therefore less effective) as participants get used to the cues (Ginis et al., 2018).

Compared to open-loop, closed-loop strategies adjust cues based on the participant's real-time performance, which may address cue-dependency and habituation, and potentially provide greater gait and postural improvement (Mancini et al., 2018). Closed-loop cueing requires the participant's gait performance to be quantified, which can be measured using smartphones and/or wearable devices (e.g., Ginis et al., 2016; Chomiak et al., 2019). With the gait-monitoring capabilities, cues can be provided on-demand, only when symptoms of freezing occur (Ginis et al., 2016), or can be synchronized to each step (Mancini et al., 2018). However, many of these methods focus on the events leading up to the cue provision. There is a lack of adaptation to change the feedback based on the user's response. One example of cue adaptation is Zhang et al. (2020), where the speed of the cues is adjusted using a proportional-integral controller to minimize the difference between the user's walking speed and target speed. Our previous work proposed a human-in-the-loop (HIL) optimization strategy that models the participant's real-time response to cues (Wu et al., 2021). Recently, Zhang et al. (2022) developed a framework that can first estimate the user's maximum walking speed online, then uses reinforcement learning and fuzzy logic to adapt an intermediate, guiding speed to help the participant reach their maximum speed. While all the aforementioned adaptation strategies have been effective in changing healthy participants' gait performance, they have not yet been validated with PwP or other representative groups (Mancini et al., 2018).

We adapt the HIL framework and the study methodology originally evaluated with healthy participants in Wu et al. (2021) in this case study with PwP. In the HIL framework, a model of the person's response to cues is learned online using a Gaussian Process (GP). The GP model is then used in an optimization function to generate cues to improve gait performance. Compared to our previous work, this work evaluates adaptive cue generation for PwP and provides an analysis of the cue-selection mechanism. The study utilizes auditory cues due to the low development complexity (i.e., only needing a speaker, compared to visual/haptics cues that require other hardware). However, the framework generalizes to other cueing modalities. As a feasibility study, it is also important to determine whether PwP in the early stages of the disease can respond to cues.

Compared to the work by Zhang et al. (2022), the HIL framework can provide insights into the person's response to cues by explicitly modeling the response using GPs. The optimization framework guarantees that the selected cue is optimal and personalized given the person-specific cue response model. Finally, the HIL framework may allow for more practical clinical use, as the therapist would only need to select a target cadence, rather than defining the fuzzy rules that are needed for Zhang et al. (2022). The

target selection being grounded in clinical metrics and the ability for person-specific adaptation are also the advantage of the HIL framework over the PI controller approach in Zhang et al. (2020), as the controller gains do not have meaningful clinical associations and lack the ability to adapt to the user's real-time condition.

2. Materials and methods

2.1. Summary of proposed framework

The HIL framework consists of three subcomponents: estimating gait parameters online, learning the individualized cue-response model, and providing cues using an optimization function. The framework block diagram is presented in Figure 1A. An Inertial Measurement Unit (IMU) sensor is used to capture cadence as the main gait performance metric. Cadence in Hertz (Hz) is estimated using the canonical dynamical system (CDS) proposed by Petrič et al. (2011).

To learn the individualized cue-response model, a Gaussian Process (GP) is used to learn the relationship between the current cadence as a function of the past cadence and past cue frequency as shown in Equation (1).

$$\begin{aligned} \mathbf{X} &= [\hat{\omega}_{k-1}, c_{k-1}], \text{ for } k \in (0, 1, \dots, K-1) \\ \mathbf{Y} &= [\hat{\omega}_j], \text{ for } j \in (1, 2, \dots, K) \\ \mathbf{Y} &= f(\mathbf{X}) + \beta, \\ \text{where } f(\mathbf{X}) &\sim GP(m(\mathbf{X}), cov(\mathbf{X}, \mathbf{X}')) \end{aligned} \quad (1)$$

\mathbf{X} and \mathbf{Y} are the input-output data pairs of the GP, with a total of K number of pairs. $\hat{\omega}_k$ is the CDS estimate at the current sampling index k , which happens every four strides roughly at heel strike. \mathbf{Y} consists of $(\hat{\omega}_j, j \in [1, 2, \dots, K])$ is a vector of current cadence as the GP output data up to the current index k . \mathbf{X} consists of a vector of past cadences $(\hat{\omega}_{k-1})$ and past cues (c_{k-1}) up to index $k-1$, which are the GP input data. The GP has a mean function, $m(\mathbf{X})$, a covariance, $cov(\mathbf{X}, \mathbf{X}')$, and a constant basis β and is trained online and used to predict how the participant would respond to a given cue using Equation (2). This approach is inspired by previous works implementing the HIL framework for exoskeletons (e.g., Kim et al., 2017; Zhang et al., 2017).

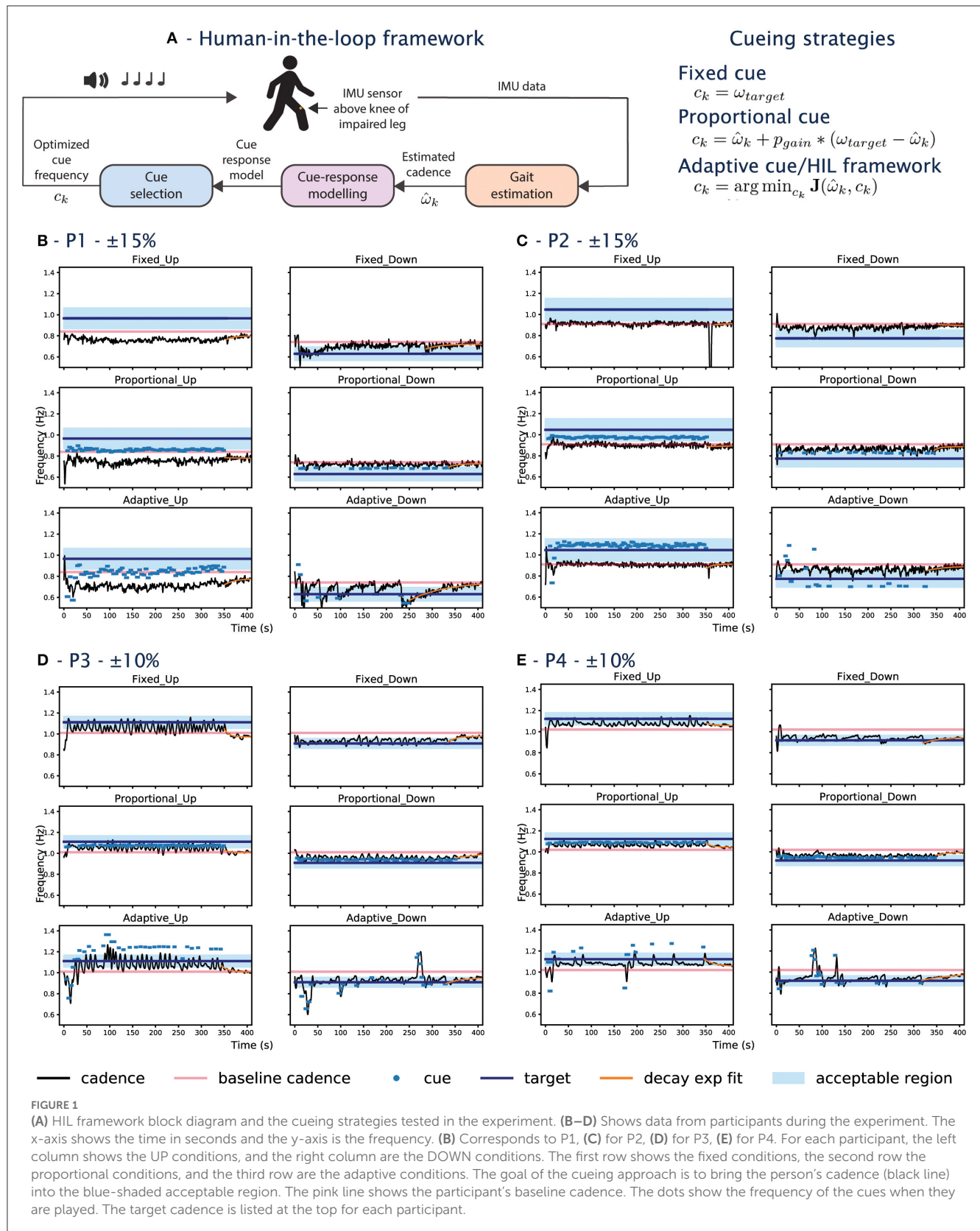
Finally, a cost function is minimized to provide feedback as shown in Equation (3) and subject to the constraints in Equation (4).

$$\hat{\omega}_{k+1}(\hat{\omega}_k, c_k) = f(\hat{\omega}_k, c_k) + \beta \quad (2)$$

$$\begin{aligned} J(\hat{\omega}_k, c_k) &= (\omega_{target} - \hat{\omega}_{k+1}(\hat{\omega}_k, c_k))^2 \\ c_k &= \arg \min_{c_k} J(\hat{\omega}_k, c_k), \text{ subject to} \end{aligned} \quad (3)$$

$$\max(-20\%\omega_k, -35\%\omega_{baseline}) \leq c_k \leq \min(+20\%\omega_k, +35\%\omega_{baseline}) \quad (4)$$

Where J is the cost function that minimizes the squared difference between the target cadence and the predicted cadence to provide feedback, c_k . The cost function is subject to the constraints in Eq 4, with bounds of $\pm 20\%$ of the current cadence and the ceiling/floor at $\pm 35\%$ of the person's baseline cadence ($\omega_{baseline}$).



The constraints for the cost function were reduced compared to our work in Wu et al. (2021). The constraint prevents the cues from changing to the theoretical maximum/minimum in one iteration

to prevent participants from needing to change their gait rapidly which may increase tripping risks. At runtime, the optimizer relies on the GP having learned the cue-response model, which requires

training samples. A random exploration is initiated at the start of the experiment for each participant to collect samples until the gradient can be estimated, which leads to two-phase behavior that we called the exploration and the converged phases. The GP is trained continuously regardless of the phase, but we analyze the performance of the framework with respect to these two phases, where the exploration is the first 70 seconds of the experiment, and the converged phase is as the GP prediction error becomes sufficiently low as shown in [Figure 3J](#).

2.2. Experimental conditions

2.2.1. Cueing strategies

The experiment compares three different cueing strategies: fixed, proportional, and adaptive. The fixed cue condition provides cues with frequency at the target cadence, representing the current state-of-the-art open-loop cueing strategy. In the proportional condition, cue frequency proportional to the error between the current cadence and the target cadence is provided. The proportional condition represents a one-size-fits-all closed-loop cueing strategy as a constant error gain is used for all participants. The error gain was set to 0.5, as determined empirically in [Wu et al. \(2021\)](#). Finally, the adaptive cue provides cues using the HIL framework described in Section , which allows personalized cues to be provided. A summary of the cueing strategies can be found in [Figure 1A](#).

2.2.2. Target cadence selection

As the PD participants of the current study do not experience gait impairment, the goal is to alter their baseline walking to a new cadence. This is similar to the usage of cues during FoG, where cues are used to guide the patient to a non-freezing pace. Two target cadences (i.e., UP/DOWN speed conditions) are set based on each participant's baseline cadence, $\omega_{baseline}$. In this study, the targets are $\pm 15\% \omega_{baseline}$ for the first two participants. We observe during the experiment that both participants were unable to respond to the $+15\%$ conditions and lower the targets to $\pm 10\% \omega_{baseline}$ for the next two participants. The targets have been used in previous studies (e.g., [Arias and Cudeiro, 2008](#); [Hoppe et al., 2020](#)). To account for natural variation in the walking and the gait estimation error, the target cadence constraint is relaxed to an acceptable boundary during implementation. This means cues would only play if the participant's cadence falls out of the boundary. The bounds are $\pm 10\% \omega_{target}$ for the first two participants with $\pm 15\% \omega_{baseline}$ as the target. The next two participants have the $\pm 10\% \omega_{baseline}$ as the targets with the bounds of $\pm 5\% \omega_{target}$. The acceptable boundary tightens for the later two participants to avoid the overlap with the baseline cadence. The change in acceptable boundary range enforces a minimum of 5% cadence change for all participants. The acceptable boundary check occurs every 4 strides, during which 8 beats are provided, to allow time for the participant to converge to the new cadence. The combination of targets and cueing approaches result in a total of 6 experimental conditions.

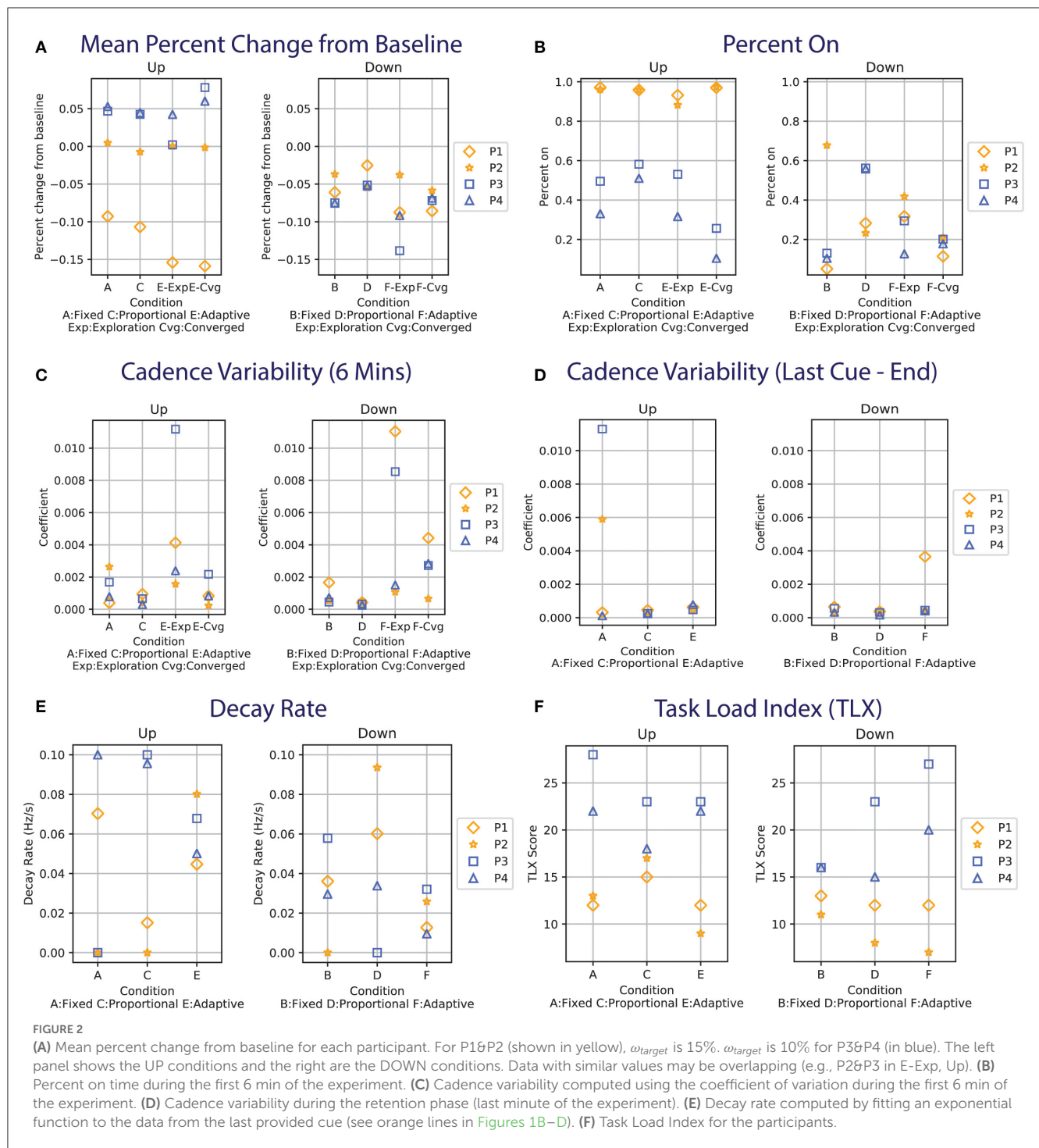
2.3. Participants

Four participants with PD were recruited by a clinician at the Movement Disorder Clinic, Kingston Center. Participants needed to have Hoehn and Yahr score¹ of less than or equal to two regardless of medication state to participate and have no hearing impairments/allergies to adhesives. The criterion excludes those who experience gait impairment based on the clinician's assessment (i.e., freezing of gait, tremor in the lower legs, may be at risk of falls) in this feasibility study. All participants were tested during their subjective medication-ON state (if they are on medication). The study (ID 22556) was approved by the Monash University Human Research Ethics Committee.

2.4. Protocol

Participants watched an introductory video at the start of the experiment. Participants provided consent once they had a chance to have their questions addressed. Different from the previous study, the IMU sensor was fixed onto what participants self-reported as the more disease-affected leg. A familiarization session was provided where participants practiced syncing to 88 beats per minute. Instructions were given to sync each step to a beat. Afterwards, participants were told walk at their comfortable and natural pace for 7 minutes to measure $\omega_{baseline}$. Participants filled in a demographic survey after the baseline measurement. The 6 experiment conditions were then provided in random order and blinded from the participants. During the experiment, cues were played based on the condition described in Section for the first 6 min (as per the standard 6-min Walk Test). No cues were played in the last minute of the condition to examine retention. Participants were instructed to sync their walking to cues to the best of their ability, but were not explicitly told to maintain the new cadence in the absence of beats. The researcher walked a few steps behind the participant throughout the experiment to provide support if needed. Participants were given breaks while they filled in a survey between experiments, which included filling in a NASA Task Load Index (TLX) and if/how the participants thought their gait changed during each experiment. The break was extended on demand to avoid fatigue. Once participants completed all experiment conditions, an exit interview was conducted to fill in a system usability scale (SUS) and gather information on the participant's qualitative experience, followed by a debrief session. The debrief explained the conditions of the experiment and the participants also had a chance to review their data in relation to the goal and the experimental conditions. The study took 1.5 hours to complete.

¹ Hoehn and Yahr score (HY) is a clinical scale that is used to classify the motor function of Parkinson's Disease. The scale rating goes from 1 to 5 and the progression in the HY score corresponds to more severe motor impairment ([Bhidayasiri and Tarsy, 2012](#)). Functionally, $HY \leq 2$ means participants can perform their daily routine independently or with minimal assistance.



2.5. Materials

The same setup in Wu et al. (2021) was used and summarized below. The motion data was recorded using an IMU sensor from the WaveTrack Inertial System at 285 Hz (Cometa Systems, Milan, IT) and streamed wirelessly into a custom C# program. The C# program ran on a laptop (Windows 10, i7 core with no GPU), which controlled the timing of the auditory cues played from a speaker (Phillips BT50A). The program also interfaced with MATLAB, where the Statistics and Machine Learning and Optimization

Toolboxes were used for the HIL framework. The GP was initialized with $X = [0, 0]$, $Y = [0]$ for each participant.

2.6. Analysis

No statistical analysis was conducted due to the small sample size. The analysis will focus on reporting the individual raw data and metrics, combined with the participant's subjective ratings.

3. Results

3.1. Demographics

Four participants enrolled in the study (2M/2F; age 70 ± 5 ; height 165.25 ± 12.1 ; weight 64.25 ± 16.31 ; years since diagnosis 3.5 ± 1.5). The participants' self-reported lower body symptoms are as follows, with the number of participants who reported in brackets: stiffness (1), slowed movement (2), trouble balancing (2), and dyskinesia (1). One participant does not experience any symptoms and others indicated that these symptoms rarely occur. All participants exercise 3+ times a week, with the most common exercise being walking (4), strength/resistance training (2), and stretching/balance training (2). No participant had prior experience with strategy training (i.e., visual cueing, audio cueing, haptic feedback, vibration therapy).

3.2. Cueing strategies comparison

3.2.1. Mean percent change from baseline

The mean percent change from the baseline (δ_{BL}) is shown in Figure 2A. This metric is an indicator of whether the approach is able to sustainably influence the person's cadence. We hypothesize that a positive percent change from baseline will be observed in the UP conditions and a negative percent change for the DOWN conditions. For instance, the δ_{BL} for P1&P2 (in yellow) would be close to +0.15 in the right panel and -0.15 in the left panel in Figure 2A. The comparison focuses on the converged adaptive cue after the model has been learned in the exploration phase.

In the UP conditions, P1's cadence does not reach +0.15 regardless of the cueing approach. The behavior can also be seen in the raw data, where the participant's cadence (black line) is always below the baseline cadence (pink line) for the UP conditions (left column) in Figure 2B. For the DOWN conditions, while the target of -0.15 was not reached for all approaches, the adaptive-DOWN condition showed the largest mean percent change from the target as seen in Figure 2A.

The cadence for P2 is similar to the baseline across all UP conditions (Figure 2A), even during the exploration phase of the adaptive condition where a series of random cues is provided. This is illustrated in Figure 1C, where the random cues are seen within the first 50 s of the adaptive approach (last row), but the participant's cadence tracks the baseline (i.e., the black line oscillates around the pink line). The largest change is seen around 350 s in the Fixed-UP condition in Figure 1C. The cadence dropped because it was the first condition and the participant paused walking when the cue stopped playing for the first time. The most significant change in δ_{BL} is in the adaptive-down condition, where P2 responded best to the slower cue provided in the adaptive condition compared to the fixed/proportional approach.

For P3&P4, the target is set to $\pm 10\%$, meaning the blue shapes in Figure 2A should ideally be close to +0.1/-0.1 for the right/left panel. The target was lowered for P3&P4 after observing that the first two participants were unable to reach the fast target. The adaptive approach for P3&P4 in both UP/DOWN conditions is comparable to the state-of-the-art fixed approach in terms of δ_{BL} .

In the UP condition, the converged adaptive approach achieves the highest mean percent change from baseline for P3 and P4, especially for P3 as the participant had the highest δ_{BL} among all conditions and all participants.

3.2.2. Percent on

The percent on metric examines the percentage of time the cue is provided in the first 6 min of the study, which is shown in Figure 2B. The metric is a measure of cue efficiency. The participant's cadence did not converge to the cues despite the constant presence of cues in the UP conditions for P1&2. For P3&4, the adaptive-UP condition requires the least percent on time to keep participants at the target boundary.

In the DOWN conditions, the converged adaptive condition (F-Cvg in Figure 2B) shows good performance across all participants. Despite the fixed-DOWN (Figure 2B) condition having the lowest percent on time among the three, it is ineffective for P2. The proportional cue has a similar percent on time between the UP/DOWN conditions for P3&4, but is drastically different between the UP/DOWN conditions for P1&2 (i.e., always on for UP, relatively low for DOWN).

3.2.3. Gait variability

The coefficient of variation of the participant's cadence is computed for the first 6 min of the experiment (Figure 2C) and during the retention phase from the last cue to the end (Figure 2D), following the definition in Lo et al. (2017). The variability is the highest during the adaptive condition exploration phase when cues with the largest variance are provided (see Figures 1B–E). The proportional approach has the lowest variability, as cues of similar frequencies are provided. In the fixed/converged-adaptive approaches, the variability is similar in the UP conditions, but the adaptive DOWN has a higher variability. This might be due to the adaptive approach undergoing a second exploration, which happened in both P3&4. P1's variability is also high in the adaptive down condition as the participant's cadence experience sharp changes (sudden dip in cadence when cues are provided, see Figure 1B).

During the retention phase when no cue was played, the cadence variability is generally low except for P3 in Fixed UP, P2 in Fixed UP, and P1 in Fixed DOWN. P3 had the highest variability as the participant's cadence varied from the UP target to a value lower than the baseline. P2 had a high variability in Fixed UP due to the participant stopping/starting as described in Section . While a manual offset is applied to skip the pause/start, the data should be considered an outlier. P1 in Adaptive DOWN also had high variability due to the larger variance around $t=350$ s. Overall, the variability is higher when cues are played, as participants actively change their cadence to match the cue. The variability is immediately decreased when there is no cue.

3.2.4. Decay rate

An exponential function of the form of $y = \alpha e^{-\eta x} + \gamma$ is fitted to the cadence data from the last provided cue to the end of the experiment to examine the rate at which participants settle to a

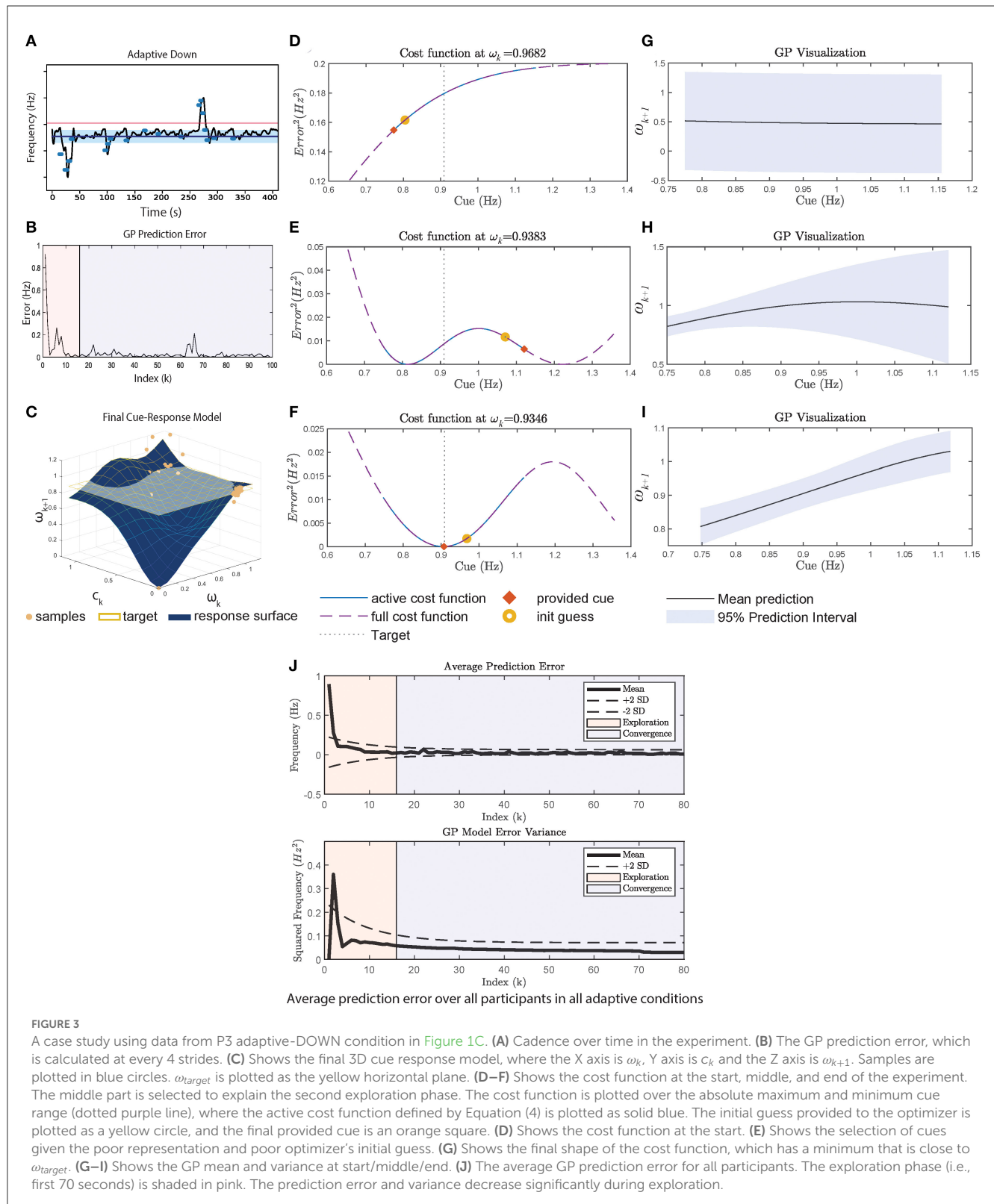


FIGURE 3

A case study using data from P3 adaptive-DOWN condition in Figure 1C. (A) Cadence over time in the experiment. (B) The GP prediction error, which is calculated at every 4 strides. (C) Shows the final 3D cue response model, where the X axis is ω_k , Y axis is c_k and the Z axis is ω_{k+1} . Samples are plotted in blue circles. ω_{target} is plotted as the yellow horizontal plane. (D–F) Shows the cost function at the start, middle, and end of the experiment. The middle part is selected to explain the second exploration phase. The cost function is plotted over the absolute maximum and minimum cue range (dotted purple line), where the active cost function defined by Equation (4) is plotted as solid blue. The initial guess provided to the optimizer is plotted as a yellow circle, and the final provided cue is an orange square. (D) Shows the cost function at the start. (E) Shows the selection of cues given the poor representation and poor optimizer's initial guess. (F) Shows the final shape of the cost function, which has a minimum that is close to ω_{target} . (G–I) Shows the GP mean and variance at start/middle/end. (J) The average GP prediction error for all participants. The exploration phase (i.e., first 70 seconds) is shaded in pink. The prediction error and variance decrease significantly during exploration.

cadence in the absence of cue. The absolute value of the decay rate, η , is presented in Figure 2E. The function is plotted in orange in Figures 1B–E. Participants can settle back to their baseline cadence (e.g., P3, Proportional UP in Figure 1D), a faster cadence (e.g., P4, Adaptive UP in Figure 1E), or a slower cadence (e.g., P1, Adaptive

UP in Figure 1B). A higher value would indicate a faster settlement. A low value indicates a minimal change from the baseline or from a new cadence.

Overall, the decay rates for the fixed and proportional approaches in UP have a higher variance compared to the adaptive

condition. The results can be attributed to participants not being responsive to cues (e.g., P1&P2) or the fast pace being hard for participants to maintain (as the cadence for P3&4 both drop significantly once the cue is removed). There is no clear difference between the cueing approaches in the UP conditions. In the down condition, the adaptive approach on average has the lowest decay rate, as well as the lowest variance. Since participants are all able to slow down, the result suggests that participants are able to better maintain the new DOWN target using the adaptive approach. The proportional approach in the DOWN condition again had the largest variance and the fastest average decay rate.

3.3. Adaptive framework cue-selection mechanism: Strengths and limitations

The mechanism of the adaptive framework is discussed in this section with illustrations shown in Figure 3, considering the Adaptive-DOWN condition for P3, shown in Figure 3A. The condition is interesting as the framework undergoes 2 exploration periods (once at the start and once at $t \approx 260$ s).

The initial exploration phase lowers the prediction error as seen in Figure 3B, until reaching $t \approx 260$ s, $k \approx 60$ in B. GP undergoes another exploration period until the prediction error settles again. In the analysis, we visualize the cost function at each ω_k at $k = 5, 60, 94$ (index for start/second exploration/end) (Figures 3D–F) and the corresponding GP realization (Figures 3G–I).

At the start, the GP posterior mean prediction starts off flat across the range of cues as shown in Figure 3G. During this phase, the constraints defined in Equation (4) are in effect, causing cues at the maximum/minimum to be provided, as shown in Figure 3D.

Between 0 and 250 s in Figure 3A, cues with frequency of < 1 Hz are provided. Through repeated sampling, GP captures the participant's response and the prediction variance also decreases significantly between Figures 3G, H in the < 1 Hz region. This prediction variance remains large for cues > 1 Hz due to the lack of samples. This demonstrates a limitation of the random initial exploration technique as it does not adequately cover the state space, which results in a poor model in regions where there are insufficient samples. The large uncertainty and the optimizer's initial guess leads to the second exploration phase, where the upper range of the cue is explored, resulting in a cue at the upper bound to be provided.

The GP visualization toward the end of the session is plotted in Figure 3I. Once the GP model has low variance across the range of cues, the cost function minimum approaches $\omega_{target} = 0.9$ as seen in Figure 3F, since the participant is generally responsive to cues (i.e., able to walk at the pace of the cue). However, the participant does not synchronize exactly to the cue, so a cue slightly below the target is more effective. Similarly for the UP condition, the adaptive framework provides cues at a much higher pace than the fixed approach. In general, the minimum of the cost function represents the participant's best performance in relation to the target given that the GP has been adequately explored. The continuous learning ability of the adaptive framework may provide a mechanism to handle habituation as the framework can alter the cues based on the current user model. In addition, the explicit modeling of the user's

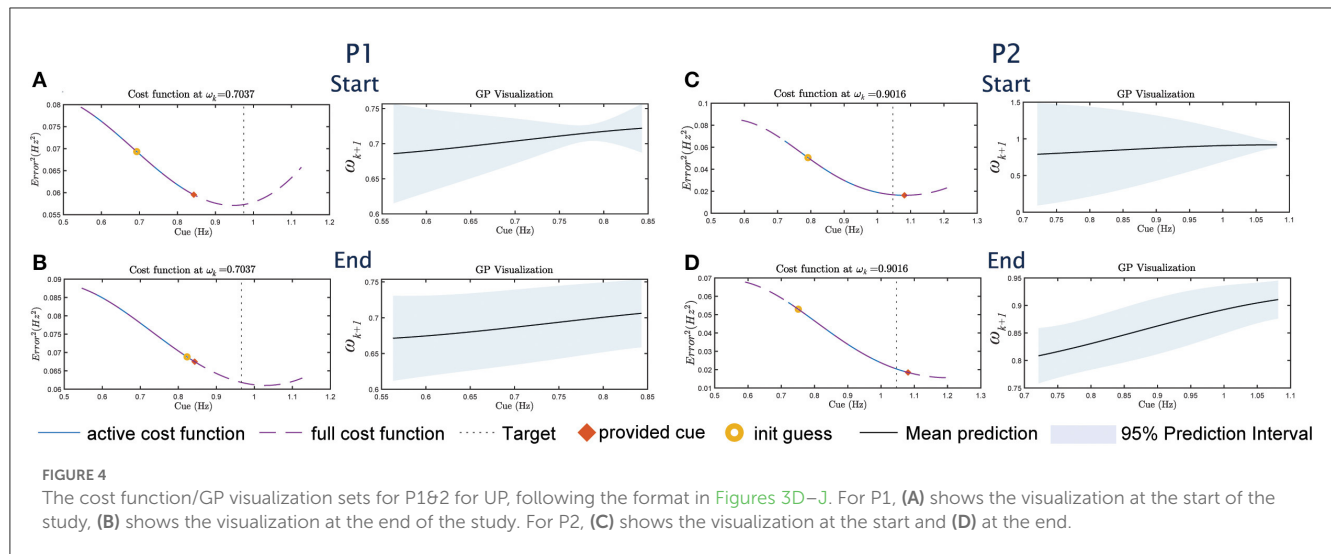
response to cues through GP may provide clinicians with insights about changes in the user's motor capability and users with better transparency and explainability. The final cue-response surface of P3 is plotted in Figure 3C.

3.4. Subjective rating and responses

The Task Load Index (TLX) is administered after each condition and the result is plotted in Figure 2F. Overall, P1&2 rated the mental workload for the experiment to be lower compared to P3&4. The UP and DOWN conditions have similar TLX scores (UP: 17.83 ± 1.4 , DOWN: 15 ± 1.75). The adaptive condition has the lowest mean in the UP condition despite P3&4 both experiencing two phases of rapid cue changes. The result is not due to practice effect. As stated by a participant in the post-study interview, cue synchronization "[becomes] like a game." In each post-condition survey, participants are asked whether their walking changed compared to normal (in the form of yes/no). Out of the 24 total experimental conditions across the 4 participants, there are 9 reports (37.5%) for no change in walking (2 Fixed-UP, 1 Fixed-DOWN, 4 Proportional-UP/DOWN, 2 Adaptive-UP). All participants answered "no" in at least one condition. All participants felt their gait changed in adaptive-DOWN (i.e., answered "yes"). PD participants reported no change at a much higher rate compared to the previous study with healthy participants ($19/150 = 12.7\%$ reported no change; the target is $\pm 20\%$). In the post-study interview, P1&2 both mentioned that they thought their natural cadence matched the UP targets, which was surprising given that these two participants failed to increase their cadence in response to any cue strategy. The overall cue-provision system scored an average of 78.75 ± 13.77 out of 100 on the system usability scale using the calculation detailed in Brooke (1996). Most participants found the system easy to use, would like to use the system frequently if they need it in the future but emphasize on the need for help during initial setup.

4. Discussion

In this experiment, we first evaluate whether participants can respond to the cue, especially when cues are not fixed. The results show that all three cueing approaches are able to influence the participants' cadences in the DOWN conditions. Specifically, the adaptive approach performs similarly to the benchmark fixed approach in slowing the cadence. The benefit of the adaptive approach is the efficiency and robustness across participants, meaning it does not cue the participants as frequently in the converged phase and works equally well across participants as seen by the low variance in the data. In addition, the adaptive approach in the DOWN cases has the best retention given by the lowest decay rate. The better retention could be attributed to the adaptive condition providing slower cues compared to the other two strategies, combined with the target being feasible to maintain. Clinically, the impaired ability to regulate step length could be the fundamental challenge in PD, which is compensated by the increase in cadence (Morris et al., 1994). In Morris et al. (1994), the authors observed improvement in stride length in the $-10\% \omega_{target}$ speed



condition. While later studies have also shown other metronome settings to be effective (e.g., Willems et al., 2006; Arias and Cudeiro, 2008 tested ranges from -70% to $+120\%$), the implication of the current study is that by successfully modulating the participant's cadence, the step length may be improved. Another clinical aspect examined is the cadence variability. While cues generally increase variability (typically associated with the increased risk of falls Lo et al., 2017), the variability is an intended study effect as participants need to actively change their pace. In addition, the variability decreases immediately in the absence of cues, which demonstrates the short-lasting effect in a single-session study.

As mentioned by Zhang et al. (2022), the target speed selection during gait rehabilitation is still an open research question. In our experiment, the performance of the cueing approaches was impacted by the selection of the initial target, as seen especially in the UP $+15\%\omega_{baseline}$ case for P1&2, where all three cueing strategies were unsuccessful in influencing the participants' cadences. When participants are not responsive to cues, the benefit of the adaptive approach is allowing a better understanding of the participant's response landscape. Overall, there is no clear benefit of the proportional approach based on the metrics of the study.

The GP model combined with the cost function results in the optimal selection of cue given the constraint in Equation (4). This is illustrated in Figure 4, where the provided cue (marked in red x) is the minimum within the constraint boundaries. However, the boundaries represent a trade-off between safety and convergence. By limiting the change in cue amplitude, participants do not need to rapidly change their cadence, which reduces the risk of tripping. However, the boundary prevents the global minimum from being selected (as illustrated by the dashed lines in Figure 4). Since P1&2 did not change their cadence during the experiment, the adaptive approach is therefore stuck within the boundary in Eq. 4. The convergence of the GP as indicated by the variance is also not as drastic as in Figure 3I for P3. Overall, in addition to the reliance on the GP model, the adaptive framework performance may also be influenced by the optimizer's initial guess (as seen in Figure 3E), and the boundary constraint.

The experiment task (i.e., walking and syncing to the beats) may have been challenging due to dual-task interference and impaired beat perception, particularly for P1&2. Parkinson's disease disrupts the basal ganglia (BG) function in the brain, which is involved in both motor and other cognitive functions. Particularly, BG is used to carry out automatic, learned movements such as walking (Wu et al., 2015). In therapy, cueing can be used to bring attention to the walking task and therefore bypass the automatic control for walking. However, when walking while listening to the beats, the attention may be split between walking and keeping track of the beats, which may result in decreased performance for both tasks (i.e., dual-task interference). In addition, Schwartz et al. (2011) has shown that BG damages can lead to poor beat perception. PD participants also experience difficulty in acquiring new motor skills (i.e., sync walking to beats) (Rochester et al., 2010; Wu et al., 2015) and therefore participants may need more time to execute the new skills (Ghai et al., 2018), which may explain why P1&2 were unable to match the UP targets compared to the DOWN targets.

Potential confounding variables include fatigue and learning effect. Multiple participants requested a longer break as the experiment progressed, potentially indicating fatigue. Despite these factors, no trend is found when ordering the main metrics of the study by the experimental order, meaning the participant's performance did not get better or worse over time. This finding is consistent with our previous study with healthy participants. The major limitations of this study are the small sample size and the lack of an age-matched control group, which we plan to address in the follow-up study. In addition, further research will need to be conducted to bridge the perception gap potentially with different cueing modalities.

Data availability statement

The raw data supporting the conclusions of this article will be made available by the authors, without undue reservation.

Ethics statement

The studies involving human participants were reviewed and approved by Monash University Human Research Ethics Committee (ID 22556). The patients/participants provided their written informed consent to participate in this study.

Author contributions

TW is responsible for conducting the studies, performing analysis, and writing the manuscript. AM is responsible for recruiting participants and providing clinical insights. CC is responsible for providing feedback on technical development. DK is responsible for overseeing the project and providing feedback on all components of the study and the manuscript. All authors contributed to the ideation of the study. All authors contributed to the article and approved the submitted version.

Funding

DK was supported by an Australian Research Council Future Fellowship (FT200100761).

References

- Arias, P., and Cudeiro, J. (2008). Effects of rhythmic sensory stimulation (auditory, visual) on gait in Parkinson's disease patients. *Exp. Brain Res.* 186, 589–601. doi: 10.1007/s00221-007-1263-y
- Bhidayasiri, R., and Tarsy, D. (2012). *Parkinsons Disease: Hoehn and Yahr Scale*. Totowa, NJ: Humana Press.
- Brooke, J. (1996). Sus-a quick and dirty usability scale. *Usability Evaluat. Ind.* 189, 4–7.
- Chomiak, T., Sidhu, A. S., Watts, A., Su, L., Graham, B., Wu, J., et al. (2019). Development and validation of ambulosono: a wearable sensor for bio-feedback rehabilitation training. *Sensors* 19, 686. doi: 10.3390/s19030686
- Ghai, S., Ghai, I., Schmitz, G., and Effenberg, A. O. (2018). Effect of rhythmic auditory cueing on parkinsonian gait: a systematic review and meta-analysis. *Sci. Rep.* 8, 1–19. doi: 10.1038/s41598-017-16232-5
- Ginis, P., Nackaerts, E., Nieuwboer, A., and Heremans, E. (2018). Cueing for people with Parkinson's disease with freezing of gait: a narrative review of the state-of-the-art and novel perspectives. *Ann. Phys. Rehabil. Med.* 61, 407–413. doi: 10.1016/j.rehab.2017.08.002
- Ginis, P., Nieuwboer, A., Dorfman, M., Ferrari, A., Gazit, E., Canning, C. G., et al. (2016). Feasibility and effects of home-based smartphone-delivered automated feedback training for gait in people with Parkinson's disease: a pilot randomized controlled trial. *Parkinsonism Related Disord.* 22, 28–34. doi: 10.1016/j.parkreldis.2015.11.004
- Hoppe, M., Chawla, G., Browner, N., and Lewek, M. D. (2020). The effects of metronome frequency differentially affects gait on a treadmill and overground in people with Parkinson disease. *Gait Posture* 79, 41–45. doi: 10.1016/j.gaitpost.2020.04.003
- Kim, M., Ding, Y., Malcolm, P., Speeckaert, J., Sivi, C. J., Walsh, C. J., et al. (2017). Human-in-the-loop bayesian optimization of wearable device parameters. *PLoS ONE* 12, 1–15. doi: 10.1371/journal.pone.0184054
- Lirani-Silva, E., Lord, S., Moat, D., Rochester, L., and Morris, R. (2019). Auditory cueing for gait impairment in persons with Parkinson disease: a pilot study of changes in response with disease progression. *J. Neurol. Phys. Therapy* 43, 50–55. doi: 10.1097/NPT.0000000000000250
- Lo, O.-Y., Halko, M. A., Zhou, J., Harrison, R., Lipsitz, L. A., and Manor, B. (2017). Gait speed and gait variability are associated with different functional brain networks. *Front. Aging Neurosci.* 9, 390. doi: 10.3389/fnagi.2017.00390
- Mancini, M., Smulders, K., Harker, G., Stuart, S., and Nutt, J. G. (2018). Assessment of the ability of open-and closed-loop cueing to improve turning and freezing in people with Parkinson's disease. *Sci. Rep.* 8, 1–9. doi: 10.1038/s41598-018-31156-4
- McCandless, P. J., Evans, B. J., Janssen, J., Selfe, J., Churchill, A., and Richards, J. (2016). Effect of three cueing devices for people with Parkinson's disease with gait initiation difficulties. *Gait Posture* 44, 7–11. doi: 10.1016/j.gaitpost.2015.11.006
- Morris, M. E., Iansek, R., Matyas, T. A., and Summers, J. J. (1994). The pathogenesis of gait hypokinesia in Parkinson's disease. *Brain* 117, 1169–1181. doi: 10.1093/brain/117.5.1169
- Muthukrishnan, N., Abbas, J. J., Shill, H. A., and Krishnamurthi, N. (2019). Cueing paradigms to improve gait and posture in Parkinson's disease: a narrative review. *Sensors* 19, 5468. doi: 10.3390/s19245468
- Nieuwboer, A., Kwakkel, G., Rochester, L., Jones, D., van Wegen, E., Willems, A. M., et al. (2007). Cueing training in the home improves gait-related mobility in Parkinson's disease: the rescue trial. *J. Neurol. Neurosurg. Psychiatry* 78, 134–140. doi: 10.1136/jnnp.200X.097923
- Petrič, T., Gams, A., Ijspeert, A. J., and Žlajpah, L. (2011). On-line frequency adaptation and movement imitation for rhythmic robotic tasks. *Int. J. Rob. Res.* 30, 1775–1788. doi: 10.1177/0278364911421511
- Rochester, L., Baker, K., Hetherington, V., Jones, D., Willems, A.-M., Kwakkel, G., et al. (2010). Evidence for motor learning in Parkinson's disease: acquisition, automaticity and retention of cued gait performance after training with external rhythmical cues. *Brain Res.* 1319, 103–111. doi: 10.1016/j.brainres.2010.01.001
- Schwartz, M., Keller, P. E., Patel, A. D., and Kotz, S. A. (2011). The impact of basal ganglia lesions on sensorimotor synchronization, spontaneous motor tempo, and the detection of tempo changes. *Behav. Brain Res.* 216, 685–691. doi: 10.1016/j.bbr.2010.09.015
- Sweeney, D., Quinlan, L. R., Browne, P., Richardson, M., Meskell, P., and ÓLaighin, G. (2019). A technological review of wearable cueing devices addressing freezing of gait in Parkinson's disease. *Sensors* 19, 1277. doi: 10.3390/s19061277
- Willems, A. M., Nieuwboer, A., Chavret, F., Desloovere, K., Dom, R., Rochester, L., et al. (2006). The use of rhythmic auditory cues to influence gait in patients with Parkinson's disease, the differential effect for freezers and non-freezers, an explorative study. *Disabil. Rehabil.* 28, 721–728. doi: 10.1080/09638280500386569
- Wu, T., Hallett, M., and Chan, P. (2015). Motor automaticity in Parkinson's disease. *Neurobiol. Dis.* 82, 226–234. doi: 10.1016/j.nbd.2015.06.014

Acknowledgments

We acknowledge the support of the Natural Sciences and Engineering Research Council of Canada (NSERC), Monash Institute of Medical Engineering (MIME), the Commonwealth Scientific and Industrial Research Organization (CSIRO), and Monash Partners. We also acknowledge the help from Fight Parkinson's and the support from the members of the community.

Conflict of interest

The authors declare that the research was conducted in the absence of any commercial or financial relationships that could be construed as a potential conflict of interest.

Publisher's note

All claims expressed in this article are solely those of the authors and do not necessarily represent those of their affiliated organizations, or those of the publisher, the editors and the reviewers. Any product that may be evaluated in this article, or claim that may be made by its manufacturer, is not guaranteed or endorsed by the publisher.

Wu, T. L., Murphy, A., Chen, C., and Kulić, D. (2021). Human-in-the-loop auditory cueing strategy for gait modification. *IEEE Rob. Autom. Lett.* 6, 3521–3528. doi: 10.1109/LRA.2021.3062580

Zhang, H., Li, S., Zhao, Q., Rao, A. K., Guo, Y., and Zanotto, D. (2022). Reinforcement learning-based adaptive biofeedback engine for overground walking speed training. *IEEE Rob. Autom. Lett.* 7, 8487–8494. doi: 10.1109/LRA.2022.3187616

Zhang, H., Yin, Y., Chen, Z., Zhang, Y., Rao, A. K., Guo, Y., et al. (2020). Wearable biofeedback system to induce desired walking speed in overground gait training. *Sensors* 20, 4002. doi: 10.3390/s20144002

Zhang, J., Fiers, P., Witte, K. A., Jackson, R. W., Poggensee, K. L., Atkeson, C. G., et al. (2017). Human-in-the-loop optimization of exoskeleton assistance during walking. *Science* 356, 1280–1284. doi: 10.1126/science.aal5054



OPEN ACCESS

EDITED BY

Emilio Trigili,
Sant'Anna School of Advanced Studies, Italy

REVIEWED BY

Mahdi Tavakoli,
University of Alberta, Canada
Nitin Sharma,
North Carolina State University, United States

*CORRESPONDENCE

Marcia K. O'Malley
✉ omalleym@rice.edu

RECEIVED 20 December 2022

ACCEPTED 06 March 2023

PUBLISHED 06 April 2023

CITATION

Dunkelberger N, Berning J, Scheerer EM and
O'Malley MK (2023) Hybrid FES-exoskeleton
control: Using MPC to distribute actuation for
elbow and wrist movements.
Front. Neurobot. 17:1127783.
doi: 10.3389/fnbot.2023.1127783

COPYRIGHT

© 2023 Dunkelberger, Berning, Scheerer and
O'Malley. This is an open-access article
distributed under the terms of the [Creative
Commons Attribution License \(CC BY\)](#). The use,
distribution or reproduction in other forums is
permitted, provided the original author(s) and
the copyright owner(s) are credited and that
the original publication in this journal is cited, in
accordance with accepted academic practice.
No use, distribution or reproduction is
permitted which does not comply with these
terms.

Hybrid FES-exoskeleton control: Using MPC to distribute actuation for elbow and wrist movements

Nathan Dunkelberger¹, Jeffrey Berning¹, Eric M. Scheerer² and
Marcia K. O'Malley^{1*}

¹Department of Mechanical Engineering, Mechatronics and Haptics Interfaces Laboratory, Rice
University, Houston, TX, United States, ²Center for Human Machine Systems, Department of Mechanical
Engineering, Cleveland State University, Cleveland, OH, United States

Introduction: Individuals who have suffered a cervical spinal cord injury prioritize the recovery of upper limb function for completing activities of daily living. Hybrid FES-exoskeleton systems have the potential to assist this population by providing a portable, powered, and wearable device; however, realization of this combination of technologies has been challenging. In particular, it has been difficult to show generalizability across motions, and to define optimal distribution of actuation, given the complex nature of the combined dynamic system.

Methods: In this paper, we present a hybrid controller using a model predictive control (MPC) formulation that combines the actuation of both an exoskeleton and an FES system. The MPC cost function is designed to distribute actuation on a single degree of freedom to favor FES control effort, reducing exoskeleton power consumption, while ensuring smooth movements along different trajectories. Our controller was tested with nine able-bodied participants using FES surface stimulation paired with an upper limb powered exoskeleton. The hybrid controller was compared to an exoskeleton alone controller, and we measured trajectory error and torque while moving the participant through two elbow flexion/extension trajectories, and separately through two wrist flexion/extension trajectories.

Results: The MPC-based hybrid controller showed a reduction in sum of squared torques by an average of 48.7 and 57.9% on the elbow flexion/extension and wrist flexion/extension joints respectively, with only small differences in tracking accuracy compared to the exoskeleton alone.

Discussion: To realize practical implementation of hybrid FES-exoskeleton systems, the control strategy requires translation to multi-DOF movements, achieving more consistent improvement across participants, and balancing control to more fully leverage the muscles' capabilities.

KEYWORDS

model predictive control (MPC), hybrid control (HC), functional electrical stimulation (FES), movement assistance, upper limb exoskeleton

1. Introduction

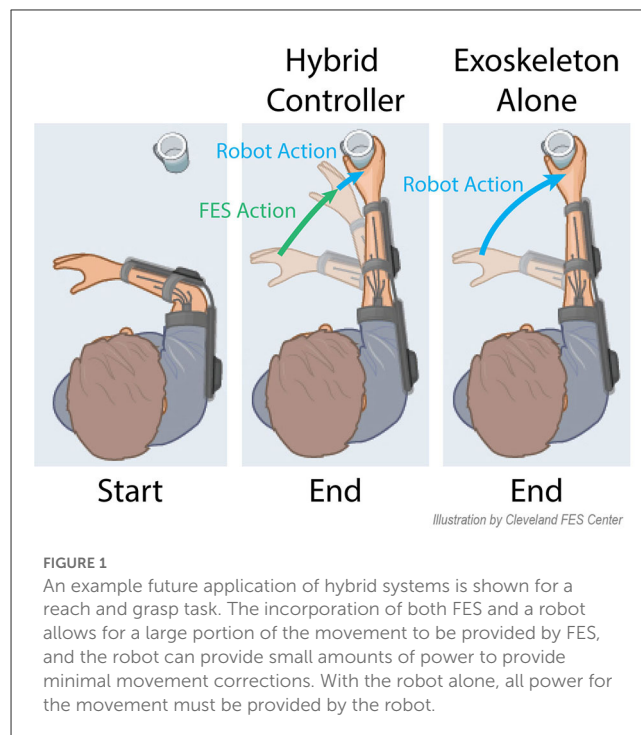
There are ~291,000 people in the United States living with spinal cord injuries, and the majority of these are cervical level injuries, resulting in tetraplegia (NSCISC, 2019). Injuries at such a high level of the spinal cord create severe arm and hand disabilities, resulting in an inability to complete Activities of Daily Living (ADLs). As a result, 71% of individuals with tetraplegia currently require assistance with ADLs (Collinger et al., 2013). Given this, it is not surprising that restoration of arm and hand function is a top priority among people with tetraplegia due to cervical spinal cord injuries (SCI) (Anderson, 2004). With scarce rehabilitation and assistive technology options, these individuals are largely dependent on full-time caregivers for feeding, grooming, and many other activities of daily

living. Regaining the ability to perform these tasks independently will reduce requirements on caregivers and increase opportunities for individuals to return to social participation in their communities, both of which are highly correlated to quality of life (Dijkers, 1997).

Recovery of arm and hand function through rehabilitation can be achieved for individuals with some residual muscle capability (Dietz et al., 2002; Beekhuizen and Field-Fote, 2005), and there are promising results that show that the same intensive robotic rehabilitation that has been successful for inducing plasticity and recovery following stroke (Reinkensmeyer et al., 2000; Charles et al., 2005; Lum et al., 2012; Blank et al., 2014) can be effective for SCI (Kadivar et al., 2012; Fitle et al., 2015; Francisco et al., 2017; Frullo et al., 2017; Yozbatiran and Francisco, 2019). For those *without* residual motor capability, however, or for those for whom rehabilitation interventions have not been able to restore functional movement, assistive technologies are a more viable option for replacing lost function. Such approaches incorporate mechanical devices that are attached to the limb and have the capability to move the limb or hand, or approaches that electrically stimulate the existing muscles, causing muscle contraction and inducing motion of the upper limb.

Functional electrical stimulation (FES) is a promising assistive technology to restore arm and hand function. By activating a person's own paralyzed muscles via surface electrodes placed on the skin or surgically implanted electrodes, limb movements can be generated. This approach requires very low energy consumption and exhibits high embodiment by the person; however, FES cannot produce sufficient torques to enable whole-arm reaching movements in people with tetraplegia, as many muscles are unresponsive to FES (Peckham et al., 1976; Mulcahey et al., 1999). Further, general multi-joint motions are notoriously hard to control with FES even with the most advanced systems (Ajiboye et al., 2017), often resulting in fine-tuned feed-forward implementations due to the physiological delays in muscle response to applied stimulation, and difficulty in accurately modeling the response to muscle activation. Augmenting FES with an assistive robot offers additional torque to support whole arm reaching while also offering improved movement accuracy, but this comes at the expense of increased bulkiness and decreased wearability of the combined FES-robotic system. An optimal combination of FES and an assistive robot would maximize the contribution of FES to minimize size and power requirements of the robot (Dunkelberger et al., 2020).

This combination of FES with robotic devices is starting to gain traction, and is termed hybrid FES-robot (or FES-exoskeleton) control. A conceptual representation of using FES with a robot is shown in Figure 1, where both robotic and FES action can complement each other to assist in the completion of activities of daily living. Many of the early approaches to bring this concept to reality did not truly combine and coordinate the actuation strategies for upper limb movements (Dunkelberger et al., 2020). Instead, each of the actuation types was used to achieve separate functions. For example, robotic devices have been used to lock degrees of freedom (Klauer et al., 2014; Ambrosini et al., 2017) or as gravity compensation (Cannella et al., 2016) enabling the muscles to relax and preventing fatigue. Other works have used robotic support devices to actuate one set of degrees of freedom, while FES



is used to actuate another set (Varoto et al., 2008; Schulz et al., 2011; Ajiboye et al., 2017). Typically the robot controls motions that need precision or require larger torques and forces to support, such as elbow flexion and extension, while FES is used for coarse movements, such as grasping. For upper limb motions with coupled degrees of freedom, such as shoulder, elbow, and wrist movements, these existing control strategies pit FES against a robot-imposed locked-joint, gravity, or single-joint motion constraint, essentially wasting the free actuation from FES and transferring it to the robot. Recently, single-joint hybrid systems that do share actuation on the same joint have been explored, but research has been limited, testing only in the elbow flexion extension joint with biceps electrodes in a minimum jerk trajectory (Wolf et al., 2017; Burchielli et al., 2022), or in simulation (Bardi et al., 2021).

In lower limb applications, more advanced hybrid control algorithms have been explored, largely enabled by the repetitive nature of gait motions (Bulea et al., 2014; del Ama et al., 2014; Ha et al., 2016). These lower limb hybrid systems often use a version of iterative learning control that takes advantage of the repetitive movements to fine-tune control over several cycles. Some recent research has begun to use model predictive control (MPC) algorithms, which can be more readily adapted to non-cyclic movements in the lower limbs (Kirsch et al., 2018; Bao et al., 2021), and which are more similar to the non-cyclic movements required of upper-limb movements. Results from these studies using MPC have shown the ability to follow a step reference trajectory and hold a position, and the algorithms should generalize to arbitrary trajectories.

A truly shared approach for hybrid FES and robotic control of upper limb reaching movements is needed to combine these techniques in a manner that achieves generalized upper limb movement assistance in an optimal manner. In this paper, we

present a model-based control approach to hybrid FES-exoskeleton control. Recent works have demonstrated the first steps toward this vision. Wolf and Scheerer (2022) demonstrated the use of model-based algorithms to power FES in combination with gravity compensation from a robot. Our group has also demonstrated shared control of elbow flexion and extension movements with FES and exoskeleton assistance acting in coordination to follow a desired trajectory (Dunkelberger et al., 2022b). In that work, we showed that a model-based controller for our upper limb exoskeleton, which has knowledge of the expected contributions of FES, requires significantly less robot torque than a standard PD control algorithm, with minimal loss in trajectory following accuracy. Here, we expand our initial demonstration along a number of fronts. First, we present an MPC algorithm that removes the integral term used previously and incorporates an additional proportional-integral-derivative (PID) controller acting in parallel, resulting in improved performance in both trajectory following and reduction in torque requirements from the exoskeleton compared to our initial controller. We incorporate a sophisticated model of the user's arm dynamics that accurately captures behavior across the exoskeleton workspace. We experimentally demonstrate the performance of the hybrid FES-exoskeleton controller in able-bodied participants completing two trajectories for two degrees-of-freedom of the exoskeleton (elbow flexion-extension and wrist flexion-extension), and we compare the performance of the hybrid controller to an exoskeleton-alone case, as illustrated in Figure 1. Finally, we examine longitudinal performance of the hybrid FES-exoskeleton control for a subset of participants to determine how performance changes 1 week after the initial experiment trials.

2. Materials and methods

2.1. Participants

Nine able-bodied participants (four female, avg age 22.9) participated in a single session of the experiment after providing informed consent. Three of the nine participants, who had experience with FES prior to the initial experimental session, also completed a second session of testing using the same protocol at least 1 week after their first experimental session. The study was approved by the institutional review boards at Rice University (IRB #FY2017-461) and Cleveland State University (IRB #30213-SCH-HS).

2.2. Procedure

The goal of this study is to develop a new hybrid controller that distributes actuation between an exoskeleton system and an FES system. The goal of such a controller is that it can reduce the power requirements in comparison to an exoskeleton alone system, which can lead to more portable devices in the future that can assist individuals with SCI in completing general activities of daily living. To test the effectiveness, the developed hybrid controller is used to provide movements on two different degrees of freedom (DOF), elbow flexion/extension, and wrist flexion/extension. To understand how this compares to available exoskeleton systems, the

resulting torque and position profiles for the hybrid controller are compared with an exoskeleton-alone controller in following two different trajectories.

2.3. Materials

The hybrid FES-exoskeleton system is comprised of two main subsystems that provide actuation. The first subsystem, which provides FES, is a transdermic electrical stimulation system (Trier et al., 2001) which provides eight output channels of bipolar stimulation. In this study, two channels are used for the elbow flexion/extension joint, and two channels are used for the wrist flexion/extension joint. To provide varying levels of output using the FES subsystem, the amplitude and frequencies are kept at a constant value for each channel, and the pulsewidth is varied.

The second subsystem is the robot, the MAHI Open Exoskeleton (Dunkelberger et al., 2022a). This robot provides four DOFs of movement support, namely elbow flexion/extension, forearm pronation/supination, wrist flexion/extension, and wrist radial/ulnar deviation, and each of these joints line up with the equivalent anatomical degree of freedom of a person using the exoskeleton. These will also be referred to by joint number throughout this paper, which are joints 1–4, respectively. The exoskeleton has an adjustable counterweight to account for varying arm masses, an adjustable slider to account for varying forearm lengths, and an adjustable shoulder abduction angle to keep the participant comfortable. The counterweight and forearm slider parameters are adjusted for each subject at the beginning of the experiment, and locked for the experiment duration. This shoulder abduction angle was kept at a value of 30° for all participants.

2.4. Methods

The study consists of several model characterization steps related to each of the subsystems, followed by experimental testing of the hybrid controller which makes use of these characterizations. First, the electrodes are placed in appropriate locations, and comfortable ranges of stimulation are found. Recruitment curves are characterized for each set of electrodes to define the relationship between commanded pulse width and muscle activation level. Gaussian process regression models are created to characterize torque output for each electrode based on the orientation of the upper-limb. The mass properties of the participant's arm are then characterized so that a combined dynamic model can be created for the arm-exoskeleton subsystem. The hybrid controller is created using the characterizations of each of the components. These characterization steps are more completely described in Sections 2.4.1–2.4.5. The hybrid controller is then compared against an exoskeleton alone controller in a scenario of following two trajectories for each DOF.

In this study, the elbow flexion/extension and wrist flexion/extension DOFs are tested independently. Each of the experimental steps is performed with the elbow flexion/extension joint and corresponding electrodes, followed by the wrist

flexion/extension joint with corresponding electrodes. The explanations that follow apply to both DOFs.

2.4.1. FES electrode placement

The experimental protocol began by placing the electrodes on the participants. Each of the electrode pairs were placed and tested one at a time. A set of electrodes was placed as agonist/antagonist pairs for each of the active degrees of freedom. This means for the elbow flexion/extension joint, one set of electrodes was placed to target elbow flexion, and another set was placed to target elbow extension using two inch square electrodes. For the wrist flexion/extension joint, one set of electrodes was placed to target wrist flexion, and another set of electrodes was placed to target wrist extension using one inch round electrodes. Electrode placement locations for each of these movements were chosen based on pilot testing based on which locations could reliably provide the desired movement. These general chosen locations are shown in Figure 2.

For the elbow flexion electrode placement, a reference electrode was placed, and a Compex motor point pen was used to find a specific point that generates biceps contraction, and the second electrode was placed there. For the remaining electrodes, the pair of electrodes were placed in a nominal location, and the pulse width was increased slowly. The resulting movement with the participant's arm on a table was observed, and the electrodes were adjusted if the desired movement was not produced. The electrodes were then wrapped with medical bandage to ensure that the electrodes stayed in the original location.

2.4.2. Threshold identification

Once the electrodes have been placed, the minimum and maximum pulsewidth values that will be used for each participant need to be identified. The robot and arm were moved to a neutral configuration, and held there using independent PD controllers on all joints. For each electrode placed, the minimum value that produced a change in torque output in the PD controller is considered the minimum pulse width value, pw_{min} . The discomfort threshold is then found by increasing the pulsewidth until the participant verbally indicates their maximum value which is still comfortable. The maximum pulsewidth value used throughout the experiment, pw_{max} , is taken as a slight reduction from the discomfort threshold. A ramp from the pw_{min} to pw_{max} is then used to verify that the participant remains comfortable throughout the range, and that the pw_{min} is just below the threshold of providing torque output.

2.4.3. Recruitment curve characterization

With the thresholds defined, a mathematical representation between the pulsewidth range and muscle activation is found, defined as a recruitment curve. Previous research has shown that functional electrical stimulation produces a muscle recruitment curve in the form of a sigmoid (Durfee and MacLean, 1989). To characterize this recruitment curve, the robot is again moved to a neutral configuration, and held there using independent PD controllers on each joint. Each of the electrodes sequentially

performs four impulses at pw_{max} , followed by four linear ramps between pw_{min} and pw_{max} , as shown in Figure 3.

The ramp deconvolution method is used (Durfee and MacLean, 1989) with the input of pulsewidth values and the corresponding torques generated from the stimulation to generate smooth curves to be characterized. The sigmoid is then fitted using Equation 3 with free parameters of c_1 and c_2 , where pw^* and pw_{max}^* are defined as pulsewidths normalized so that a pw^* value of 0, corresponds a pw_{min} as defined in Equations 1, 2.

$$pw^* = pw - pw_{min} \quad (1)$$

$$pw_{max}^* = pw_{max} - pw_{min} \quad (2)$$

$$\alpha^* = \frac{c_1}{1 + e^{-c_2(pw^* - \frac{pw_{max}^*}{2})}} - \frac{c_1}{1 + e^{\frac{c_2 pw_{max}^*}{2}}} \quad (3)$$

$$\alpha = \frac{\alpha^*}{c_1} \quad (4)$$

This equation results in a sigmoid with a minimum value of 0 and a maximum value of c_1 . The term c_2 is related to the slope of the function as it crosses the midpoint. To turn this characterization into the standard definition of a recruitment curve which varies from 0 to 1, α^* is divided by c_1 to arrive at an equation for activation, α .

2.4.4. Gaussian process regression model creation

The last component needed to mathematically represent the FES subsystem is a representation of the torque output based on the arm joint configuration of the participant. A Gaussian Process Regression (GPR) model is used to characterize this relationship torque when each of the FES electrode pairs is at a maximum activation as a function of the arm configuration. In this case, the black-box representation of the GPR models also implicitly capture some of the complex muscle dynamics. For each of the degrees of freedom, eight evenly spaced positions are taken between the minimum and maximum values that each joint will see throughout the experiment. At each of these positions, PD controllers on each of the individual robot DOFs are used to keep the robot at the desired position. The exoskeleton torque required to hold the pose when no muscles are stimulated is recorded as $\tau_{passive}$. One electrode is increased to its maximum activation, and the exoskeleton torque required to hold that pose is recorded as τ_{hold} . We consider the difference between the two values as the torque produced by the electrode τ_{record} .

$$\tau_{record} = \tau_{hold} - \tau_{passive} \quad (5)$$

The position tested and τ_{record} at that position are saved as training data for the tested electrode. This is repeated for the other electrode active for the current DOF, and at each of the other positions, three times in a randomized order. The collected training points are then used to generate a GPR model for each electrode using Matlab's `fitrmp` function. An example of trained GPR models for elbow flexion/extension torque output resulting

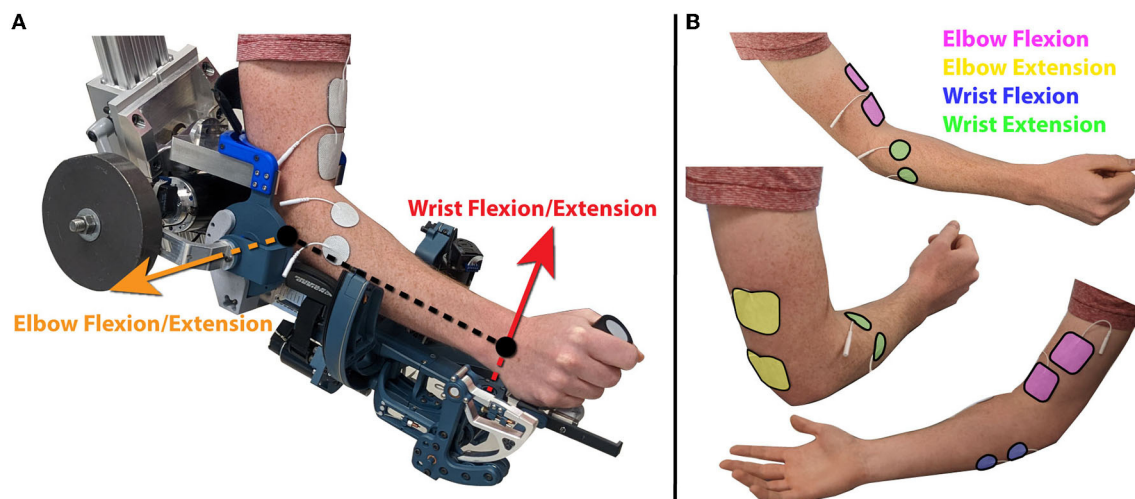


FIGURE 2 (A) A participant with their arm in the robot in the experimental setup, with the axes of rotation for the active joints indicated by orange and red arrows for the elbow flexion/extension and wrist flexion/extension joints respectively. (B) Placement of each of the four sets of electrodes. Electrodes were placed over the biceps for elbow flexion over the triceps for elbow extension. Electrodes were placed on the flexor carpi ulnaris for wrist flexion, and extensor carpi radialis longis and extensor carpi ulnaris muscles for wrist extension.

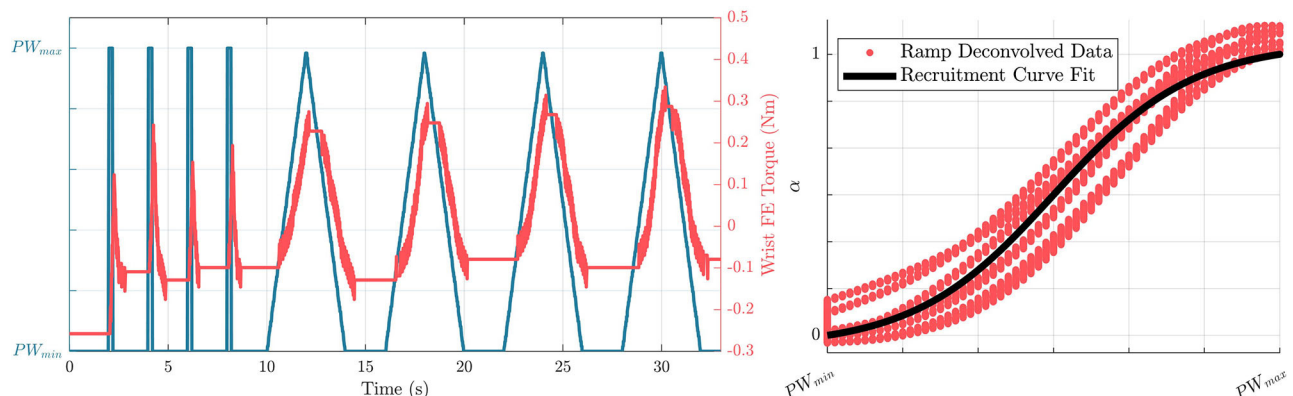


FIGURE 3 (Left) Profiles of commanded pulsewidths, and resulting torque outputs due to stimulation from the wrist extension electrode in the recruitment curve characterization process. (Right) Resulting characterized recruitment curve in the form of a sigmoid based on the ramp deconvolved data.

from the elbow flexion and elbow extension electrodes for a single subject is shown in Figure 4. This results in the following equation

$$\tau_{fes} = P(q)\alpha \quad (6)$$

where $P(q) \in \mathbb{R}^{1 \times 2}$ and where column i is an individual GPR model that provides an estimated output torque when electrode set i is at maximum stimulation, and the robot is at position q . Recall that this is implemented for each joint separately, so there is one $P(q)$ that corresponds to the elbow flexion/extension joint and uses the elbow flexion/extension position as an input, and one $P(q)$ that corresponds to the wrist flexion/extension joint and used the wrist flexion/extension position as an input.

2.4.5. Arm model characterization

An accurate model of the dynamic system is needed for effective MPC implementation. Previous work has developed a model of the exoskeleton without an arm (Dunkelberger et al., 2022a). In this study, an optimization problem was solved to find an estimate of dynamic properties for the arm to be used with the exoskeleton dynamic model, including masses, moments of inertia, and friction components.

To add these dynamic properties of the arm to the dynamic model of the exoskeleton, each joint in the arm was assumed to be a rigid body rigidly connected to the corresponding joint on the exoskeleton. With this assumption, the mass of each arm joint can be added to the mass of the robot joint, and the inertia of each arm joint can be combined with the inertia of each robot joint using the parallel axis theorem. While this study mainly focuses on the impact on the elbow flexion/extension and wrist flexion/extension

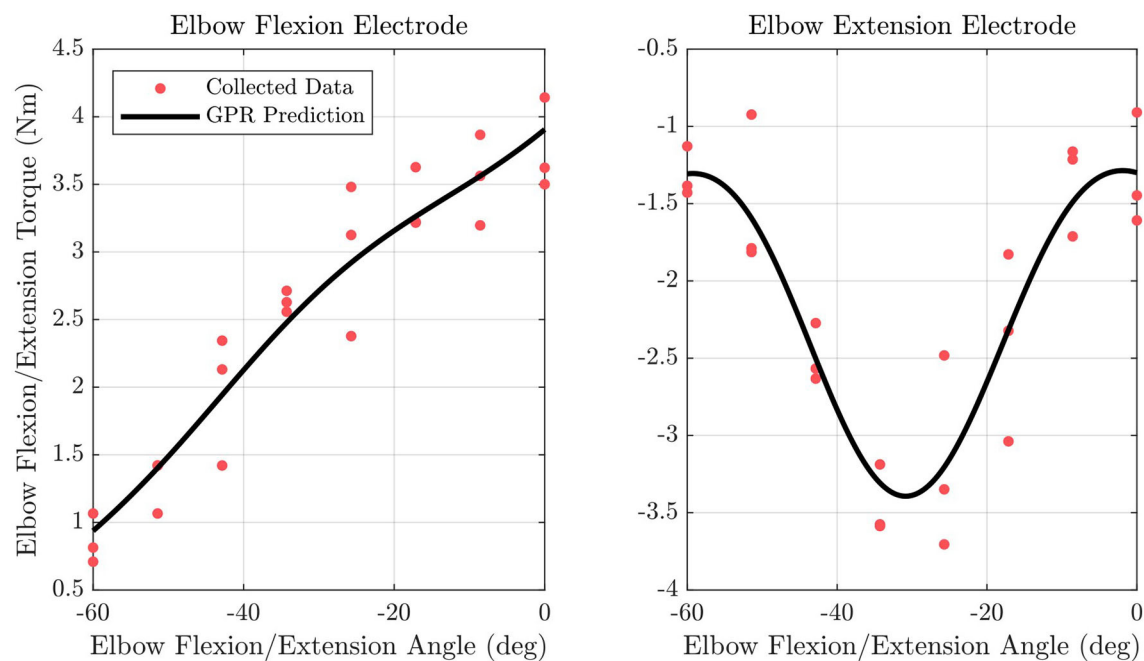


FIGURE 4

Fitted GPR models are shown along with data points used to fit the model for the elbow flexion/extension joint for the elbow flexion and elbow extension electrode.

joints, this arm characterization process utilizes all four joints of the exoskeleton to create a full dynamic model as shown in Equation 7, which can then be reduced to the single-joint components for the controller.

$$\tau = M(\mathbf{q})\ddot{\mathbf{q}} + \mathbf{V}(\mathbf{q}, \dot{\mathbf{q}}) + \mathbf{G}(\mathbf{q}) + \mathbf{F}_f(\dot{\mathbf{q}}) \quad (7)$$

In Equation 7, $\tau \in \mathbb{R}^{4 \times 1}$ is a vector consisting of the torques at each joint. $M \in \mathbb{R}^{4 \times 4}$ is known as the mass matrix and consists of different combinations of the mass and inertial terms of each joint. $\mathbf{V} \in \mathbb{R}^{4 \times 1}$ is the vector of centrifugal and Coriolis terms. $\mathbf{G} \in \mathbb{R}^{4 \times 1}$ is the gravity vector and gives the affects of gravity on each joint, and $\mathbf{F}_f \in \mathbb{R}^{4 \times 1}$ gives friction on each joint. \mathbf{q} is a vector of all joint positions, $\dot{\mathbf{q}}$ is a vector of all joint velocities, and $\ddot{\mathbf{q}}$ is a vector of all joint accelerations. M , \mathbf{V} , \mathbf{G} , and \mathbf{F}_f were calculated using the same methods as previous work (Dunkelberger et al., 2022a), but with the combined arm and robot properties serving as lumped parameters in the formulation.

Equation 7 can be used to characterize the unknown arm mass properties that appear in the equation, given experimentally recorded values for τ , \mathbf{q} , and $\dot{\mathbf{q}}$. To collect these data for characterization, the user's arm was placed inside the robot and secured. A chirp signal was used as a position reference for the wrist radial/ulnar deviation joint while the other three joints were commanded to remain stationary using independent PD controllers. This process was then repeated for each more proximal joint. The torque required to complete the motions and the resulting joint positions and velocities were recorded. The recorded

velocities were filtered, and a finite difference derivative was calculated to approximate the accelerations. With these values, the difference between the left side and right side of Equation 7, recorded and calculated torques respectively, could be found given a guess of mass properties. The difference between these two values at every time step is the error in the dynamic model, and this error was used as the optimization criteria to estimate the mass properties of the arm when combined with the mass properties of the exoskeleton found in previous work (Dunkelberger et al., 2022a).

To keep the number of optimization variables small, the problem was solved one joint at a time, starting with the most distal joint, wrist radial/ulnar deviation. This joint was the first to be optimized because for any given joint, only the more distal joints impact the current mass property analysis. Each more proximal joint was then optimized in order, ending with the elbow flexion/extension joint. At each joint, the inertia about the axis of rotation and the distances to the center of mass in the other two axes were optimization variables. When running the optimization on any joint except wrist radial/ulnar deviation, the next distal joint's distance to the center of mass along the distal joint's axis of rotation was also included as an optimization variable. This was added because this value does not appear in the calculations for the joint moving, but does impact the more proximal joints. Lastly, two optimization variables were added to each joint corresponding to the joint kinetic and viscous friction, which were considered to be added to the coefficients previously characterized for the exoskeleton by itself. A constant mass was assumed for each joint because the mass only appears multiplied by the distance to the center of mass terms. The

TABLE 1 Holding position of inactive joints throughout testing.

Active joint	q_{hold_1}	q_{hold_2}	q_{hold_3}	q_{hold_4}
Elbow F/E	N/A	0°	0°	0°
Wrist F/E	-30°	-30°	N/A	0°

formulation of this optimization problem can be seen in Equations 8, 9.

$$\arg \min_{\mathbf{p}_d} e_d = \sum_{t=1}^M (\tau_{calc_d_t} - \tau_{meas_d_t})^2 \quad (8)$$

$$\mathbf{p}_d = \begin{cases} [I_{czz_d}, r_{cx_d}, r_{cy_d}, r_{cx_d+1}, F_{k_d}, B_d] & \text{if } 1 \leq d \leq 3 \\ [I_{czz_d}, r_{cx_d}, r_{cy_d}, F_{k_d}, B_d] & \text{if } d = 4 \end{cases} \quad (9)$$

In these equations, \mathbf{p}_d represents the vector of parameters for a given joint, d . A d of 1 represents the elbow flexion/extension joint and $d = 4$ being the wrist radial ulnar/deviation joint, e_d refers to the torque error between the calculated torque, τ_{calc} , and measured torque, τ_{meas} , t represents a given time step up to M total time steps, I_{czz} is the moment of inertia about the axis of rotation taken about the center of mass, and r_{cx} , r_{cy} , and r_{cz} represent the distance from the axis of rotation to the center of mass in the x , y , and z directions respectively.

The optimization problem was solved using `fmincon` in Matlab, with initial guesses of zero for all optimization variables. The optimal properties found using this method were combined into the lumped arm and robot system used in the remainder of this study.

2.5. Hybrid controller design

We first present the full four-DOF dynamics for the FES-exoskeleton hybrid system, which we will then reduce to the single-DOF dynamics for the control formulation. This is similar to the dynamics of the robot and arm system in Equation 7, but the inputs to the system arise from both the exoskeleton and the FES system, so we separate the torque term into the two components.

$$\tau_{fes} + \tau_{exo} = M(\mathbf{q})\ddot{\mathbf{q}} + \mathbf{V}(\mathbf{q}, \dot{\mathbf{q}}) + \mathbf{G}(\mathbf{q}) + \mathbf{F}_f(\dot{\mathbf{q}}) \quad (10)$$

In this equation, $\tau_{exo} \in \mathbb{R}^{4 \times 1}$ and $\tau_{fes} \in \mathbb{R}^{4 \times 1}$ are torques supplied along each of the robot joints due to robot torque outputs, and torques provided by FES respectively.

As in the previous sections, the control problem will be described once, but the equations presented apply to either the elbow flexion/extension or the wrist flexion/extension DOF. To limit the full dynamics in Equation 10 to analyze a single DOF with the rest of the joints remaining stationary, all inactive joints can be constrained such that $q_j = q_{hold_j}$, $\dot{q}_j = 0$, $\ddot{q}_j = 0$ for all joints j that are inactive. Here, q_{hold_j} is the holding position of joint j when it is inactive, as shown in Table 1. This results with the following equation to describe the dynamics of a single DOF system, either in the elbow flexion/extension or wrist flexion/extension case.

$$P(q)\alpha + \tau_{exo_mpc} = m\ddot{q} + g \sin(q - q_{eq}) + f_f(\dot{q}) \quad (11)$$

For the DOF of interest, m represents the estimated lumped inertia, g represents the gravitational effects, f_f represents the friction effects, and q_{eq} represents the natural resting position of the combined arm-robot system for the DOF of interest. In Equation 11, and throughout the remainder of the paper, all variables that appear in equations are referring to a single DOF, and the values of these variables are different in the elbow flexion/extension DOF and the wrist flexion/extension DOF, but the symbolic expressions apply to both DOFs. For example, when this equation is applied to the elbow flexion/extension joint, q , \dot{q} , and \ddot{q} are the position, velocity, and acceleration of the robot elbow flexion/extension joint, and α is the vector $[\alpha_1, \alpha_2]^T$, which are the activation levels of the electrodes placed to induce elbow flexion, and elbow extension.

To develop our control problem, we define the following quantities as the system state, \mathbf{x} , system output, \mathbf{y} , and control input, \mathbf{u} , where C is the output matrix describing the variables we can observe.

$$\mathbf{x} = [q, \dot{q}]^T \quad (12)$$

$$C = I_2 \quad (13)$$

$$\mathbf{y} = C\mathbf{x} \quad (14)$$

$$\mathbf{u} = [\tau_{exo_mpc}, \alpha_1, \alpha_2]^T \quad (15)$$

To use standard analysis techniques, we would like to have our dynamics in the form of $\dot{\mathbf{x}} = f(\mathbf{x}, \mathbf{u})$, which by definition is the vector $[\dot{q}, \ddot{q}]^T$. By solving Equation 11 for \ddot{q} as follows, we can obtain an explicit definition for the representation of $f(\mathbf{x}, \mathbf{u})$.

$$\ddot{q} = \frac{1}{m}(P(q)\alpha + \tau_{exo_mpc} - g \sin(q - q_{eq}) - f_f(\dot{q})) \quad (16)$$

To implement real time control, it is beneficial to use a linearized form of the dynamics to reduce computation time. We can then convert the dynamics to a linearized form by calculating the Jacobian of the dynamics about time k with respect to the input and output. The following gives an estimate for the dynamic equations at time i , linearized at time k .

$$A_k = \left. \frac{\partial f}{\partial \mathbf{x}} \right|_{\mathbf{x}=\mathbf{x}_k, \mathbf{u}=\mathbf{u}_k} \quad (17)$$

$$B_k = \left. \frac{\partial f}{\partial \mathbf{u}} \right|_{\mathbf{x}=\mathbf{x}_k, \mathbf{u}=\mathbf{u}_k} \quad (18)$$

$$\dot{\hat{\mathbf{x}}}_i = A_k \hat{\mathbf{x}}_i + B_k \mathbf{u}_i + \dot{\mathbf{x}}|_{\mathbf{x}=\mathbf{x}_k, \mathbf{u}=\mathbf{u}_k} \quad (19)$$

These linearized dynamics are then used in the MPC formulation. The cost function is as follows, where i represents a discrete point in time in the standard MPC formulation.

$$J_i = (\mathbf{r}_i - \bar{\mathbf{y}}_i)^T Q (\mathbf{r}_i - \bar{\mathbf{y}}_i) + \Delta \mathbf{u}_i^T R \Delta \mathbf{u}_i + \mathbf{u}_i^T R_m \mathbf{u}_i \quad (20)$$

The matrices $Q \in \mathbb{R}^{2 \times 2}$, $R \in \mathbb{R}^{3 \times 3}$, and $R_m \in \mathbb{R}^{3 \times 3}$ are positive diagonal matrices used to weight predicted trajectory error, control input rate of change, and control input magnitude respectively.

In this equation, the control input rate of change at timestep i is defined as $\Delta u_i = u_i - u_{i-1}$. Initial values for these gains were chosen based on pilot studies that provided desired behavior as described below.

$$Q = \begin{bmatrix} Q_{pos} & 0 \\ 0 & Q_{vel} \end{bmatrix} \quad (21)$$

$$R = \begin{bmatrix} R_{exo} & 0 & 0 \\ 0 & R_{fes} & 0 \\ 0 & 0 & R_{fes} \end{bmatrix} \quad (22)$$

$$R_m = \begin{bmatrix} R_{m_exo} & 0 & 0 \\ 0 & R_{m_fes} & 0 \\ 0 & 0 & R_{m_fes} \end{bmatrix} \quad (23)$$

The general ideology behind the choice of gains in the hybrid controller is as follows. The gains for Q represent the importance for the controller to follow the desired trajectory, with higher gains indicating better tracking, but less stable behavior if there are model errors. The gains for R_m are chosen so that $R_{m_exo} \gg R_{m_fes}$, which is the main method by which the hybrid control strategy reduces exoskeleton torque compared to a strategy which only uses an exoskeleton. Additionally, these gains are chosen such that $(\bar{\mathbf{y}}_i - \mathbf{r}_i)^T Q (\bar{\mathbf{y}}_i - \mathbf{r}_i) \gg \mathbf{u}_i^T R_m \mathbf{u}_i$, so that trajectory accuracy is not sacrificed to allow for overall torque reduction. The gains for R are chosen so that $R_{fes} \gg R_{exo}$ so that the FES system, which has significant delay, remains stable by mainly responding with low-frequency changes in torque while the exoskeleton does mostly quick corrective actions. This combination of chosen gains for R and R_m are intended to have the general effect of the FES subsystem providing low frequency, high amplitude torque, allowing it to provide a bulk of the power requirement, yet maintain smooth motions despite the time delay. The exoskeleton subsystem provides high frequency, low amplitude torque, which provides necessary quick corrections without requiring too much power consumption. As a reminder, separate controllers are used for the elbow flexion/extension joint and for the wrist flexion/extension joint, and the gains for each of the two joints are created independently.

Because the R_{fes} and R_{m_fes} gains place costs on activation levels rather than FES torque outputs, in some cases, it was necessary to adjust these values for each participant upon initial testing with the hybrid controller to account for variations in torque productions for the same activation level. To account for this, when the hybrid controller was first tested in the experiment, these gains were increased by a factor of two from the original values if there was oscillatory behavior, or decreased by a factor of two if activation levels were lower than expected.

The final cost function used in the MPC implementation is as follows.

$$\arg \min_{\mathbf{u}(\cdot)} J_{tot} = \sum_{i=1}^N J_{k+i} \quad (24)$$

$$\text{subject to } \bar{\mathbf{y}}_{k+i+1} = \bar{\mathbf{y}}_{k+i} + \dot{\bar{\mathbf{x}}}_{k+i} T_s,$$

$$0 \leq \alpha_e \leq 1, e = \{1, 2\}$$

In Equation 24, k represents the current point in time, and future discretized timesteps at time $k + i$ are T_s seconds apart, for N time steps. The dynamics at these future time points are approximated using Euler integration as shown by the first constraint on the optimization problem, with the bars representing that these are estimated values. The second constraint restricts the activation level, α , of each electrode, e , to fall between 0 and 1. An additional constraint could be implemented to limit the maximum allowable exoskeleton torque; however, in this study, the torque required from the exoskeleton always remained below the maximum allowable torque, which meant that this constraint did not need to be implemented. The result of the optimization is $\mathbf{u}(\cdot)$ which represents the optimal control inputs over the time prediction horizon, $u_{k+1}, u_{k+2}, \dots, u_{k+N}$.

This MPC formulation is created in C++ using the nonlinear optimization framework CasADi (Andersson et al., 2019). The solver for the dynamic problem is compiled into a dll file which can be loaded at runtime and interfaced with the Interior Point Solver, IPOPT (Wächter and Biegler, 2006), to solve the MPC problem. This MPC problem is solved as fast as possible in a separate thread, and each time a solution is found, the solution of the minimization, $\mathbf{u}(\cdot)$, is sent to the main thread, where those successive control solutions are used until the next solution is found. From \mathbf{u} , τ_{exo_mpc} is used directly, and α_1 and α_2 are converted to pulsewidth commands to send to the stimulator using Equation 4 which describes the recruitment curve.

To tune the gains for the MPC algorithm, Q and R were first tuned to achieve smooth movements and low tracking error, with R_m values kept at 0. Following this, the R_m gains were chosen to achieve meaningful reduction in the exoskeleton torque, while maintaining similar tracking accuracy. As R_m gains were tuned, Q and R were further adjusted as necessary.

To account for model error in the MPC formulation, a PID controller using only exoskeleton torque is implemented in parallel as shown in Figure 5. This has the effect of allowing the MPC portion to control most of the action, while still providing a high accuracy on the resulting trajectory tracking. The torque provided by the PID controller is defined as τ_{exo_fb} , and the gains for this controller were chosen in pilot testing to achieve between 1 and 1.5° RMS tracking error. In the tuning of this controller, the gains were slowly increased, and tuned only after fully tuning the MPC system independently, so that the controller dynamics achieved from the MPC algorithm were the driving component. This additional controller does not change the output applied by the FES subsystem, but the torque applied to the exoskeleton becomes

$$\tau_{exo_tot} = \tau_{exo_mpc} + \tau_{exo_fb} \quad (25)$$

To test the effectiveness of the hybrid controller design, it is compared against a purely exoskeleton controller, defined as the *exoskeleton alone* control case. In this test case, the same general structure is used with the MPC controller paired with a PID controller, but Equation 15 becomes

$$\mathbf{u} = [\tau_{exo}] \quad (26)$$

which results in R and R_m being single values rather than matrices.

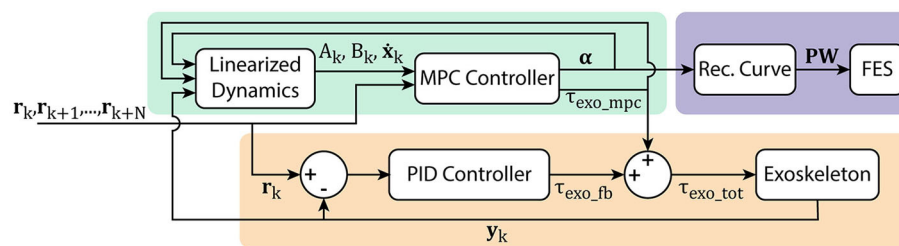


FIGURE 5

Hybrid FES-exoskeleton control block diagram, showing how the different components of the hybrid controller work together to provide torque commands to the robot and pulse width commands to the stimulator given a desired input trajectory.

2.6. Experimental validation

After a participant completed each of the model characterization steps and the MPC problem was generated, the experimental validation was conducted. Participants were assisted in completing two different trajectories in two different conditions, using the hybrid controller that combined the FES and exoskeleton action, and using the exoskeleton alone. The first trajectory is referred to as the *cup* trajectory, and it is based on a study that tracked healthy individuals' joint-level movements to move a cup to various target locations with differing grasps (Valevicius et al., 2019). The movement profile for each of the joints was taken independently and spaced so that it spanned a useful and comfortable trajectory space for the exoskeleton used in this study which was 30° flexed to 90° flexed from full extension for elbow flexion/extension and 15° extended to 45° flexed for wrist flexion/extension. The *cup* trajectory is useful to observe how the hybrid controller behaves when following natural motions that would be expected under normal use. The second trajectory is referred to as the *sinusoidal* trajectory, and it is an artificially created trajectory that is the summation of multiple sinusoidal waves at different amplitudes and frequencies. This trajectory was created to test the controllers' ability to generalize to different movements. The trajectories are relatively similar in terms of difficulty for the elbow flexion/extension joint, but the wrist flexion/extension joint movement is significantly easier in the *cup* trajectory than the *sinusoidal* trajectory. Both trajectories take 42.4 s to complete, which is four times the time it took an average able-bodied individual to complete the *cup* trajectory in Valevicius et al. (2019). A four times reduction was chosen because the original trajectory moved through the workspace very quickly, and this reduction empirically felt an appropriate length to safely perform movements with a human in the robot. Visualizations of these trajectories are shown in the results in Figures 8, 9.

Each DOF was tested for ten trials on the *cup* trajectory, split evenly between hybrid controller and exoskeleton alone controller, and 10 trials on the *sinusoidal* trajectory, also split evenly between hybrid controller and exoskeleton alone controller. While each DOF was being tested, all other DOFs were kept at their q_{hold} values as shown in Table 1 using independent PD controllers on those joints. Collection of the experimental data began by running four elbow flexion/extension trials, consisting of one of each possible combination of trajectory and controller type. This

was followed by four wrist flexion/extension trials, again consisting of each possible combination of trajectory and controller. This sequence was repeated until all 40 total trials had been collected. Throughout each of the trials, position of the active DOF, total exoskeleton torque commanded, and activation levels of electrodes were collected at a rate of 1 kHz using a Quanser Q8-USB data acquisition device.

Three of the nine participants repeated the entire protocol (including characterization steps) at least 1 week after they completed the first set of data collection. These data were collected to provide insight into whether results remain similar between sessions within the same participant, rather than only comparing between participants.

2.7. Data analysis

The primary objective of these experiments is to understand the extent to which exoskeleton power consumption can be reduced in a hybrid system compared to a exoskeleton alone system. We compare power consumption by taking the sum of the squared total exoskeleton torque throughout the trajectory for each of the conditions tested as shown in Equation 27, averaged across each of the five trials with that set of conditions. This value is labeled as τ_{ss_exo} for the exoskeleton alone control condition, and τ_{ss_hybrid} for the hybrid control condition. Because participants have different arm sizes, and require the robot to be in different configurations, it is expected that participants will require different amounts of sum of squared torque from the system to move through the *cup* and *sinusoidal* trajectories. To normalize the data to compare across subjects, the reduction in sum of squared torque in the hybrid control case compared to the exoskeleton alone control case is shown by Equation 28. This allows us to analyze the varying power consumption both between exoskeleton alone and hybrid controllers, as well as how the relative controller performance translates between two different trajectories.

$$\tau_{ss} = \sum_{i=1}^N \tau_{exo_tot}^2 \quad (27)$$

$$\%Imp = 100(1 - \frac{\tau_{ss_exo} - \tau_{ss_hybrid}}{\tau_{ss_exo}}) \quad (28)$$

In Equation 27, N is the number of data points collected. With this representation, a value of $\%Imp = 0$ would represent equal amounts of torque being used in both control cases, which would indicate no improvement, a value of $\%Imp > 0$ would indicate a reduction in power consumption using the hybrid controller with a value of $\%Imp = 100$ indicating no exoskeleton power was consumed, and a value of $\%Imp < 0$ would indicate that the hybrid controller required more exoskeleton power than the exoskeleton alone case. A paired t -test was performed to understand whether there was a statistically significant difference between in the sum of squared torque in the exoskeleton alone control case, and in the hybrid control case for each of the trajectories.

The secondary objective of these experiments is to understand how the tracking accuracy compares when using the two options for controllers. The RMS tracking error is calculated as

$$e_{rms} = \frac{\sum_{i=1}^N \sqrt{(y_i - r_i)^2}}{N} \quad (29)$$

A paired t -test was performed to understand whether there was a statistically significant difference between the RMS errors in the exoskeleton alone control case, and in the hybrid control case for each of the trajectories.

One subject was unable to get any detectable torque output from one of the electrodes on the wrist flexion/extension DOF, and therefore, did not complete data collection for that DOF. Because of this, there are nine sets of data analyzed for the elbow flexion/extension results, and eight sets of data analyzed for the wrist flexion/extension results.

3. Results

A summary of the sum of squared torque reduction findings is presented in Figure 6 as boxplots with individual subject data overlaid on top. These results show a mean sum of squared torque reduction of 48.8 and 48.6% for the *cup* and *sinusoidal* trajectories respectively for the elbow flexion/extension joint when comparing the hybrid controller to the exoskeleton alone controller. These values for individual participants spanned from 11.8 to 71.6% for the *cup* trajectory, and from 8.8 to 77.2% for the *sinusoidal* trajectory, with the lowest data point being an outlier. A mean sum of squared torque reduction of 59.3 and 56.5% was shown for the *cup* and *sinusoidal* trajectories respectively for the wrist flexion/extension joint when comparing the hybrid controller to the exoskeleton alone controller. These values for individual participants spanned from 33.4 to 82.9% for the *cup* trajectory, and from 39.3 to 79.0% for the *sinusoidal* trajectory. The statistical tests showed that the sum of squared torques were significantly lower in the hybrid control case compared to the exoskeleton alone control case in both DOFs and in both trajectories, with p -values being < 0.01 in both trajectories for the elbow flexion/extension joint, and p -values being < 0.001 in both trajectories for the wrist flexion/extension joint.

A summary of the trajectory tracking accuracy findings is presented in Figure 7 as box plots with individual subject data overlaid on top. For the elbow flexion/extension joint, mean RMS errors in the *cup* trajectory were 1.04 and 1.24° for the

exoskeleton alone and hybrid controllers respectively. RMS errors in the *sinusoidal* trajectory were 1.10 and 1.26° for the exoskeleton alone and hybrid controllers respectively. These results indicate that there is a mean increase of 0.18° in RMS error when using the hybrid controller compared to using the exo alone controller in the elbow flexion/extension joint. This difference was shown to be statistically significant in the paired t -test, with p -values for each of the trajectories < 0.01 .

For the wrist flexion/extension joint, RMS errors in the *cup* trajectory were 1.21 and 1.12° for the exoskeleton alone and hybrid controllers respectively. RMS errors in the *sinusoidal* trajectory were 1.53 and 1.48° for the exoskeleton alone and hybrid controllers respectively. These results indicate that there is a mean decrease of 0.07° in RMS error when using the hybrid controller compared to using the exoskeleton alone controller in the wrist flexion/extension joint. This difference was again shown to be statistically significant in the paired t -test, with p -values for each of the trajectories again remaining < 0.01 .

Figures 8, 9 show time series representations of torque profiles for the best performing subject (represented by the Δ symbol in Figures 6, 7) and movement profiles averaged across all subjects. In the representative plots of torque profiles, the exoskeleton torque used during the hybrid trials exhibits a smaller magnitude than the exoskeleton torque used during exoskeleton alone trials. This result shows that the hybrid controller is able to replace a significant amount of the torque requirement from the exoskeleton with FES torque. The plots for movement profiles demonstrate how well each of the controllers are able to track the trajectory. In all combinations of trajectories and DOFs, the trajectories almost entirely overlap each other, showing similar accuracy regardless of controller.

The reduction in maximum torque for the torque profile averaged across participants profiles across participants is also analyzed, for the hybrid controller compared to the exoskeleton alone controller. For this metric, it is interesting to observe both the change in maximum and minimum values, as many cable-driven systems would likely require one actuator for each agonist and antagonist pair. In the elbow flexion/extension DOF, the maximum torque was reduced by 44.2 and 43.7% in the *cup* and *sinusoidal* trajectories respectively, and the minimum torque for the mean profile was reduced by 31 and 27.1% for the *cup* and *sinusoidal* trajectories respectively. In the wrist flexion/extension DOF, the maximum torque was reduced by 67.1 and 65.3% in the *cup* and *sinusoidal* trajectories respectively, and the minimum torque for the mean profile was reduced by 36.9 and 36.6% for the *cup* and *sinusoidal* trajectories respectively.

4. Discussion

There is a need for devices to provide assistance in completing activities of daily living for individuals with SCI. For this population, return of upper-limb function is among their top priorities (Anderson, 2004). Both FES and exoskeletons provide some framework to assist with movement, but each of these technologies has fundamental limitations preventing meaningful assistance for the upper-limbs in activities of daily living. FES is unable to provide accurate and repeatable movements by itself, and using feedback control causes instability due to the inherent

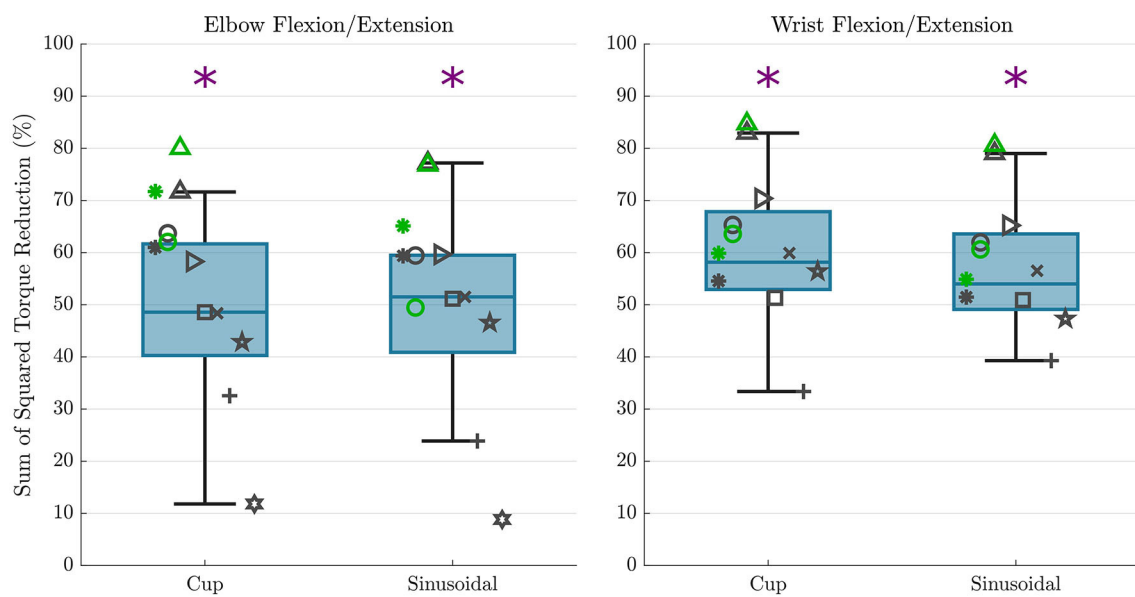


FIGURE 6

Sum of squared torque reduction results are shown for all subjects for each trajectory for the elbow flexion/extension DOF (**left**) and wrist flexion/extension DOF (**right**). The overlaid scatterplot shows individual subject results, with the same symbol representing a single subject across figures. Points in green show the repeated data collection for the first three subjects, but repeated data collection does not contribute to boxplot presentation. The purple "*" above the plots represents a that there was a statistically significant difference in the sum of squared torque between the hybrid and exoskeleton alone control cases.

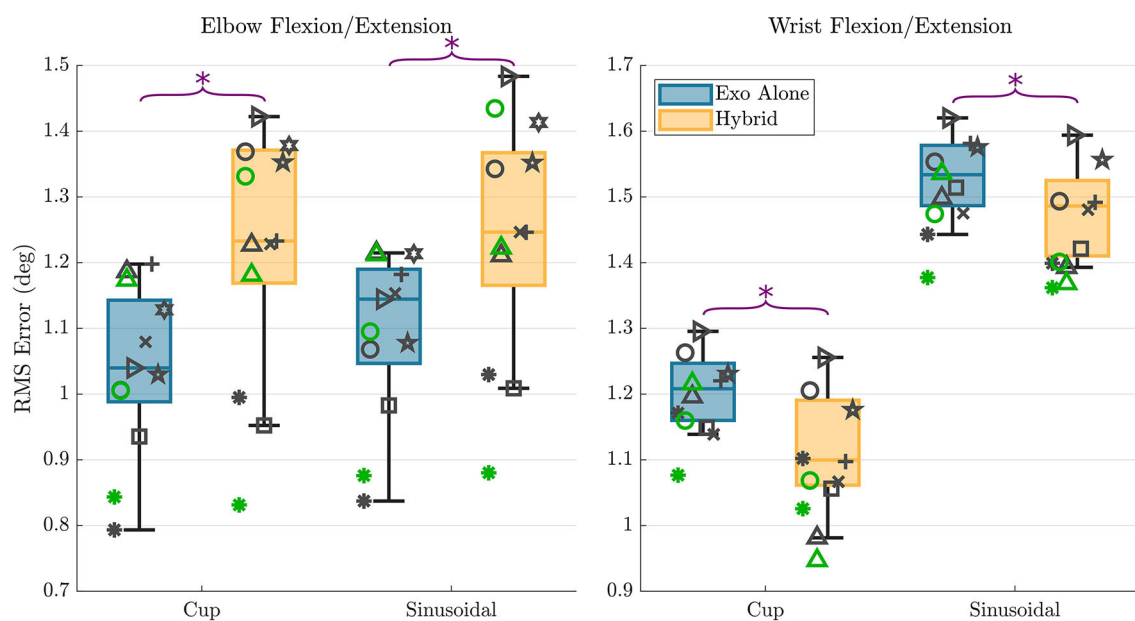


FIGURE 7

RMS error results are shown for all subjects for each trajectory and each controller type for the elbow flexion/extension DOF (**left**) and wrist flexion/extension DOF (**right**). The overlaid scatterplot shows individual subject results, with the same symbol representing a single subject across figures. Points in green show the repeated data collection for the first three subjects. The purple "*" above the plots represents a that there was a statistically significant difference in the RMS errors between the two control types.

time delays in muscle response to stimulation. Exoskeletons are able to provide accurate and repeatable movements, but require bulky systems and large amounts of power to support upper-limb movements against gravity. In this paper, we have

proposed a hybrid FES-exoskeleton controller that combines the two technologies, with the goal of reducing power consumption compared to a robot alone, and providing accurate movement, similar to that of an exoskeleton alone. This controller uses the

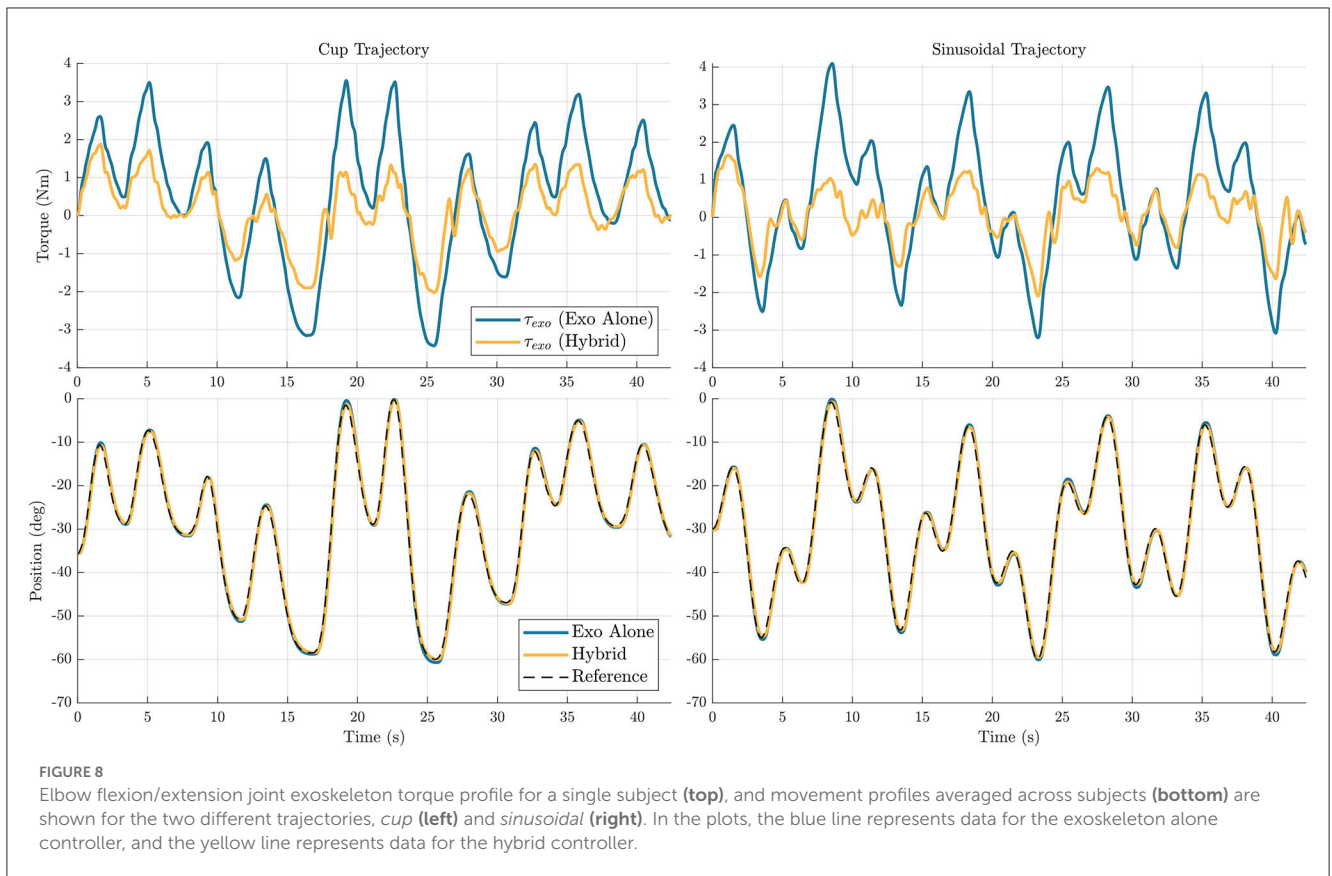


FIGURE 8

Elbow flexion/extension joint exoskeleton torque profile for a single subject (**top**), and movement profiles averaged across subjects (**bottom**) are shown for the two different trajectories, *cup* (**left**) and *sinusoidal* (**right**). In the plots, the blue line represents data for the exoskeleton alone controller, and the yellow line represents data for the hybrid controller.

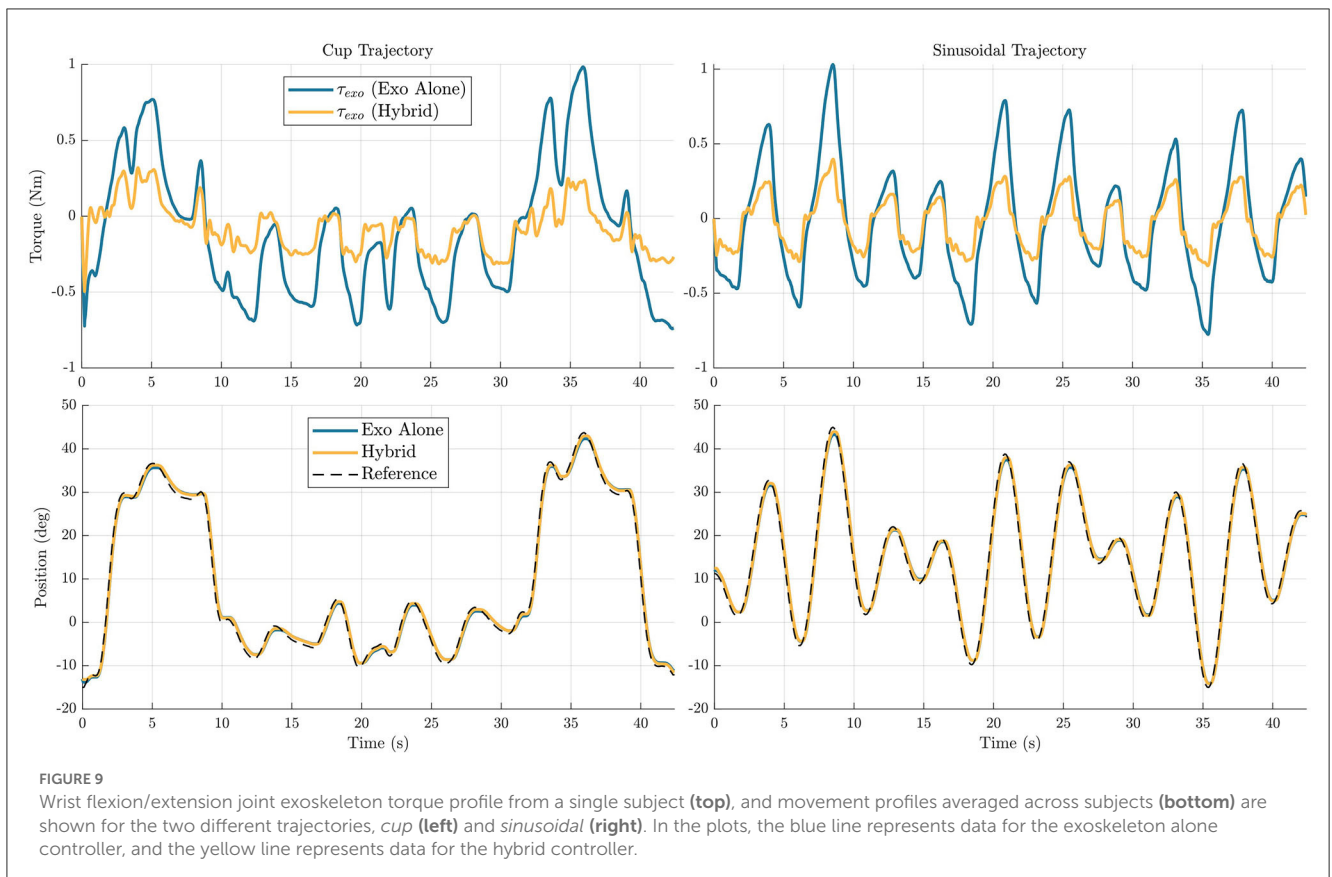


FIGURE 9

Wrist flexion/extension joint exoskeleton torque profile from a single subject (**top**), and movement profiles averaged across subjects (**bottom**) are shown for the two different trajectories, *cup* (**left**) and *sinusoidal* (**right**). In the plots, the blue line represents data for the exoskeleton alone controller, and the yellow line represents data for the hybrid controller.

model predictive control cost function to leverage the strengths of each of the subsystems, while minimizing the weaknesses of each.

4.1. Torque reduction

An average reduction of 48.7 and 57.9% of sum of squared torque was found on the elbow flexion/extension and wrist flexion/extension DOFs respectively with the use of the hybrid controller compared to the exoskeleton alone controller. These results in the EFE joint are an improvement over the 32.1% reduction found in our previous implementation using only the *cup* trajectory (Dunkelberger et al., 2022b). This improvement shows that the inclusion of the feedback controller instead of using an integral term, and the incorporation of a more sophisticated arm model, resulted in greater benefits in this hybrid control scheme, while even extending to more generalized trajectory cases. This shows promise for meaningful power consumption reduction for a hybrid system when comparing to an exoskeleton alone controller. Practically, this could mean that a portable hybrid system could be powered for roughly twice as long as an equivalent exoskeleton alone system, given the same battery capacity. In the future, this could lead to more portability and longevity in hybrid assistive devices for impaired populations.

It is worth noting that while the participants are able-bodied and can move their arm through the desired trajectories without assistance, we should not expect to see a torque reduction of 100%. With FES we often cannot achieve the full capabilities of the user's muscles, and in this study, many of the participants were not able to produce the maximum required torque solely through FES, even at maximum activation. Additionally, FES is known to not provide accurate or repeatable movements by itself, so at a minimum, the exoskeleton needs to provide corrective torques to account for these inaccuracies.

The average reduction in minimum and maximum torques shows potential for actuator sizes to be reduced while still achieving the same resultant motion, which would result in less bulky assistive robotic systems. In the future, this could be more directly tested by artificially limiting the maximum torque of the exoskeleton joints to observe how the FES can make up for the lack of torque.

4.2. Accuracy

FES systems by themselves do not provide reliable repeatability when trying to perform generalized movements. The goal of hybrid FES and exoskeleton systems is to achieve trajectory-following accuracies significantly better than FES systems by themselves, ideally approaching accuracies that are achievable using exoskeleton-alone systems. In the elbow flexion/extension joint, the hybrid algorithm had on average 0.20 and 0.16° more RMS tracking error on the *cup* and *sinusoidal* trajectories, respectively, when comparing the hybrid controller to the exoskeleton alone controller. While this was a decrease in accuracy, this still resulted in a very similar motion over the trajectory, as shown in Figure 8. To put this in perspective, for a forearm length of 30 cm, the RMS error in positioning the wrist, given the error in angular

tracking, is ~ 1 mm. For the wrist flexion/extension joint, the hybrid controller had on average 0.09 and 0.05° less RMS tracking error on the *cup* and *sinusoidal* trajectories, respectively. Again, while there is a small decrease in accuracy, the resultant trajectories are very similar, as shown in Figure 9. These results demonstrate that the hybrid controller is able to achieve similar tracking accuracies to the exoskeleton alone controller in both of the individual DOFs.

It is worth noting the difference in tracking accuracy between the *cup* and *sinusoidal* trajectories on the wrist flexion/extension joint. Recall that the *cup* trajectory requires significantly less movement, with an average velocity of 7.3 °/s compared to the sinusoidal trajectory with an average velocity of 14.3 °/s. The difference in difficulty between the trajectories is likely the cause for more tracking error in the *sinusoidal* trajectory. Still, we see that the general relationship of the hybrid controller having a 0.06° RMSE improvement is similar to the 0.09 degree RMSE improvement on the *cup* trajectory.

A benefit of the proposed control architecture is that the feedback controller portion can be adjusted independently of the model predictive control portion. This means that if a specific movement needs high-precision, the gains of the feedback controller can be modified in a straightforward manner to increase accuracy, although it would result in an increase in exoskeleton torque usage. Additionally, while this study focused on the challenging task of tracking time-varying trajectories, it would also be an interesting translation to modify the implementation to achieve desired setpoint positions, where FES could be used for a majority of the movement generation when it is far from the target, and the exoskeleton could be used to fine-tune the position when it is close to the desired setpoint.

4.3. Generalization across tasks

Many of the previous applications using FES for assistance provide the stimulation using a pre-programmed profile for a specific movement. An important feature of the proposed hybrid controller is that it does not rely on knowing the desired trajectory before use, and works with any given input trajectory. By testing two different trajectories, we were able to observe how the different outcome metrics varied in different movements. Tracking performance across several tasks has been reported by a few studies that use both FES and exoskeletons (Rohm et al., 2013; Memberg et al., 2014; Ajiboye et al., 2017), but none of these studies use a controller to distribute actuation between the two systems on the same joint.

The sum of squared torque reduction was similar between the two trajectories for both the elbow flexion/extension DOF and the wrist flexion/extension DOF. Along with the means and ranges being the same, the general spacing of the participants within the range of results remained the same between the two trajectories. This means that the benefits in power reduction did generalize well to these different trajectories, and that users could expect similar results on trajectories that require similar motions. It is especially interesting that a similar level of sum of squared torque reduction was found on the two different trajectories for the wrist

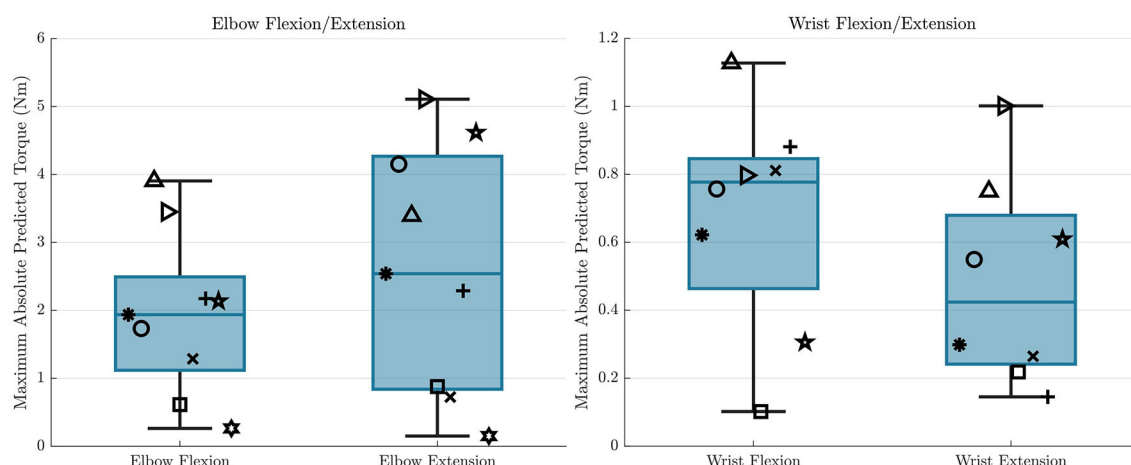


FIGURE 10

The maximum absolute values of the GPR predictions throughout the workspace for all participants are shown for each electrode, and for each DOF. This represents how different participants are able to achieve different levels of torque from FES when the participant is receiving maximum stimulation. The symbols here correspond to the same symbols from Figures 6, 7.

flexion/extension joint, especially because one of the trajectories was significantly more challenging than the other.

While the elbow flexion/extension DOF saw similar tracking accuracies in the two different trajectories when comparing the two controllers, the wrist flexion/extension DOF did see a difference in trajectory tracking accuracy on the two different trajectories. Despite this, the relationship between the exoskeleton-alone tracking accuracy and the hybrid tracking accuracy remained similar in all cases, with the elbow flexion/extension DOF showing average increase of 19.2 and 14.5% in RMS error on the *cup* and *sinusoidal* trajectories respectively, and the wrist flexion/extension DOF showing average reduction of 7.4 and 3.3% on the *cup* and *sinusoidal* trajectories respectively.

While not implemented in this paper, another benefit of this proposed controller is the ability to intuitively adjust controller behavior to generalize to different objectives of movement. If a specific task requires high precision in a movement, the gains of the Q matrix or feedback could be increased to favor more accurate movement at a cost of more torque. If there is an onset of fatigue, the weights of the R_m matrix can be adjusted to prefer more exoskeleton torque, and allow the muscles to recover.

4.4. Consistency across participants

While the results between trajectories were consistent within participants, there is a significant distribution of results between participants, especially for the sum of squared torque reduction observed for the hybrid controller compared to the exoskeleton alone controller. Even though all results showed improvement, except for the single participant who could not achieve an FES response in one of the wrist flexion/extension electrodes, some participants had significantly better results than others. There are many factors that can impact the effectiveness of FES, including electrode placement, size of muscles, body fat levels, and fatigue,

many of which are not modifiable. These variations in ability to produce torques due to FES can be visualized across participants in Figure 10, where the maximum absolute value that the GPR model predicts that each participant can produce throughout the workspace is shown. We can see that there are wide variations in the predicted amount of FES torque production. As an example, one participant cannot produce more than about 0.25 Nm of torque throughout the entire workspace with either the elbow flexion or elbow extension electrodes, but two other participants can produce more than 3 Nm in both of these cases. With these differences in mind, it is clear that some participants would never be able to achieve high reductions in power consumption with this hybrid control approach. To increase consistency between participants, it would be interesting to test with implanted FES systems, which are more reliable and targeted, and to model fatigue, which can help modify the controller in real-time to account for it.

When observing the results of the three participants who performed the same protocol twice separated by at least a week, we see that the results remained similar between the two time points. The difference between sessions in sum of squared torque reduction when comparing the hybrid controller to the exoskeleton alone controller remained within 17% across participants for the elbow flexion/extension DOF, and below 10% for the wrist flexion/extension DOF. The difference between sessions in RMS tracking error for the hybrid controller compared to the exoskeleton alone controller remained below 7% across participants for the elbow flexion/extension DOF, and below 12% on the wrist flexion/extension DOF. It is encouraging that even though it is difficult to generalize across participants, these preliminary repeatability results seem to indicate that results hold steady within users if the same implementation procedure is followed during each use. It is important to note here that the participants repeated the entire protocol, and it is expected that the model that the FES production will change (especially when using surface electrodes), meaning that the model

will necessarily have to be tuned for each use, even for the same participant.

One factor of this controller implementation that does not generalize across participants is that it relies on the relative weighting between exoskeleton torque inputs and FES activation levels. While the exoskeleton torque outputs are relatively consistent across participants, the activation levels do not map directly to torque outputs, because each participant produces a different amount of torque, given an activation level. In this case, the R_{fes} and R_{m_fes} parameters as defined in Equations 22, 23 must be scaled for each participant, based on the torque outputs expected from the GPR models. However, once the parameters are scaled once they should only need to be modified if electrodes need to be moved, or if fatigue occurs.

One participant had a particularly weak response to the FES, with a very low response from the elbow flexion/extension electrodes, and no response from the wrist flexion/extension electrodes. This difference compared to the remainder of participants shows the importance in characterizing each individual's FES behavior to understand the potential effectiveness of using the proposed hybrid controller.

4.5. Future work

An area of interest in observing the behavior of hybrid systems would be to identify how maximum torque allowed by the exoskeleton changes the resulting behavior in terms of torque output and tracking error. We observed the maximum torque used by the exoskeleton in this study, but it was not limited in any particular way to influence controller behavior. We should expect the controllers to behave differently if the maximum torques are limited at the start, as the future-looking MPC controller is able to predict a torque limit onset and proactively compensate for it.

Modeling of fatigue is another area of interest when using FES, and has received much attention in the FES research community. While this study aimed to keep the stimulation time to a minimum to reduce the effects of fatigue, there were likely at least some effects of fatigue present in results. Modeling and compensating for fatigue would be a meaningful addition to the hybrid controller to see improved performance.

The overall results from this study show promise for power reduction while maintaining high accuracy when performing movements with a single-DOF through the implementation of the hybrid FES-exoskeleton controller. Importantly, these algorithms should translate to a multi-DOF use case with only small modifications. To realize truly shared control for generalized upper-limb movements, these algorithms should be tested in multi-DOF circumstances to understand potential benefits and complications in this scenario.

5. Conclusion

In this paper, we presented a model-based control approach to hybrid FES-exoskeleton control. We experimentally demonstrated the benefits of using this model-based controller to distribute robot and FES contributions to control elbow and wrist movements with

a hybrid FES-exoskeleton system. This control strategy reduced exoskeleton torque for the hybrid system with similar tracking accuracy compared to using the exoskeleton alone. To realize practical implementation of hybrid FES-exoskeleton systems, the control strategy requires translation to multi-DoF movements, achieving more consistent improvement across participants, and balancing control to more fully leverage the muscles' capabilities.

Data availability statement

The datasets presented in this study can be found in online repositories. The names of the repository/repositories and accession number(s) can be found at: <https://github.com/mahilab/SingleDofHybridControlDataFrontiers/releases>.

Ethics statement

The studies involving human participants were reviewed and approved by Rice University IRB #FY2017-461 and Cleveland State University IRB #30213-SCH-HS. The patients/participants provided their written informed consent to participate in this study.

Author contributions

ND, JB, ES, and MO'M contributed to conception, design of the study, and wrote sections of the manuscript. ND conducted the experiments, performed the statistical analysis, and wrote the first draft of the manuscript. All authors contributed to manuscript revision, read, and approved the submitted version.

Funding

This material is based upon work supported by the National Science Foundation under Grants NSF CBET 2025130 and 2025142.

Acknowledgments

We acknowledge the contributions of Skye A. Carlson and Kyra C. Stovicek to the development of this study.

Conflict of interest

The authors declare that the research was conducted in the absence of any commercial or financial relationships that could be construed as a potential conflict of interest.

Publisher's note

All claims expressed in this article are solely those of the authors and do not necessarily represent those of

their affiliated organizations, or those of the publisher, the editors and the reviewers. Any product that may be evaluated in this article, or claim that may be made by its manufacturer, is not guaranteed or endorsed by the publisher.

References

- Ajiboye, A. B., Willett, F. R., Young, D. R., Memberg, W. D., Murphy, B. A., Miller, J. P., et al. (2017). Restoration of reaching and grasping movements through brain-controlled muscle stimulation in a person with tetraplegia: A proof-of-concept demonstration. *Lancet* 389, 1821–1830. doi: 10.1016/S0140-6736(17)30601-3
- Ambrosini, E., Ferrante, S., Zajc, J., Bulgheroni, M., Baccinelli, W., D'Amico, E., et al. (2017). The combined action of a passive exoskeleton and an EMG-controlled neuroprosthesis for upper limb stroke rehabilitation: First results of the RETRAINER project. *IEEE Int. Conf. Rehabil. Robot.* 2017, 56–61. doi: 10.1109/ICORR.2017.8009221
- Anderson, K. D. (2004). Targeting recovery: Priorities of the spinal cord-injured population. *J. Neurotrauma* 21, 1371–1383. doi: 10.1089/NEU.2004.21.1371
- Andersson, J. A. E., Gillis, J., Horn, G., Rawlings, J. B., and Diehl, M. (2019). CasADi – A software framework for nonlinear optimization and optimal control. *Math. Progr. Comput.* 11, 1–36. doi: 10.1007/s12532-018-0139-4
- Bao, X., Sheng, Z., Dicianno, B. E., and Sharma, N. (2021). A tube-based model predictive control method to regulate a knee joint with functional electrical stimulation and electric motor assist. *IEEE Trans. Contr. Syst. Technol.* 29, 2180–2191. doi: 10.1109/TCST.2020.3034850
- Bardi, E., Dalla Gasperina, S., Pedrocchi, A., and Ambrosini, E. (2021). “Adaptive cooperative control for hybrid fes-robotic upper limb devices: A simulation study,” in *2021 43rd Annual International Conference of the IEEE Engineering in Medicine and Biology Society (EMBC)* (Mexico), 6398–6401.
- Beekhuizen, K. S., and Field-Fote, E. C. (2005). Massed practice versus massed practice with stimulation: Effects on upper extremity function and cortical plasticity in individuals with incomplete cervical spinal cord injury. *Neurorehabil. Neural Repair* 19, 33–45. doi: 10.1177/1545968305274517
- Blank, A. A., French, J. A., Pehlivan, A. U., and O'Malley, M. K. (2014). Current trends in robot-assisted upper-limb stroke rehabilitation: Promoting patient engagement in therapy. *Curr. Phys. Med. Rehabil. Rep.* 2, 184–195. doi: 10.1007/s40141-014-0056-z
- Bulea, T. C., Kobetic, R., Audu, M. L., Schnellenberger, J. R., Pinault, G., and Triolo, R. J. (2014). Forward stair descent with hybrid neuroprosthesis after paralysis: Single case study demonstrating feasibility. *J. Rehabil. Res. Dev.* 51, 1077. doi: 10.1682/JRRD.2013.12.0257
- Burchielli, D., Lotti, N., Missiroli, F., Bokranz, C., Pedrocchi, A., Ambrosini, E., et al. (2022). “Adaptive hybrid fes-force controller for arm exosuit,” in *2022 International Conference on Rehabilitation Robotics (ICORR)* (Rotterdam), 1–6.
- Cannella, G., Laila, D. S., and T. Freeman, C. (2016). Design of a hybrid adaptive support device for FES upper limb stroke rehabilitation. *New Trends Med. Serv. Robot.* 38, 13–22. doi: 10.1007/978-3-319-23832-6_2
- Charles, S. K., Krebs, H. I., Volpe, B. T., Lynch, D., and Hogan, N. (2005). “Wrist rehabilitation following stroke: Initial clinical results,” in *International Conference on Rehabilitation Robotics (ICORR)* (Piscataway, NJ: IEEE), 13–16.
- Collinger, J. L., Boninger, M. L., Bruns, T. M., Curley, K., Wang, E., and Weber, D. J. (2013). Functional priorities, assistive technology, and brain-computer interfaces after spinal cord injury. *J. Rehabil. Res. Dev.* 50, 145–160. doi: 10.1682/jrrd.2011.11.0213
- del Ama, A. J., Gil-Agudo, A., Pons, J. L., and Moreno, J. C. (2014). Hybrid FES-robot cooperative control of ambulatory gait rehabilitation exoskeleton. *J. Neuroeng. Rehabil.* 11, 1–15. doi: 10.1186/1743-0003-11-27
- Dietz, V., Müller, R., and Colombo, G. (2002). Locomotor activity in spinal man: Significance of afferent input from joint and load receptors. *Brain* 125, 2626–2634. doi: 10.1093/brain/awf273
- Dijkers, M. (1997). Quality of life after spinal cord injury: A meta analysis of the effects of disablement components. *Spinal Cord* 35, 829–840. doi: 10.1038/sj.sc.3100571
- Dunkelberger, N., Berning, J., Dix, K. J., Ramirez, S. A., and O'Malley, M. K. (2022a). “Design, characterization, and simulation of the mahi open exoskeleton upper limb robot (in review),” in *IEEE/ASME International Conference on Advanced Intelligent Mechatronics* (Sapporo).
- Dunkelberger, N., Carlson, S. A., Berning, J., Stovicek, K. C., Scheerer, E. M., and O'Malley, M. K. (2022b). “Shared control of elbow movements with functional electrical stimulation and exoskeleton assistance,” in *2022 International Conference on Rehabilitation Robotics (ICORR)* (Rotterdam), 1–6.
- Dunkelberger, N., Scheerer, E. M., and O'Malley, M. K. (2020). A review of methods for achieving upper limb movement following spinal cord injury through hybrid muscle stimulation and robotic assistance. *Exp. Neurol.* 328, 113274. doi: 10.1016/j.expneurol.2020.113274
- Durfee, W. K., and MacLean, K. E. (1989). Methods for estimating isometric recruitment curves of electrically stimulated muscle. *IEEE Trans. Biomed. Eng.* 36, 654–666. doi: 10.1109/10.32097
- Fitle, K. D., Pehlivan, A. U., and O'Malley, M. K. (2015). “A robotic exoskeleton for rehabilitation and assessment of the upper limb following incomplete spinal cord injury,” in *IEEE International Conference on Robotics and Automation (ICRA)* (Seattle, WA), 4960–4966.
- Francisco, G. E., Yozbatiran, N., Berliner, J., O'malley, M. K., Pehlivan, A. U., Kadivar, Z., et al. (2017). Robot-assisted training of arm and hand movement shows functional improvements for incomplete cervical spinal cord injury. *Am. J. Phys. Med. Rehabil.* 96, S171–S177. doi: 10.1097/PHM.0000000000000815
- Frullo, J. M., Elinger, J., Pehlivan, A. U., Fitle, K., Nedley, K., Francisco, G. E., et al. (2017). Effects of assist-as-needed upper extremity robotic therapy after incomplete spinal cord injury: A parallel-group controlled trial. *Front. Neurobot.* 11, 26. doi: 10.3389/fnbot.2017.00026
- Ha, K. H., Murray, S. A., and Goldfarb, M. (2016). An approach for the cooperative control of fes with a powered exoskeleton during level walking for persons with paraplegia. *IEEE Trans. Neural Syst. Rehabil. Eng.* 24, 455–466. doi: 10.1109/TNSRE.2015.2421052
- Kadivar, Z., Sullivan, J., Eng, D., Pehlivan, A., Malley, M., Yozbatiran, N., et al. (2012). RiceWrist robotic device for upper limb training: Feasibility study and case report of two tetraplegic persons with spinal cord injury. *Int. J. Biol. Eng.* 2, 27–38. doi: 10.5923/j.jibe.20120204.01
- Kirsch, N. A., Bao, X., Alibeji, N. A., Dicianno, B. E., and Sharma, N. (2018). Model-based dynamic control allocation in a hybrid neuroprosthesis. *IEEE Trans. Neural Syst. Rehabil. Eng.* 26, 224–232. doi: 10.1109/TNSRE.2017.2756023
- Klauer, C., Schauer, T., Reichenfeller, W., Karner, J., Zwicker, S., Gandolla, M., et al. (2014). Feedback control of arm movements using neuro-muscular electrical stimulation (NMES) combined with a lockable, passive exoskeleton for gravity compensation. *Front. Neurosci.* 8, 1–16. doi: 10.3389/fnins.2014.00262
- Lum, P. S., Godfrey, S. B., Brokaw, E. B., Holley, R. J., and Nichols, D. (2012). Robotic approaches for rehabilitation of hand function after stroke. *Am. J. Phys. Med. Rehabil.* 91, S242–S254. doi: 10.1097/PHM.0b013e31826bcd6b
- Memberg, W. D., Polasek, K. H., Hart, R. L., Bryden, A. M., Kilgore, K. L., Nemunaitis, G. A., et al. (2014). Implanted neuroprosthesis for restoring arm and hand function in people with high level tetraplegia. *Archiv. Phys. Med. Rehabil.* 95, 1201–1211. doi: 10.1016/j.apmr.2014.01.028
- Mulcahey, M., Smith, B., and Betz, R. (1999). Evaluation of the lower motor neuron integrity of upper extremity muscles in high level spinal cord injury. *Spinal Cord* 37, 585. doi: 10.1038/sj.sc.3100889
- NSCISC (2019). *Spinal Cord Injury Facts and Figures at a Glance*. Birmingham, AL: National Spinal Cord Injury Statistical Center.
- Peckham, P., Mortimer, J., and Marsolais, E. (1976). Upper and lower motor neuron lesions in the upper extremity muscles of tetraplegics. *Spinal Cord* 14, 115–121. doi: 10.1038/sc.1976.19
- Reinkensmeyer, D. J., Kahn, L. E., Averbuch, M., McKenna-Cole, A., Schmit, B. D., and Rymer, W. Z. (2000). Understanding and treating arm movement impairment after chronic brain injury: Progress with the ARM guide. *J. Rehabil. Res. Dev.* 37, 653–662. doi: 10.1007/s00115-016-0187-9
- Rohm, M., Schneiders, M., Müller, C., Kreiling, A., Kaiser, V., Müller-Putz, G. R., et al. (2013). Hybrid brain-computer interfaces and hybrid neuroprostheses for restoration of upper limb functions in individuals with high-level spinal cord injury. *Artif. Intell. Med.* 59, 133–142. doi: 10.1016/j.artmed.2013.07.004

Author disclaimer

Any opinions, findings, and conclusions or recommendations expressed in this material are those of the authors and do not necessarily reflect the views of the National Science Foundation.

- Schulz, S. B. S. R. W., Pylatiuk, C., and Reischl, M. (2011). "The hybrid fluidic driven upper limb orthosis—Orthojacket," in *Proceedings of the 2011 MyoElectric Controls/Powered Prosthetics Symposium Fredericton* (New Brunswick).
- Trier, S., Buckett, J., Campean, A., Miller, M., Montague, F., Vrabec, T., et al. (2001). "A modular external control unit for functional electrical stimulation," in *Annual Conference of the International Functional Electrical Stimulation Society* (Cleveland, OH).
- Valevicius, A. M., Boser, Q. A., Lavoie, E. B., Chapman, C. S., Pilarski, P. M., Hebert, J. S., et al. (2019). Characterization of normative angular joint kinematics during two functional upper limb tasks. *Gait Post.* 69, 176–186. doi: 10.1016/j.gaitpost.2019.01.037
- Varoto, R., Barbarini, E. S., and Cliquet, A. Jr. (2008). A hybrid system for upper limb movement restoration in quadriplegics. *Artif. Org.* 32, 725–729. doi: 10.1111/j.1525-1594.2008.00597.x
- Wächter, A., and Biegler, L. T. (2006). On the implementation of an interior-point filter line-search algorithm for large-scale nonlinear programming. *Math. Progr.* 106, 25–57. doi: 10.1007/s10107-004-0559-y
- Wolf, D., Dunkelberger, N., McDonald, C. G., Rudy, K., Beck, C., O'Malley, M. K., et al. (2017). "Combining functional electrical stimulation and a powered exoskeleton to control elbow flexion," in *2017 International Symposium on Wearable Robotics and Rehabilitation (WeRob)* (Houston, TX), 1–2.
- Wolf, D., and Scheerer, E. (2022). Trajectory optimization and model predictive control for functional electrical stimulation-controlled reaching. *IEEE Robot. Automat. Lett.* 7, 3093–8. doi: 10.1109/LRA.2022.3145946
- Yozbatiran, N., and Francisco, G. E. (2019). Robot-assisted therapy for the upper limb after cervical spinal cord injury. *Phys. Med. Rehabil. Clin.* 30, 367–384. doi: 10.1016/j.pmr.2018.12.008



OPEN ACCESS

EDITED BY

Emilio Trígili,
Sant'Anna School of Advanced Studies, Italy

REVIEWED BY

Wenbin Chen,
Huazhong University of Science
and Technology, China
Clara Beatriz Sanz-Morere,
Hospital Los Madroños, Spain

*CORRESPONDENCE

Christian Di Natali
✉ christian.dinatali@iit.it

RECEIVED 19 December 2022

ACCEPTED 06 April 2023

PUBLISHED 11 May 2023

CITATION

Di Natali C, Ortiz J and Caldwell DG (2023)
Quasi-passive lower limbs exosuit: an
in-depth assessment of fatigue, kinematic
and muscular patterns while comparing
assistive strategies on an expert subject's gait
analysis.
Front. Neurobot. 17:1127694.
doi: 10.3389/fnbot.2023.1127694

COPYRIGHT

© 2023 Di Natali, Ortiz and Caldwell. This is an
open-access article distributed under the terms
of the [Creative Commons Attribution License](#)
(CC BY). The use, distribution or reproduction
in other forums is permitted, provided the
original author(s) and the copyright owner(s)
are credited and that the original publication in
this journal is cited, in accordance with
accepted academic practice. No use,
distribution or reproduction is permitted which
does not comply with these terms.

Quasi-passive lower limbs exosuit: an in-depth assessment of fatigue, kinematic and muscular patterns while comparing assistive strategies on an expert subject's gait analysis

Christian Di Natali*, Jesus Ortiz and Darwin G. Caldwell

Laboratory XoLab, Department of Advanced Robotics (ADVR), Istituto Italiano di Tecnologia (IIT),
Genova, Italy

Wearable robots are becoming a valuable solution that helps injured, and elderly people regain mobility and improve clinical outcomes by speeding up the rehabilitation process. The XoSoft exosuit identified several benefits, including improvement of assistance, usability, and acceptance with a soft, modular, bio-mimetic, and quasi-passive exoskeleton. This study compares two assistive configurations: (i) a bilateral hip flexion (HA, hips-assistance) and (ii) a bilateral hip flexion combined with ankle plantarflexion (HAA, hips-ankles-assistance) with the main goal of evaluating compensatory actions and synergetic effects generated by the human- exoskeleton interaction. A complete description of this complex interaction scenario with this actuated exosuit is evaluated during a treadmill walking task, using several indices to quantify the human-robot interaction in terms of muscular activation and fatigue, metabolic expenditure, and kinematic motion patterns. Evidence shows that the HAA biomimetic controller is synergetic with the musculature and performs better concerning the other control strategy. The experimentation demonstrated a metabolic expenditure reduction of 8% of Metabolic Equivalent of Task (MET), effective assistance of the muscular activation of 12.5%, a decrease of the muscular fatigue of 0.6% of the mean frequency, and a significant reduction of the compensatory actions, as discussed in this work. Compensatory effects are present in both assistive configurations, but the HAA modality provides a 47% reduction of compensatory effects when considering muscle activation.

KEYWORDS

exoskeleton, soft robot applications, assistive device, wearable robots: exoskeletons and exosuits, human-robot interaction, biologically inspired robotics, biological control systems

1. Introduction

The world's elderly population is expected to increase significantly by 2,050 (estimated to rise to almost 22% of the worldwide population), reaching about 2 billion and doubling the proportion from 2002 (World Health Organization [WHO], 2015). Against such a background, a major concern that is attracting growing attention concerning the quality of elderly life is the link with physical activities (Dunn et al., 1998). Indeed, when physical activity is reduced, there is a strong correlation with psychosocial problems such as social isolation, unhappiness, or depression. At the same time, a lack of physical activities leads to further muscle degeneration in the lower limbs, with elderly persons potentially falling into a negative cycle of depression, skeletal muscle decline and further decreases in physical activity (Rejeski and Mihalko, 2001).

Mobility is a key component of health throughout all phases of the lifespan, and it is vital to ensuring that older adults can maintain independent functioning and autonomy (Richardson et al., 2015). Mobility limitations, defined as difficulty walking a one-quarter mile or climbing one flight of stairs, are reported by 30–40% of adults aged 65 years and older (Shumway-Cook et al., 2005). Because of these walking difficulties caused by age-related skeletal muscle decline of the lower limbs, many elderly persons partake in fewer and shorter physical activities than young people (Rosenbloom, 1988). One of the main causes of muscle degeneration is that many older adults do not engage in regular walking activities (Colley et al., 2011). Relatively slow gait speed is always detected in the elderly. This is an adaptive response to conserve energy (Alexander et al., 2010). As peak aerobic capacity (VO_2 peak) declines with increasing age (Waters et al., 1983), the energetic requirements of walking at a given speed increase relative to VO_2 peak, such that normal walking becomes more intense. Indeed, evidence suggests that energy requirements during walking play a central role in the development of mobility limitation in older adults (Fiser et al., 2010; Schrack et al., 2010).

It is critical to remain active and mobile to slow down the degrading of overall physical health and cognitive functions (Volkers et al., 2012). Indeed many elderly people, due to neuromotor deficits, make use of assistive devices such as canes, walkers, and orthoses to enable walking at home (Jutai et al., 2007). However, many of these devices substitute or complement the functional loss but do not encourage the activation or rehabilitation of the legs. Robotic research is actively trying to address some of the most pertinent problems of an aging society.

Wearable robots may be a solution that helps elderly people to regain their mobility. Recent years have seen the development of powered exoskeletons designed to restore walking in individuals who are unable to walk (Dollar and Herr, 2008; Goldfarb et al., 2013)). The main characteristic of these exoskeletons is the rigid structure that can support their weight and provide high levels of assistance to the wearer. While these devices are actively being studied as an alternative to wheelchairs for paralyzed people, they are too complex and expensive for users with a low to moderate degree of impairment (Ortiz et al., 2021). For the individuals who need some, but less, assistance, a new generation of exoskeletons based on soft technologies is in development, which has excellent promise in terms of usability and performance. They specifically

target users that retain some degree of mobility, and consequently, the exoskeleton only provides partial assistance/support. This is well suited to current soft technologies. For example, the Harvard soft exosuit (Awad et al., 2017), or MyoSuit (Haufe et al., 2019), share common elements, such as cable-driven actuation, although they use different approaches in their implementation. The presented trend underlines the need in several applications and target users, where wearability and acceptability become critical features to drive the shift from heavy rigid exoskeletons to light, soft wearable devices. In the XoSoft project, we introduced Quasi-Passive Actuations (QPA) to create a biomimetic device. These QPAs are composed of a Textile-Based Clutch (TBC) (Sadeghi et al., 2019) together with an Elastic Tendon (ET) that forms the passive mechanical element, which is connected in series. From an assessment point of view, the analysis of a passive device is more complex because of the continuous energy exchange between the user and the ETs.

Most of the scientific efforts are focused on conducting kinematic, dynamic and metabolic assessments (Wehner et al., 2013; Shamaei et al., 2014; Di Natali et al., 2019; Zhou et al., 2020), rather than carrying out analysis on the muscle activity (Van Dijk et al., 2011). Inconclusive answers are reported in this (Van Dijk et al., 2011), mainly because of the complexity of the experimental protocol that has been carried out, e.g., multiple subjects, high variability in gender, age and physical characteristics, and the effects of the learning curve in the use of new technological devices. That protocol also has to cope with the high sensitivity and variability of the measurement equipment used (surface EMG for muscular activation measurement). This technology deserves a more accurate analysis to underpin the effective and potential results that this equipment could bring. Thus, a systematic comparative analysis of similar technology (i.e., passive or quasi-passive actuated exosuit) is relevant to better understanding what happens at the muscular level.

2. Background and motivation

The rationale behind the assistive approach is based on the typical muscular pattern during walking. During walking, the main muscles activated are the gluteus, gastrocnemius and rectus femoris, acting during stance, push-off and swing phases, respectively, (Winter, 2009). Typical gait assistive strategies proposed in rehabilitation exoskeletons that aim to reduce fatigue during walking, support alternatively hip flexion (Jin et al., 2016), hip extension (Asbeck et al., 2015), or ankle plantarflexion (Collins et al., 2015). Hybrid approaches (Asbeck et al., 2013; Ding et al., 2014) also report good effectiveness in reducing muscular activation or metabolic consumption between 5 and 15%.

During normal walking, as shown in Figure 1B, power is expended by the body primarily at the transitions of support from one leg to the other. This power is mainly provided by the hip (represented in blue) and ankle (represented in green) (Winter, 2009). During stance, the gastrocnemius contracts isometrically, stretching the Achilles tendon due to the body's natural motion falling forward. Subsequently, these muscles contract concentrically, and the Achilles tendon recoils, giving a large positive power burst from 40 to 60% of the gait cycle

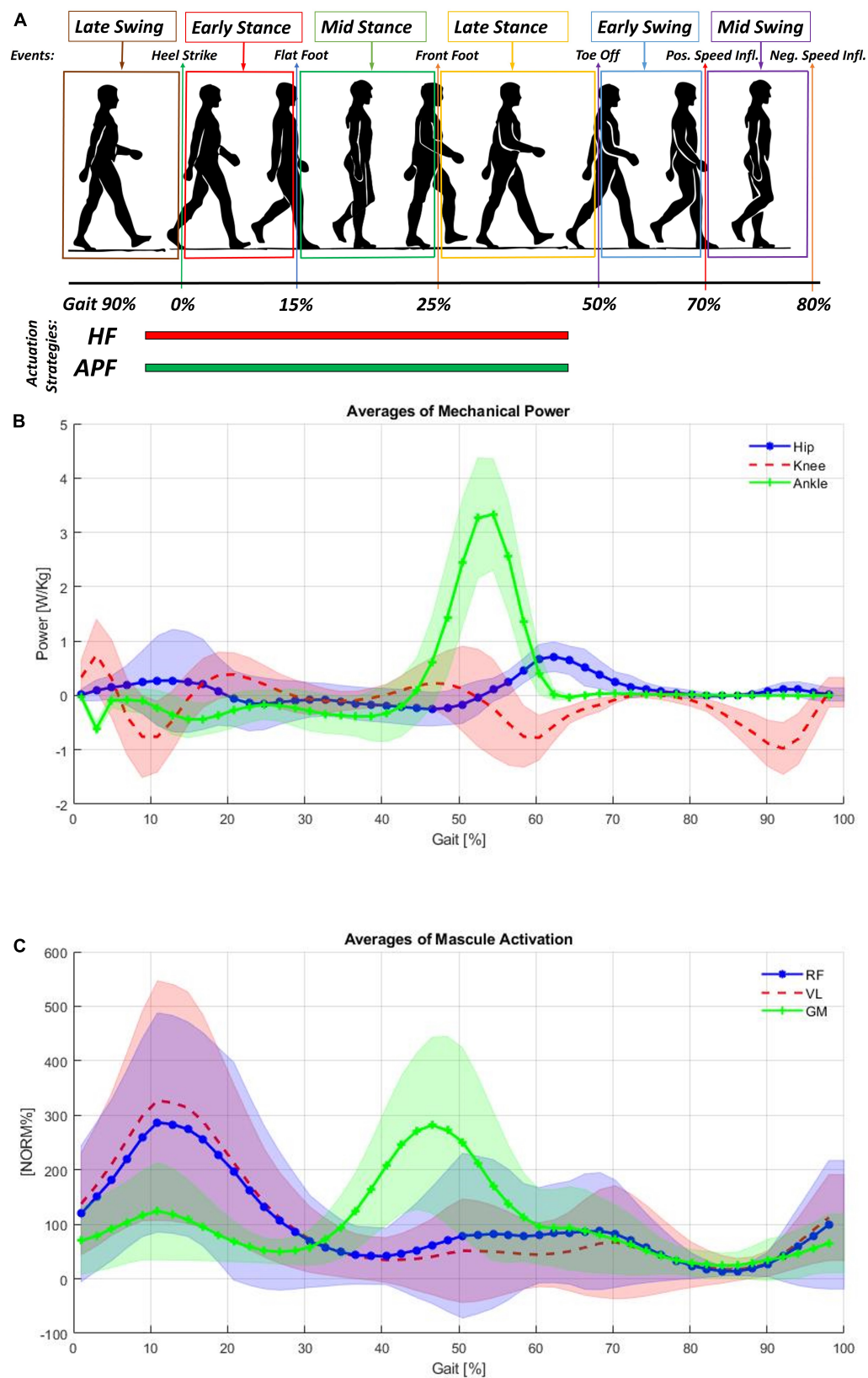


FIGURE 1

(A) Cyclical gait representation, (B) averages of mechanical power measured at the hips, knees and ankles normalized for the subject weight (Winter, 2009). (C) Shows the averages of muscular activation of the rectus femoris (RF), vastus lateralis (VL), and gastrocnemius medialis (GM). Each subject's mean EMG was normalized to 100% prior to averaging (Winter, 2009).

to propel the body upward and forward (shown in **Figure 1C** with the activation of the gastrocnemius medialis). The muscles at the front of the thigh (such as the rectus femoris, shown in **Figure 1C**) provide a smaller power burst at the hip and a period of power absorption during the transition between legs. The power absorption occurs from 35 to 50% of the gait cycle. The power burst occurs from 50 to 75% of the gait cycle, providing energy to help swing the leg. It is reported (DeVita and Hortobagyi, 2000; McGibbon, 2003) that elderly persons if compared with young persons, are characterized by reduced power generation at the ankle plantar flexors compensated by more power at the hip flexors to guarantee step length. By assisting the hip flexors, the burden on the hip joint would be reduced, and the lower limbs would be lifted sufficiently high that ground clearance of the feet is achieved, and tripping could be prevented (Sposito et al., 2018; Di Natali et al., 2019).

Important aspects, which are also correlated to passive exoskeletons performance (Rahman et al., 2006), are evaluating the effects on gait for the kinematic patterns and muscular activity. Before receiving assistive forces, passive exoskeletons require the user to input energy into the system to elongate the elastic elements. The storing of potential energy causes an increase in muscle activity (Fanti et al., 2022). Moreover, it could also generate changes in motion patterns. Thus, evaluating these changes is critical to understanding the actual efficacy of this complex human-exoskeleton interaction.

In addition, by investigating how the musculature of a healthy subject responds to the assistive and resistive cycles provided by the QPA-based exosuit (Di Natali et al., 2020), we aim to define the technology's potential for improving mobility and enabling personalized, effective rehabilitation. Consequently, the system acts also as continuous muscle training (Di Natali et al., 2021), which is, in turn, a secondary benefit of the system to help regain mobility by improving gait and postural patterns (Di Natali et al., 2019). Ultimately, considering the complexity of the human musculoskeletal system and the assistance provided, compensatory and synergetic effects on the musculature were studied.

3. Objectives and hypotheses

The primary objective of this foundational study is to assess the effective reduction in walking energy consumption and hence quantify the energy exchanges in healthy individuals by using the XoSoft exosuit technology employing QPAs. Moreover, changes in the motion patterns are not evitable. Thus, a synergetic analysis of kinematic and muscular patterns is critical to understand the overall effectiveness of the interaction with the exosuit. Two different assistive modalities have been assessed: (i) bilateral hip flexion (HF) assistance; and (ii) bilateral HF assistance and bilateral ankle plantarflexion (APF) assistance. These two assistance strategies are those most commonly adopted in literature to reduce the energy burden during walking with active exosuits (Asbeck et al., 2013; Ding et al., 2014; Jin et al., 2016; Awad et al., 2017; Haufe et al., 2019). The hypothesis of this study is a comprehensive evaluation of human-exoskeleton interaction focusing on several different indexes that provide positive and negative effects on the system energy exchange and motion patterns during walking

activities, which is particularly important for elderly people. The target evaluation will focus on assessing an effective reduction in metabolic expenditure, a decrease in muscular fatigue, and a minimal change of kinematic patterns while reducing muscle activation.

This study is conducted on a single healthy subject with several hours of experience using a quasi-passive exosuit. Exoskeletons perform differently as a function of experience, fitting, particular motion patterns and many other aspects necessary for optimization to improve cross-subject effectiveness (Zhang et al., 2017). Therefore, a personalized assistive approach must be considered a standard approach. Moreover, a generalization of the effectiveness over a small number of subjects in a single testing run is always difficult to be reliable (Van Dijk et al., 2011). This aspect is essential, particularly when considering the effects of the learning curve on the user's motion style and neuro-motor coordination, particularly when considering changes in the walking pattern and due to the mutual adaptation in which robot and human effectively cooperate and exchange forces (Moreno et al., 2009; Afzal et al., 2020).

Moreover, this work (Theurel and Desbrosses, 2019) underlines the need for more evidence on the impact of assistive forces on neuromuscular coordination and joint kinematics. Therefore, this study has performed long walking tests on an expert exoskeleton wearer and repeated them over multiple days. We aim to measure the effectiveness of the wearer's interaction with the exosuit without bias due to the bad fitting and learning curve effects. In addition, multiple test repetitions will be essential to apply statistical analysis to the gathered data while investigating the exoskeleton interaction at the muscle activity level over several gaits (Galle et al., 2017).

This work's main contribution lays on the hypothesis that the assistance targeted on the hip flexion and ankle assistance would promote a more comprehensive and bio-inspired propulsive force from the muscles activated during walking and, simultaneously, reduce the energetic burden associated with locomotion. This aspect is not obvious, particularly when considering passive (or quasi-passive) exoskeletons interacting with such a complex as the human system. In principle, The XoSoft exosuit generates forces on the body during both storing (elastic elongation) and releasing phases, thus mimicking the behavior of muscles and tendons. These forces generate assistance during the realigning phase. The elastic tendon has already accumulated potential energy and releases it to the user.

In contrast, the storing phase is characterized by storing energy from the elastic tendon the user provides. This phenomenon of the wearer's interaction with a passive actuated exoskeleton is fundamental when considering the overall exchange of forces and energy balance. Moreover, this study also impacts the understanding the fundamental interaction with passive exoskeletons.

4. Materials and methods

4.1. XoSoft platform

The XoSoft EU project developed a user-centered design-based exosuit. This soft, modular, bio-mimetic and quasi-passive exoskeleton assists users such as the elderly, and post-stroke and

TABLE 1 Characteristics of the ET used in experimental trials.

ET for specific joint	Stiffness (N/mm)	ET length (mm)	Force at 50% of ET elongation (N)
Hip flexion (HF)	1.6	50	40
Ankle plantarflexion (APF)	2.5	20	25

partial spinal cord injury subjects with low to moderate mobility impairments (Di Natali et al., 2019). The XoSoft-Gamma prototype demonstrated in Di Natali et al. (2020), features reconfigurable and modular soft pneumatic QPAs to deliver bilateral gait assistance for hip and knee flexion and extension and ankle plantar and dorsiflexion. QPAs relying on variable stiffness mechanical elements, the TBC (Sadeghi et al., 2019), are used to modulate the forces generated by the passive elements employed to store the mechanical energy.

The XoSoft exosuit was designed to support the user at the hips and ankles in this work. The ETs characteristics and possible control strategies are extensively presented in Di Natali et al. (2020). The ETs selected for this study are reported in Table 1. The exosuit is designed to assist power absorption through controlled modulation of the extension of the passive element. The exosuit is actuated for both hip flexion (HF) and ankle plantarflexion (APF) actuation from 5 to 65% of the gait cycle (the timing of both control strategies are shown in Figure 1A, with the hip flexion presented in red, and the ankle plantarflexion in green).

The wearer, thus, before receiving assistance, has to exert a force to elongate the ETs in an energy-storing phase. Subsequently, the exosuit returns this stored energy to the wearer in the releasing phase (see Figures 2B, C). If the system efficiency were ideal at the end of the cycle, the physical energy balance would be the same. Still, previous works demonstrated that control strategies could modify this balance toward a surplus value of assistance (Di Natali et al., 2019, 2020, 2021).

Figure 2A shows the subject wearing the XoSoft exosuit configured with the assistive modules, i.e., QPA hip flexion and QPA ankle plantarflexion to assist at the hip and ankle, respectively. The effective elongation and the torque generated by each actuator are a function of the corresponding articulation angle shown in Figures 2B, C. Walking is a cyclical motion characterized by oscillating trends of the lower limbs. This determines the gait cycle portions to be exploited for the elongation of the ET (storing phase) and the subsequent releasing phase (the effective assistance). We hypothesized that the extraction and storage of mechanical energy during stance would have less impact than its release during the swing, thus shifting the energy balance toward a net assistive condition. The specific HA (hips assistance) strategy engages the QPA between 5 and 65% of the gait cycle, where the elastic energy is accumulated during the stance and then returned during the swing. The HAA (Hips-ankles-assistance) strategy also assists the gastrocnemius between 5 and 65% of the gait cycle to propel the body upward.

Similarly, the QPA requires a storing phase before releasing assistance to the target ankle. During stance, the QPA ankle plantarflexion is engaged. Consequently, the ET stretches thanks to the body's motion "falling" forward. Subsequently, when the person starts pushing, and the ankle angle reaches its minimum, the user actively contracts the calf muscles. The ET contracts to its original length, releasing the stored mechanical energy and aiding

the propulsion of the body upward. Figures 2B, C show the concept underpinning both the storing and releasing phases of the HA and HAA strategies as functions of the corresponding joints.

4.2. Design of the study

The experimentation focused on evaluating, during treadmill walking, the effects of the QPA-based exosuit on healthy gait mechanics and energetics. The assessment of the reduction in walking energy requirements was evaluated in three experimental configurations (i) the baseline (NOE), (ii) the HA and (iii) the HAA configurations.

This study aims to meticulously detail the effects of using a QPA-based exosuit on muscle patterns, muscle synergy, and compensatory effects. Experimentation is conducted on a single healthy subject with experience in using XoSoft to reduce subject-specific performance variability, which was involved in completing each test repetition with and without the exoskeleton worn. The test is repeated five times on different days applying for the following order between the three conditions: NOE, HA, and HAA. Moreover, the test was performed five times on different days to reduce set-up variability due to exosuit wearing and sensor placement. In addition, we imposed a rest period of 20 min between each repetition, during which the subject recovered, and the investigators controlled the equipment. Single-subject experimentation is critical, particularly when measuring errors introduced by intra-subject variability and subject-specific performance variability. The main objective is to analyze muscular and kinematic pattern changes and compensatory effects while reducing any possible risk of affecting measurements due to the errors introduced by the experimental protocol, e.g., multiple measurements, donning-doffing wearable devices, dynamic movements, and sweating.

A 5-day testing protocol was used to evaluate the effects of the two different exosuit assistive configurations (HA and HAA). During any single testing day, the three different walking tests were performed for 10 min on a treadmill at a natural self-selected walking speed of 3 km/h (0.83 m/s), taking approximately 600 steps for each leg. Data were recorded for the monitored muscles, namely: Rectus Femoris (RF), Vastus Medialis (VM), Tibialis Anterior (TA), and Gastrocnemius Lateralis (GL). Apart from the gluteus, these four selected muscles are the most relevant for gait analysis. The gluteus was not selected due to possible interference with the exosuit. The Biceps Femoris or the hamstrings are also relevant in the walking pattern. In this work, the hamstrings were not monitored since the main assistive effects of the exosuit of the hips motion would mainly exert on the hip flexors. Moreover, our previous work (Fanti et al., 2022) reports results on a similar exosuit assistive configuration on the semimembranosus, which is responsible of hip extension. To apply a statistical approach, right and left muscle activations were averaged for each stride,

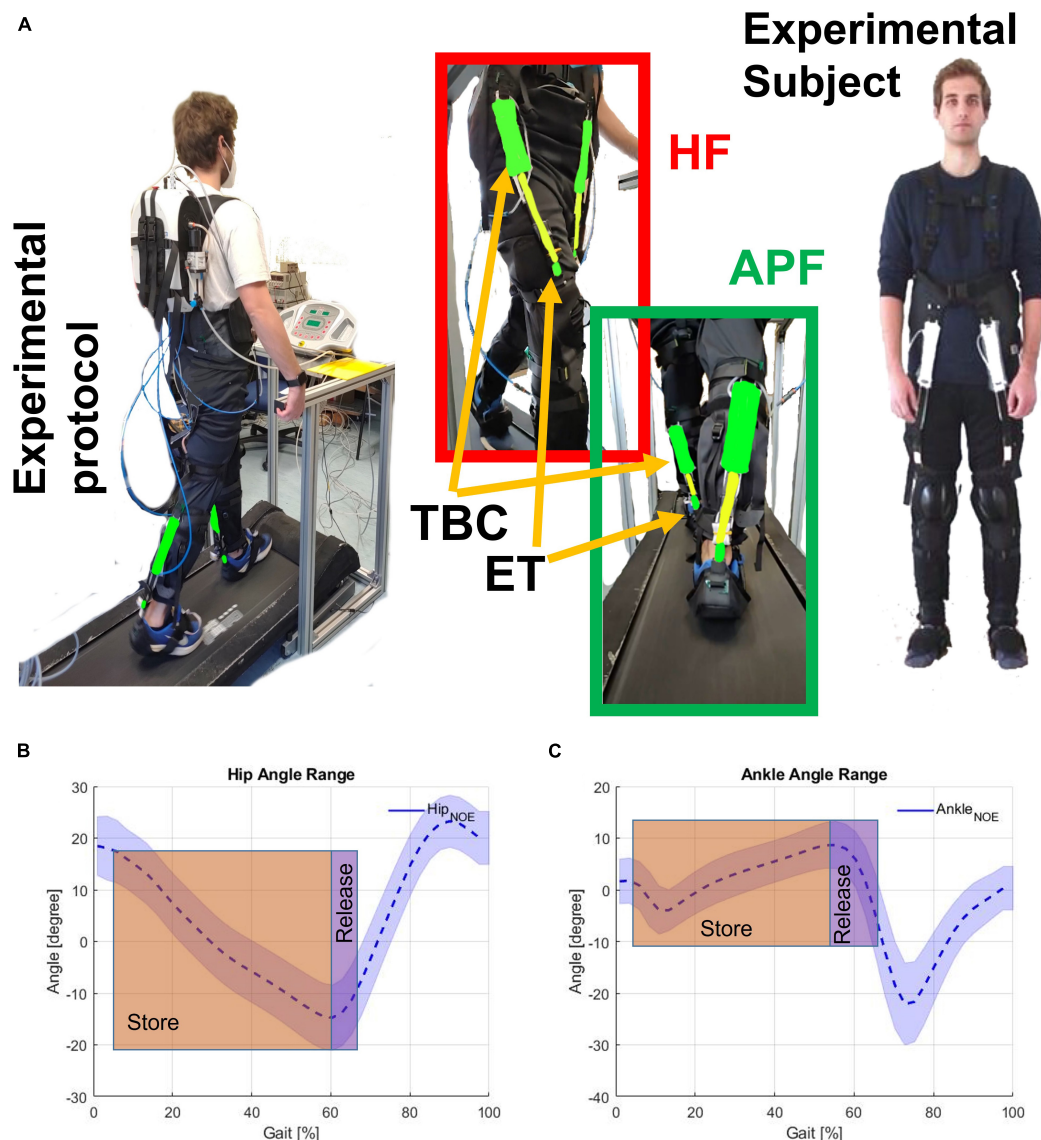


FIGURE 2

(A) Experimental subject wearing the exosuit. Hip flexion (HF) and ankle plantar flexion (APF) are shown together with the textile-based clutch (TBC) and the elastic tendon (ET). Store and release phases on the (B) HF (hip angle), and (C) APF (ankle angle). The human subject gave permission for the use of their image.

determining the overall behavior for each studied configuration and analyzed muscles. Each test modality was compared against the specific daily baseline (NOE) to minimize the day-to-day variability of the participant.

4.3. Experimental protocol

This work aims to evaluate if specific assistive exosuit control profiles reduce metabolic energy and muscle fatigue during walking at a fixed rate. Biomechanics and energetic considerations are reported during treadmill walking on three experimental conditions: (i) the reference condition without the exoskeleton being worn (NOE), (ii) the hip flexion assistance study referred to as HA, and (iii) the hip flexion and ankle plantarflexion assistance study referred to as HAA. Two primary outcomes were assessed:

the activity of four muscles (RF, VM, TA, and GL), and the energy cost of walking, defined as mass normalized oxygen consumption ($\text{ml O}_2/\text{kg}$). From a kinematic point of view, maximum extension and flexion are evaluated, along with the range of motion (RoM) of the hip, knee, and ankle. All trends are plotted within each gait cycle and are expressed as a percentage of the stride period. 0% refers to the heel strike, and 100% to the next consecutive heel strike. All results are reported by combining right and left signals over a 10-min walking test, repeated five times for each test scenario, thus averaging approximately three thousand strides. Muscle activations were normalized over the Maximal Voluntary Exertions (MVE) computed as the 95th percentile of the baseline distribution of the four EMG measurements taken during normal walking at 3 km/h. This approach prevents the false selection of maximum muscle activations due to erroneous EMG spikes. The muscle activations

vary from 0 to 1 of MVE (where 1 corresponds to 100% of MVE of each muscle during walking) in all four measured muscles.

The experiment was approved by the Ethical Committee of Liguria (protocol reference number: CER Liguria 001/2019) and complied with the Helsinki Declaration. A healthy adult participated in the study (male, age 35 years, height 1.70 m, weight 70 kg). After fully explaining the experimental procedure, the subject signed a consent form before participating. We recorded the participant's fully-body kinematics, lower limb surface electromyography (EMG) and metabolic expenditure during the test. An Xsens wearable motion tracking system was used to record full-body kinematics (MTw Awinda 3D Wireless Motion Tracker, Xsens Technologies B.V. Enschede, Netherlands) at a sampling rate of 100 Hz. An 8-channel Wi-Fi transmission surface electromyography (FreeEMG 300 System, BTS, Milan, Italy) was used to acquire the surface myoelectric signals (sEMG) at a sampling rate of 1,000 Hz. K5 metabolic wearable technology (K5 COSMED Srl, Roma, ITALIA) was used to measure the metabolic expenditure. After skin preparation, bipolar Ag/AgCl surface electrodes (diameter 2 cm) prepared with electro-conductive gel were placed over the muscle belly of RF, VM, TA, and GL in the direction of the muscle fibers (distance of 2 cm between the center of the electrodes) according to the European recommendation for surface electromyography (Hermens et al., 2000) and the atlas of muscle innervation zones (Barbero et al., 2012). The baseline muscle activity and energy expenditure were recorded without the exoskeleton. Each repetition was conducted on a treadmill, with the speed set to the participant's natural and self-selected overground walking speed (approximately 3 km/h).

4.4. Data analysis

Data were processed using MATLAB software (MATLAB 2020, MathWorks, Natick, MA, USA). The raw EMG signals were band-pass filtered using a zero-lag third-order Butterworth filter (20–450 Hz), rectified, and low-pass filtered with a zero-lag fourth-order Butterworth filter (10 Hz). The time scale was normalized by interpolating individual gait cycles over 1,200 points. Then, the EMG signal from each muscle was normalized to the MVE value across all trials. The MVE is recorded at the start of each experimental day when the muscles were fresh and then used as the maximal values across the successive measurements. The Results section reports the trends of each muscle activation against the baseline (NOE), particularly highlighting the resistive and assistive phases of the gait (Di Natali et al., 2020). The resistive phase is when the muscle activity is higher than the baseline, while the assistive phase is when muscle activity is lower than the baseline. The specific assistive strategy (HA and HAA) can strongly affect the oscillation of the muscle activity about the baseline value. The Results section extensively studies and reports the phases of resistance and assistance.

The root means square (RMS), and the Mean Frequency (MF) of the power spectrum of the EMG signals were calculated to investigate the effect of the exosuit on muscle fatigue. For each stride, the RMS was computed over specific intervals of

the gait cycle for each muscle, according to the following formula:

$$RMS = \sqrt{\frac{1}{N} \sum_{i=1}^N EMG_i^2}$$

Where EMG_i is the value of the i th sample of the envelope of each muscle and N is the number of samples of each interval. For each muscle and each stride, the MF was computed as the ratio between the spectral moments of order 1 and 0 (Ament et al., 1993; Dimitrov et al., 2006):

$$MF = \frac{\int_{t_1}^{t_2} f PSD(f) \delta f}{\int_{t_1}^{t_2} PSD(f) \delta f}$$

Where t_1 and t_2 are the initial and final instants of each stride, $PSD(f)$ is the power spectrum density of the EMG signal, and f is the frequency.

The estimation of the metabolic cost is based on an indirect measurement of the oxygen consumption and respiratory quotient as presented in Goedecke et al. (2000); Jin et al. (2016). The mathematical equation used to derive the metabolic energy expenditure (EE) expressed in watts [W], is a function of oxygen consumption (V_{O_2}) and the respiratory exchange ratio (RER) as in:

$$EE = c_1 V_{O_2} (c_2 RER + c_3)$$

Where the conversion factors are: $c_1 = 69.7$, $c_2 = 1.2341$, and $c_3 = 3.8124$, the respiratory exchange ratio ($RER = V_{CO_2}/V_{O_2}$), as reported in Jansson (1982), is the ratio between the CO_2 produced and the O_2 used during metabolism.

Joint angles were calculated based on the standards defined by the International Society of Biomechanics (Grood and Suntay, 1983). All kinematic data were plotted from 0 to 100% of the gait cycle, where 0 and 100% are the consecutive touches of the same heel. The measurements of each lower leg joint angle were averaged over each right and left gait segmentation to estimate and display averaged trends.

Both kinematic, muscular, and exoskeleton data are fully synchronized with a common triggering signal. As previously mentioned, the data is then segmented, and the analysis is represented over the gait cycle. The objective is to evaluate the averaged behavior of muscles and joint angles over multiple test days. The reason for multiple testing days is not to propose a longitudinal test but to enlarge the data set without impacting the user's fatigue due to longer trials. A multiple testing days approach will also provide a big data set that, averaging each signal over the gait cycle, will allow achieving mean behaviors of the target signals over the gait cycle. Thus, sudden errors and irregular motions would be smoothed down while similar motions would be emphasized. The statistical analysis was performed for the MF and the estimation of the metabolic cost data using SPSS 20.0 software (IBM). P -values < 0.05 were considered statistically significant. We used the Shapiro–Wilk test (Ghasemi and Zahediasl, 2012) to verify that the data was from a normal distribution. Then we applied a parametric paired t -test to detect any significant differences. For the muscle and kinematic representation, a descriptive statistical analysis was applied to evaluate the average behavior and variations (STD) over the 6,000 strides (600 strides for leg for each of the 5 days of test) for each assistive modality (NOE, HA, and HAA). The bold line in the muscles and kinematic trend plots represents

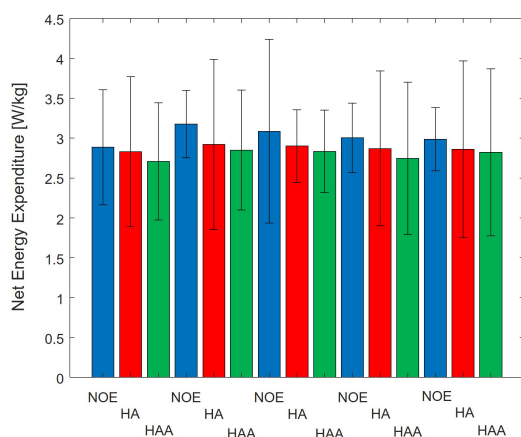


FIGURE 3

Comparison of Baseline vs. Hips-assistance (HA) and Hips-Ankles-assistance (HAA) modalities of the metabolic consumption trends of all 5-day tests. Numerical results are normalized on the subject mass.

the averaged behavior of muscle activities and joint angles. At the same time, the shaded region covers about 68% of the variation of the data around the mean values.

5. Results

5.1. Metabolic energy consumption results

In this section, both assistive strategies (HA and HAA) are assessed against baselines and compared regarding metabolic expenditure variation. **Figure 3** reports the energy cost associated with 10 min of walking for the three configurations. The average metabolic expenditure normalized for the subject's weight of normal walking measured over five tests using the NOE configuration is 3.02 ± 0.62 W/kg, (2.6 Metabolic Equivalent of Task - MET). Where 1 MET is equal to 1.162 W/kg. For the HA configuration, the metabolic expenditure is 2.88 W/kg (2.5 MET), while the HAA configuration reports consumption of 2.79 W/kg (2.4 MET). **Table 2** shows the relative reduction and *p*-value of the *t*-test.

5.2. Muscle fatigue analysis results averaged over 5 days: HA and HAA comparison

This analysis shows the main change in the EMG signal in the frequency domain with a spectrum translation toward lower frequencies (Cifrek et al., 2009). Thus, if the specific MF of a single muscle decreases during the test, the user perceives increased fatigue in that muscle. The MF is calculated as shown in the Data analysis section for each stride (18,160 strides in total if considering the right and left leg of the NOE, HA, and HAA configurations). Subsequently, each trend is normalized using the

initial value of the baseline. **Figure 4** shows the normalized MF of each muscle as the difference between the initial and final stride. The baseline of the MF for all four muscles, measured without the exosuit (NOE), shows negative values, underlining the presence of a certain degree of muscular fatigue that occurs during the task. The MF trend decreases linearly in all muscles and configurations as the number of strides increases. A linear envelope is used to average the whole trend for each MF. The barplot of **Figure 4** represents the decrease in the MF over the entire walking test, thus indicating muscular fatigue. The same approach has been taken for exoskeleton configurations and all four measured muscles shown in **Figures 4A-D**. Focusing on the baseline, the MF of the RF during the walking test decreases by 6.9% on average, corresponding to 5.4 Hz at an initial value of 78.8 Hz. The VM starts at 73.4 Hz and decreases by 6.4 Hz. Thus, the mean decrement in 10 min of walking is 8.7%. The TA starts from 77.8 Hz and decreases by 1.7 Hz, thus the mean reduction during the test is 2.2%. Finally, the GL starts from 85.5 Hz and decreases by 1.0 Hz, giving a mean reduction of 1.2%.

We hypothesize that using an exosuit would lead to a smaller decrease in the MF, which indicates of reduced fatigue. This should occur even though the user has to carry the extra weight of the device. For the HA, the results show an increased negative trend of MF for all four evaluated muscles. The RF decrease is 6.6 Hz, which is 8.4% of the initial baseline value. The VM decrease is 9.5 Hz, which is 13.0% of the initial baseline value. The TA decrease is 2.1 Hz, which is 2.7% of the initial baseline value. Finally, the GL decrease is 1.9 Hz, which is 2.3% of the initial baseline value.

For the HAA, the results show an effective reduction of the negative trend of the MF for three of the four muscles under evaluation. The RF decrease is 5.7 Hz, which is 7.2% of the initial baseline value. The VL decrease is 5.3 Hz, which is 7.2% of the initial baseline value. The TA decrease is 1.3 Hz, which is 1.6% of the initial baseline value. Finally, the GL decrease is 0.4 Hz, which is 0.4% of the initial baseline value.

The average of the relative difference in MF across all four muscles of the HA configuration presented in **Table 3**, shows an increment of the relative difference of the muscle fatigue of 1.8%. The HAA configuration shows a reduction in fatigue of 0.6%, which is also measured as the average of the relative difference of MF for the HAA.

5.3. HA and HAA assistance strategies comparison on the kinematic analysis

5.3.1. HA: hips-assistance kinematic analysis

In this section, the HA strategy is assessed against the baseline. The participant produced a physiological range of motions for each of the three lower limb joints (hips, knees, and ankles) while walking on the treadmill at 3 km/h (0.83 m/s). The RoM for the ankle varied from -22° to $9^\circ \pm 15^\circ$ (**Figure 5A**). For the knee, the range was from 5° to $60^\circ \pm 15^\circ$ (**Figure 5B**), and for the hip, the RoM was from -15° to $25^\circ \pm 15^\circ$ (**Figure 5C**). **Figures 5A-C** shows the joint angle displacements generated using the HA modality. These displacements are averaged over the right and left

TABLE 2 Comparison of HA and HAA strategies concerning the baseline (NOE): 5 days average of the relative reduction of metabolic expenditure and *p*-value.

	Relative reduction of metabolic expenditure (%)	<i>t</i> -test, <i>p</i> < 0.05
HA vs. NOE	4.98	0.0191
HAA vs. NOE	7.75	0.0031

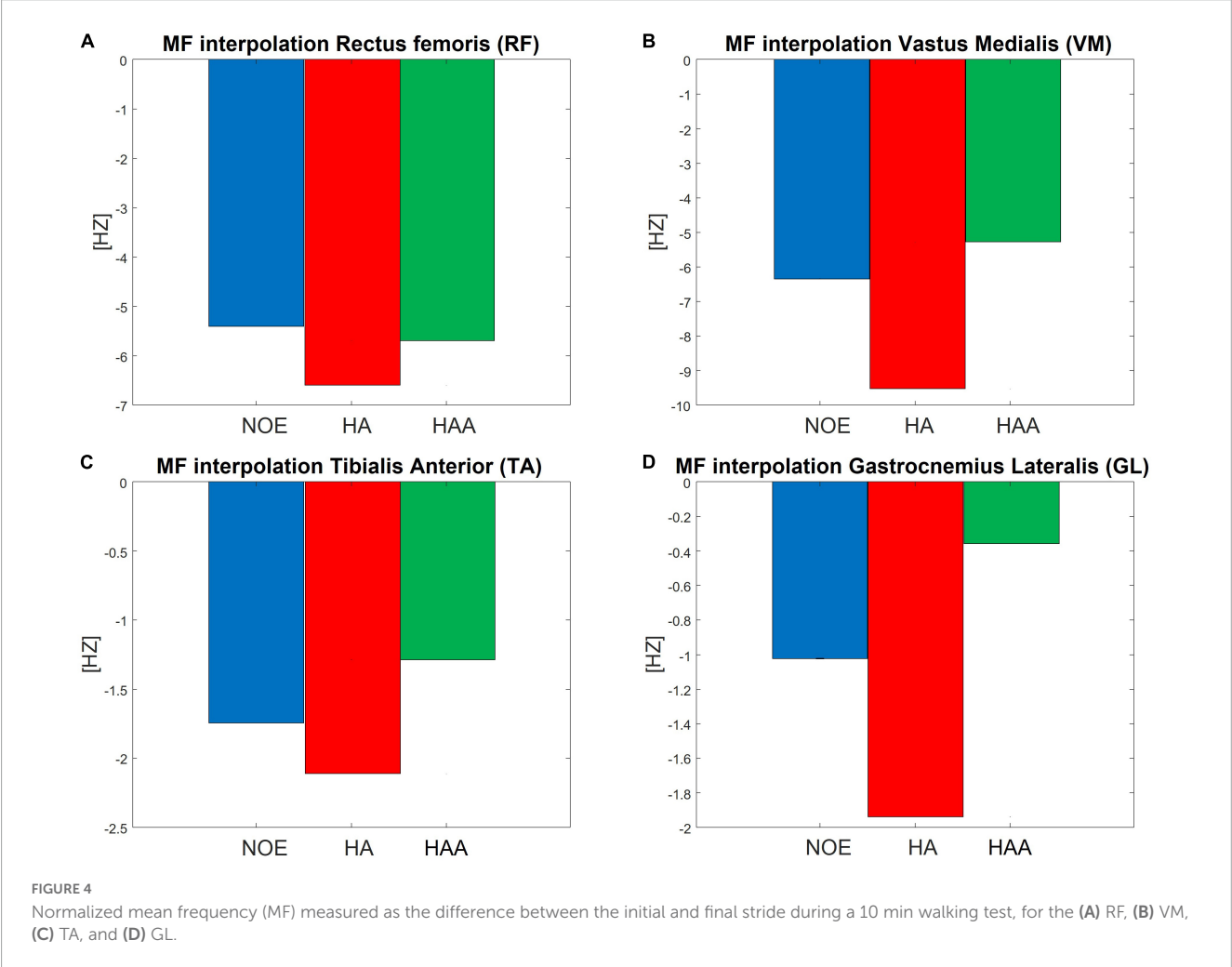


TABLE 3 Comparison on the 5 days average of the relative reduction of MF for the HA and HAA strategies with respect to the baseline (NOE).

	Absolute difference of MF (Hz)	Relative difference of MF (%)
HA vs. NOE @ Rectus femoris (RF)	1.2	1.5
HA vs. NOE @ Vastus medialis (VM)	3.2	4.3
HA vs. NOE @ Tibialis anterior (TA)	0.4	0.5
HA vs. NOE @ Gastrocnemius lateralis (GL)	0.9	1.1
HAA vs. NOE @ Rectus femoris (RF)	0.3	0.4
HAA vs. NOE @ Vastus medialis (VM)	−1.1	−1.5
HAA vs. NOE @ Tibialis anterior (TA)	−0.5	−0.6
HAA vs. NOE @ Gastrocnemius lateralis (GL)	−0.7	−0.8

Positive values correspond to an increase in muscular fatigue, while negative values indicate a reduction in fatigue.

sides of the body during 10 min of consecutive striding for the ankle, knee, and hip, respectively. Biomechanical consideration of the averaged modification in the behavior of joint angles due to the use of the HA assistive modality shows a slight reduction in both hip flexion ($2.24^{\circ} \pm 7.4^{\circ}$ between 85 and 100% of the gait cycle) and hip extension ($1.4^{\circ} \pm 8.17^{\circ}$ from 50 to 70% of the gait

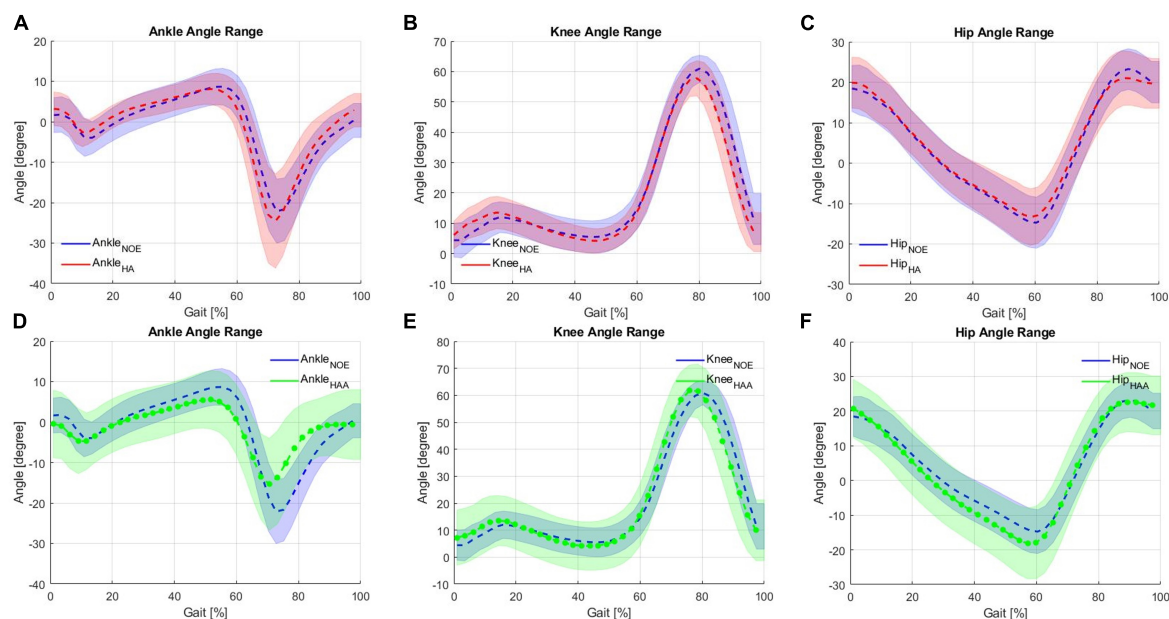


FIGURE 5

Kinematic analysis comparison on the Hips-assistance (HA) modality for the (A) ankle, (B) knee and (C) hip against baseline during walking on a treadmill, and Hips-Ankles-assistance (HAA) modality for the (D) ankle, (E) knee and (F) hip.

cycle) during the late swing and stance phases, respectively, shown in **Figure 5C**. The exosuit with HA modality reduces the extension by about $3.63^\circ \pm 7.85^\circ$. This is due to the force generated by the exoskeleton while raising the leg and approaching the swing phase. Consequently, to elongate the ET of the QPA at the beginning of the stance phase, the hip extension is then increased. Hence, the user compensates for this reduction in extension by increasing flexion. The plots for the knee and ankle show similar effects when using the HA modality (shown in **Figures 5A-B**). The ankle angle, specifically dorsiflexion, increases from 0 to 30% of the gait cycle by $1.57^\circ \pm 5.98^\circ$. From 50 to 70% of the gait cycle, plantarflexion is also increased by $2.46^\circ \pm 14.33^\circ$ showing an overall increase in RoM of $1.88^\circ \pm 14.26^\circ$ when compared to the baseline. The knee flexion angle is reduced by about $3.17^\circ \pm 6.59^\circ$ during late swing (70–100% of the gait cycle), while the RoM is also reduced by approximately $2.96^\circ \pm 7.4^\circ$.

These changes in the angular displacements, which are very little (varying from 1.5 to 3.5° approximately of the knees and ankles), underline the fact that, due to the exchange of forces with the exosuit, the walking pattern of the user has been slightly modified. Considering these as compensatory effects, the changes in ROMs are almost negligible compared to natural variations. Moreover, the first external force encountered by the user during the initial part of the gait cycle is in the opposite direction to the user's motion, which is required to elongate the ET. This force causes the user to compensate slightly for the interference created by the ET by varying the RoM of all three articulations. The ankle shows an increase in the RoM of approximately 6.1%, the knee shows a reduction in RoM of 5.2%, and the hip also indicates a decrease of the RoM of 9.6%. A slight reduction in the RoM of all three articulations is desirable, meaning that the assistance does not significantly affect the natural movement.

5.3.2. HAA: hips-ankles-assistance strategy kinematic analysis

In this section, the HAA strategy is assessed against baselines. **Figures 5D-F** shows the joint angle displacements compared to the configuration when the exoskeleton is not worn (NOE). Use of the HAA strategy causes decreased dorsiflexion (this effect is visible from 30 to 70% of the gait cycle) of $3.18^\circ \pm 9.47^\circ$ and reduced plantarflexion of $6.73^\circ \pm 11.63^\circ$, from 70 to 95% of the gait cycle shown in **Figure 5D**. This behavior shows an overall relative reduction of 32.2% in the RoM and an absolute ankle angle variation of $9.9^\circ \pm 13.5^\circ$ over an average baseline range of 30.75° . **Figure 5E** shows the knee angle trend. The initial angle during extension and flexion is slightly increased by approximately $2.83^\circ \pm 11.64^\circ$ during the extension phase at 0–20% of the gait cycle and by approximately $0.75^\circ \pm 9.27^\circ$ during the flexion phase (60–80% of the gait cycle). For the hip angle, a slight shift of the hip extension (from 10 to 65% of the gait cycle) generates an increase of $3.4^\circ \pm 10.76^\circ$ shown in **Figure 5F**. The knee shows a relative reduction in the RoM of 1.86%, and the hip shows a reduction in RoM of 7.3%. These changes in angular displacements, particularly for the ankles, underline a certain degree of unwanted influence and compensatory effects arising from the external forces generated by the exosuit (i.e., forces required to elongate the ETs). This effect is more pronounced on the ankle, where there is an RoM reduction of about 32%, with an average range of 20.8° [residual RoM of 68% concerning the baseline, which is just at the limit to be acceptable before being considered as a pathologic pattern (Bonney and Armand, 2015; Serrao et al., 2017)]. On the other hand, both the hip and the knee trends show a small increase in RoM. This configuration reports a small variation of the RoM, thus not significantly affecting the natural movement.

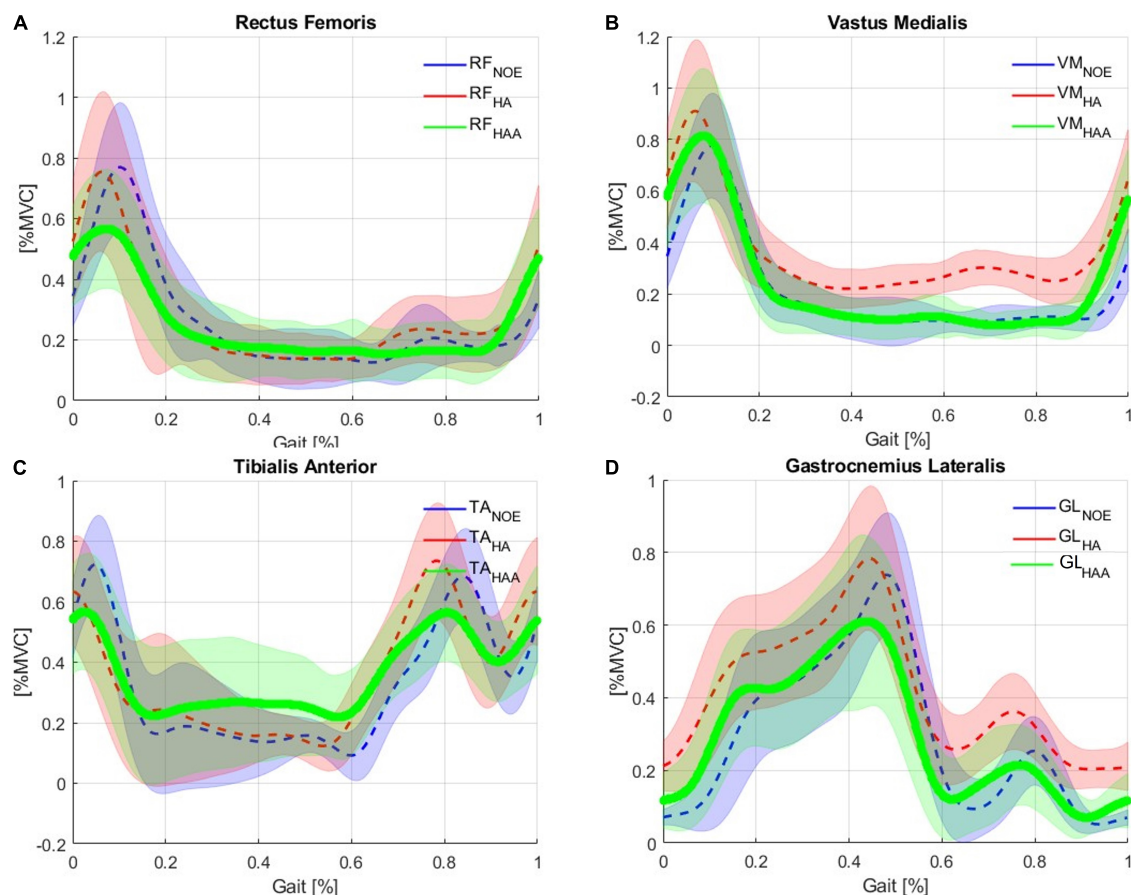


FIGURE 6 Comparison of Baseline vs. Hips-assistance (HA) and Hips-Ankles-assistance (HAA) modality of the muscle activations of the (A) RF, (B) VM, (C) TA, and (D) GL.

5.4. HA and HAA assistance strategies comparison on the muscular analysis

5.4.1. HA: hips-assistance strategy muscular analysis

Figures 6A–D shows the muscular activation of the RF, VM, TA, and GL, respectively. All the plots are segmented and averaged over each gait cycle. Figure 6 shows the data for the muscle activation averaged over approximately 600 right and left gait cycles for each of the five runs. As expected, the measurements of muscle activation and joint angles are comparable with the normal average behavior of the state-of-the-art available data as in Winter (2009). All baselines are reported in blue in Figure 6. The effects of using this exosuit, with QPA and the HA strategy, are evaluated and compared against the baseline, with the baseline shown in blue and red representing the exosuit with the HA strategy. When the muscle activity of the HA-assisted device is lower than the baseline, this means that only a small amount of muscle activity is required for that specific portion of the gait phase due to the direct assistance provided by the exosuit, or eventual positive synergetic effects from interactions between muscle activations and different walking patterns. More effort is required for that specific gait section with higher muscle activity than the baseline. This effort could be associated with the storing phases (elongation of the ET)

or possible indirect compensations arising from changes in the walking pattern. Moreover, the muscular trends show a temporal shift in the muscle activation of about 8% of the gait cycle compared to the baseline. The main numerical results are reported in Table 4.

5.4.2. HA: hips-ankles-assistance strategy muscular analysis

Figures 6A–D shows the muscular activation of the RF, VM, TA, and GL, respectively. Comparing the HAA strategy against the baseline shows a temporal shift in the muscle activation of about 5% of the gait cycle. The characteristic maximum for each of the four muscles occurs earlier in their respective gait cycles. The main numerical results are reported in Table 5.

5.5. HA and HAA muscular analysis comparison: relative assistance and resistance

To quantify and compare the assistance and resistance effects, shown in Figure 6, the average trends of muscle activity associated with the HA and HAA have been subtracted from the baseline and normalized against the maximum muscle variation across all the tests. Positive and negative relative variations of muscle activities

TABLE 4 Muscles assistance and resistance of the HA as comparison with the baseline (NOE).

Muscle	Assistance: portion of gait cycle (%)	Assistance (%MVE)	Resistance: portion of gait cycle (%)	Resistance (%MVE)
Rectus femoris (RF)	10–40	7.6 ± 15.8	60–100, and 0–10	5.2 ± 16.4
Vastus medialis (VM)	10–20	5.9 ± 20.3	20–10	16.3 ± 16.9
Tibialis anterior (TA)	0–15, and 80–90	11.0 ± 18.4	15–80	8.9 ± 13.8
Gastrocnemius lateralis (GL)	50–60	7.1 ± 17.5	60–50	14.1 ± 12.5

TABLE 5 Muscles assistance and resistance of the HAA as comparison with the baseline (NOE).

Muscle	Assistance: portion of gait cycle (%)	Assistance (%MVE)	Resistance: portion of gait cycle (%)	Resistance (%MVE)
Rectus femoris (RF)	5–30	7.7 ± 16.5	40–70, and 90–100	4.3 ± 9.8
Vastus medialis (VM)	15–30	2.1 ± 9.1	90–15	6.1 ± 16.9
Tibialis anterior (TA)	0–15, and 70–90	11.3 ± 17.7	20–70	9.4 ± 14.6
Gastrocnemius lateralis (GL)	40–60	9.1 ± 13.7	90–20	4.6 ± 11.1

of the HA and HAA strategies for each muscle are separately computed to estimate the relative assistance and resistance. Assistance is when the muscle activity is below the reference baseline, and the resistive phase is when the muscle activity is higher than the baseline. The difference in muscle activity compared to the baseline is averaged and normalized concerning the mean value of the selected baseline section. Then, the result is normalized over the ratio between the time portion of both assistive and resistive phases and the whole averaged gait time. The barplot in **Figure 7** represents, with negative values, the muscle activity that the user must provide to store energy in the exosuit (to elongate the ETs).

In contrast, the positive part of the barplot represents the assistance provided by the exosuit and reduces muscle activation. Positive assistance and negative resistance values are generated by comparing the muscle activation of the specific muscle and control strategy against the baseline. The comparison is calculated at the specific interval of the gait cycle, as reported in **Tables 4, 5** for HA and HAA, respectively. The percentage of resistance and assistance is derived as a difference between the baseline muscle activity and specific control strategy and then normalized on the baseline value. The system aids 10.0% and a resistance of 11.1% for the RF in the HA configuration. The VM shows assistance of 2.2% against the resistance of 65.5%. The TA shows assistance of 9.8% with a resistance of 19.1%, and the GL shows assistance of 2.4% and a resistance of 41.4%. The system assists 12.5% with a resistance of 6.5% for the RF in the HAA configuration. The VM shows assistance of 5.7% and a resistance of 11.4%. The TA shows assistance of 9.2% against the resistance of 21.4%, and the GL shows assistance of 10.7% against the resistance of 9.5%. When considering the improvement from the HA to the HAA modality, the resistance is reduced by 47%. This reduction is calculated as the difference of each resistance measured at the four muscles for each modality (HA and HAA). Then the differences are normalized over the resistance measured for the HA mode. It is important to underline that even if the energy can neither be created nor destroyed, the energy stored in the ETs generates unbalanced resistive and assistive effects on the muscles. This is closely correlated to the behavior of the human biomechanical

system and the fact that humans can react differently during specific gait phases, in some instances extracting or injecting energy (Di Natali et al., 2019, 2020; Fanti et al., 2022).

6. Discussion

The functionality of the QPA requires an important interaction between the user and the exosuit. This interaction is characterized by a continuous mechanical energy exchange between the wearer's biomechanical system and the actuators' ETs. Due to the high complexity of the human system, it is not too obvious that adding multiple actuators would generate a higher assistive impact. We demonstrated in previous studies that the same exosuit platform could generate assistance by reducing the torque and mechanical power of the wearer (Di Natali et al., 2020). Still, also it could provide just resistance for specific muscle training (Di Natali et al., 2021). Finally, this work (Fanti et al., 2022) shows an oscillation of both muscle activity and mechanical power about the reference signals, thus, underlying complex behaviors of the whole system composed of wearer and exosuit. These results are a function of specific assistance strategies such as actuation placement and control timing. Therefore, in this study, a comprehensive analysis of metabolic cost, muscle fatigue, muscle activity and kinematic patterns has been conducted to provide a clear view of what is happening during the interaction with the exosuit.

The detailed analysis of the performance of the exosuit shows a reduction in the metabolic cost in user fatigue using both exosuit configurations, generating better performance with the HAA. For the muscle fatigue data, we see that the fatigue is strongly reduced for the HAA configuration, but this was not found with the HA setup. The seemingly conflicting results prompted further investigation with more attention on muscle activation and kinematic analysis. The detailed muscle activation analysis showed that the four main muscles involved are sensitive to the actuation configuration. Causing a more (or less) effective net reduction in muscular activity when compared against the baseline, as shown in **Figures 6, 7**. Thus, both assistive and resistive phases, measured in all four muscles during the gait cycle, are strongly correlated

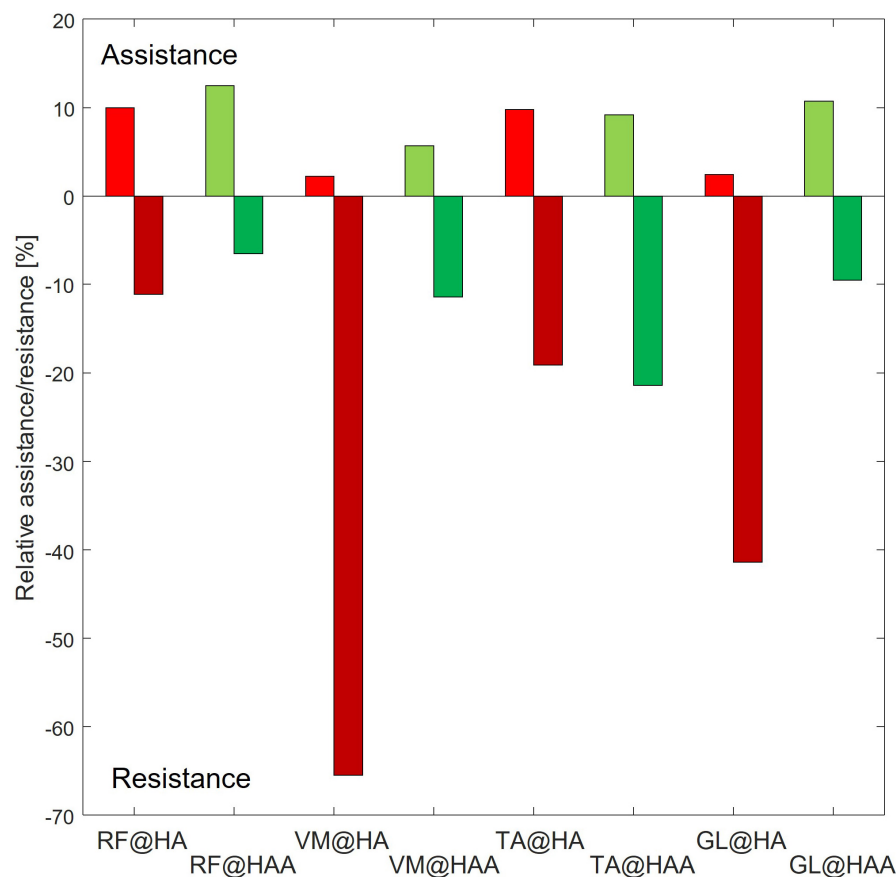


FIGURE 7

Relative assistance and resistance for each of the assessed muscles [rectus femoris (RF), vastus medialis (VM), tibialis anterior (TA), and gastrocnemius lateralis (GL)] at specific assistive configuration.

to the selected configuration. This suggests that synergetic and compensatory effects occur even if a specific control strategy at the muscle level reduces metabolic cost. Thus, it is critical to evaluate the interaction between exoskeletons and exosuit, focusing on several indexes as shown in this study. A more comprehensive analysis is necessary to assess particular side effects generated while modifying the complex balance of human motion. Therefore, when considering the full complexity of the compensatory and synergetic effects, results show that assistance applied by an exosuit might partially guarantee advantages. Moreover, the interaction between the assistive device and the whole body must be studied, analyzed, and understood. In addition, a more biomimetic control approach can generate advanced performances with reduced compensatory effects, as shown in this work when using the HAA and HA control strategies.

With this study, we want also to underline the evidence of the compensatory effects, which are shown in [Figures 6, 7](#). This is particularly evident for the VM and the GL, where a more biomimetic controller (the HAA) reduces the compensatory effects. By comparing the HAA and the HA configurations, we noticed an increment of the assistance rather than the resistive effect. This, however, is not valid when considering the TA. Indeed, there is a slight worsening (from the HA to the HAA) of both assistive and resistive effects. The TA suffers if both actuators are applied bilaterally to the hip flexion and the ankle plantarflexion. This

actuation strategy generates compensatory behaviors, modifying the standard muscular activation pattern. The development of modified control strategies that seek to address this effect will form part of future work in this area.

6.1. Discussion on the metabolic energy consumption

The principal objective was to evaluate the effective reduction of metabolic expenditure in both the HA and HAA exosuit configurations. The results, reported in [Table 2](#), show a net reduction of metabolic expenditure for both configurations concerning the baseline (NOE). Despite the added weight of the device and the interaction with the exosuit, the HA reduces 5% of the total metabolic cost, while the HAA reduces about 8%. The HAA configuration strategy performs 1.55 times better than the HA configuration when considering the metabolic cost. In other words, taking advance of the work of [Rafiq et al. \(2017\)](#), it is possible to derive a simple linear equation from the following points: a walking speed of 4 km/h requires 2.9 MET. A walking speed of 1.7 km/h requires 2.3 MET. The equation is as follows: $y = a * x + b$. Where y is the MET and x is the speed, while $a = 0.26$ and $b = 1.86$. Therefore, if we substitute the metabolic cost found

for the NOE and the HAA we can solve the equation for the hypothetical walking speed (x). The hypothetical walking speed of the NOE modality is 2.8 km/h, while the hypothetical walking speed for the HAA modality is 2 km/h. This underlines the fact that even an improvement of a few percentage points, such as is seen comparing HA to HAA, strongly impacts the reduction in metabolic consumption.

6.2. Discussion on the muscle fatigue analysis

The results obtained from the analysis of the MF do not confirm the study on metabolic consumption. In particular, the HA strategy does reduce the metabolic cost but increases muscle fatigue, while the HAA strategy reduces both the metabolic cost and muscle fatigue. This effect arises because, in HA, the lower part of the leg muscle involved in controlling the knee and ankle is required to work more. This happens mainly during the elongation of the elastic band. We see from [Figure 6](#) that the tibialis and gastrocnemius activate more than the baseline. This is particularly evident for the gastrocnemius during the period of the gait cycle when the elastic tendon is elongating (from 5 to 55%).

On the other hand, for the tibialis, the compensation (higher muscular activation than baseline) occurs during the assistance phase (60–65%), thus showing a counter effect, which could be necessary to improve balance. These results do confirm that the HAA configuration performs better than the HA arrangement ([Table 3](#)). Indeed, only the HAA generates an effective advantage on the user's energy balance.

The results confirm that the design of the assistive strategies must consider muscle synergies. When considering the HA configuration, where a single bilateral QPA is applied to the hip flexion, this assistive configuration is enough to counter the additional weight of the device and, at the same time, reduce metabolic expenditure. While the HAA configuration, which has two bilateral QPAs (hips flexion and ankles plantarflexion), performs better also, reducing muscle fatigue in three of the four assessed muscles.

6.3. Discussion on the muscle pattern analysis of the HA and HAA

The muscle activation of RF, VM, TA, and GL are evaluated during the walking task to quantify the energy exchange for both exosuit configurations. The results show that the control configuration strongly affects the muscle pattern during walking. Moreover, different control configurations, particularly this type of QPA, involve a high degree of human-robot interaction and flow of energy exchange, leading to diverse muscle activity trends, with more marked increases and decreases with respect to the baseline ([Figures 6, 7](#)).

The results show in both configurations (HA and HAA) the generation of different effects during distinct phases of the gait cycle due to the sequence of resistive and assistive phases. Therefore, the controller must be well-designed/tuned regarding actuation timing ([Di Natali et al., 2020](#)) and actuation configuration. When

comparing the HA and HAA configurations, the HAA performs better than the HA in RF, VM, and GL by increasing the assistance and decreasing the resistance ([Figures 6, 7](#)). Focusing on the normalized and weighted RF activity for both the HA (assistance of 10%, resistance of 11%), and the HAA (assistance of 12.5%, resistance of 6.5%), show that a more biomimetic assistive configuration (i.e., HAA) enhance the assistive effects at the expenses of the resistive once. Thus, the HAA provides better performance than the HA configuration. Even though the result is slight, the HA affects the balance between the assistive and the resistive effects on the RF. This has unwanted impacts on the VM, TS, and GL, with considerable resistance effects. The side effects on the VM and the GL are strongly reduced by introducing assistance for the ankle plantarflexion (as in the HAA). In the HA, the normalized and weighted VM activity (assistance of 2.2%, resistance of 65.5%) and for the GL (assistance of 2.4%, resistance of 41.4) show an equilibrium shifted toward the resistive effect when compared with the HAA (VM assistance of 5.7%, resistance of 11.4%, and GL assistance of 10.7%, resistance of 9.5%). For the TA (mostly activated during ankle dorsiflexion and providing balance), we noticed that both configurations cause similar effects, with the resistance effect being more marked (assistance of about 9.5%, resistance of about 20%). We can assume that the walking pattern is modified for both configurations. Thus, unwanted effects and compensatory behaviors have to be counteracted.

This analysis demonstrates that when the actuation strategy is designed accordingly with muscle synergy, as in the HAA, efficiency increments due to augmentation of the assistance and a reduction in the resistive effects are more evident (particularly for the RF and the GL). On the other hand, the undesirable effects on the TA could lead to rethinking the actuation strategy and timing to reduce the side effects.

7. Conclusion and future works

This study compares two assistive strategies applied at hips and ankles employing QPAs integrated on the XoSoft exosuit, particularly vital as motions of the hip and ankle are considered important in assisting the elderly with walking and may ultimately be useful in reducing or even preventing falls. Hence, this work suggests that this exosuit may provide immediate improvements in walking performance by reducing muscle fatigue and metabolic expenditure. This makes this a very promising approach that could have essential benefits in activities of daily living for the elderly.

The investigation also evaluates the effective muscular reduction as a net balance between the storage and release phases for both exosuit configurations. Also importantly, side effects on the walking pattern and muscle activation due to the wearing of an external device are found to be strongly reduced on the VM when using the HAA configuration. At the same time with the TA, compensatory behaviors in both control configurations were found to be negligible. This analysis underlines the importance of a biomimetic assistive strategy to improve results and reduce compensatory actions.

Finally, by investigating how healthy subjects respond to the assistance provided by the QPA-powered exosuit, this study serves to define the technology's potential for improving mobility and

enabling future potential rehabilitation benefits. In fact, not only could the net assistance be used to enhance activities of daily living or rehabilitation, but it may also be possible to take advantage of the resistive phase of each QPA to train muscles in specific gait phases or generate established controlled compensatory effects. Future work will evaluate the impact on inexperienced subjects and the relevance of the learning curve.

The highly encouraging results from this study will drive further investigations in a broader population (particularly the elderly and those suffering from gait disorders with low level mobility impairments) and studies into compensatory behaviors that arise when assisted by different actuation strategies.

Data availability statement

The raw data supporting the conclusions of this article will be made available by the authors, without undue reservation.

Ethics statement

The studies involving human participants were reviewed and approved by the Ethical Committee of Liguria. The patients/participants provided their written informed consent to participate in this study. Written informed consent was obtained from the individual(s) for the publication of any potentially identifiable images or data included in this article.

Author contributions

CD contributed to the conception and design of the study and conduction of the experimental section and contributed on

the manuscript drafting. All authors contributed to manuscript revision, read, and approved the submitted version.

Funding

This work has received funding from the European Union's Horizon 2020 framework program for research and innovation under grant agreement no. 688175.

Acknowledgments

The authors thank the XoSoft project consortium for the collaboration and the results achieved during the project.

Conflict of interest

The authors declare that the research was conducted in the absence of any commercial or financial relationships that could be construed as a potential conflict of interest.

Publisher's note

All claims expressed in this article are solely those of the authors and do not necessarily represent those of their affiliated organizations, or those of the publisher, the editors and the reviewers. Any product that may be evaluated in this article, or claim that may be made by its manufacturer, is not guaranteed or endorsed by the publisher.

References

- Afzal, T., Tseng, S.-C., Lincoln, J. A., Kern, M., Francisco, G. E., and Chang, S.-H. (2020). Exoskeleton-assisted gait training in persons with multiple sclerosis: A single-group pilot study. *Arch. Phys. Med. Rehabil.* 101, 599–606. doi: 10.1016/j.apmr.2019.10.192
- Alexander, N. B., Taffet, G. E., Horne, F. M., Eldadah, B. A., Ferrucci, L., Nayfield, S., et al. (2010). Bedside-to-bench conference: research agenda for idiopathic fatigue and aging. *J. Am. Geriatr. Soc.* 58, 967–975. doi: 10.1111/j.1532-5415.2010.02811.x
- Ament, W., Bonga, G. J., Hof, A. L., and Verkerke, G. J. (1993). EMG median power frequency in an exhausting exercise. *J. Electromyogr. Kinesiol.* 3, 214–220. doi: 10.1016/1050-6411(93)90010-T
- Asbeck, A. T., Dyer, R. J., Larusson, A. F., and Walsh, C. J. (2013). "Biologically-inspired soft exosuit," in *Proceedings of the 2013 IEEE 13th International Conference on Rehabilitation Robotics (ICORR)*, (Seattle, WA: IEEE), 1–8. doi: 10.1109/ICORR.2013.6650455
- Asbeck, A. T., Schmidt, K., and Walsh, C. J. (2015). Soft exosuit for hip assistance. *Robot. Auton. Syst.* 73, 102–110. doi: 10.1016/j.robot.2014.09.025
- Awad, L. N., Bae, J., O'donnell, K., De Rossi, S. M., Hendron, K., Slood, L. H., et al. (2017). A soft robotic exosuit improves walking in patients after stroke. *Sci. Transl. Med.* 9:eaa19084. doi: 10.1126/scitranslmed.aai9084
- Barbero, M., Merletti, R., and Rainoldi, A. (2012). *Atlas of muscle innervation zones: understanding surface electromyography and its applications*. Berlin: Springer Science & Business Media. doi: 10.1007/978-88-470-2463-2
- Bonnefoy, A., and Armand, S. (2015). "Normal gait," in *Orthopedic management of children with cerebral palsy: A comprehensive approach* (Hauppauge, NY: Nova Science Publishers Inc), 567.
- Cifrek, M., Medved, V., Tonković, S., and Ostojić, S. J. C. B. (2009). Surface EMG based muscle fatigue evaluation in biomechanics. *Clin. Biomech.* 24, 327–340. doi: 10.1016/j.clinbiomech.2009.01.010
- Colley, R. C., Garriguet, D., Janssen, I., Craig, C. L., Clarke, J., and Tremblay, M. S. (2011). Physical activity of Canadian adults: accelerometer results from the 2007 to 2009 Canadian Health Measures Survey. *Health Rep.* 22:7. doi: 10.1016/j.yspm.2011.03.006
- Collins, S. H., Wiggin, M. B., and Sawicki, G. S. (2015). Reducing the energy cost of human walking using an unpowered exoskeleton. *Nature* 522, 212–215. doi: 10.1038/nature14288
- DeVita, P., and Hortobagyi, T. (2000). Age causes a redistribution of joint torques and powers during gait. *J. Appl. Physiol.* 88, 1804–1811. doi: 10.1152/jappl.2000.88.5.1804
- Di Natali, C., Chini, G., Totaro, M., Lora-Millán, J. S., Rocon, E., Beccai, L., et al. (2021). Quasi-passive resistive exosuit for space activities: proof of concept. *Appl. Sci.* 11:3576. doi: 10.3390/app11083576
- Di Natali, C., Poliero, T., Sposito, M., Graf, E., Bauer, C., Pauli, C., et al. (2019). Design and evaluation of a soft assistive lower limb exoskeleton. *Robotica* 37, 2014–2034. doi: 10.1017/S0263574719000067

- Di Natali, C., Sadeghi, A., Mondini, A., Bottenberg, E., Hartigan, B., De Eyto, A., et al. (2020). Pneumatic quasi-passive actuation for soft assistive lower limbs exoskeleton. *Front. Neurobot.* 14:31. doi: 10.3389/fnbot.2020.00031
- Dimitrov, G. V., Arabadzhev, T. I., Mileva, K. N., Bowtell, J. L., Crichton, N., and Dimitrova, N. A. (2006). Muscle fatigue during dynamic contractions assessed by new spectral indices. *Med. Sci. Sports Exerc.* 38:1971. doi: 10.1249/01.mss.0000233794.31659.6d
- Ding, Y., Galiana, I., Asbeck, A., Quinlivan, B., De Rossi, S. M. M., and Walsh, C. (2014). "Multi-joint actuation platform for lower extremity soft exosuits," in *Proceedings of the 2014 IEEE International Conference on Robotics and Automation (ICRA)*, (Hong Kong: IEEE), 1327–1334. doi: 10.1109/ICRA.2014.6907024
- Dollar, A. M., and Herr, H. (2008). Lower extremity exoskeletons and active orthoses: challenges and state-of-the-art. *IEEE Trans. Robot.* 24, 144–158. doi: 10.1109/TRO.2008.915453
- Dunn, A. L., Andersen, R. E., and Jakicic, J. M. (1998). Lifestyle physical activity interventions: history, short- and long-term effects, and recommendations. *Am. J. Prev. Med.* 15, 398–412. doi: 10.1016/S0749-3797(98)00084-1
- Fanti, V., Sanguineti, V., Caldwell, D., Ortiz, J., and Di Natali, C. (2022). Assessment methodology for human-exoskeleton interactions: kinetic analysis based on muscle activation. *Front. Neurobot.* 16:982950. doi: 10.3389/fnbot.2022.982950
- Fiser, W. M., Hays, N. P., Rogers, S. C., Kajkenova, O., Williams, A. E., Evans, C. M., et al. (2010). Energetics of walking in elderly people: factors related to gait speed. *J. Gerontol. Ser. A Biomed. Sci. Med. Sci.* 65, 1332–1337. doi: 10.1093/gerona/gdq137
- Galle, S., Derave, W., Bossuyt, F., Calders, P., Malcolm, P., and De Clercq, D. (2017). Exoskeleton plantarflexion assistance for elderly. *Gait Posture* 52, 183–188. doi: 10.1016/j.gaitpost.2016.11.040
- Ghasemi, A., and Zahediasl, S. (2012). Normality tests for statistical analysis: a guide for non-statisticians. *Int. J. Endocrinol. Metab.* 10:486. doi: 10.5812/ijem.3505
- Goedeker, J. H., Gibson, A. S. C., Grobler, L., Collins, M., Noakes, T. D., and Lambert, E. V. (2000). Determinants of the variability in respiratory exchange ratio at rest and during exercise in trained athletes. *Am. J. Physiol. Endocrinol. Metab.* 279, E1325–E1334. doi: 10.1152/ajpendo.2000.279.6.E1325
- Goldfarb, M., Lawson, B. E., and Shultz, A. H. (2013). Realizing the promise of robotic leg prostheses. *Sci. Transl. Med.* 5:210815. doi: 10.1126/scitranslmed.3007312
- Grood, E. S., and Suntay, W. J. (1983). A joint coordinate system for the clinical description of three-dimensional motions: application to the knee. *J. Biomech. Eng.* 105, 136–144. doi: 10.1115/1.3138397
- Haufe, F. L., Kober, A. M., Schmidt, K., Sancho-Puchades, A., Duarte, J. E., Wolf, P., et al. (2019). User-driven walking assistance: first experimental results using the MyoSuit. *IEEE Int. Conf. Rehabil. Robot.* 2019, 944–949. doi: 10.1109/ICORR.2019.8779375
- Hermens, H. J., Freriks, B., Disselhorst-Klug, C., and Rau, G. (2000). Development of recommendations for SEMG sensors and sensor placement procedures. *J. Electromyogr. Kinesiol.* 10, 361–374. doi: 10.1016/S1050-6411(00)00027-4
- Jansson, E. (1982). On the significance of the respiratory exchange ratio after different diets during exercise in man. *Acta Physiol. Scand.* 114, 103–110. doi: 10.1111/j.1748-1716.1982.tb06958.x
- Jin, S., Iwamoto, N., Hashimoto, K., and Yamamoto, M. (2016). Experimental evaluation of energy efficiency for a soft wearable robotic suit. *IEEE Trans. Neural Syst. Rehabil. Eng.* 25, 1192–1201. doi: 10.1109/TNSRE.2016.2613886
- Jutai, J., Coulson, S., Teasell, R., Bayley, M., Garland, J., Mayo, N., et al. (2007). Mobility assistive device utilization in a prospective study of patients with first-ever stroke. *Arch. Phys. Med. Rehabil.* 88, 1268–1275. doi: 10.1016/j.apmr.2007.06.773
- McGibbon, C. A. (2003). Toward a better understanding of gait changes with age and disablement: neuromuscular adaptation. *Exerc. Sport Sci. Rev.* 31, 102–108. doi: 10.1097/00003677-200304000-00009
- Moreno, J. C., Brunetti, F., Navarro, E., Forner-Cordero, A., and Pons, J. L. (2009). Analysis of the human interaction with a wearable lower-limb exoskeleton. *Appl. Bionics Biomech.* 6, 245–256. doi: 10.1155/2009/712530
- Ortiz, J., Dinatali, C., and Caldwell, D. G. (2021). *XoSoft: Design of a Novel Soft Modular Exoskeleton*. Amsterdam: Elsevier. doi: 10.1016/B978-0-12-818538-4.00006-X
- Rafiq, A., Sklyar, E., and Bella, J. N. (2017). Cardiac evaluation and monitoring of patients undergoing noncardiac surgery. *Health Serv. Insights* 10:1178632916686074. doi: 10.1177/1178632916686074
- Rahman, T., Sample, W., Jayakumar, S., King, M. M., Wee, J., Seliktar, R., et al. (2006). Passive exoskeletons for assisting limb movement. *J. Rehabil. Res. Dev.* 43:583. doi: 10.1682/JRRD.2005.04.0070
- Rejeski, W. J., and Mihalko, S. L. (2001). Physical activity and quality of life in older adults. *J. Gerontol. A Biol. Sci. Med. Sci.* 56, 23–35. doi: 10.1093/gerona/56.suppl_2.23
- Richardson, C. A., Glynn, N. W., Ferrucci, L. G., and Mackey, D. C. (2015). Walking energetics, fatigability, and fatigue in older adults: the study of energy and aging pilot. *J. Gerontol. A Biol. Sci. Med. Sci.* 70, 487–494. doi: 10.1093/gerona/glu146
- Rosenbloom, S. (1988). "The mobility needs of the elderly," in *Paper presented by special report 218: transportation in an aging society: improving mobility and safety for older persons: technical papers*, Vol. 2, (Washington, DC: National Research Council), 21–71.
- Sadeghi, A., Mondini, A., and Mazzolai, B. (2019). A vacuum powered soft textile-based clutch. *Actuators* 8:47. doi: 10.3390/act8020047
- Schrack, J. A., Simonsick, E. M., and Ferrucci, L. (2010). The energetic pathway to mobility loss: an emerging new framework for longitudinal studies on aging. *J. Am. Geriatr. Soc.* 58, S329–S336. doi: 10.1111/j.1532-5415.2010.02913.x
- Serrao, M., Chini, G., Casali, C., Conte, C., Rinaldi, M., Ranavolo, A., et al. (2017). Progression of gait ataxia in patients with degenerative cerebellar disorders: a 4-year follow-up study. *Cerebellum* 16, 629–637. doi: 10.1007/s12311-016-0837-2
- Shamaei, K., Cenciarini, M., Adams, A. A., Gregorczyk, K. N., Schiffman, J. M., and Dollar, A. M. (2014). Design and evaluation of a quasi-passive knee exoskeleton for investigation of motor adaptation in lower extremity joints. *IEEE Trans. Biomed. Eng.* 61, 1809–1821. doi: 10.1109/TBME.2014.2307698
- Shumway-Cook, A., Ciol, M. A., Yorkston, K. M., Hoffman, J. M., and Chan, L. (2005). Mobility limitations in the Medicare population: prevalence and sociodemographic and clinical correlates. *J. Am. Geriatr. Soc.* 53, 1217–1221. doi: 10.1111/j.1532-5415.2005.53372.x
- Sposito, M., Poliero, T., Di Natali, C., Ortiz, J., Pauli, C., Graf, E., et al. (2018). "Evaluation of XoSoft Beta-1 lower limb exoskeleton on a post stroke patient," in *Proceedings of the sixth national congress of bioengineering, Milan, Italy, 25-27 June 2018*, (Milan).
- Theurel, J., and Desbrosses, K. J. (2019). Occupational exoskeletons: overview of their benefits and limitations in preventing work-related musculoskeletal disorders. *IIEE Trans. Occup. Ergon. Hum. Factors* 7, 264–280. doi: 10.1080/24725838.2019.1638331
- Van Dijk, W., Van Der Kooij, H., and Hekman, E. (2011). "A passive exoskeleton with artificial tendons: design and experimental evaluation," in *Proceedings of the 2011 IEEE international conference on rehabilitation robotics*, (Zurich: IEEE), 1–6. doi: 10.1109/ICORR.2011.5975470
- Volkers, K. M., De Kieviet, J. F., Wittingen, H. P., and Scherder, E. J. (2012). Lower limb muscle strength (LLMS): why sedentary life should never start? A review. *Arch. Gerontol. Geriatr.* 54, 399–414. doi: 10.1016/j.archger.2011.04.018
- Waters, R. L., Hislop, H. J., Perry, J., Thomas, L., and Campbell, J. (1983). Comparative cost of walking in young and old adults. *J. Orthop. Res.* 1, 73–76. doi: 10.1002/jor.1100010110
- Wehner, M., Quinlivan, B., Aubin, P. M., Martinez-Villalpando, E., Baumann, M., Stirling, L., et al. (2013). "A lightweight soft exosuit for gait assistance," in *Proceedings of the 2013 IEEE international conference on robotics and automation*, (Karlsruhe: IEEE), 3362–3369. doi: 10.1109/ICRA.2013.6631046
- Winter, D. A. (2009). *Biomechanics and motor control of human movement*. New York, NY: John Wiley & Sons. doi: 10.1002/9780470549148
- World Health Organization [WHO]. (2015). *World report on ageing and health*. Geneva: World Health Organization.
- Zhang, J., Fiers, P., Witte, K. A., Jackson, R. W., Poggensee, K. L., Atkeson, C. G., et al. (2017). Human-in-the-loop optimization of exoskeleton assistance during walking. *Science* 356, 1280–1284. doi: 10.1126/science.aal5054
- Zhou, L., Chen, W., Chen, W., Bai, S., Zhang, J., and Wang, J. (2020). Design of a passive lower limb exoskeleton for walking assistance with gravity compensation. *Mech. Mach. Theory* 150:103840. doi: 10.1016/j.mechmachtheory.2020.103840



OPEN ACCESS

EDITED BY

Alessandro Ridolfi,
University of Florence, Italy

REVIEWED BY

Jimena Quinzaños,
National Institute of Rehabilitation Luis
Guillermo Ibarra Ibarra, Mexico
Nicola Secciani,
University of Florence, Italy

*CORRESPONDENCE

Chiara Höhler
✉ choehler@schoen-klinik.de

[†]These authors share first authorship

RECEIVED 17 February 2023

ACCEPTED 12 May 2023

PUBLISHED 25 May 2023

CITATION

Höhler C, Wild L, de Crignis A, Jahn K and
Krewer C (2023) Contralaterally EMG-triggered
functional electrical stimulation during serious
gaming for upper limb stroke rehabilitation: a
feasibility study.
Front. Neurobot. 17:1168322.
doi: 10.3389/fnbot.2023.1168322

COPYRIGHT

© 2023 Höhler, Wild, de Crignis, Jahn and
Krewer. This is an open-access article
distributed under the terms of the [Creative
Commons Attribution License \(CC BY\)](#). The use,
distribution or reproduction in other forums is
permitted, provided the original author(s) and
the copyright owner(s) are credited and that
the original publication in this journal is cited, in
accordance with accepted academic practice.
No use, distribution or reproduction is
permitted which does not comply with these
terms.

Contralaterally EMG-triggered functional electrical stimulation during serious gaming for upper limb stroke rehabilitation: a feasibility study

Chiara Höhler^{1,2*†}, Laura Wild^{1†}, Alexandra de Crignis²,
Klaus Jahn^{2,3} and Carmen Krewer^{1,2}

¹Faculty of Sport and Health Science, Chair of Human Movement Science, Technical University Munich, Munich, Germany, ²Department of Neurology, Research Group, Schoen Clinic Bad Aibling, Bad Aibling, Germany, ³Ludwig-Maximilians University of Munich (LMU), German Center for Vertigo and Balance Disorders (DSGZ), Munich, Germany

Introduction: Virtual Reality/serious games (SG) and functional electrical stimulation (FES) therapies are used in upper limb stroke rehabilitation. A combination of both approaches seems to be beneficial for therapy success. The feasibility of a combination of SG and contralaterally EMG-triggered FES (SG+FES) was investigated as well as the characteristics of responders to such a therapy.

Materials and methods: In a randomized crossover trial, patients performed two gaming conditions: SG alone and SG+FES. Feasibility of the therapy system was assessed using the Intrinsic Motivation Inventory (IMI), the Nasa Task Load Index, and the System Usability Scale (SUS). Gaming parameters, fatigue level and a technical documentation was implemented for further information.

Results: In total, 18 patients after stroke (62.1 ± 14.1 years) with a unilateral paresis of the upper limb ($MRC \leq 4$) were analyzed in this study. Both conditions were perceived as feasible. Comparing the IMI scores between conditions, perceived competence was significantly increased ($z = -2.88$, $p = 0.004$) and pressure/tension during training ($z = -2.13$, $p = 0.034$) was decreased during SG+FES. Furthermore, the task load was rated significantly lower for the SG+FES condition ($z = -3.14$, $p = 0.002$), especially the physical demand ($z = -3.08$, $p = 0.002$), while the performance was rated better ($z = -2.59$, $p = 0.010$). Responses to the SUS and the perceived level of fatigue did not differ between conditions (SUS: $z = -0.79$, $p = 0.431$; fatigue: $z = 1.57$, $p = 0.115$). For patients with mild to moderate impairments (MRC 3–4) the combined therapy provided no or little gaming benefit. The additional use of contralaterally controlled FES (ccFES), however, enabled severely impaired patients (MRC 0–1) to play the SG.

Discussion: The combination of SG with ccFES is feasible and well-accepted among patients after stroke. It seems that the additional use of ccFES may be more beneficial for severely impaired patients as it enables the execution of the serious game. These findings provide valuable implications for the development of rehabilitation systems by combining different therapeutic interventions to increase patients' benefit and proposes system modifications for home use.

Clinical trial registration: <https://drks.de/search/en>, DRKS00025761.

KEYWORDS

virtual reality, neuromuscular stimulation, patient treatment, electromyography, hand recovery

1. Introduction

Due to demographic change, stroke is becoming more prevalent (Feigin et al., 2021). Worldwide, there are more than 10 million new cases each year, and more than 100 million people suffer from stroke sequelae. Stroke is the second leading cause of death and a major cause of disability (Feigin et al., 2021). Up to 40% of survivors have long-term limitations in activities of daily living (ADLs) and often rely on caregivers or are institutionalized (Luengo-Fernandez et al., 2013). Therefore, stroke is of immense public health relevance because of the burden it places on family members, the health care system, and society (Crichton et al., 2016).

A stroke often results in sudden onset of neurological symptoms like hemiparesis and hemihypesthesia, speech and visual problems, balance disturbances, and neuropsychological symptoms such as aphasia, apraxia, agnosia, and neglect. Symptoms depend on the brain area affected and usually involve a combination of several impairments. Survival probabilities after an ischemic stroke improved over the past decades (Rücker et al., 2020). Improvements in stroke management and treatment may have contributed to this. However, 15-years after stroke about one-third of survivors was living with a mild disability and one-third with a moderate or severe disability. The latter suffer long-term impairments in basic ADLs, such as dressing, and in performing instrumental ADLs such as preparing meals (Desrosiers et al., 2003; Crichton et al., 2016). Therefore, stroke survivors are often dependent on caregivers or are institutionalized (Luengo-Fernandez et al., 2013). Upper limb function is fundamental to ADLs and important for independence. Recovery of arm function is targeted by various rehabilitative intervention strategies with the overall goal of being less dependent in daily living (Desrosiers et al., 2003; Pollock et al., 2014; Platz, 2021). These intervention strategies are based on underlying mechanisms of neuroplasticity and principles of motor learning (Meier, 2021). Therefore, training has been shown to be effective for motor recovery when it is repetitive (Veerbeek et al., 2014; French et al., 2016), intensive (Pollock et al., 2014; Platz, 2021), task specific (Kleim and Jones, 2008; Veerbeek et al., 2014) and variable (Veerbeek et al., 2014; French et al., 2016). Moreover, feedback and motivation are also important for learning to be effective. The success of traditional therapies is limited and current rehabilitation methods often do not adequately incorporate evidence based on motor learning theories (Maier et al., 2019a). Therefore, new approaches are needed to address these problems. Both, functional electrical stimulation (FES) and Virtual Reality (VR)/serious gaming (SG) therapies are used in stroke rehabilitation (Pollock et al., 2014; Platz et al., 2020). Increasingly, the use of VR technologies in therapeutic interventions for neurorehabilitation is also being discussed and researched. VR technologies provide a multisensory environment that promotes brain neuroplasticity and thus contributes to the rehabilitation of motor disorders (Teo et al., 2016). Often, VR technological interventions incorporate elements of gamification to make therapy interesting and motivating (Dumas et al., 2021). Such games, which are used for education and rehabilitation purposes, are referred to as serious games (SG) (Dumas et al., 2021). Those are specifically designed to facilitate brain plasticity and recovery by incorporating principles of motor learning (Maier et al., 2019b) and provide the user with task-specific and repetitive

training, which can be individualized to the patient's ability and motivates the user (Sapoznik and Levin, 2011; Lohse et al., 2014; Veerbeek et al., 2014; Laver et al., 2017; Maier et al., 2019a). A Cochrane review, and a consecutive review published in 2021 could confirm a positive effect on motor recovery when VR technologies were used as an adjunct to conventional therapy (Laver et al., 2017; Bui et al., 2021). To enable intensive training, even in severely affected individuals with hemiplegia, electrostimulation seems to be an appropriate therapeutic method (Oujamaa et al., 2009; Meadmore et al., 2012). Electrical stimulation can be used in a functional context, referred to as FES, to assist impaired or absent function during a task (Moe and Post, 1962; Doucet et al., 2012). FES applications can be orthotic applications aiming at replacing a function or therapeutic applications which target the regain of a function. While the orthotic application on the upper limb has not been studied a lot, the positive effects of therapeutic FES interventions include improvements in muscle strength (Veerbeek et al., 2014; Küçükdeveci et al., 2018), motor function (de Kroon et al., 2005; Veerbeek et al., 2014; Hebert et al., 2016; Küçükdeveci et al., 2018; Monte-Silva et al., 2019), range of motion (Veerbeek et al., 2014), and ADLs (Veerbeek et al., 2014; Howlett et al., 2015; Eraifej et al., 2017). In addition, it has been shown that involving the patient's voluntary effort with EMG-triggered FES is more effective compared to passive stimulation (de Kroon et al., 2005). A combination of both approaches seems promising and has been investigated in only a few studies so far (e.g., Meadmore et al., 2012; Buick et al., 2016; Kumar et al., 2016; Collaborators GBDLROs et al., 2018; Lee et al., 2018; Fu et al., 2019; Chou et al., 2020; Norouzi-Gheidari et al., 2021). In all of these studies task-specific training via VR-based games was provided that incorporated FES. Various VR and gaming devices (e.g., smart glove gaming system, touch table screen, computer screens), as well as different FES systems (e.g., custom-built FES wristlet, single electrodes, and electrode arrays) were used for this purpose. Additionally, two studies also integrated an arm support system, such as Saebomas (Kutlu et al., 2016) or an unweighting exoskeleton robotic system (Meadmore et al., 2012). All games were designed to promote upper limb motor recovery including reaching, grasping and object manipulation tasks, which often mimicked ADLs such as opening a door, pressing a button, or positioning an object.

A combined approach may have the potential to positively impact treatment outcomes, as FES and SG complement each other in terms of motor learning principles that are important for effective neurorehabilitation interventions (Fu et al., 2019). In addition, the combined use of VR/SG and FES provides multimodal feedback (visual, auditory, and proprioceptive), which may further enhance the therapeutic effect (Lee et al., 2018). Preliminary results have shown improvements in motor function (Meadmore et al., 2012; Buick et al., 2016; Kumar et al., 2016; Kutlu et al., 2016; Lee et al., 2018; Fu et al., 2019; Norouzi-Gheidari et al., 2021), range of motion (Kutlu et al., 2016), and cognitive function (Fu et al., 2019). The combined interventions were also found to be interesting, motivating and challenging (Buick et al., 2016; Fu et al., 2019), and to reduce the burden on clinical therapists (Chou et al., 2020). However, there is limited evidence to support this novel approach, and most studies included small numbers of patients, had no control group and/or examined therapies for home use in chronic stroke patients. Moreover, controlling FES stimulation still

appears to be a challenge (Meadmore et al., 2012; Buick et al., 2016; Kutlu et al., 2016; Lee et al., 2018). Existing control mechanisms were either inaccurate, did not require voluntary patient effort, or were complex, expensive and time-consuming and therefore not feasible in the hospital setting. In contrast, using a contralaterally controlled FES with kinematic sensing gloves seems feasible for home use (Fu et al., 2019). A similar approach using FES with the contralateral unimpaired hand controlled via EMG with a commercially available stimulation device also appears feasible and easy to use but has not yet been studied in combination with SG (Krewer et al., 2008). Accordingly, the aim of the present work is to investigate whether the combination of SG and contralaterally EMG-triggered FES is feasible, and what factors might influence the feasibility of the combined therapy system. Another objective is to investigate the benefit from the additional use of FES while playing SG.

2. Materials and methods

2.1. Participants

Patients in an inpatient rehabilitation hospital (Schoen Clinic Bad Aibling) were screened for study eligibility based on the following inclusion criteria: (i) ischemic or hemorrhagic stroke, (ii) age ≥ 18 years, (iii) cognitively able to follow instructions, (iv) no pain or low pain level in wrist or fingers of both limbs (Numerical Rating Scale/Pain scale < 4), (v) functional impairments in wrist and fingers of one limb (Medical Research Council scale score (MRC) ≤ 4), (vi) no rigid spasticity in the affected limb (Modified Ashworth Scale (MAS) ≤ 3), and (vii) able to sit in a chair for the duration of the session (about 1 h). Study-related and device-related exclusion criteria were (i) pregnancy, (ii) severe psychiatric disorders, (iii) active implantable devices (e.g., pacemaker), or other metal implants within the stimulation area, (iv) severe or frequent epileptic seizures in the past, (v) cancer, and (vi) wounds in the application area of the electrodes or measuring equipment. In addition, patients with no sensitivity in wrist or fingers and no motion resulting from FES (e.g., due to atrophy or polyneuropathy) were excluded from the study. A botulinum toxin injection during study participation led to study termination. The study was approved by the Ethics Committee of the Ludwig-Maximilians University (LMU) Munich, Germany (registration number: 21-0270), and registered with the German Clinical Trials Register (registration number: DRKS00025761).

2.2. Study design

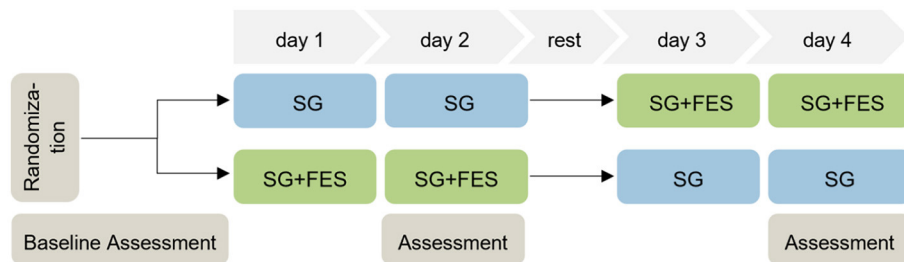
In this randomized crossover trial, the feasibility of serious gaming (SG) was compared to SG supported by FES (SG+FES). Each participant first underwent a baseline assessment to determine their current functional status. Patients received two consecutive training sessions of SG alone (control condition) and two consecutive training sessions of SG+FES (experimental condition). Whether they started with or without FES support, was randomized with an allocation ratio of 1:1. Randomization with different block

sizes of four and six, was done using sealed envelopes. Due to the nature of the trial, patients, therapists and assessors were not blind to the group allocation. Each session lasted about 45 to 60 min. Between the conditions at least an 1-day washout period was scheduled to lower the risk of carryover effects from the previous intervention (Dwan et al., 2019). All four sessions were completed within the timeframe of 2 weeks. The schematic of the study design is illustrated in Figure 1.

2.3. Intervention

The intervention in each condition consisted of performing serious gaming exercises with (SG+FES) and without (SG) FES support of the affected hand. Study participation did not affect the standard therapies during the rehabilitation stay, which took place to the usual extent.

For the gaming scenario, the Rehabilitation Gaming System (RGS; Eodyne Systems S.L., Barcelona, Spain), a VR-based rehabilitation tool, was used in both conditions. The RGS platform provides gamified and engaging exercises for effective and functional recovery of motor and cognitive functions, validated in stroke patients (Cameirão et al., 2009, 2011; Ballester et al., 2017). The system integrates a motion sensor (Leap Motion, Inc., San Francisco, United States) to capture hand movements in real time, which can be mapped to a hand- and forearm-like virtual avatar on a computer screen, allowing the player to interact with the game scenario. In the current trial, the *Bubbles* scenario was used, which targets grasping, reaching and bi-manual coordination. In this scenario, bubbles rise from a lake which need to be burst to score points by catching the bubbles with an open hand, and then closing the hand to burst. The exercise can be tailored to the user. The side of appearance of the bubbles can be adjusted. For this trial, the side of appearance of bubbles was set to the patient's paretic side to encourage the use of the impaired hand. Furthermore, the size of the bubbles can be set according to the patient's ability to open and close the hand, and the speed of the game can be adjusted by increasing the frequency of the rising bubbles. Size and speed were adjusted for each patient individually. Regarding the size, the smaller the bubbles, the less the user must open the hand, but the more they must close it to make them burst. Accordingly, smaller bubbles were chosen for patients who could not open their hand completely, or who had good ability in closing the hand, to make the task challenging. As the size equaled different scoring values, ranging from very large (one point per bubble) to very small (ten points per bubble), size and speed were adjusted only at the beginning of each game and documented for each patient to make the sessions comparable. Patients were seated in front of a large screen on which the game was displayed. The motion sensor was placed on the table in front of the patient. If needed, the proximal part of the arm (i.e., the elbow and forearm) was supported and guided by the therapist to move the arm toward the bubble, allowing the patient to concentrate on opening and closing the hand. The current total score was constantly visible at the top of the screen, and in the end of each game the performance was ranked in comparison with previous games. A briefing and explanation



During the SG+FES session, finger and wrist extension were supported by electrical stimulation using the STIWELL med 4 (MED-EL Elektromedizinische Geräte GmbH, Innsbruck, Austria). To facilitate finger and wrist extension, a pair of self-adhesive electrodes was attached to each forearm targeting extensor carpi ulnaris, extensor digitorum communis, and partially also extensor

Biphasic square-wave pulses with a frequency of 35 Hz and a pulse width of 250 μ s were used for stimulation. The muscle contraction/relaxation time ratio was set to 2/1 s on/off time. Therefore, 2 s of stimulation were followed by one second of

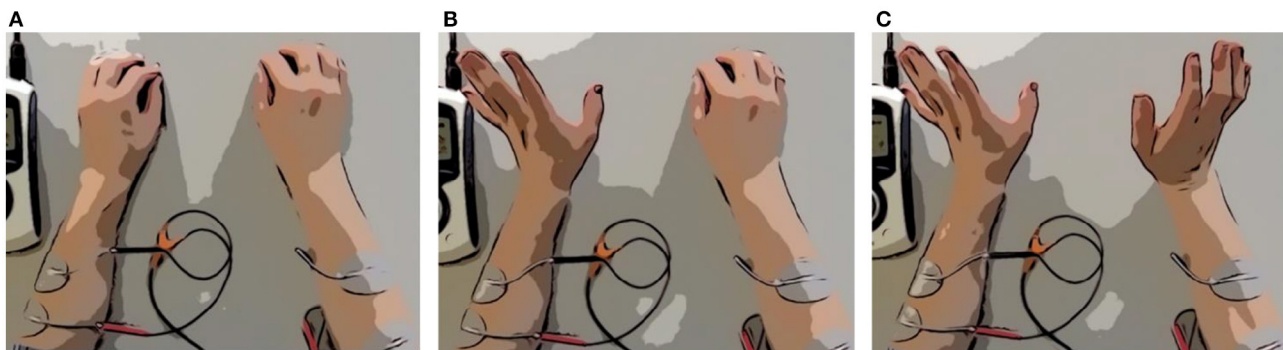


FIGURE 3

Scheme of EMG-based ccFES. Two electrodes are placed on each forearm. First, both hands are closed (A). Then the non-paretic hand (left hand) opens (B). Muscle activity is recorded by EMG and exceeds a set threshold. Stimulation of the affected paretic hand (right hand) is triggered. Wrist and finger extensor muscles of the affected hand contract and the hand opens (C).

pause. The stimulation included no ramping-up and ramping-down period to insure fast reaction on the game. However, in patients with instable wrists, a ramping-up and ramping down of 0.5 s was added to reduce strain on the structures. The stimulation intensity (mA) and EMG-threshold (μV) was set individually for each patient. Therefore, the intensity was slowly increased until the first muscle twitch was seen and was further increased to the level that produced maximum wrist and finger extension without discomfort or pain. The EMG threshold was set to trigger stimulation when the non-paretic hand was opened without much effort. For integrating the stimulation to the gaming therapy, there are two different ways: Either the patient opens the unaffected hand first, which triggers the stimulation and leads to the opening of the affected hand, or the patient opens both hands simultaneously and the function of the affected hand is supported by the stimulation. The second option is only possible if the patient can open the hand volitionally. The procedure of the game in the SG+FES condition is as follows: (i) A bubble rises from the lake, (ii) patient opens his unaffected hand/both hands at the same time, (iii) the muscle activity exceeds the EMG threshold and triggers the stimulation on the affected side, (iv) short time later the affected hand opens/the hand opening improves, (v) the hand motion is detected by the sensor and displayed as virtual motion by the avatar, (vi) the digital avatar catches the bubble with the opened hand, (vii) the bubble attaches to the avatar's hand, (viii) the patient closes the affected hand volitionally (including use of gravity) or with the support of the therapist, (ix) the bubble bursts and points are collected.

2.4. Outcome parameters

Baseline patient characteristics including sociodemographic characteristics, severity of impairment, cognition (Montreal Cognitive Assessment, MoCA) (Nasreddine et al., 2005), pain, and technical affinity were collected before the interventions. For more details see Table 1. Assessments were performed immediately after completing each condition (see Figure 1).

2.4.1. Primary outcomes

Feasibility of the therapy system was assessed after each condition using the Intrinsic Motivation Inventory (IMI), the Nasa Task Load Index (NASA-TLX), the System Usability Scale (SUS), and the vertical numerical rating scale (NRS-FRS) for perceived fatigue. Patients either filled the questionnaires by themselves or with the support of the supervising researcher.

The patients' motivation during the respective interventions was assessed using the IMI, a multidimensional questionnaire designed to evaluate motivational structures for performing given tasks in laboratory experiments (McAuley et al., 1989; Dec et al., 1994). In recent years, the use of the IMI has become widespread in stroke rehabilitation research. Monardo, Pavese (Monardo et al., 2021) also recommend the use of the IMI to assess patient motivation and satisfaction during technology-assisted rehabilitation. For the purpose of the study, a shorter version with a total of 20 items was selected (Bergmann et al., 2018). It contains the following five subscales relevant for our study: interest/enjoyment, value/usefulness, effort, perceived competence, and felt pressure and tension. Four items per subscale were included and rated on a seven-point Likert scale from "strongly disagree"/1 to "strongly agree"/7. The original questionnaire was translated into German and slightly modified to adapt them to the given task. The subscale *interest/enjoyment* directly reflects the patient's intrinsic motivation, whereas the other concepts influence intrinsic motivation and self-regulatory behavior. For example, it is assumed that individuals internalize and become self-regulating when they can identify with an activity's value (Dec et al., 1994). The total score and the score per subscale were calculated by averaging the respective items.

The NASA-TLX is a multidimensional rating scale for measuring a person's subjectively perceived workload during or shortly after completing a given task (Hart and Staveland, 1988). The measurement tool comprises a total of six subdimensions of workload: mental demand, physical demand, temporal demand, performance, effort, and frustration. The subscales are presented on straight lines with the endpoints low and high on which patients mark the point that best represents their subjective perception of workload of the given task (NASA Ames Research Center, 1986).

TABLE 1 Demographic and clinical patient characteristics ($n = 18$).

Parameter	<i>M (SD), min-max; or number</i>
Age [years]	62.1 (14.1), 40–86
Sex (men/women)	15/3
Type of stroke (ischemia/hemorrhage)	11/7
Side of paresis (left/right)	7/11
Time after stroke [months]	2.4 (1.6), 1.0–7.3
Fugl-Meyer Assessment (FMA)	
FMA—upper extremity motor function (0–66)	26.1 (18.6), 4–59
FMA—hand/part C (0–14)	6.4 (4.6), 0–13
FMA—sensory function (0–12)	9.1 (3.7), 0–12
Categorization (severe, 0–28/moderate, 29–42/mild, 43–66)	11/3/4
Montreal Cognitive Assessment (MoCA, 0–30)	23.7 (5.6), 10–28 (12 normal, 2 mild, 4 moderate)
Modified ashworth scale (max value; 0/1/1+/2/3)*	5/4/5/2/2
Tardieu scale (max value; 0/1/2/3/4)*	5/2/7/4/0
Medical research council scale*	
Finger extensors (0/1/2/3/4/5)	3/8/1/2/4/0
Wrist extensors (0/1/2/3/4/5)	4/6/1/4/3/0
Mean maximum grip strength [kg]	
Paretic hand	4.9 (6.4), 0–22.8
Non-paretic hand	30.5 (11.0), 7.6–48
Technical Affinity questionnaire—Total score (TA-EG, 0–5)	3.6 (0.7), 2.5–4.5
TA-EG—Enthusiasm (0–5)	3.6 (1.1), 1.6–5.0
TA-EG—Competence (0–5)	3.8 (0.9), 1.8–5.0
TA-EG—Positive attitude (0–5)	3.9 (0.8), 2–5
TA-EG—Negative attitude (0–5)	3.2 (0.6), 1.8–4.4

A MoCA score of 26 or above is considered normal; a score from 18–25 is considered a mild, 10–17 a moderate, and less than 10 points a severe cognitive impairment. *individual values are shown in [Supplemental Table 1](#).

For scoring, the line is divided into 20 equal intervals marked by vertical ticks. The position of the marker is then rated numerically on a scale from 0 to 100, with five points for each interval. If a subject marks between two ticks, the value is rounded up. The value of each subscale is measured and represents a unique score. The mean value of the subscales gives the overall RAW-TLX score between 0 and 100, whereas a higher score indicates greater perceived workload ([Hart, 2006](#)). The German version of the RAW-TLX was used. The term NASA-TLX is retained in the following for simplification.

Testing usability during and after the development of a product or system is an incredibly important process ([Peres et al., 2013](#)). The patients' perceived usability of the therapy system (SG and SG+FES) was assessed using the SUS. Thereby usability is defined as the appropriateness of a system or tool to a purpose or to a

context in terms of effectiveness (success), efficiency (effort), and satisfaction (level of comfort). The SUS comprises a total of ten items, which are rated on a five-point Likert scale from “strongly disagree”/0 to “strongly agree”/4 ([Brooke, 1996](#)). The SUS was proven to be a valid and reliable instrument (even with small samples) for assessing the overall perceived usability of a wide range of products and services (including health care devices). In this study, a translated German version of the SUS was used and the term “system” was changed to “therapy system” for better suitability ([Bangor et al., 2008](#)). In addition, a rating scale was used to determine the degree to which the patient perceived ccFES as supportive or as disturbing. The rating scale consists of a ten-centimeter horizontal line divided into 20 equal intervals marked by vertical ticks with the endpoints “disturbing”/0 and “supportive”/10. The higher the value, the more supportive the ccFES was perceived to be.

After each therapy session, the level of perceived fatigue was assessed using a vertical numerical rating scale supplemented by faces (NRS-FRS) ([Chuang et al., 2015](#)). The tool is easy to administer and has shown a high sensitivity and specificity in assessing fatigue intensity in patients with stroke. In addition, compared to the normal numerical rating scale (NRS), it may be more suitable for patients who lack cognitive and visuospatial functions. The NRS-FRS scale consists of a ten-centimeter vertical line with a rating scale from “no fatigue”/0 to “worst possible fatigue”/10 and six facial expressions (from smiling to crying). Patients were asked to rate their perceived overall fatigue level by pointing to a number on the scale that best represented it. Based on the score assigned, fatigue can be categorized as no fatigue (0), mild (1–3), moderate (4–6), or severe fatigue (7–10).

Lastly, adverse events were documented.

2.4.2. Secondary outcomes

Gaming parameters (duration and score) were recorded during each session to assess the orthotic efficacy of the therapy system. The gaming duration was defined as the amount of time spent performing the serious game per session, whereas the score was defined as the total number of points achieved during therapy per session. To make the scores comparable between the sessions and conditions, the total number of points were divided by the level of difficulty (bubble size). Thus, the number of points also corresponds to the number of successful hand opening and closing repetitions. The patient's performance was automatically saved in a remote medical information management system and additionally noted on a documentation sheet. For both parameters, the mean value for each condition was used for analyses.

2.5. Data and statistical analysis

Descriptive statistics (mean, M ; standard deviation, SD ; median, Mdn ; $Q1$ – $Q3$, quartile 1–quartile 3) are used to describe the study population and outcome variables. Outcome variables were first tested for normality using the Shapiro-Wilk test. For between-condition comparisons, paired-sample t -tests or Wilcoxon signed-rank tests were performed. In addition, subgroup

Wilcoxon tests were performed with classification of patients based on disease severity and spearman rank correlations (non-parametric test for ordinal or metric data) were used to analyze relationships between feasibility and (1) time since stroke, (2) age, (3) technical affinity, and (4) degree of cognitive impairment. The alpha level was set to 0.05. Inferential analysis was performed using IBM SPSS Statistics 27 and visualization was done in RStudio.

3. Results

3.1. Baseline

Between June and September 2021, and April and November 2022 inpatients at the Schoen Clinic Bad Aibling were screened for eligibility (see criteria in Section 2.1). Figure 4 shows the patients' flow through the study. Of 400 patients who were assessed for eligibility, 294 patients did not meet the previously defined inclusion criteria. The top three reasons for not meeting the inclusion criteria were: only fine motor impairments in the paretic hand (inclusion criteria v), not being able to sit upright for more than 1 h (inclusion criteria vii), or not being able to follow instructions due to cognitive or language impairments (inclusion criteria iii), in 21%, 13%, or 12% of the excluded patients, respectively. Three patients declined to participate. Other reasons for not being able to participate ($n = 82$) were e.g., a hospital stay shorter than 2 weeks, or a language barrier due to the inability to understand or speak German.

In the end, 21 of the screened patients were included in the study of which one patient dropped out before study participation and two patients after baseline assessment (see Figure 4). Demographic and clinical characteristics of analyzed patients ($n = 18$) are shown in Table 1.

3.2. Primary outcome parameters

The IMI, NASA-TLX and SUS questionnaires as well as the perceived fatigue level provide subjective measures of feasibility. Questionnaire results are reported for both conditions in Table 2.

Comparing the IMI scores between conditions, the statistical values indicate a significant increase in the patients' perceived competence ($z = -2.88$, $p = 0.004$) and a decrease in the perceived pressure/tension during ccFES supported training ($z = -2.13$, $p = 0.034$). Furthermore, the task load was rated significantly lower in the SG+FES condition ($z = -3.14$, $p = 0.002$). The subscale of physical demand showed lower values ($z = -3.08$, $p = 0.002$) and performance higher values ($z = -2.59$, $p = 0.010$) for the SG+FES condition. Responses to the SUS did not differ significantly between conditions ($z = -0.79$, $p = 0.431$). Also, the perceived level of fatigue showed no significant difference ($z = 1.57$, $p = 0.115$).

The technical and user documentation revealed that the addition of ccFES was perceived as very supportive ($Mdn = 9.0$, $Q1-Q3 = 7.8-10.0$). However, 16 of the 18 patients (mild: 2/4, moderate: 3/3, severe: 11/11) needed proximal support of the paretic arm, which was given by the therapist.

3.3. Factors influencing feasibility

A subgroup analysis reveals the severity of the hemiparesis as a factor that had an influence on the feasibility of using SG+FES compared to SG alone. Mildly and moderately impaired patients perceived no difference in feasibility between conditions ($p \geq 0.068$). However, patients with a severe hemiparesis remarked a significantly higher task load during the therapy when they were not supported by ccFES ($Mdn_{SG} = 50.0$, $Q1-Q3_{SG} = 41.7-58.3$, $Mdn_{SG+FES} = 35.8$, $Q1-Q3_{FES+SG} = 16.7-47.5$, $z = -2.1$, $p = 0.033$). Furthermore, their intrinsic motivation was higher when playing the game with ccFES support ($Mdn_{SG} = 4.9$, $Q1-Q3_{SG} = 4.6-5.5$, $Mdn_{SG+FES} = 5.5$, $Q1-Q3_{SG+FES} = 5.3-5.8$, $z = -2.0$, $p = 0.046$).

The patients' technical affinity showed a positive correlation ($r = 0.46$) with the feasibility of the SG+FES condition, assessed by the SUS, which is tending toward statistical significance ($p = 0.053$). Factors such as age, time since stroke and the degree of cognitive impairment (according to the MoCA) did not correlate with any feasibility assessment of the SG+FES condition ($p \geq 0.192$).

3.4. Secondary outcome parameters

Since one patient (severely impaired) received physical support in hand opening and closing by the therapist, the online effect of ccFES was analyzed in 17 patients. Gaming parameters (i.e., the gaming score and the session duration) were compared between SG+FES and SG condition. Overall, the support by ccFES showed a significant effect on the gaming duration ($z = -2.41$, $p = 0.016$) enabling longer training times. With the support of ccFES, patients played on average 27.7 ($SD = 4.5$, $min = 16.3$) minutes, while the training lasted on average 17.8 ($SD = 14.2$, $min = 0$) minutes without ccFES. In Figure 5, the difference in gaming duration is grouped according to the severity of impairment. For patients with a mild or moderate hemiparesis, the therapy duration was not expanded by the addition of ccFES support. However, only few severely impaired patients (4/10), were able to play the therapy game without ccFES support at all (10.3 ± 14.2 min), but the support by ccFES enabled them to train on average 28.0 ($SD = 4.2$) minutes ($z = -2.41$, $p = 0.016$). Overall, the gaming duration of ccFES supported trials ranged from 20 to 30 min. Factors preventing the patients from finishing the 30 min of therapy included muscle fatigue, general fatigue, shoulder pain, and time pressure due to the patient's therapy schedule.

With respect to the gaming score, patients achieved a 50.5 points higher score when they were supported by ccFES (183.0 ± 97.5 points) compared to no support (132.5 ± 146.2 points). This effect reached statistical significance ($t_{(16)} = -2.17$, $p = 0.045$). Subgroup analyses reveal a significant online effect of ccFES leading to an increase of on average 84.9 (95%CI = 22.8–147.0) points in the group of severely impaired patients ($t_{(9)} = -3.09$, $p = 0.013$). As visualized in Figure 6, there is no clear pattern for mildly and moderately impaired patients; some profited from ccFES support, others achieved less points in the SG+FES condition.

3.5. Harms

Neither FES nor the gaming scenario itself led to any serious adverse events. By following the manufacturer's instructions, device-related exclusion criteria were set to reduce the risk of harms. During recruitment, attention was given to not include patients with allergies to adhesive material. Reactions to the stimulation include temporary redness of the skin, most likely induced by an increase in blood flow. Pain in the shoulder or at the back of the hand was recorded as side effect of the general intervention by two patients, leading to an earlier termination of the therapy session (after 15–20 min).

4. Discussion

4.1. Feasibility of the system

The feasibility of combining a SG application with ccFES was investigated within the population of subacute stroke patients in

the design of a randomized crossover study. It was demonstrated that the combination of SG with EMG-based ccFES is feasible, safe and well-accepted among patients after stroke. Overall, both conditions were perceived as motivating, and were rated to be at an appropriate task load. The SUS score was high in both conditions, with 85.0 points in SG and 82.5 points in SG+FES condition, which is considered as good according to the existing literature (Bangor et al., 2008, 2009). Thus, the results indicate that both systems are easy to learn for most people, easy to use without much technical support and not too complex, inconsistent or awkward. In addition, most subjects felt confident in using the therapy systems and could imagine using those regularly. The results of the IMI show that both conditions were with a median score of 5.5 (SG+FES) and 5.3 (SG) perceived as enjoyable and valuable, and thus patients were motivated during therapy. This is in line with previous work (Buick et al., 2016; Fu et al., 2019; Doumas et al., 2021). When ccFES support was provided, patients perceived a significantly higher level of competence and experienced significantly less pressure. This is also evident in the results of the NASA-TLX, which show a significantly lower

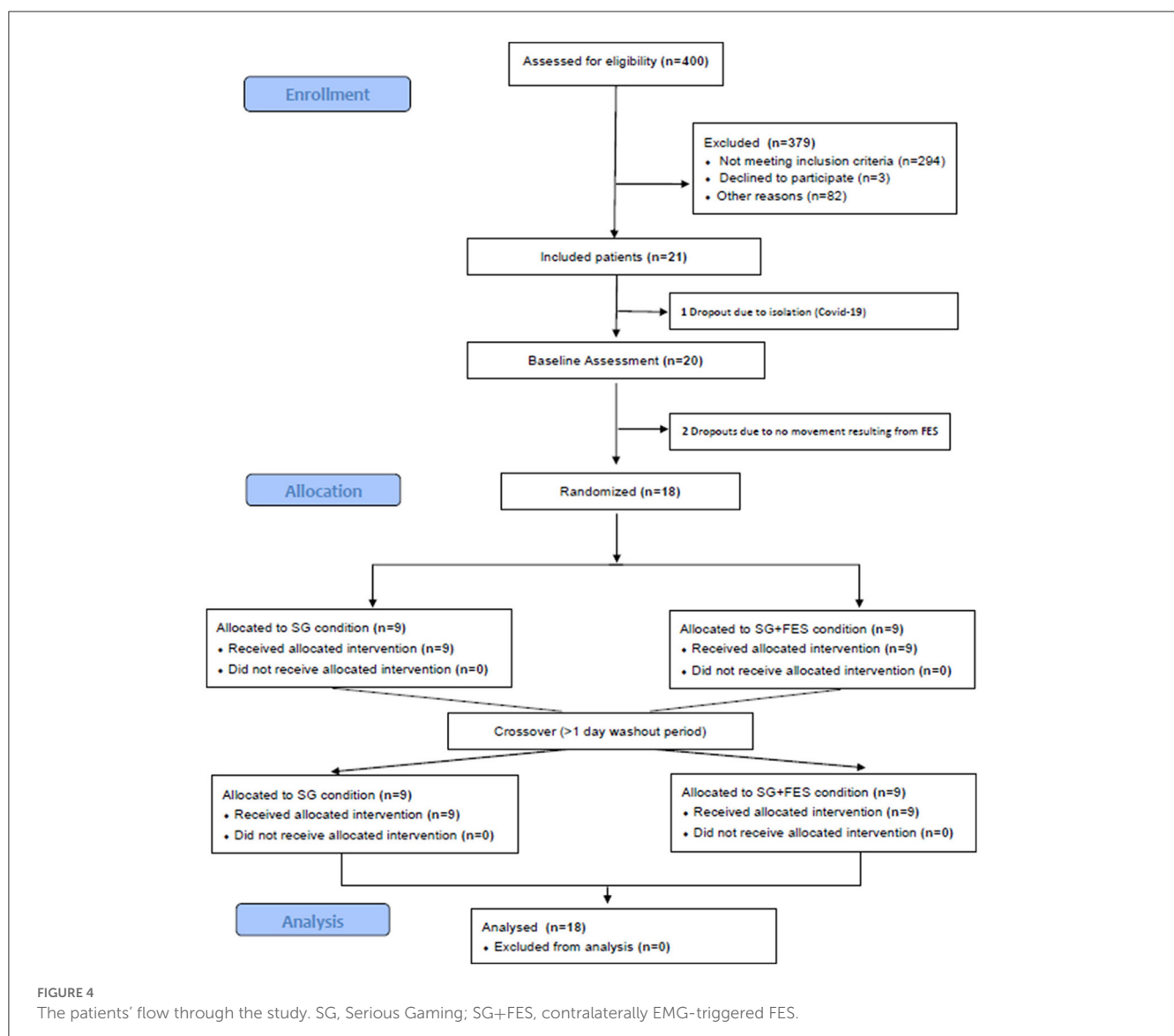
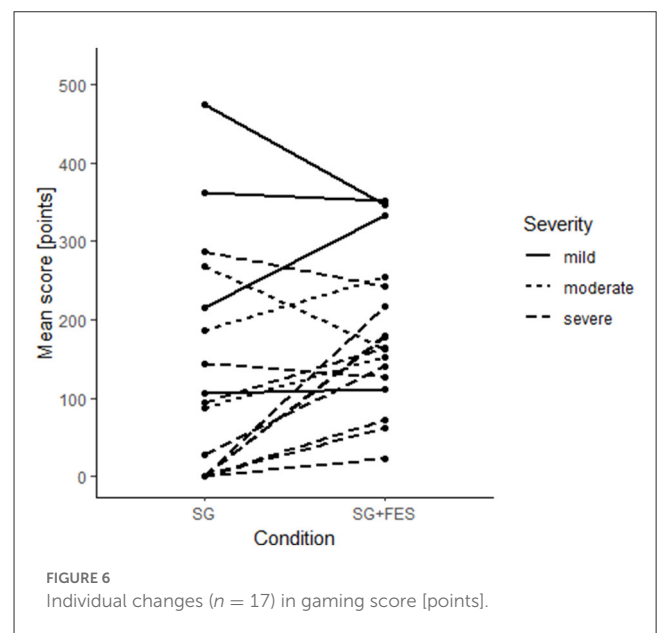
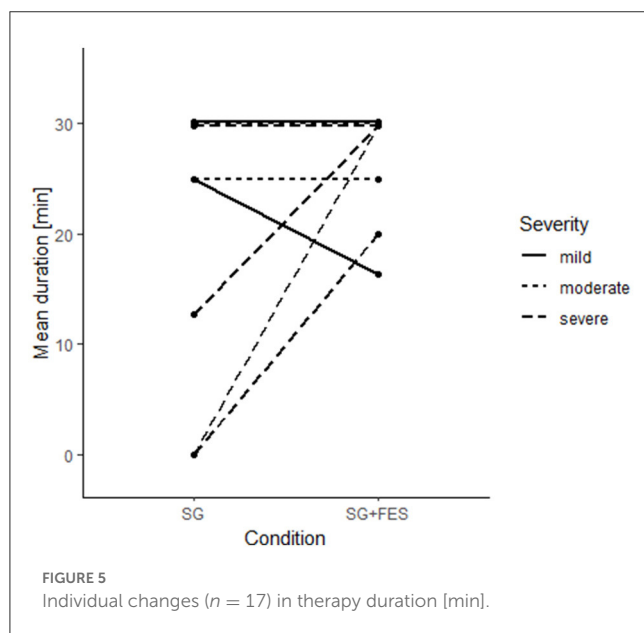


TABLE 2 Feasibility scores for both conditions and the inferential comparison between conditions.

Outcome parameters	SG+FES Mdn (Q1–Q3)	SG Mdn (Q1–Q3)	Statistical values
IMI (0–7)*	5.5 (5.3–5.8)	5.3 (4.8–5.5)	$z = -1.66, p = 0.097$
Interest/enjoyment	7.0 (6.8–7.0)	6.7 (6.2–7.0)	$z = -1.11, p = 0.265$
Value/usefulness	6.8 (6.0–7.0)	6.8 (6.2–7.0)	$z = -0.61, p = 0.539$
Effort	7.0 (6.4–7.0)	6.8 (5.5–7.0)	$z = -0.72, p = 0.473$
Perceived competence	5.9 (4.8–6.6)	4.9 (2.5–5.5)	$z = -2.88, p = 0.004$
Pressure/tension	1.8 (1.0–2.5)	2.3 (1.0–3.0)	$z = -2.13, p = 0.034$
NASA-TLX (0–100)*	32.9 (22.9–46.9)	49.2 (37.1–58.7)	$z = -3.14, p = 0.002$
Mental demand	47.5 (25.0–76.3)	50.0 (17.5–53.8)	$z = -0.42, p = 0.678$
Physical demand	50.0 (13.8–76.3)	72.5 (50.0–90.0)	$z = -3.08, p = 0.002$
Temporal demand	42.5 (18.8–50.0)	50.0 (23.8–50.0)	$z = -0.54, p = 0.593$
Performance	20.0 (10.0–37.5)	52.5 (25.0–96.3)	$z = -2.59, p = 0.010$
Effort	30.0 (20.0–52.5)	62.5 (23.8–50.0)	$z = -1.85, p = 0.064$
Frustration	5.0 (0.0–25.0)	12.5 (3.8–31.3)	$z = -1.07, p = 0.284$
SUS (0–100)*	85.0 (71.9–90.6)	82.5 (74.4–88.1)	$z = -0.79, p = 0.431$
Perceived fatigue level (0–10)*	4.5 (2.3–6.5)	2.5 (0.0–6.1)	$z = 1.57, p = 0.115$

IMI, Intrinsic Motivation Inventory; NASA-TLX, Nasa Task Load Index; SG, Serious Gaming; SG+FES, Serious Gaming plus contralaterally EMG-triggered FES; SUS, System Usability Scale.

*individual values are shown in [Supplementary Table 2](#).



workload when the movement was support by ccFES with a median of 32.9 points, compared so SG only with a median of 49.3 points. Specifically, the physical and temporal demand was significantly lowered by ccFES. In general, patients rated the stimulation as supportive rather than distracting. However, almost 90% of patients needed proximal anti-gravity support in order to participate in the therapy. This points out the strong need of adding a proximal robotic component (e.g., lightweight exoskeleton) to the system.

Our results thus proof that the combination of SG and EMG-based ccFES is as feasible as SG alone, and in some aspects even superior to SG alone. According to previous research, the implementation of such a combined therapy is expected to have additional benefits on motor recovery. By adding ccFES to SG, the following principles are incorporated and complement each other. SG delivers individualized, task-specific training in a multisensory environment, including visual and auditory feedback on performance and results (Cameirão et al., 2009). In addition, it

promotes the active execution of movements of the paretic limb and observation of movement through an avatar representation on the computer screen (Cameirão et al., 2009). Moreover, controlling FES with the contralateral side encourages bilateral arm movements, which can be beneficial in improving motor recovery after stroke (Cauraugh and Kim, 2002). Dumas, Everard (Dumas et al., 2021) demonstrated that a greater focus on these principles increases the efficacy of SG therapies.

The investigation of factors that influence the feasibility of the combined system revealed the severity of the upper limb hemiparesis as one aspect. Especially, severely impaired patients rated the SG+FES condition as motivating and supportive, in terms of reducing the task load. Since the age of the participants, the time since stroke and the degree of cognitive impairments had no influence on the feasibility of the combined training, the results imply no restrictions in therapy prescription. However, it has to be highlighted that the time since stroke for the investigated study cohort was seven months or shorter (without specification in the inclusion and exclusion criteria). Solely, technical affinity is a potential influencing factor of feasibility. Patients with a higher technical affinity tend to rate the combined approach even more positive, potentially because they are in general more open for new technologies and less afraid to use them.

4.2. Orthotic effect

Only patients with sufficient residual movement activity were able to play the game under the SG condition without ccFES, while it was possible for all patients under the SG+FES condition regardless of impairment. This becomes evident in the significant increase in therapy time in the combined training compared to unassisted SG. More than half of the severely impaired patients were not able to perform the game without assistance, so ccFES enabled them to execute the SG at all. Obviously, this group of severely impaired patients were those who had the strongest orthotic effect in terms of therapy duration. ccFES facilitated these patients to increase the therapy intensity and the number of repetitions of hand opening, which could potentially lead to an increased rehabilitation outcome for the severely affected patients.

When comparing the success achieved in the game indicated by the resulting scores, ccFES led to an orthotic effect. However, only the performance of patients with a severe hemiparesis significantly improved under ccFES support. In contrast, patients with mild to moderate impairment showed little or no gain in their performance in the SG+FES condition.

Although moderately and mildly impaired patients did not show any orthotic effect, a therapeutic effect of the combined SG+FES application might still be possible due to the increased sensory information. It is worth to highlight that the control of the additional ccFES component did not lead to any disadvantage, neither in feasibility nor in work load. A therapeutic effect, however, needs to be investigated in future studies, as this was not addressed in the here presented trial. That would even mean to focus on different outcome parameters to investigate the therapeutic effect (e.g., Action Research Arm Test, Barthel Index, Functional Independence Measure).

4.3. Strengths and limitations

To our knowledge, this is one of the few studies demonstrating the feasibility of combining serious gaming with ccFES using a randomized controlled design and the first study using ccFES for this purpose. Some study-related weaknesses, however, were identified that limit the interpretability and generalizability of the results. The patients and the research team were not blinded with respect to the applied interventions. However, the research team itself did not rate feasibility nor the orthotic efficacy of the system. Rather was the assessment of the orthotic effect captured by means of the gaming system. Also, regarding the subjective report of feasibility by the participating patients, the patients have to be aware of the different gaming conditions to better evaluate the feasibility. Therefore, the potential risk of bias due to the lack of blinding is considered to be low. Despite possible biases due to self-reporting, such as recall bias, the inclusion of patients' opinions and needs in a participatory design is necessary for the rehabilitation system to be user-friendly and accepted by patients. Since the vast majority of patients did not show cognitive impairments, it is not expected that many patients could not recall the therapy sessions, which were performed right before answering the questionnaires. Regarding the sample size, it is important to note that the focus of this work was to demonstrate the feasibility of the concepts of combining serious gaming with EMG-based ccFES in a hospital setting, instead of testing the efficacy in upper limb rehabilitation. Future work is needed to verify these results with a larger number of participants, especially to perform higher powered sub-group analysis according to the severity of the hemiparesis. Lastly, there are some limitations of the system when thinking about using it at home. For an application of the system at home, it is necessary to allow the patient to train without support of a therapist, and therefore the following implications were derived. The goal of the *Bubbles* scenario of the RGS system was to burst bubbles by opening and closing the hand. The extension of the fingers and the opening of the hand were supported by ccFES. However, to successfully score points, finger bending is also essential, which was not supported in the current study. For patients with very limited flexion, it was not possible to play the game without the therapist manually closing the hand. Therefore, not only the extensor but also the flexor muscles of the fingers should be stimulated with ccFES. Furthermore, the bubble game of the RGS system required a good proximal arm function to be able to hold the hand independently over the motion sensor and thus to be able to play the game. However, since proximal arm function was not sufficient in almost all patients and no arm support system was planned for the study, the therapist had to physically assist the proximal joints.

Our findings provide valuable implications for the development of rehabilitation systems by combining different therapeutic interventions to increase patients benefit. The combined approach provides individualized, task-specific rehabilitation with the potential to increase therapy intensity, especially for severely impaired patients with muscle weakness, and to maintain patients' motivation and engagement. To bring this therapy system from a hospital setting to home use, the integration of an additional arm support system (e.g., exoskeleton) would be necessary, as shown to be feasible in two studies investigating SG+FES

(Meadmore et al., 2012; Kutlu et al., 2016). Such a hybrid combination of robotic and FES has already been studied and makes a proportion of about 25% of existing hybrid systems, as shown in a recent review (Höhler et al., 2023). As another solution, either in addition or as an alternative to FES, the distal functions could also be supported by integrating a hand support system [e.g., hand exoskeleton (Prange-Lasonder et al., 2017)]. The combined use of robotic and FES support for hand functions, however, has not yet been studied (Höhler et al., 2023).

Data availability statement

The original contributions presented in the study are included in the article/Supplementary material, further inquiries can be directed to the corresponding author.

Ethics statement

The studies involving human participants were reviewed and approved by Ethics Committee of the Ludwig-Maximilians University (LMU) Munich, Germany. The patients/participants provided their written informed consent to participate in this study.

Author contributions

Conceptualization: AC and CK. Methodology: CH, AC, and CK. Formal analysis and visualization: CH and LW. Investigation: LW, AC, and KJ. Resources and supervision: KJ and CK. Data curation: LW and AC. Writing—original draft: CH, LW, and CK. Writing—review and editing: AC and KJ. Project administration: AC, KJ, and CK. Funding acquisition: CK. All authors contributed to the article and approved the submitted version.

References

- Ballester, B. R., Nirme, J., Camacho, I., Duarte, E., Rodriguez, S., Cuxart, A., et al. (2017). Domiciliary VR-based therapy for functional recovery and cortical reorganization: randomized controlled trial in participants at the chronic stage post stroke. *JMIR Ser. Games*. 5, e15. doi: 10.2196/games.6773
- Bangor, A., Kortum, P. T., and Miller, J. T. (2008). An empirical evaluation of the system usability scale. *Int. J. Human-Comp. Interact.* 24, 574–94. doi: 10.1080/10447310802205776
- Bangor, A., Kortum, P. T., and Miller, J. T. (2009). Determining what individual SUS scores mean: adding an adjective rating scale. *J. Usabili. Stud.* 4, 114–23.
- Bergmann, J., Krewer, C., Bauer, P., Koenig, A., Riener, R., Muller, F., et al. (2018). Virtual reality to augment robot-assisted gait training in non-ambulatory patients with a subacute stroke: a pilot randomized controlled trial. *Eur. J. Phys. Rehabil. Med.* 54, 397–407. doi: 10.23736/S1973-9087.17.04735-9
- Brooke, J. (1996). SUS: A “quick and dirty” usability scale. In *Usability Evaluation in Industry*, eds P. W. Jordan, B. A. Thomas, Weerdmeester, and I. L. McClelland (London: Taylor & Francis), 189–194.
- Bui, J., Luauté, J., and Farné, A. (2021). Enhancing upper limb rehabilitation of stroke patients with virtual reality: a mini review. *Front. Virtual Real.* 2, 5771. doi: 10.3389/frvir.2021.595771
- Buick, A. R., Kowalczewski, J., Carson, R. G., and Prochazka, A. (2016). Tele-supervised FES-assisted exercise for hemiplegic upper limb. *IEEE Trans. Neural. Syst. Rehabil. Eng.* 24, 79–87. doi: 10.1109/TNSRE.2015.2408453
- Cameirão, M. S., Badia, S. B., Oller, E. D., and Verschure, P. F. (2009). The rehabilitation gaming system: a review. *Stud. Health Technol. Inform.* 145, 65–83. doi: 10.3233/978-1-60750-018-6-65
- Cameirão, M. S., Badia, S. B., Oller, E. D., and Verschure, P. F. (2011). Virtual reality based rehabilitation speeds up functional recovery of the upper extremities after stroke: a randomized controlled pilot study in the acute phase of stroke using the rehabilitation gaming system. *Restor. Neurol. Neurosci.* 29, 287–98. doi: 10.3233/RNN-2011-0599
- Cauraugh, J. H., and Kim, S. (2002). Two coupled motor recovery protocols are better than one: electromyogram-triggered neuromuscular stimulation and bilateral movements. *Stroke* 33, 1589–94. doi: 10.1161/01.STR.0000016926.77114.A6
- Chou, C. H., Wang, T., Sun, X., Niu, C. M., Hao, M., Xie, Q., et al. (2020). Automated functional electrical stimulation training system for upper-limb function recovery in poststroke patients. *Med. Eng. Phys.* 84, 174–83. doi: 10.1016/j.medengphy.2020.09.001
- Chuang, L. L., Lin, K. C., Hsu, A. L., Wu, C. Y., Chang, K. C., Li, Y. C., et al. (2015). Reliability and validity of a vertical numerical rating scale supplemented with a

Funding

This project has received funding from the European Unions Horizon 2020 research and innovation programme ReHyb under grant agreement no 871767.

Acknowledgments

The authors would like to thank Jasmin Fuchs for supporting patient recruitment and investigation, and creating the flow chart. The authors would also like to thank Eodyne Systems S.L. (Barcelona, Spain) for providing the serious gaming system (Rehabilitation Gaming System, RGS).

Conflict of interest

The authors declare that the research was conducted in the absence of any commercial or financial relationships that could be construed as a potential conflict of interest.

Publisher's note

All claims expressed in this article are solely those of the authors and do not necessarily represent those of their affiliated organizations, or those of the publisher, the editors and the reviewers. Any product that may be evaluated in this article, or claim that may be made by its manufacturer, is not guaranteed or endorsed by the publisher.

Supplementary material

The Supplementary Material for this article can be found online at: <https://www.frontiersin.org/articles/10.3389/fnbot.2023.1168322/full#supplementary-material>

faces rating scale in measuring fatigue after stroke. *Health Qual. Life Outcomes* 13, 91. doi: 10.1186/s12955-015-0290-9

Collaborators GBDLROs, Feigin, V. L., Nguyen, G., Cercy, K., Johnson, C. O., Alam, T., et al. (2018). Global regional and country-specific lifetime risks of stroke, 1990 and 2016. *N. Engl. J. Med.* 379, 2429–37. doi: 10.1056/NEJMoa1804492

Crichton, S. L., Bray, B. D., McKeivitt, C., Rudd, A. G., and Wolfe, C. D. (2016). Patient outcomes up to 15 years after stroke: survival, disability, quality of life, cognition and mental health. *J. Neurol. Neurosurg. Psychiatry* 87, 1091–8. doi: 10.1136/jnnp-2016-313361

de Kroon, J. R., Ijzerman, M. J., Chae, J., Lankhorst, G. J., and Zilvold, G. (2005). Relation between stimulation characteristics and clinical outcome in studies using electrical stimulation to improve motor control of the upper extremity in stroke. *J. Rehabil. Med.* 37, 65–74. doi: 10.1080/16501970410024190

Deci, E. L., Eghrari, H., Patrick, B. C., and Leone, D. R. (1994). Facilitating internalization: the self-determination theory perspective. *J. Pers.* 62, 119–42. doi: 10.1111/j.1467-6494.1994.tb00797.x

Desrosiers, J., Malouin, F., Bourbonnais, D., Richards, C. L., Rochette, A., Bravo, G., et al. (2003). Arm and leg impairments and disabilities after stroke rehabilitation: relation to handicap. *Clin. Rehabil.* 17, 666–73. doi: 10.1191/0269215503cr662oa

Doucet, B. M., Lam, A., and Griffin, L. (2012). Neuromuscular electrical stimulation for skeletal muscle function. *Yale. J. Biol. Med.* 85, 201–15.

Doumas, I., Everard, G., Dehem, S., and Lejeune, T. (2021). Serious games for upper limb rehabilitation after stroke: a meta-analysis. *J. Neuroeng. Rehabil.* 18, 100. doi: 10.1186/s12984-021-00889-1

Dwan, K., Li, T., Altman, D. G., and Elbourne, D. C. O. N. S. O. R. T. (2019). 2010 statement: extension to randomised crossover trials. *BMJ* 366, 14378. doi: 10.1136/bmj.l4378

Eraifej, J., Clark, W., France, B., Desando, S., and Moore, D. (2017). Effectiveness of upper limb functional electrical stimulation after stroke for the improvement of activities of daily living and motor function: a systematic review and meta-analysis. *Syst. Rev.* 6, 40. doi: 10.1186/s13643-017-0435-5

Feigin, V. L., Stark, B. A., Johnson, C. O., Roth, G. A., Bisignano, C., Abady, G. G., et al. (2021). Global, regional, and national burden of stroke and its risk factors, 1990–2019: a systematic analysis for the Global Burden of Disease Study 2019. *Lancet Neurol.* 20, 795–820. doi: 10.1016/S1474-4422(21)00252-0

French, B., Thomas, L. H., Coupe, J., McMahon, N. E., Connell, L., Harrison, J., et al. (2016). Repetitive task training for improving functional ability after stroke. *Cochrane Database Syst. Rev.* 11, Cd006073. doi: 10.1002/14651858.CD006073.pub3

Fu, M. J., Harley, M. Y., Hisel, T., Busch, R., Wilson, R., Chae, J., et al. (2019). Ability of people with post-stroke hemiplegia to self-administer FES-assisted hand therapy video games at home: an exploratory case series. *J. Rehabil. Assist. Technol. Eng.* 6, 2055668319854000. doi: 10.1177/2055668319854000

Hart, S. G. (2006). NASA-Task Load Index (NASA-TLX) 20 Years Later. *Proceedings of the Human Factors and Ergonomics Society Annual Meeting*. 50, 904–8. doi: 10.1177/154193120605000909

Hart, S. G., and Staveland, L. E. (1988). *Development of NASA-TLX (Task Load Index): Results of empirical and Theoretical Research*. Hancock PA, Meshkati N, editors. North-Holland. doi: 10.1016/S0166-4115(08)62386-9

Hebert, D., Lindsay, M. P., McIntyre, A., Kirtan, A., Rumney, P. G., Bagg, S., et al. (2016). Canadian stroke best practice recommendations: stroke rehabilitation practice guidelines, update 2015. *Int. J. Stroke Soc.* 11, 459–84. doi: 10.1177/1747493016643553

Höhler, C., Trigili, E., Astarita, D., Hermsdörfer, J., Jahn, K., Krewer, C., et al. (2023). The efficacy of hybrid neuroprostheses in the rehabilitation of upper limb impairment after stroke, a systematic review with a meta-analysis. *Res. Square*. 3, 1. doi: 10.21203/rs.3.rs-2910291/v1

Howlett, O. A., Lannin, N. A., Ada, L., and McKinstry, C. (2015). Functional electrical stimulation improves activity after stroke: a systematic review with meta-analysis. *Arch. Phys. Med. Rehabil.* 96, 934–43. doi: 10.1016/j.apmr.2015.01.013

Kleim, J. A., and Jones, T. A. (2008). Principles of experience-dependent neural plasticity: implications for rehabilitation after brain damage. *J. Speech Lang. Hear. Res.* 51, S225–39. doi: 10.1044/1092-4388(2008)018

Krewer, C., Sikorski, C., Blechschmidt, C., Müller, F., and Quintern, J. (2008). *From Mind to Movement—Contralateral EMG-Triggered Electrical Stimulation for Bilateral Movements in Hemiparetic Patients*. Freiburg: IFESS.

Küçükdeveci, A. A., Stibrant Sunnerhagen, K., Golyk, V., Delarque, A., Ivanova, G., Zampolini, M., et al. (2018). Evidence-based position paper on Physical and Rehabilitation Medicine professional practice for persons with stroke. The European PRM position (UEMS PRM Section). *Eur. J. Phys. Rehabil. Med.* 54, 957–70. doi: 10.23736/S1973-9087.18.05501-6

Kumar, D., Verma, S., Bhattacharya, S., and Lahiri, U. (2016). Audio-visual stimulation in conjunction with functional electrical stimulation to address upper limb and lower limb movement disorder. *Eur. J. Transl. Myol.* 26, 6030. doi: 10.4081/ejtm.2016.6030

Kutlu, M., Freeman, C. T., Hallewell, E., Hughes, A. M., and Laila, D. S. (2016). Upper-limb stroke rehabilitation using electrode-array based functional electrical

stimulation with sensing and control innovations. *Med. Eng. Phys.* 38, 366–79. doi: 10.1016/j.medengphys.2016.01.004

Laver, K. E., Lange, B., George, S., Deutsch, J. E., Saposnik, G., Crotty, M., et al. (2017). Virtual reality for stroke rehabilitation. *Cochrane Database Syst. Rev.* 11, CD008349. doi: 10.1002/14651858.CD008349.pub4

Lee, S. H., Lee, J. Y., Kim, M. Y., Jeon, Y. J., Kim, S., Shin, J. H., et al. (2018). Virtual reality rehabilitation with functional electrical stimulation improves upper extremity function in patients with chronic stroke: a pilot randomized controlled study. *Arch. Phys. Med. Rehabil.* 99, 1447–53. e1. doi: 10.1016/j.apmr.2018.01.030

Lohse, K. R., Hilderman, C. G. E., Cheung, K. L., Tatla, S., and Van Der Loos, H. F. M. (2014). Virtual reality therapy for adults post-stroke: a systematic review and meta-analysis exploring virtual environments and commercial games in therapy. *PLoS ONE* 9, e93318. doi: 10.1371/journal.pone.0093318

Luengo-Fernandez, R., Paul, N. L., Gray, A. M., Pendlebury, S. T., Bull, L. M., Welch, S. J., et al. (2013). Population-based study of disability and institutionalization after transient ischemic attack and stroke: 10-year results of the Oxford vascular study. *Stroke* 44, 2854–61. doi: 10.1161/STROKEAHA.113.001584

Maier, M., Ballester, B. R., Duff, A., Oller, E. D., and Verschure, P. F. (2019a). Effect of specific over non-specific vr-based rehabilitation on poststroke motor recovery: a systematic meta-analysis. *Neurorehabil. Neural Repair* 33, 112–29. doi: 10.1177/1545968318820169

Maier, M., Ballester, B. R., and Verschure, P. F. (2019b). Principles of neurorehabilitation after stroke based on motor learning and brain plasticity mechanisms. *Front. Syst. Neurosci.* 13, 74. doi: 10.3389/fnsys.2019.00074

McAuley, E., Duncan, T., and Tammen, V. V. (1989). Psychometric properties of the Intrinsic Motivation Inventory in a competitive sport setting: a confirmatory factor analysis. *Res. Q. Exerc. Sport*. 60, 48–58. doi: 10.1080/02701367.1989.10607413

Meadmore, K. L., Hughes, A. M., Freeman, C. T., Cai, Z., Tong, D., Burrage, J. H., et al. (2012). Functional electrical stimulation mediated by iterative learning control and 3D robotics reduces motor impairment in chronic stroke. *J. Neuroeng. Rehabil.* 9, 32. doi: 10.1186/1743-0003-9-32

Meier, P. (2021). Plastizität und motorisches Lernen. In: Schick T, editor. *Funktionelle Elektrostimulation in der Neurorehabilitation: Synergieeffekte von Therapie und Technologie*. Berlin, Heidelberg: Springer, 9–19. doi: 10.1007/978-3-662-61705-2_2

Moe, J., and Post, H. (1962). Functional electrical stimulation for ambulation in hemiplegia. *J. Lancet*. 82, 285–8.

Monardo, G., Pavese, C., Giorgi, I., Godi, M., and Colombo, R. (2021). Evaluation of patient motivation and satisfaction during technology-assisted rehabilitation: an experiential review. *Games Health J.* 10, 13–27. doi: 10.1089/g4h.2020.0024

Monte-Silva, K., Piscitelli, D., Norouzi-Gheidari, N., Batalla, M., Archambault, P., Levin, M. F., et al. (2019). Electromyogram-related neuromuscular electrical stimulation for restoring wrist and hand movement in poststroke hemiplegia: a systematic review and meta-analysis. *Neurorehabil. Neural. Repair*. 33, 96–111. doi: 10.1177/1545968319826053

NASA Ames Research Center (1986). NASA Task Load Index (TLX): Paper and Pencil Package. Available online at: <https://humansystems.arc.nasa.gov/groups/TLX/downloads/TLX.pdf> (accessed March 11, 2023).

Nasreddine, Z. S., Phillips, N. A., Bédirian, V., Charbonneau, S., Whitehead, V., Collin, I., et al. (2005). The montreal cognitive assessment MoCA: a brief screening tool for mild cognitive impairment. *J. Am. Geriatr. Soc.* 53, 695–9. doi: 10.1111/j.1532-5415.2005.53221.x

Norouzi-Gheidari, N., Archambault, P. S., Monte-Silva, K., Kairy, D., Sveistrup, H., Trivino, M., et al. (2021). Feasibility and preliminary efficacy of a combined virtual reality, robotics and electrical stimulation intervention in upper extremity stroke rehabilitation. *J. Neuroeng. Rehabil.* 18, 61. doi: 10.1186/s12984-021-00851-1

Oujamaa, L., Relave, I., Froger, J., Mottet, D., and Pelissier, J. Y. (2009). Rehabilitation of arm function after stroke. Literature review. *Ann. Phys. Rehabil. Med.* 52, 269–93. doi: 10.1016/j.rehab.2008.10.003

Peres, S., Pham, T., and Phillips, R. (2013). Validation of the system usability scale (SUS). *Proceedings of the Human Factors and Ergonomics Society Annual Meeting*. 57, 192–6. doi: 10.1177/1541931213571043

Platz, T. (2021). *Clinical Pathways in Stroke Rehabilitation: Evidence-based Clinical Practice Recommendations*. Cham: Springer International Publishing. 1–13. p. doi: 10.1007/978-3-030-58505-1

Platz, T., Fheodoroff, K., Mehrholz, J., Nyffeler, T., Roschka, S., Schupp, W., et al. (2020). *S3-Leitlinie Rehabilitative Therapie bei Armparese nach Schlaganfall*. Available online at: https://www.awmf.org/uploads/tx_szleitlinien/080-0011_S3_Rehabilitative_Therapie_bei_Armparese_nach_Schlaganfall_2020-07.pdf (accessed March 01, 2023).

Pollock, A., Farmer, S. E., Brady, M. C., Langhorne, P., Mead, G. E., Mehrholz, J., et al. (2014). Interventions for improving upper limb function after stroke. *Cochrane Database Syst. Rev.* 3, CD010820. doi: 10.1002/14651858.CD010820.pub2

Prange-Lasonder, G. B., Radder, B., Kottink, A. I. R., Melendez-Calderon, A., Bourke, J. H., and Rietman, J. S., editors. (2017). Applying a soft-robotic glove as assistive device and training tool with games to support hand function after stroke: preliminary results on feasibility and potential clinical impact. 2017

International Conference on Rehabilitation Robotics (ICORR). 17–20 July 2017. doi: 10.1109/ICORR.2017.8009444

Rücker, V., Heuschmann, P. U., O'Flaherty, M., Weingärtner, M., Hess, M., Sedlak, C., et al. (2020). 20-year time trends in long-term case-fatality and recurrence rates after ischemic stroke stratified by etiology. *Stroke* 51, 2778–85. doi: 10.1161/STROKEAHA.120.029972

Saposnik, G., and Levin, M. (2011). Outcome Research Canada (SORCan) Working Group. Virtual reality in stroke rehabilitation: a meta-analysis and implications for clinicians. *Stroke* 42, 1380–6. doi: 10.1161/STROKEAHA.110.605451

Teo, W. P., Muthalib, M., Yamin, S., Hendy, A. M., Bramstedt, K., Kotsopoulos, E., et al. (2016). Does a combination of virtual reality, neuromodulation and neuroimaging provide a comprehensive platform for neurorehabilitation?—A narrative review of the literature. *Front. Hum. Neurosci.* 10, 284. doi: 10.3389/fnhum.2016.00284

Veerbeek, J. M., van Wegen, E., van Peppen, R., van der Wees, P. J., Hendriks, E., Rietberg, M., et al. (2014). What is the evidence for physical therapy poststroke? A systematic review and meta-analysis. *PLoS ONE* 9, e87987. doi: 10.1371/journal.pone.0087987



OPEN ACCESS

EDITED BY
Emilio Trigili,
Institute of BioRobotics, Italy

REVIEWED BY
Alireza Mohammadi,
University of Michigan-Dearborn, United States
Antonio Di Lallo,
University of Pisa, Italy

*CORRESPONDENCE
Carlos A. Cifuentes
✉ carlos.cifuentes@uwe.ac.uk

RECEIVED 07 November 2022
ACCEPTED 26 May 2023
PUBLISHED 15 June 2023

CITATION
Maldonado-Mejía JC, Múnera M, Diaz CAR,
Wurdemann H, Moazen M, Pontes MJ, Vieira
Segatto ME, Monteiro ME and Cifuentes CA
(2023) A fabric-based soft hand exoskeleton for
assistance: the ExHand Exoskeleton.
Front. Neurobot. 17:1091827.
doi: 10.3389/fnbot.2023.1091827

COPYRIGHT
© 2023 Maldonado-Mejía, Múnera, Diaz,
Wurdemann, Moazen, Pontes, Vieira Segatto,
Monteiro and Cifuentes. This is an open-access
article distributed under the terms of the
[Creative Commons Attribution License \(CC BY\)](https://creativecommons.org/licenses/by/4.0/).
The use, distribution or reproduction in other
forums is permitted, provided the original
author(s) and the copyright owner(s) are
credited and that the original publication in this
journal is cited, in accordance with accepted
academic practice. No use, distribution or
reproduction is permitted which does not
comply with these terms.

A fabric-based soft hand exoskeleton for assistance: the ExHand Exoskeleton

Juan C. Maldonado-Mejía^{1,2}, Marcela Múnera^{2,3},
Camilo A. R. Diaz¹, Helge Wurdemann⁴, Mehran Moazen⁴,
Maria José Pontes¹, Marcelo Eduardo Vieira Segatto¹,
Maxwell E. Monteiro⁵ and Carlos A. Cifuentes^{3,6*}

¹Telecommunications Laboratory (LabTel), Electrical Engineering Department, Federal University of Espírito Santo (UFES), Vitória, Brazil, ²Department of Biomedical Engineering, Colombian School of Engineering Julio Garavito, Bogotá, Colombia, ³Bristol Robotics Laboratory, University of the West of England, Bristol, United Kingdom, ⁴Department of Mechanical Engineering, University College London, London, United Kingdom, ⁵Federal Institute of Espírito Santo (IFES), Serra, Brazil, ⁶School of Engineering, Science and Technology, Universidad del Rosario, Bogotá, Colombia

Introduction: The rise of soft robotics has driven the development of devices for assistance in activities of daily living (ADL). Likewise, different types of actuation have been developed for safer human interaction. Recently, textile-based pneumatic actuation has been introduced in hand exoskeletons for features such as biocompatibility, flexibility, and durability. These devices have demonstrated their potential use in assisting ADLs, such as the degrees of freedom assisted, the force exerted, or the inclusion of sensors. However, performing ADLs requires the use of different objects, so exoskeletons must provide the ability to grasp and maintain stable contact with a variety of objects to lead to the successful development of ADLs. Although textile-based exoskeletons have demonstrated significant advancements, the ability of these devices to maintain stable contact with a variety of objects commonly used in ADLs has yet to be fully evaluated.

Materials and methods: This paper presents the development and experimental validation in healthy users of a fabric-based soft hand exoskeleton through a grasping performance test using The Anthropomorphic Hand Assessment Protocol (AHAP), which assesses eight types of grasping with 24 objects of different shapes, sizes, textures, weights, and rigidities, and two standardized tests used in the rehabilitation processes of post-stroke patients.

Results and discussion: A total of 10 healthy users (45.50 ± 14.93 years old) participated in this study. The results indicate that the device can assist in developing ADLs by evaluating the eight types of grasps of the AHAP. A score of $95.76 \pm 2.90\%$ out of 100% was obtained for the Maintaining Score, indicating that the ExHand Exoskeleton can maintain stable contact with various daily living objects. In addition, the results of the user satisfaction questionnaire indicated a positive mean score of 4.27 ± 0.34 on a Likert scale ranging from 1 to 5.

KEYWORDS

hand exoskeleton, soft robotics, soft actuators, activities of daily living, assistive technologies

1. Introduction

Stroke is a leading cause of mortality and disability worldwide (Feigin et al., 2022). Common effects of stroke include communication impairments, balance and coordination deficits, reduced strength and motor control, and joint stiffness caused by spasticity (Murphy and Werring, 2020). In addition to these physical impairments, stroke survivors often

experience dependence on others for activities of daily living (ADLs), altered mood, and impaired social interaction (Schultz et al., 1997), which can significantly diminish their overall quality of life.

Hand function loss is one of the most common impairments experienced by stroke survivors (Liu et al., 2018). Given that the hand is critical for performing many activities of daily living, including self-care, eating, writing, washing, and dressing, this impairment can significantly affect a person's independence and quality of life. The hand's complexity, with more than 20 degrees of freedom (DoFs) and a wide range of motion (RoM) in each joint, enables it to execute various movement patterns for grasping different objects (Kapandji, 1971). Thus, restoring hand function is essential for the rehabilitation of a stroke survivor.

The primary goal of stroke rehabilitation is to improve patients' quality of life and achieve the highest level of independence possible for each individual (Kelley and Borazanci, 2009; Good et al., 2011). This process typically begins with an evaluation of the patient's condition, which may include the use of outcome measures (Fetters and Tilson, 2018). Based on this assessment, the therapist will develop an individualized rehabilitation program that includes a series of exercises aimed at improving motor recovery and increasing hand and finger strength, dexterity, and range of motion (RoM).

However, hand rehabilitation is a long-term process that requires patience, persistence, and many repetitive exercise routines that involve interaction between the patient and therapist, making it a laborious and costly process. As a result, many stroke survivors discontinue therapy before achieving the maximum potential for hand function recovery (Mohammadi et al., 2018).

Advancements in technology have led to the emergence of hand exoskeletons, which aid in rehabilitation therapies and assist with activities of daily living (ADLs). Hand exoskeletons are soft robotics devices that are inspired by biological systems and are designed to be safer for humans (Hsiao et al., 2019). This technology uses soft and flexible components such as polymers (Rus and Tolley, 2015; Whitesides, 2018) to reduce size, complexity, weight, and cost (Ferguson et al., 2020). Furthermore, soft robotics has inspired the development of actuator designs for hand exoskeletons that perform movements kinematically similar to natural human joint movements (Whitesides, 2018). As a result, safe, lightweight, portable, and affordable devices have been developed.

Hand exoskeletons based on soft robotics have proven to be effective in recovering hand function (Aisen et al., 1997; Carmeli et al., 2011). In particular, these devices have drastically reduced the rehabilitation process's cost and the workload of therapists by enabling patients to perform intense repetitive movements (Wolf et al., 2006; Kutner et al., 2010).

Recently, the use of textile-based pneumatic actuation has been explored in the development of hand exoskeletons, leveraging the lightness, softness, flexibility, durability, and biocompatibility of fabrics (Sanchez et al., 2021; Fu et al., 2022). These properties are crucial for developing assistive devices (Boser et al., 2020; du Plessis et al., 2021). For example, researchers have shown that geometric variations in the textile structure can enhance the anisotropy, allowing for a wider range of motion and increased force generated by fabric-based actuators (Cappello et al.,

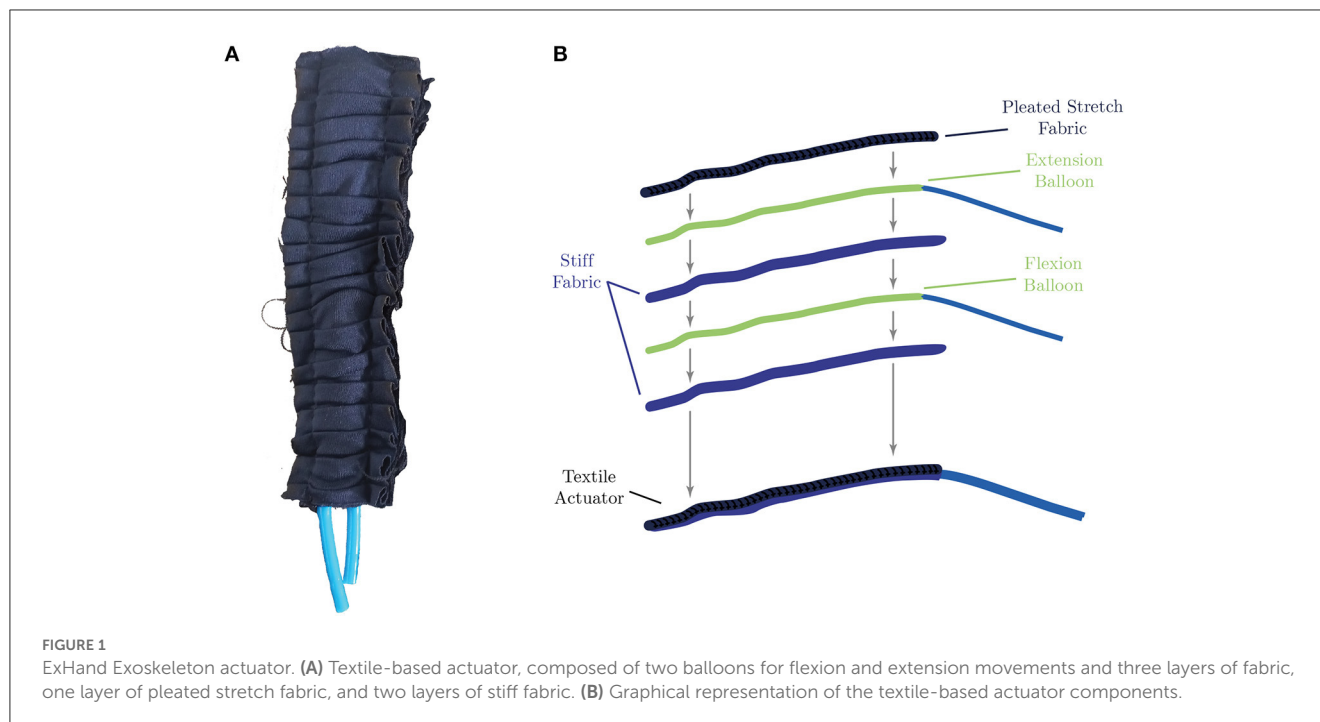
2018a,b). Soft robotic gloves have been developed using flexible thermoplastic polyurethane (TPU) coated fabrics for bidirectional actuation (Yap et al., 2017), and multi-articular actuators and textile-based capacitance soft sensors have been incorporated into the next generation of gloves (Zhou et al., 2019). Furthermore, a study has been conducted to investigate the mechanical properties of various fabrics, leading to the design of a glove that can assist in thumb abduction, finger flexion, and extension movements (Ge et al., 2020). The development of textile-based hand exoskeletons shows promising results and is an emerging field that could have significant implications for stroke rehabilitation and ADL assistance.

Textile-based exoskeletons have shown great potential in assisting with activities of daily living (ADLs) for post-stroke patients, particularly in the execution of repetitive motions such as flexion, extension, and thumb abduction movements. These devices can generate the necessary force to grasp most objects commonly used in daily life, which are estimated to require a distal tip force of around 7.3 N, as most everyday objects weigh no more than 1.5 kg (Matheus and Dollar, 2010). For example, the devices presented by Zhou et al. (2019) and Ge et al. (2020) can exert forces of 37 and 47.9 N, respectively.

In addition, a study by Cappello et al. (2018b) demonstrated how their exoskeleton was able to assist in the rehabilitation therapy of spinal cord injury (SCI) patients through the Toronto Rehabilitation Institute Hand Function Test (TRI-HFT), which includes a manipulation test of 10 objects used in ADLs. However, while these devices have successfully provided the necessary force for grasping objects, their ability to maintain stable contact with various objects commonly used in ADLs has yet to be fully evaluated. For instance, Gerez et al. (2020) evaluated the grasping ability of a hybrid exoskeleton on 13 objects from the Yale-CMU-Berkeley object set, which is a collection of daily living objects that facilitates benchmarking in robotic manipulation and grasping (Calli et al., 2015).

Overall, while textile-based exoskeletons have shown promise in assisting with ADLs, further evaluation of their ability to grasp and maintain stable contact with various objects is needed to fully assess their effectiveness in daily life scenarios.

This paper builds upon the work of Ramos et al. (2022) by integrating textile actuators into an assistive device. In their study, Ramos et al. demonstrated that pleated textile actuators with a length of 16 cm and a width of 2 cm are capable of achieving a distal tip force of 9.18 ± 1.16 N, which is sufficient force to aid patients in manipulating various daily objects. Based on this finding, we present the development of a fabric-based hand exoskeleton, named the ExHand Exoskeleton, designed to assist stroke survivors with activities of daily living (ADL). Before its use on post-stroke patients, we experimentally validate the device on healthy subjects using the Anthropomorphic Hand Assessment Protocol (AHAP), a protocol developed by Llop-Harillo et al. (2019) for evaluating anthropomorphic robotic and prosthetic devices. The AHAP uses 25 objects from the Yale-CMU-Berkeley object set and quantifies the device's ability to hold the objects through eight relevant grasp types. Additionally, we evaluate the device's functionality through two outcome measures commonly used in the rehabilitation process of post-stroke



patients. Finally, we evaluate the usability of the device through a questionnaire.

This document is structured as follows: Section 2 details the development and experimental validation of the ExHand Exoskeleton. Section 3 presents the evaluation results, and Section 4 compares our results with those of related work while highlighting advantages and limitations. Finally, we conclude and outline future work in Section 5.

2. Materials and methods

2.1. The ExHand Exoskeleton

As previously stated, this work presents the development and evaluation of the ExHand Exoskeleton. This section presents the exoskeleton actuators, the construction of the hand exoskeleton ExHand (its mechatronic system and its functionalities), and finally, the experimental validation of the exoskeleton.

2.2. Exoskeleton actuators

Before using the textile actuators on the hand exoskeleton, their structure and operation are detailed. Elastic and inelastic fabric and thermoplastic elastomer (TPE) materials are used to construct the actuators. Specifically, a rigid fabric and an elastic fabric type, Lycra (Lycra-Nilon POWER ID-0019-056, Facol, Colombia), were used to construct the actuator. The construction process is done by creating a pocket from two layers of rigid fabric and adding a pleated elastic fabric on top. The fabric-based actuator comprises three layers of fabric (two layers of rigid material and one layer of pleated stretch fabric) and two TPE balloons housed in the pockets generated by the fabric layers, as shown in [Figure 1](#). Thus, flexion

and extension movements are achieved by selective pressurization of the inner balloons.

2.3. Exoskeleton construction

The construction of the ExHand Exoskeleton is first carried out by searching for a suitable glove. The glove selection was based on the anthropometric measurements of the Colombian population (target population) and the glove sizing system used in Colombia, which uses two dimensions: metacarpal perimeter and hand length. [Figure 2](#) and [Table 1](#) present anthropometric measurements of the hand of the Colombian population divided by gender and percentiles, and [Table 2](#) presents the glove sizes in Colombia.

An anthropometric design requires adapting the products to 90% of the user population. For this reason, the most commonly used percentiles in ergonomic design are 5 (smaller people) and 95 (larger people), representing 90% of the population ([Robinette, 2012](#)). Therefore, the 95 percentile of the male is selected to ensure most users' comfortable use of the exoskeleton. Thus, glove size nine is the most appropriate for these measurements, as it has a metacarpal perimeter of 22.9 cm and a hand length of 19.2 cm, which is very close to the anthropometric measurements of the 95th percentile of the male (metacarpal perimeter of 22.15 cm and hand length of 19.90 cm).

Once the glove is obtained, the actuators are placed. To facilitate the attachment of the actuators to the glove, a cutout is made to place them from the tip of the finger to the dorsal area of the glove. As a result, each actuator measured 13, 18.6, 19.6, 18.7, and 16 cm for the thumb, index, middle, ring, and little finger, respectively. Thus, the textile actuators were sewn around each finger from the tip of the finger to the dorsal part of the hand, and a silicone coating

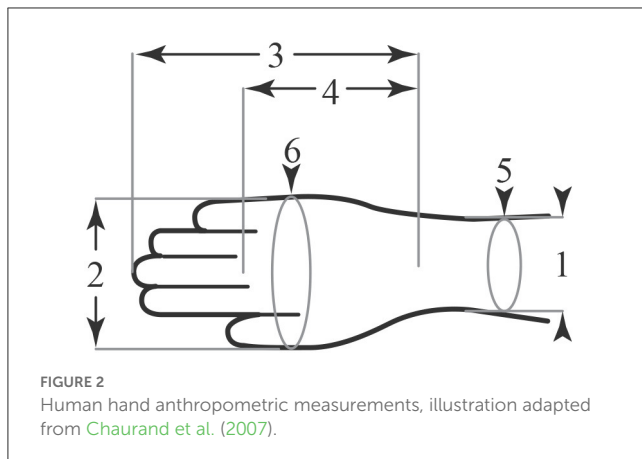


TABLE 1 Anthropometric measures of the hand in the Colombian population, males ($n = 1,315$) and females ($n = 785$) between 20 and 59 years old (Chaurand et al., 2007).

Gender	Female			Male		
Percentile	5	50	95	5	50	95
1. Wrist width (cm)	4.48	4.93	5.43	5.00	5.58	6.05
2. Hand width (cm)	6.85	7.45	8.03	7.78	8.45	9.08
3. Hand length (cm)	15.43	16.60	17.95	16.83	18.30	19.90
4. Palm length (cm)	8.48	9.23	10.08	9.28	10.28	11.23
5. Wrist perimeter (cm)	13.53	14.68	16.10	15.20	16.53	17.98
6. Metacarpal perimeter (cm)	16.58	17.95	19.40	18.85	20.45	22.15

TABLE 2 Glove dimensions according to the Colombian sizing system (Rincón Becerra and Garc-a-Acosta, 2014).

Glove size	Metacarpal perimeter of the glove (cm)	Hand length of the glove (cm)
6	15.20	16.00
7	17.80	17.10
8	20.30	18.20
9	22.90	19.20
10	25.40	20.40
11	27.90	21.50

of Ecoflex 00-30 (Smooth-On, USA) was applied on the palmar area to generate a non-slip surface to improve grip. Finally, an elastic band with Velcro was added to fix the glove to the patient's wrist. The ExHand Exoskeleton is shown in Figure 3.

2.4. Mechatronics system

The pneumatic system of the ExHand Exoskeleton is composed of an air pump ROB-10398 (Sparkfun Electronics, USA) of 32 psi of pressure. The ROB-10398 air pump can be used either as a vacuum pump or an air pump; in this case, the air pump is

used for the ExHand Exoskeleton. For the selective pressurization of the balloons, a system of 11 solenoid electrovalves (Adafruit, USA) of three ways in two positions is implemented. Thus, 10 electrovalves control the flexion/extension movements performed by the selective pressurization of the internal balloons, and one electrovalve controls the air output. In addition, ten pressure sensors (MPX4250DP, NXP, Netherlands) have been added to measure the air pressure entering each of the inner balloons. Thus, air leakage due to over-pressurization is prevented, and the pressure can be adjusted to the user's requirements. The pneumatic schematic of the ExHand Exoskeleton is presented in Figure 4.

The control of each internal balloon gives the exoskeleton the ability for the extension balloons to work simultaneously with the flexion balloons; this enables the exoskeleton to perform different combinations resulting in different types of grasp such as power grip, pulp pinch, tripod pinch commonly used in ADL, or actuate each finger separately if needed. Figure 5 shows some configurations.

A web interface was developed for the operation of the exoskeleton; in this interface, different modes of operation are established, for example, the extension of all fingers, different grips such as power grip, pulp pinch or tripod pinch, and depressurization of the system. Also, a configuration panel was added to adjust the pressure limits for each internal balloon as required by the user.

Regarding the electronics system, 3 ADCs (ADS1115, Adafruit, New York, USA) are configured at 860 samples per second to read the pressure sensors' data. In addition, four 4-channel MOSFET switching modules were implemented as electric switches for the air pump and solenoid valves. Thus, as soon as a command is received from the web interface, the air pump, and solenoid valves corresponding to the requested motion are turned on, as shown in Figure 5A or Figure 5B. Once the pressure set by the user is reached, the air pump and solenoid valves are turned off to prevent over-pressurization. In the event of an air leak due to damage to the internal balloons, the air pump and corresponding solenoid valve will be kept until the user sends a different command from the web interface. All the processing and control of the device is performed by one single board computer (Raspberry Pi 3 B+) with the official operating system for Raspberry Pi systems based on Debian, Raspbian OS, and running Robot Operating System (ROS). In terms of consumption, the Raspberry Pi 3 B+ is sufficient to power the ADCs and pressure sensors, as each ADC consumes 5 V/150 μ A, and each pressure sensor consumes 5 V/7.0 mA. As for the air pump (12 V, 1 A) and the solenoid valves (5 V, 220 mA), a separate 12 V/5 A power supply and a DC-DC voltage regulator (LM2596, DFRobot, Shanghai, China) set to 5 V are used. Finally, Figure 6 illustrates the electronic system and its connections for clarity.

2.5. ExHand Exoskeleton features

The study by Ramos et al. (2022) found that the textile-based actuators used to construct the ExHand Exoskeleton achieved a maximum distal tip force of 9.18 ± 1.16 N and a full bending time of 1.01 ± 0.33 s. Afterwards, benchtop experiments are performed

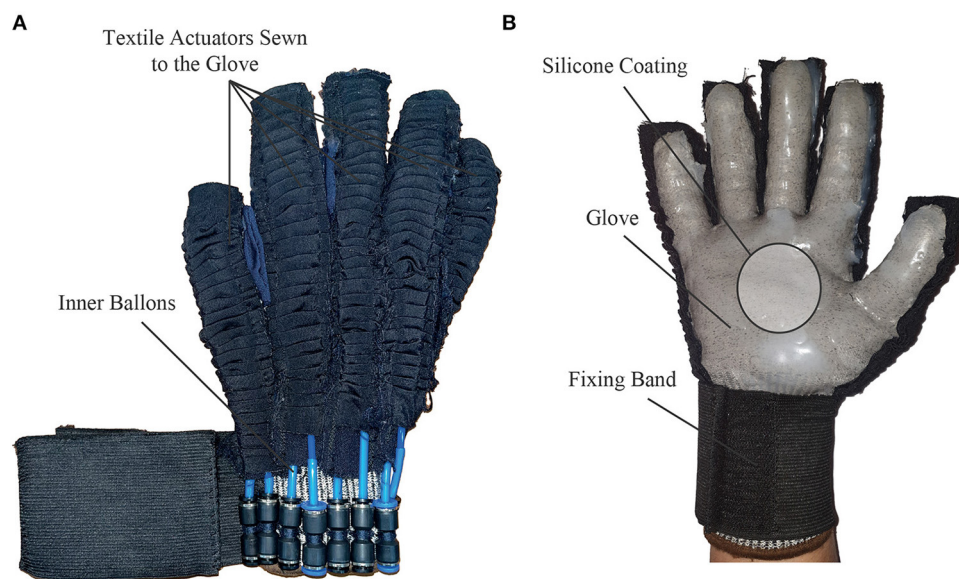


FIGURE 3

The ExHand Exoskeleton. (A) Dorsal side of the ExHand Exoskeleton shows the placements of the textile actuators on the glove. (B) Palmar side of the ExHand Exoskeleton, the coating of EcoFlex 00-30, and how the elastic band fixes to the user's wrist are shown here.

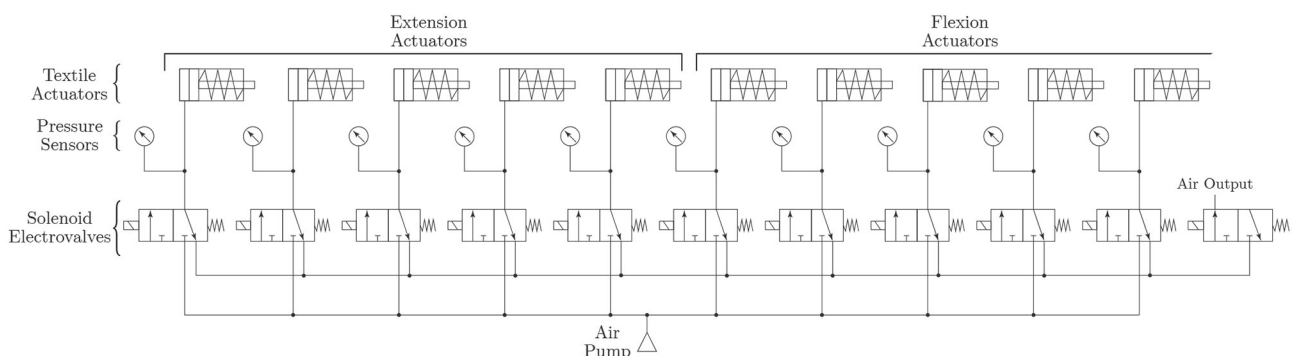


FIGURE 4

Schematic of the pneumatic system of the ExHand Exoskeleton.

to evaluate the time required to fully open and close the hand exoskeleton and the maximum force that can be exerted during grasping/holding.

2.5.1. Time required to fully open and close

To measure the time required to open and close the exoskeleton completely, a volunteer was invited to done the exoskeleton while performing flexion and extension movements until the user's hand closed and opened as much as possible. The tests were recorded with a side camera, and the time was taken using a stopwatch from starting to pressurize the exoskeleton until the full flexion/extension movement was achieved.

2.5.2. Exoskeleton maximum grasping/holding force

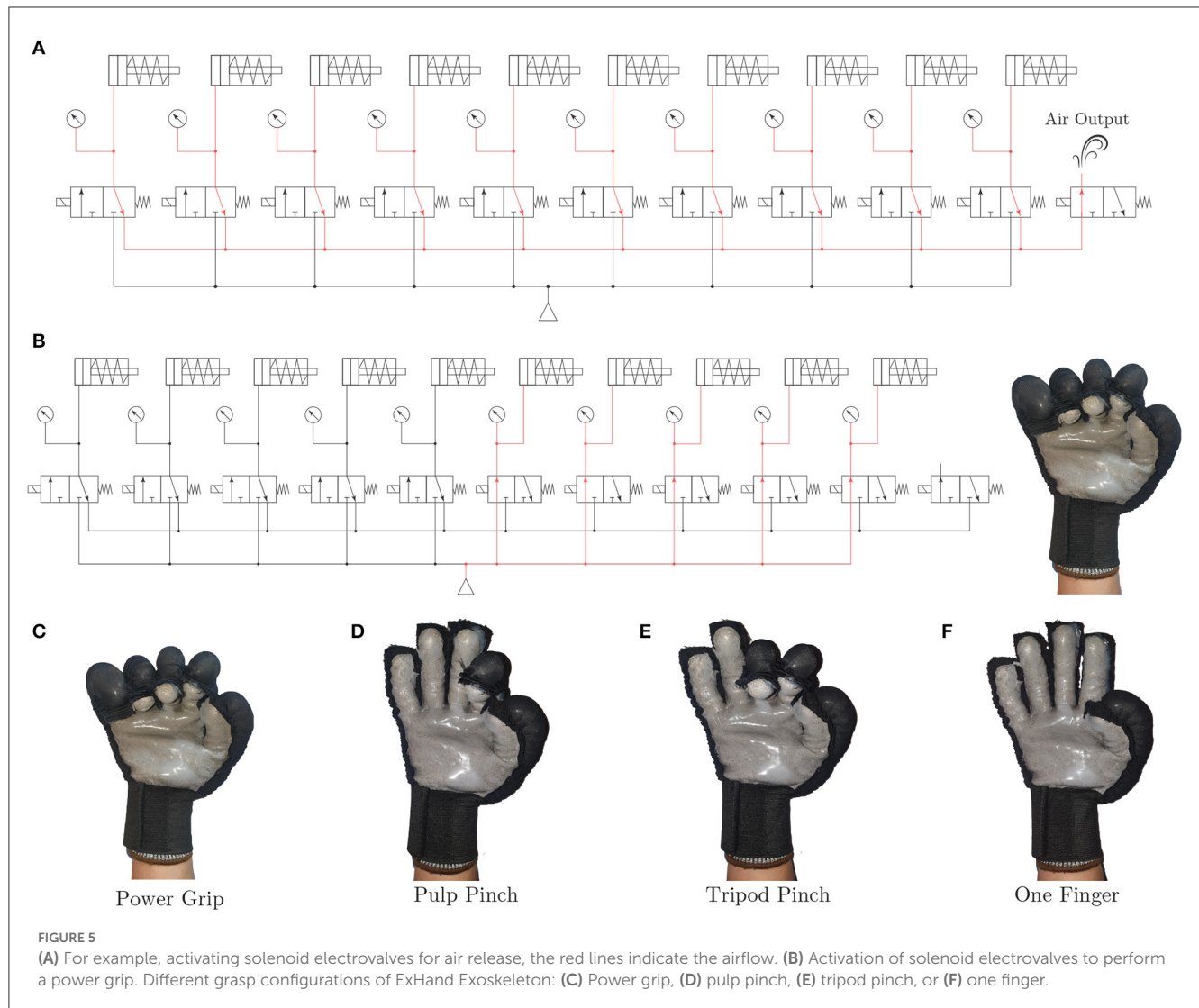
To evaluate the maximum grasping/holding force of the ExHand Exoskeleton, a 90 kg manual electronic dynamometer

(Instruterm, Brazil) was used, and an experiment similar to that of Zhou et al. (2019) was performed, where grasping/holding force was evaluated as the bending force required to extend the pressurized flexion actuators of all fingers without the thumb. A 3D printing that included the flexion DoFs of the fingers was placed inside the glove.

2.6. Experimental validation with healthy users

2.6.1. Participants

To evaluate the functionality and usability of the ExHand Exoskeleton, healthy users between 18 and 70 years of age, normal hand motor function, and the ability to perform gross and light gripping actions without discomfort or pain were included. The Ethical Committee in the Colombian School of Engineering Julio Garavito approved the study. All participants were informed about



the scope and purpose of the study, and all participating individuals signed an informed consent form.

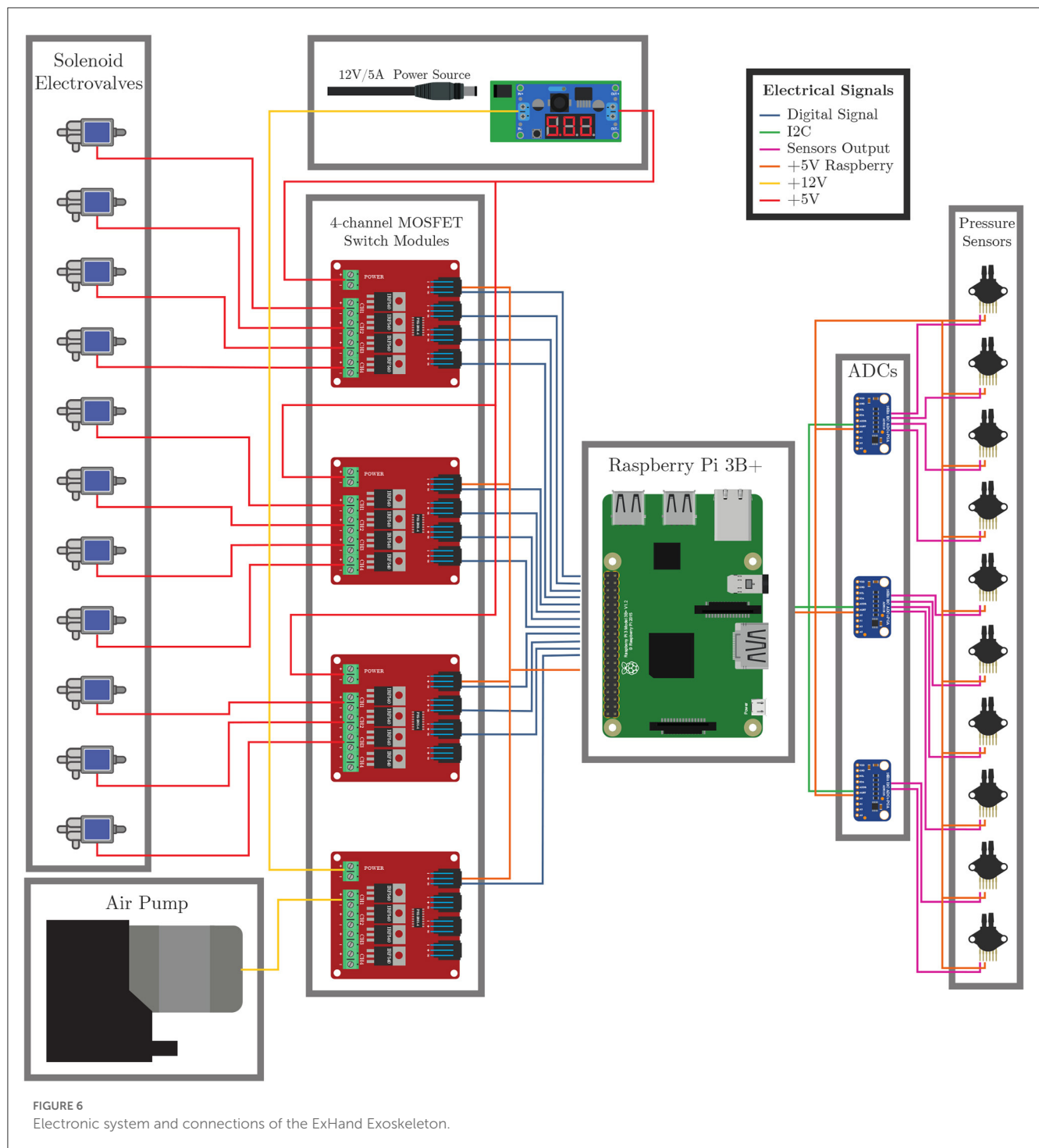
2.6.2. Functional tests

As previously mentioned, the functionality of the ExHand Exoskeleton is evaluated through the AHAP and two outcome measures used in the rehabilitation process of post-stroke patients. For the development of the tests, the participants were instructed to relax their muscles and let the exoskeleton actuation assist the flexion and extension movements of the fingers. After reading and signing the informed consent, the exoskeleton is donned to the participant, and the test procedure is explained. Furthermore, the exoskeleton was controlled by an operator using the web application. The operator adjusts the air pressure value entering each inner balloon according to the user's hand to perform complete flexion and extension movements before starting the tests. Before grasping any object, the operator activates the extension movement, depressurizes the exoskeleton, and then activates the flexion movement according to the most appropriate grip for each

object; once the object is released, the exoskeleton is depressurized again. All interventions were recorded using two cameras, one in front of the participant to capture a top view and the second on the side.

2.6.2.1. Grasping performance test

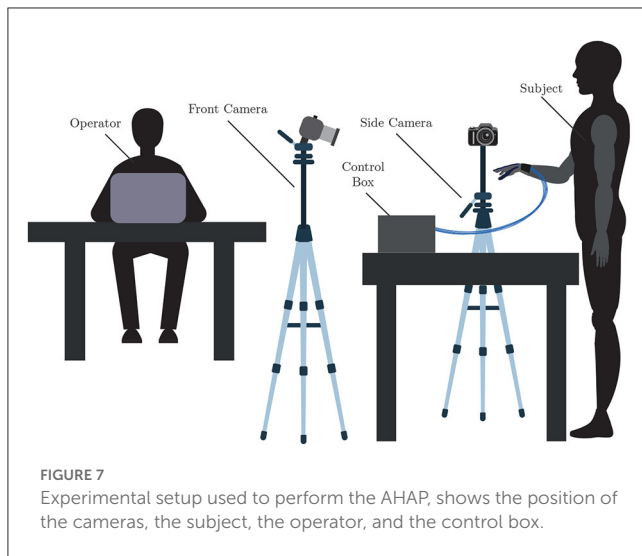
The Anthropomorphic Hand Assessment Protocol (AHAP) (Llop-Harillo et al., 2019) was chosen to evaluate the ability of the textile-based ExHand Exoskeleton to grasp various everyday objects. This protocol defines a total score that quantifies the ability to perform everyday grasps using a set of internationally available objects. AHAP uses the YCB set of objects proposed by Calli et al. (2015), including 25 objects of daily life with different shapes, sizes, textures, weights, and rigidities. Within the objects are food items, kitchen items, tools, form items, and task items. Although the AHAP is focused on anthropomorphic hands for robotic and prosthetic applications, the results obtained by the protocol provide a baseline for comparison and a way to recognize possible improvements in the design of the devices, such as hand exoskeletons.



AHAP involves two non-grasp postures and eight different grasps: hook grip, spherical grip, tripod pinch, extension grip, cylindrical grip, diagonal volar grip, lateral pinch, and pulp pinch. In this case, the two non-grasp postures and one object associated with these postures were excluded since the evaluation of these postures would not provide revealing results for the analysis of grasping of the hand exoskeleton.

For the execution of the protocol, the participant must be standing and positioned near a table, as shown in Figure 7.

Thus, the participant is instructed on the correct grasping posture for each object according to Llop-Harillo et al. (2019) and can practice with the object for 1 min. The objects are handed to the participant by the operator. Subsequently, the participant holds the grasp for 3 s. The participant naturally rotates the hand with low acceleration for the palm to point downwards (180°) and keeps the grip for another 3 s. Finally, the operator depressurizes the system to release the object.



The protocol is repeated three times for each object, and the score is divided as follows: the ability of the device to perform the grip correctly, similar to a healthy subject (*Grasping*) and the ability to hold the object without it moving (*Maintaining*). *Grasping* score and *Maintaining* score are scored from when the object is attempted to be grasped to when the object is released. In addition, *Grasping* is scored with values of 0, 0.5, and 1, being 1 if the grasping is completed with the correct grasping type, 0.5 if the grasping posture is different from the correct grasping type and 0 if the device cannot grasp the object. In the same way, *Maintaining* is scored with values of 0, 0.5, and 1, 1 if the object remains static while being held, 0.5 if the object moves and 0 if the object is dropped. The *Grasping* and *Maintaining* scores of the three objects of each type of grip are added together to obtain the final score for each grasp. Afterwards, a final score obtained from the two previous scores is calculated; this score is named the Grasping Ability Score (GAS) and quantifies the device's ability to perform all grasps. All scores are presented as a percentage. A GAS score of 100% means that the device can perform the different grasps in the same form as a healthy person (Llop-Harillo et al., 2019). To score the ExHand Exoskeleton, three external evaluators provided the *Grasping*, *Maintaining*, and GAS scores for each type of grasp using the video recorded during each test.

2.6.2.2. Box and Blocks Test

Another test performed is the Box and Blocks Test (BBT). BBT is a common outcome measure used to assess the unilateral gross manual dexterity in various populations, including stroke survivors with mild-to-moderate deficits (Thompson-Butel et al., 2015; Kontson et al., 2017). This test complements the AHAP as its results provide information on how the use of the device may affect the user's dexterity to perform ADLs that require a precise grip. The BBT contains 150 wooden cubes of 2.5 cm of sides and a wooden box (dimensions 53.7 × 25.4 × 8.5 cm) divided into two compartments by a partition of 15.2 cm in height. The test consists of moving, one by one, the maximum number of blocks from one compartment of the box to the other within 60 s (Mathiowetz et al., 1985). The participant performed the test seated close to a table.

TABLE 3 Air pressure values to reach complete extension and flexion movements in all fingers.

Finger	Air pressure for extension movement (psi)	Air pressure for flexion movement (psi)
Thumb	8.90 ± 0.16	4.63 ± 0.16
Index	9.95 ± 0.08	8.34 ± 0.28
Middle	10.45 ± 0.08	8.85 ± 0.37
Ring	9.95 ± 0.08	8.59 ± 0.22
Little finger	9.35 ± 0.24	5.57 ± 0.09

The box was placed on the table on the participant's midline and oriented lengthwise, with the compartment containing the blocks oriented toward the hand evaluated (Mathiowetz et al., 1985). The final score is the number of blocks transferred from one box compartment to another in 60 s.

2.6.2.3. Jebsen Taylor Hand Function Test

The Jebsen Taylor Hand Function Test (JTHFT) is another common outcome measure and has been used in clinical and research settings in different patient populations. The JTHFT assesses hand motor function through different ADL-related tasks (Jebsen, 1969). This consists of seven subtasks, including:

- Writing a 24-letter sentence.
- Turning over five cards of 7.6 × 12.7 cm (page turning simulation).
- Grasping five small objects (e.g., pennies, paper clips, bottle caps) and placing them in a container.
- Stacking five checkers.
- Simulated feeding.
- Moving five large empty cans.
- Moving five large heavy cans (450 g).










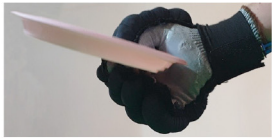




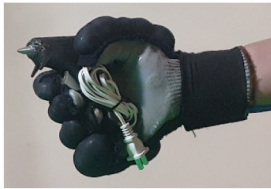
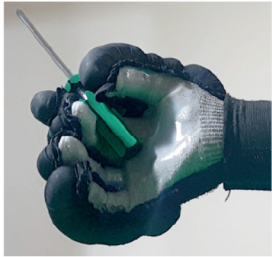


The participant must be seated close to a table to start the test. A stopwatch is used to record the time taken in each subtask. The total score is the sum of time taken for each subtask, where shorter times indicate better performance (Jebsen, 1969; Takla et al., 2018).

2.6.3. Usability assessment

The Quebec User Evaluation of Satisfaction with Assistive Technology (QUEST) 2.0 has been applied to assess the participant's perception. This questionnaire was designed to assess people's satisfaction with assistive devices. QUEST includes the rating of 12 items using a 5-point Likert scale (1: not satisfied at all, 2: not very satisfied, 3: more or less satisfied, 4: quite satisfied, and 5: very satisfied) and is divided into three scores: *Device*, *Services*, and Total QUEST (Demers et al., 2000).

To identify the level of satisfaction or dissatisfaction of users when using the ExHand Exoskeleton, QUEST 2.0 was adapted to evaluate only six items corresponding to the *Device* score: Dimensions, weight, adjustment, safety, comfort, and effectiveness. The participants answered the questionnaire once the functional tests were completed.

TABLE 4 The ExHand Exoskeleton performs the different types of grasps and objects of the AHAP.

Grasp Type	Objects		
Hook			
Spherical grip			
Tripod pinch			
Extension grip			
Cylindrical grip			
Diagonal volar grip			

(Continued)

TABLE 4 (Continued)

Grasp Type	Objects		
Lateral pinch			
Pulp pinch			

3. Results

The development of the ExHand Exoskeleton with fabric-based actuation has been carried out. A glove with an approximate weight of 137 g and an approximate system weight (weight of the power supply, the air pump, the electrovalves, the pressure sensors, the ADCs, and the single board computer) of 971 g was obtained. In addition, ten participants (five males and five females, 45.50 ± 14.93 years old) performed the tests and completed the study successfully. All results were expressed as mean values with standard deviation.

First, the ExHand Exoskeleton achieves a full opening and closing time of 2.00 ± 0.35 and 3.47 ± 0.30 s, respectively. Furthermore, the exoskeleton's maximum grasping/holding force is 87.98 ± 1.55 N. Also, The air pressure values to perform complete flexion and extension movements are presented in Table 3. Table 3 shows that the extension values were slightly higher than the flexion values, indicating that greater force is required to open the hand than to close it. Furthermore, less air pressure was required to achieve complete flexion of the thumb and little finger with values of 4.63 ± 0.16 and 5.57 ± 0.09 psi, respectively.

Second, Table 4 shows how the exoskeleton performs the different types of grasps with the objects of the AHAP and the scores obtained are presented in Table 5. Thus, the exoskeleton achieved a *Maintaining* high score in each of the different types of grasp. However, the *Grasping* score was only successful in the Hook grip and above 50% for the rest of the grasps, indicating that the ExHand Exoskeleton can hold the objects but not in the way indicated by the test. Finally, a GAS score of $80.80 \pm 2.10\%$ was obtained.

Third, the number of blocks transferred during the BBT was presented in Table 6, indicating a total of 4.10 ± 0.57 blocks per minute using the exoskeleton. This value is minimally small compared to the 61.59 ± 7.75 blocks per minute without the exoskeleton.

Fourth, the JTHFT all subtasks scores and total performance time are shown in Table 7. The full performance time to complete de JTHFT with the ExHand Exoskeleton was 495.77 ± 31.38 s, and the better times using the exoskeleton were for the Writing Simulation and Feeding subtasks.

The times obtained in the JTHFT and the results of the BBT complement the AHAP results, as they demonstrate that the exoskeleton assists in the execution of various daily living tasks, such as feeding and writing. However, although the exoskeleton assists in ADLs, it performs these tasks more slowly than a healthy person.

Finally, the QUEST 2.0 scores are shown in Table 8. According to the scores, the device satisfaction means score for the participants was 4.27 ± 0.34 out of a maximum score of 5.

4. Discussion

A fabric-based soft hand exoskeleton for assistance in ADL was developed and evaluated, and a glove with a weight of 137 g and a system weight of ~ 971 g was obtained. Compared with other related devices, the weight of the ExHand Exoskeleton is similar to the glove of Ge et al. (2020), which weighs 128 g, or the glove of Yap et al. (2017) with a weight of 99 g. In terms of the maximum force exerted by the exoskeleton, a total of 87.98 ± 1.55 N was achieved. Comparing the force with similar devices, such as Ge's device, which achieved a force of 47.9 N (Ge et al., 2020), or the 37 N force of Zhou's device (Zhou et al., 2019), the ExHand Exoskeleton achieved a force above these devices. This difference in grasping/holding force with the other devices may be due to the method applied and to the silicone layer applied on the palmar side of the glove, which creates a non-slip surface. However, a better comparison would have to be made with the same materials and methods as those applied by Zhou et al. (2019) or Ge et al. (2020).

The experimental validation of the ExHand Exoskeleton in healthy users shows the exoskeleton successfully assists the participants in accomplishing all tasks. In the first instance, the pressure results indicate pressure values for extension movement between 8.90 ± 0.16 and 10.45 ± 0.08 psi and pressure values for flexion movement between 4.63 ± 0.16 and 8.85 ± 0.37 psi. In comparison with other similar fabric-based soft actuation devices, a similar value is found in the study of Yap et al. (2017), which requires 70 kPa (~ 10 psi) of input pressure to perform extension and flexion movements, contrary to other studies such as

TABLE 5 Grasping performance test scores divided into *Grasping*, *Maintaining*, and total GAS scores for the different types of grasp.

Grasp type	Grasping score (%)	Maintaining score (%)	GAS score (%)
Hook	100.00 ± 0.00	99.44 ± 0.48	99.72 ± 0.24
Spherical grip	73.33 ± 1.66	94.44 ± 4.81	83.89 ± 3.15
Tripod pinch	59.44 ± 3.15	93.33 ± 5.77	76.39 ± 1.34
Extension grip	63.88 ± 6.36	100.00 ± 0.00	81.94 ± 3.18
Cylindrical grip	68.33 ± 9.61	92.22 ± 4.19	80.28 ± 3.78
Diagonal volar grip	50.00 ± 0.00	93.89 ± 3.94	71.94 ± 1.97
Lateral pinch	61.66 ± 2.5	98.33 ± 1.44	80.00 ± 1.91
Pulp pinch	50.00 ± 0.83	94.44 ± 2.55	72.22 ± 1.20
Final score	65.83 ± 3.02	95.76 ± 2.90	80.80 ± 2.10

The gray color indicates the highest score in the grasping performance test.

TABLE 6 Score of BBT with and without the ExHand Exoskeleton.

BBT score without Exoskeleton	BBT score with Exoskeleton
61.50 ± 7.76	4.10 ± 0.57

TABLE 7 Total performance time and scores of all subtasks of JTHFT with and without the ExHand Exoskeleton.

Subtask	Performance time without Exoskeleton (s)	Performance time with Exoskeleton (s)
Writing	12.74 ± 1.54	25.33 ± 3.18
Cards turning	5.18 ± 0.79	84.78 ± 7.77
Grasping small objects	5.02 ± 0.59	85.48 ± 8.03
Stacking checkers	6.48 ± 1.60	78.78 ± 4.56
Simulated feeding	9.47 ± 1.04	26.26 ± 3.84
Large empty cans	4.16 ± 0.64	93.21 ± 17.31
Large heavy cans	5.05 ± 1.17	101.94 ± 16.37
Total performance time	48.1 ± 5.43	495.77 ± 31.38

Cappello et al. (2018a,b) require a pressure of 172 kPa (~ 25 psi) or Ge et al. (2020) pressurizing their glove with 140 kPa (~ 20 psi).

In addition, the results of the AHAP show that the ExHand Exoskeleton can assist users in grasping objects of daily life with different shapes, sizes, textures, weights, and rigidities. It is evidenced by the *Maintaining* Score of $95.76 \pm 2.90\%$ in which a percentage higher than 90% was obtained for all types of grasps. However, it is observed that the lowest percentages were for the Tripod Pinch, Cylindrical Grip, and Diagonal Volar Grip with percentages of $93.33 \pm 5.77\%$, $92.22 \pm 4.19\%$, $93.89 \pm 3.94\%$, respectively, due to the large and heavy objects such as a skillet, chips can or a tuna can, in which the contact of the glove with the object was not sufficient to maintain a stable contact. Therefore, the

TABLE 8 Mean QUEST 2.0 scores.

Item	Level of satisfaction
Dimensions	4.20 ± 0.39
Weight	4.10 ± 0.44
Adjustment	4.40 ± 0.26
Safety	4.10 ± 0.37
Comfort	4.30 ± 0.34
Effectiveness	4.50 ± 0.26
Device satisfaction	4.27 ± 0.34

TABLE 9 Box and Blocks Test (BBT) results in different studies found in the literature.

References	Participants	BBT score	
		Without exoskeleton	With exoskeleton
Zhou et al. (2019)	Two C4 and, one C5 SCI participants	3.67 ± 3.51	4.11 ± 3.17
Tran et al. (2020)	One C6 SCI participant	13	4
Thimabut et al. (2022)	20 stroke survivors	2.2 ± 0.6	8.60 ± 2.00
Dudley et al. (2021)	A stroke survivor	5	10
Radder et al. (2018)	65 older adults with different diseases and diagnoses	About 50	About 45
Polygerinos et al. (2015b)	A participant with muscular dystrophy	10	14

object moved, slipped or fell during the test. Therefore, although force tests are performed on the hand exoskeletons, combining them with grasping tests with different objects is important to verify that the devices assist and facilitate the grasping of different objects related to ADLs.

Also, a score of $65.83 \pm 3.02\%$ obtained in the *Grasping* score demonstrated the exoskeleton's incorrect grasping of different objects. Furthermore, the lowest percentages are obtained for pinch grasps, such as the tripod pinch, lateral pinch, or pulp pinch, similar to the findings of Cappello et al. (2018b) in the TRI-HFT administered to patients with SCI using the soft robotic glove.

Lastly, a GAS Score of $80.80 \pm 2.10\%$ is obtained, possibly related to the lack of movements such as abduction, adduction, and opposition to the thumb. Since the thumb represents the most important finger of the hand due to its ability to perform flexion, extension, and opposition, and more than 50% of types of grasps require thumb movements (Feix et al., 2009). Some exoskeletons have added active or passive actuators to add abduction/adduction movements to their devices. For example, Ge et al. (2020)

TABLE 10 Jebsen Taylor Hand Function Test (JTHFT) results in different studies found in the literature.

References	Participants	JTHFT results		
		Subtask	Performance time without Exoskeleton (s)	Performance time with Exoskeleton (s)
Tran et al. (2020)	One C6 SCI participant	Writing	28.20	27.70
		Cards turning	18.70	68.50
		Grasping small objects	34.30	113.00
		Stacking checkers	15.80	14.4
		Simulated feeding	14.10	65.20
		Large empty cans	9.70	*
		Large Heavy Cans	49.30	*
Radder et al. (2018)	65 older adults with different diseases and diagnoses	Total performance time without Exoskeleton (s)	Total performance time with Exoskeleton (s)	
		About 78	About 95	
Van Ommeren et al. (2018)	Five chronic stroke patients	Total performance time without Exoskeleton (s)	Total performance time with Exoskeleton (s)	
		118.62	134.43	
Polygerinos et al. (2015a)	A healthy participant	Subtask	Performance time with exoskeleton (s)	
		Cards turning	44	
		Stacking checkers	26	
		Large empty cans	29	
		Large heavy cans	39	

implemented a textile actuator between the thumb and index finger to achieve thumb abduction. Li et al. (2019) placed actuators made of NinjaFlex 85A TPU between each finger to perform abduction/adduction movements. Gerez et al. (2020) developed a hybrid exoskeleton in which pneumatic chambers are added between each finger and an extra thumb to perform a secure and stable grip by increasing the contact area between the object and the glove.

Furthermore, the present study showed the performance of the ExHand Exoskeleton with 4.10 ± 0.28 blocks per minute for the BBT and a Total Performance Time of 495.77 ± 31.38 s in the JTHFT. Tables 9, 10 show similar studies to compare with other devices and analyze the performance of the ExHand Exoskeleton in the BBT and JTHFT.

On the one hand, compared to the study by Zhou et al. (2019), which also used a textile-based actuation glove, similar results were obtained in the BBT, showing that the ExHand Exoskeleton is slightly better by getting a lower standard deviation, it is also considered that our study was performed on healthy users so a better comparison will be made once the experimental validation of our device with pathological users is achieved. On the other hand, when comparing devices of different actuation, studies such as Tran et al. (2020), Radder et al. (2018), and Polygerinos et al. (2015a) found that the use of exoskeletons increases the time to

complete the tests but assisted patients who failed to complete the test without the exoskeleton. Even so, the ExHand Exoskeleton showed a decrease in BBT and JTHFT performance. This could be related to the fact that the activities were performed with complete flexion and extension movements for every grasp, and the time required for the exoskeleton to perform the extension movement of 2.00 ± 0.35 s and the flexion movement of 3.47 ± 0.30 s, in addition to the deflation time which is about second. This can be seen in the times of the JTHFT subtasks, as the longer times are related to multi-object tasks, as opposed to the Writing subtask and Simulated Feeding subtask, as only one extension and one flexion movement were required to grasp a single object, a pen for the Writing subtask and a piece of cutlery for the Simulated Feeding subtask, which resulted in the shortest times of the ExHand Exoskeleton (times of 25.33 ± 3.18 and 26.26 ± 3.84 s, respectively) and similar to those presented by Van Ommeren et al. (2018) and Tran et al. (2020).

One way to improve the results in future evaluations is to create an internal balloon pressurization configuration that performs movements similar to those of the healthy person, considering that most of the grip types required partial extension or flexion movements instead of complete movements, thus decreasing the pressurization and depressurization times of the device. Also, more sensors such as bending, strain, or force sensors are considered for inclusion in future works to provide

adequate grip force and posture feedback. Polymer optical fibers (POFs) are an emerging alternative for instrumentation in different applications. These sensors have been used to measure parameters such as angle, pressure, temperature, humidity, force, strain, and acceleration (Leal-Junior et al., 2019). In addition, POFs are immune to electromagnetic fields, have multiplexing capabilities, and are compact (Leal-Junior et al., 2019; De Arco et al., 2023), characteristics that make these types of sensors potentially suitable for use in soft hand exoskeletons. Another limitation is that the ExHand Exoskeleton does not recognize the human user's intention. Although a web interface is developed for easy operation of the device, future work will include a brain-computer interface (BCI), electroencephalography (EEG), or electromyography (EMG) signals as control signals to associate the patient's movement intention with the exoskeleton movement. Likewise, it is proposed to implement a control system using a combination of sensors to improve precision and thus promote better assistance.

Experimental validation also shows a mean positive score of 4.27 ± 0.34 for the QUEST 2.0 survey, i.e., an overall "quite satisfied" result. A value is similar to the studies conducted by Yoo et al. (2019) and Dudley et al. (2021) and the studies presented by Radder et al. (2019) and Tsai et al. (2019) in the System Usability Scale (SUS) questionnaire, another usability test. Surveys show people's acceptance of using these devices to assist or restore hand function, so using these surveys is recommended to provide researchers with information about user requirements and user satisfaction to compare subjectively with other devices (Pei et al., 2017; Yoo et al., 2019). Nevertheless, although healthy participants positively valued the ExHand Exoskeleton, users with anthropometric measurements lower than those of the glove mentioned that sometimes they did not perceive the grip of some objects, especially the smaller ones. Hence, it is considered the fabrication of various sizes of actuators according to different anthropometric measures and avoids the use of a glove. Furthermore, the involvement of clinicians and pathological users is needed to further validate the product's usability. Moreover, it is important to mention that the breathability of the glove was affected by applying a layer of silicone on the palmar side. Although the users were not uncomfortable, a study in post-stroke patients should consider procedures for device sanitization to avoid the risk of contamination by using the device in different users. Moreover, future works may involve the development of a device that leaves the users' palmar area free and thus avoids using a glove.

Finally, it is demonstrated that a textile-based exoskeleton, such as the ExHand Exoskeleton, can perform different grasps by evaluating its performance of 24 daily living objects of different shapes, sizes, textures, weights, and stiffness by achieving a score of $80.80 \pm 2.10\%$, considering 100% means that the grips are performed in the same way as a healthy person. Likewise, it is highlighted that using 11 electrovalves to control the movement of each finger allows different grasp configurations as required by the user. Therefore, applying the AHAP (Llop-Harillo et al., 2019), a protocol for evaluating and comparing prostheses and robotic hands, is also a valuable tool in developing and comparing hand exoskeletons. Besides, the experimental

validation of the exoskeleton with ten healthy subjects showed the repeatability of the study and similar results to the similar devices reported in the literature, confirming the device's suitability to perform a stable contact with a variety of daily living objects.

5. Conclusions and future works

The development and validation of a soft fabric-based hand exoskeleton assistance in ADL were presented. The results validate the ability of the application of the ExHand Exoskeleton to assist in grasping different types of objects used in ADLs. However, several challenges remain for the ExHand Exoskeleton to be addressed in future works, mainly the addition of low-cost, lightweight sensors; the development of actuators capable of different movements such as adduction and abduction, and opposition of the thumb; and lastly, the evaluation and validation of the device in stroke survivors.

Data availability statement

The original contributions presented in the study are included in the article/supplementary material, further inquiries can be directed to the corresponding author/s.

Ethics statement

The study was approved by the Ethical Committee in the Colombian School of Engineering Julio Garavito. All participants were informed about the scope and purpose of the study, and all participating individuals signed an informed consent form. The patients/participants provided their written informed consent to participate in this study.

Author contributions

JM-M, HW, MMA, MMú, and CC contributed to the development and design of the hand exoskeleton and the performance of the study. JM-M performed the statistical analysis and wrote the first draft of the manuscript. All authors contributed to the manuscript revision, read, and approved the submitted version.

Funding

This work was supported by The Royal Academy of Engineering—Industry-Academia Partnership Programme Colombia/UK (IAPP18-19\264), PrExHand Project, and the partial support of FAPES (209/2018—Edital Especial CPID and 459/2021), CNPq (310668/2021-2), and MCTI/FNDCT/FINEP (2784/20).

Acknowledgments

The authors would like to thank the members of the Center for Biomechanics and the healthy volunteers for participating in the study.

Conflict of interest

The authors declare that the research was conducted in the absence of any commercial or financial relationships

References

- Aisen, M. L., Krebs, H. I., Hogan, N., McDowell, F., and Volpe, B. T. (1997). The effect of robot-assisted therapy and rehabilitative training on motor recovery following stroke. *Arch. Neurol.* 54, 443–446. doi: 10.1001/archneur.1997.00550160075019
- Boser, Q. A., Dawson, M. R., Schofield, J. S., Dziwenko, G. Y., and Hebert, J. S. (2020). Defining the design requirements for an assistive powered hand exoskeleton: a pilot explorative interview study and case series. *Prosthet. Orthot. Int.* 2020:0309364620963943. doi: 10.1177/0309364620963943
- Calli, B., Walsman, A., Singh, A., Srinivasa, S., Abbeel, P., and Dollar, A. M. (2015). Benchmarking in manipulation research: using the Yale-CMU-Berkeley object and model set. *IEEE Robot. Autom. Mag.* 22, 36–52. doi: 10.1109/MRA.2015.2448951
- Cappello, L., Galloway, K. C., Sanan, S., Wagner, D. A., Granberry, R., Engelhardt, S., et al. (2018a). Exploiting textile mechanical anisotropy for fabric-based pneumatic actuators. *Soft Robot.* 5, 662–674. doi: 10.1089/soro.2017.0076
- Cappello, L., Meyer, J. T., Galloway, K. C., Peisner, J. D., Granberry, R., Wagner, D. A., et al. (2018b). Assisting hand function after spinal cord injury with a fabric-based soft robotic glove. *J. Neuroeng. Rehabil.* 15, 1–10. doi: 10.1186/s12984-018-0391-x
- Carmeli, E., Peleg, S., Bartur, G., Elbo, E., and Vatin, J.-J. (2011). Handtutor enhanced hand rehabilitation after stroke—a pilot study. *Physiother. Res. Int.* 16, 191–200. doi: 10.1002/pri.485
- Chaurand, R. Á., León, L. R. P., and Muñoz, E. L. G. (2007). *Dimensiones Antropométricas de Población Latinoamericana*. Universidad de Guadalajara; CUAAD.
- De Arco, L., Pontes, M. J., Segatto, M. E., Monteiro, M. E., Cifuentes, C. A., and Díaz, C. A. (2023). Soft-sensor system for grasp type recognition in underactuated hand prostheses. *Sensors* 23:3364. doi: 10.3390/s23073364
- Demers, L., Weiss-Lambrou, R., and Ska, B. (2000). *Quebec User Evaluation of Satisfaction With Assistive Technology Version 2.0*. Webster, NY: The Institute for Matching Persons and Technology. doi: 10.1037/t35218-000
- du Plessis, T., Djouani, K., and Oosthuizen, C. (2021). A review of active hand exoskeletons for rehabilitation and assistance. *Robotics* 10:40. doi: 10.3390/robotics10010040
- Dudley, D. R., Knarr, B. A., Siu, K.-C., Peck, J., Ricks, B., and Zuniga, J. M. (2021). Testing of a 3d printed hand exoskeleton for an individual with stroke: a case study. *Disabil. Rehabil.* 16, 209–213. doi: 10.1080/17483107.2019.1646823
- Feigin, V. L., Brainin, M., Norrving, B., Martins, S., Sacco, R. L., Hacke, W., et al. (2022). World stroke organization (WSO): global stroke fact sheet 2022. *Int. J. Stroke* 17, 18–29. doi: 10.1177/17474930211065917
- Feix, T., Pawlik, R., Schmiedmayer, H.-B., Romero, J., and Kragic, D. (2009). “A comprehensive grasp taxonomy,” in *Robotics, Science and Systems: Workshop on Understanding the Human Hand for Advancing Robotic Manipulation*, Vol. 2 (Seattle, WA), 2–3.
- Ferguson, P. W., Shen, Y., and Rosen, J. (2020). Hand exoskeleton systems-overview. *Wearab. Robot.* 149–175. doi: 10.1016/B978-0-12-814659-0.00008-4
- Fettters, L., and Tilson, J. (2018). *Evidence Based Physical Therapy*. Philadelphia, PA: FA Davis.
- Fu, C., Xia, Z., Hurren, C., Nilghaz, A., and Wang, X. (2022). Textiles in soft robots: current progress and future trends. *Biosens. Bioelectron.* 196:113690. doi: 10.1016/j.bios.2021.113690
- Ge, L., Chen, F., Wang, D., Zhang, Y., Han, D., Wang, T., et al. (2020). Design, modeling, and evaluation of fabric-based pneumatic actuators for soft wearable assistive gloves. *Soft Robot.* 7, 583–596. doi: 10.1089/soro.2019.0105
- Gerez, L., Dwivedi, A., and Liarokapis, M. (2020). “A hybrid, soft exoskeleton glove equipped with a telescopic extra thumb and abduction capabilities,” in *2020 IEEE International Conference on Robotics and Automation (ICRA)* (Paris), 9100–9106. doi: 10.1109/ICRA40945.2020.9197473
- Good, D. C., Bettermann, K., and Reichwein, R. K. (2011). Stroke rehabilitation. *CONTINUUM* 17, 545–567. doi: 10.1212/01.CON.0000399072.61943.38
- Hsiao, J.-H., Chang, J.-Y., and Cheng, C.-M. (2019). Soft medical robotics: clinical and biomedical applications, challenges, and future directions. *Adv. Robot.* 33, 1099–1111. doi: 10.1080/01691864.2019.1679251
- Jebsen, R. H. (1969). An objective and standardized test of hand function. *Arch. Phys. Med. Rehabil.* 50, 311–319.
- Kapandji, I. (1971). The physiology of the joints, volume i, upper limb. *Am. J. Phys. Med. Rehabil.* 50:96.
- Kelley, R. E., and Borazanci, A. P. (2009). Stroke rehabilitation. *Neurol. Res.* 31, 832–840. doi: 10.1179/016164109X12445505689689
- Kontson, K., Marcus, I., Myklebust, B., and Civallico, E. (2017). Targeted box and blocks test: normative data and comparison to standard tests. *PLoS ONE* 12:e0177965. doi: 10.1371/journal.pone.0177965
- Kutner, N. G., Zhang, R., Butler, A. J., Wolf, S. L., and Alberts, J. L. (2010). Quality-of-life change associated with robotic-assisted therapy to improve hand motor function in patients with subacute stroke: a randomized clinical trial. *Phys. Ther.* 90, 493–504. doi: 10.2522/ptj.20090160
- Leal-Junior, A. G., Diaz, C. A., Avellar, L. M., Pontes, M. J., Marques, C., and Frizera, A. (2019). Polymer optical fiber sensors in healthcare applications: a comprehensive review. *Sensors* 19:3156. doi: 10.3390/s19143156
- Li, M., Zhuo, Y., He, B., Liang, Z., Xu, G., Xie, J., et al. (2019). “A 3d-printed soft hand exoskeleton with finger abduction assistance,” in *2019 16th International Conference on Ubiquitous Robots (UR)* (Jeju), 319–322. doi: 10.1109/URAI.2019.8768611
- Liu, Z., Zhao, L., Yu, P., Yang, T., Li, N., Yang, Y., et al. (2018). “A wearable bionic soft exoskeleton glove for stroke patients,” in *2018 IEEE 8th Annual International Conference on CYBER Technology in Automation, Control, and Intelligent Systems (CYBER)* (Tianjin), 932–937. doi: 10.1109/CYBER.2018.8688106
- Llop-Harillo, I., Pérez-González, A., Starke, J., and Asfour, T. (2019). The anthropomorphic hand assessment protocol (AHAP). *Robot. Auton. Syst.* 121:103259. doi: 10.1016/j.robot.2019.103259
- Matheus, K., and Dollar, A. M. (2010). “Benchmarking grasping and manipulation: properties of the objects of daily living,” in *2010 IEEE/RSJ International Conference on Intelligent Robots and Systems* (Taipei), 5020–5027. doi: 10.1109/IROS.2010.5649517
- Mathiowetz, V., Volland, G., Kashman, N., and Weber, K. (1985). Adult norms for the box and block test of manual dexterity. *Am. J. Occup. Ther.* 39, 386–391. doi: 10.5014/ajot.39.6.386
- Mohammadi, A., Lavranos, J., Choong, P., and Oetomo, D. (2018). “Flexo-glove: a 3D printed soft exoskeleton robotic glove for impaired hand rehabilitation and assistance,” in *2018 40th Annual International Conference of the IEEE Engineering in Medicine and Biology Society (EMBC)* (Honolulu, HI: IEEE), 2120–2123. doi: 10.1109/EMBC.2018.8512617
- Murphy, S. J., and Werring, D. J. (2020). Stroke: causes and clinical features. *Medicine* 48, 561–566. doi: 10.1016/j.mpmed.2020.06.002
- Pei, Y.-C., Chen, J.-L., Wong, A. M., and Tseng, K. C. (2017). An evaluation of the design and usability of a novel robotic bilateral arm rehabilitation device for patients with stroke. *Front. Neurobot.* 11:36. doi: 10.3389/fnbot.2017.00036

that could be construed as a potential conflict of interest.

Publisher's note

All claims expressed in this article are solely those of the authors and do not necessarily represent those of their affiliated organizations, or those of the publisher, the editors and the reviewers. Any product that may be evaluated in this article, or claim that may be made by its manufacturer, is not guaranteed or endorsed by the publisher.

- Polygerinos, P., Galloway, K. C., Sanan, S., Herman, M., and Walsh, C. J. (2015a). "EMG controlled soft robotic glove for assistance during activities of daily living," in *2015 IEEE International Conference on Rehabilitation Robotics (ICORR)* (Singapore), 55–60. doi: 10.1109/ICORR.2015.7281175
- Polygerinos, P., Galloway, K. C., Savage, E., Herman, M., O'Donnell, K., and Walsh, C. J. (2015b). "Soft robotic glove for hand rehabilitation and task specific training," in *2015 IEEE International Conference on Robotics and Automation (ICRA)* (Seattle, WA), 2913–2919. doi: 10.1109/ICRA.2015.7139597
- Radder, B., Prange-Lasonder, G. B., Kottink, A. I., Holmberg, J., Sletta, K., Van Dijk, M., et al. (2018). The effect of a wearable soft-robotic glove on motor function and functional performance of older adults. *Assist. Technol.* 32, 9–15. doi: 10.1080/10400435.2018.1453888
- Radder, B., Prange-Lasonder, G. B., Kottink, A. I., Holmberg, J., Sletta, K., van Dijk, M., et al. (2019). Home rehabilitation supported by a wearable soft-robotic device for improving hand function in older adults: a pilot randomized controlled trial. *PLoS ONE* 14:e0220544. doi: 10.1371/journal.pone.0220544
- Ramos, O., Múnera, M., Moazen, M., Wurdemann, H., and Cifuentes, C. A. (2022). Assessment of soft actuators for hand exoskeletons: pleated textile actuators and fiber-reinforced silicone actuators. *Front. Bioeng. Biotechnol.* 10:924888. doi: 10.3389/fbioe.2022.924888
- Rincón Becerra, O., and García-Acosta, G. (2014). Adaptabilidad antropométrica de guantes de protección: importancia del desarrollo integral de sistemas de tallaje, XIII Congreso Colombiano de Ergonomía.
- Robinette, K. M. (2012). Anthropometry for product design. *Handb. Hum. Fact Ergon.* 4, 330–346. doi: 10.1002/9781118131350.ch11
- Rus, D., and Tolley, M. T. (2015). Design, fabrication and control of soft robots. *Nature* 521, 467–475. doi: 10.1038/nature14543
- Sanchez, V., Walsh, C. J., and Wood, R. J. (2021). Textile technology for soft robotic and autonomous garments. *Adv. Funct. Mater.* 31:2008278. doi: 10.1002/adfm.202008278
- Schultz, S. K., Castillo, C. S., Rosier, J. T., and Robinson, R. G. (1997). Generalized anxiety and depression: assessment over 2 years after stroke. *Am. J. Geriatr. Psychiatry* 5, 229–237. doi: 10.1097/00019442-199700530-00007
- Takla, M. K., Mahmoud, E. A., and El-Latif, N. A. (2018). Jebson taylor hand function test: gender, dominance, and age differences in healthy Egyptian population. *Bull. Facul. Phys. Ther.* 23, 85–93. doi: 10.4103/bfpt.bfpt_11_18
- Thimabut, W., Terachinda, P., and Kitisomprayoonkul, W. (2022). Effectiveness of a soft robotic glove to assist hand function in stroke patients: a cross-sectional pilot study. *Rehabil. Res. Pract.* 2022:3738219. doi: 10.1155/2022/3738219
- Thompson-Butel, A. G., Lin, G., Shiner, C. T., and McNulty, P. A. (2015). Comparison of three tools to measure improvements in upper-limb function with poststroke therapy. *Neurorehabil. Neural Repair* 29, 341–348. doi: 10.1177/1545968314547766
- Tran, P., Jeong, S., Wolf, S. L., and Desai, J. P. (2020). Patient-specific, voice-controlled, robotic flexotendon glove-ii system for spinal cord injury. *IEEE Robot. Autom. Lett.* 5, 898–905. doi: 10.1109/LRA.2020.2965900
- Tsai, Y.-L., Huang, J.-J., Pu, S.-W., Chen, H.-P., Hsu, S.-C., Chang, J.-Y., et al. (2019). Usability assessment of a cable-driven exoskeletal robot for hand rehabilitation. *Front. Neurobot.* 13:3. doi: 10.3389/fnbot.2019.00003
- Van Ommeren, A., Radder, B., Buurke, J. H., Kottink, A. I., Holmberg, J., Sletta, K., et al. (2018). "The effect of prolonged use of a wearable soft-robotic glove post stroke-a proof-of-principle," in *2018 7th IEEE International Conference on Biomedical Robotics and Biomechatronics (Biorob)* (Enschede), 445–449. doi: 10.1109/BIOROB.2018.8487906
- Whitesides, G. M. (2018). Soft robotics. *Angew. Chem. Int. Edn.* 57, 4258–4273. doi: 10.1002/anie.201800907
- Wolf, S. L., Winstein, C. J., Miller, J. P., Taub, E., Uswatte, G., Morris, D., et al. (2006). Effect of constraint-induced movement therapy on upper extremity function 3 to 9 months after stroke: the excite randomized clinical trial. *JAMA* 296, 2095–2104. doi: 10.1001/jama.296.17.2095
- Yap, H. K., Khin, P. M., Koh, T. H., Sun, Y., Liang, X., Lim, J. H., et al. (2017). A fully fabric-based bidirectional soft robotic glove for assistance and rehabilitation of hand impaired patients. *IEEE Robot. Autom. Lett.* 2, 1383–1390. doi: 10.1109/LRA.2017.2669366
- Yoo, H.-J., Lee, S., Kim, J., Park, C., and Lee, B. (2019). Development of 3D-printed myoelectric hand orthosis for patients with spinal cord injury. *J. Neuroeng. Rehabil.* 16, 1–14. doi: 10.1186/s12984-019-0633-6
- Zhou, Y. M., Wagner, D., Nuckols, K., Heimgartner, R., Correia, C., Clarke, M., et al. (2019). "Soft robotic glove with integrated sensing for intuitive grasping assistance post spinal cord injury," in *2019 International Conference on Robotics and Automation (ICRA)* (Montreal, QC), 9059–9065. doi: 10.1109/ICRA.2019.8794367



OPEN ACCESS

EDITED BY

Florian Röhrbein,
Technische Universität Chemnitz, Germany

REVIEWED BY

Simona Maria Carmignano,
University of Salerno, Italy
Satoshi Yamamoto,
Ibaraki Prefectural University of Health
Sciences, Japan

*CORRESPONDENCE

Jesús Tornero
✉ jesus.tornero@lmh.es

RECEIVED 23 February 2023

ACCEPTED 09 June 2023

PUBLISHED 05 July 2023

CITATION

Urrutia R, Miren Gutiérrez-Muto A,
Sanz-Morère CB, Gómez A, Politi AM,
Lunardini F, Baccini M, Cecchi F, León N,
Oliviero A and Tornero J (2023) Spasticity
evaluation with the Amadeo Tyromotion device
in patients with hemispheric stroke.
Front. Neurobot. 17:1172770.
doi: 10.3389/fnbot.2023.1172770

COPYRIGHT

© 2023 Urrutia, Miren Gutiérrez-Muto,
Sanz-Morère, Gómez, Politi, Lunardini, Baccini,
Cecchi, León, Oliviero and Tornero. This is an
open-access article distributed under the terms
of the [Creative Commons Attribution License
\(CC BY\)](https://creativecommons.org/licenses/by/4.0/). The use, distribution or reproduction
in other forums is permitted, provided the
original author(s) and the copyright owner(s)
are credited and that the original publication in
this journal is cited, in accordance with
accepted academic practice. No use,
distribution or reproduction is permitted which
does not comply with these terms.

Spasticity evaluation with the Amadeo Tyromotion device in patients with hemispheric stroke

Rocío Urrutia^{1,2}, Ane Miren Gutiérrez-Muto¹,
Clara B. Sanz-Morère^{1,3}, Arantxa Gómez¹, Angela M. Politi⁴,
Francesca Lunardini¹, Marco Baccini⁴, Francesca Cecchi^{4,5},
Natacha León¹, Antonio Oliviero¹ and Jesús Tornero^{1*}

¹Center for Clinical Neuroscience, Hospital Los Madroños, Madrid, Spain, ²Joint PhD Program in Neuroscience, University of Castilla La Mancha, Albacete, Spain, ³Neural Rehabilitation Group, Cajal Institute, Spanish National Research Council (CSIC), Madrid, Spain, ⁴Fondazione Don Carlo Gnocchi, Scientific Institute, Florence, Italy, ⁵Department of Experimental and Clinical Medicine, University of Florence, Florence, Italy

Objective: The objective of this study is to verify the reliability and the concurrent and discriminant validity of the measurements of spasticity offered by the robotic device, quantifying the (1) test–retest reliability, (2) correlation with the clinical evaluation using the Modified Ashworth Scale (MAS), (3) inter-rater reliability between the two physiotherapists, and (4) ability to discriminate between healthy and stroke patients.

Methods: A total of 20 stroke patients and 20 healthy volunteers participated in the study. Two physical therapists (PT1 and PT2) independently evaluated the hand spasticity of stroke subjects using the MAS. Spasticity was assessed, both in healthy and stroke patients, with the Amadeo device at three increasing velocities of passive movement for three consecutive repeated assessments, while raw data of force and position were collected through an external program.

Data analysis: The intraclass correlation coefficient (ICC) and the weighted kappa were computed to estimate the reliability of the Amadeo device measurements, the inter-rater reliability of MAS, and the correlation between the MAS and Amadeo device measurements. The discriminant ability of the Amadeo device was assessed by comparing the stroke and healthy subjects' spasticity measurements with the percentage of agreements with 0 in MAS for healthy subjects.

Results: The test–retest reliability of the Amadeo device was high with ICC at all three velocities (ICC = 0.908, 0.958, and 0.964, respectively) but lower if analyzed with weighted kappa correlation (0.584, 0.748, and 0.749, respectively) as mean values for each velocity. The correlation between Amadeo and the clinical scale for stroke patients with weighted kappa correlation was poor (0.280 ± 0.212 for PT1 and 0.290 ± 0.155 for PT2). The inter-rater reliability of the clinical MAS was high (ICC = 0.911).

Conclusion: Both MAS and Amadeo spasticity scores showed good reliability. The Amadeo scores did not show a strong clinical correlation with the MAS in stroke patients. Hitherto, Amadeo evaluation shows trends that are consistent with the characteristics of spasticity, such as an increase in spasticity as the speed of muscle stretching increases. The ability of the device to discriminate between stroke patients and healthy controls is low. Future studies adopting an instrumental gold standard for spasticity may provide further insight into the validity of these measurements.

KEYWORDS

muscle spasticity, muscle tone, rehabilitation, stroke, Amadeo, upper limb

1. Introduction

Spasticity is usually defined as a motor alteration or disorder characterized by an increase in the excitability of the myotatic or stretch reflex, causing an increase in tone. The speed is a determining factor, as the higher the speed, the greater the stretch-resistant reflex contraction (Thibaut et al., 2013; Wissel et al., 2015; Spasticity, 2017). This can highly interfere with movement, speech, and the patient's activities of daily living (Balci, 2018; Roman et al., 2022).

Stroke is among the neurological pathologies causing spasticity. Stroke-induced spasticity is a neurological disorder resulting from damage to the first motor neuron and can be difficult to treat in the initial periods after brain damage (Sünnerhagen, 2016). It is a complex phenomenon due to the heterogeneity of its symptoms and its effects on motor control (Sáinz-Pelayo et al., 2020). This causes patients to experience hypertonia, clonus, flexor, and extensor spasms. Spasticity presents in different forms depending on the site of the lesion, the time since lesion, and its size (Balci, 2018).

Both spasticity and muscle weakness caused by neurological damage (spastic paresis) are the most common motor disorders after stroke and markedly influence the patient, becoming a challenge during the rehabilitation process (Meseguer-Henarejos et al., 2018). Moreover, spasticity also causes other associated symptomatology such as pain, shortening of tendons and connective tissue, contractures, decreased joint range, or further muscle weakness (Thibaut et al., 2013; Meseguer-Henarejos et al., 2018). These factors have repercussions on the rehabilitation process due to delays or changes in the treatment that alter or modify the functional recovery (Wissel et al., 2015). In addition, spasticity is related to an alteration of normal posture, which aggravates associated factors and increases fatigue, disturbs the person's sleep, and decreases the sense of safety, resulting in the need for increased medical attention and home care (Meseguer-Henarejos et al., 2018). Spasticity is often a fluctuating condition that can be exacerbated or attenuated by different factors (temperature, infection, stress, etc.) and its assessment may be difficult.

The clinical assessment process remains challenging (Balci, 2018). Traditionally, the evaluation of spasticity has been based on the application of scales, such as the Modified Ashworth Scale (MAS), Tardieu Scale, Spasm Severity Scale, or Triple Spasticity Scale (TSS), among others (Balci, 2018; Sáinz-Pelayo et al., 2020). However, these existing scales are based on the clinician's perception, experience, and training over the years (Johnson, 2002). Among the measurement methods, MAS (Pandyan et al., 1999) is the most widely used to measure muscle tone and spasticity, measuring the resistance exerted by the muscle to stretching until the full range of motion (ROM) of the joint is achieved (Meseguer-Henarejos et al., 2018). Notwithstanding the spread use in clinical practice, the main limitation of this scale is that the administration velocity is not strictly determined, leading to the possibility to influence the result. Determining the degree of spasticity in an accurate and reliable way is critical and can compromise the patient's evaluation and the selection of the most appropriate rehabilitation process.

In the last years, new electromechanical devices have been developed, with a specific interest in robotic devices. Therapies using robotic devices can accelerate the process of neuroplasticity due to the constant stimulation provided by haptic interaction and the amount of proprioceptive and sensory information (Calabr et al., 2019). For instance, patients can receive timely feedback on their performance from robotic devices and achieve better adherence to treatment with an introduction of interactive games or tasks (Chien et al., 2020). In addition to provide repetitive, high-intensity training, stroke survivors can perform independent training with less supervision from therapists (Mehrholtz et al., 2018; Chien et al., 2020).

Therapies using robotic devices have been implemented in rehabilitation sessions and are now recommended in several guidelines for stroke patients (Serrano-López Terradas et al., 2022). Robotic devices are a support tool for the therapist to intensify motor relearning, assist the patients according to their needs, quantify performance by providing feedback during therapy, and allow repetitive and high-intensity training (Jakob et al., 2018; Dehem et al., 2019; Aprile et al., 2020; Esquenazi et al., 2021). Robotic devices are also capable of measuring patient's performance, helping professionals by providing an objective assessment of various components of motor impairment (Keller et al., 2015; Dehem et al., 2017). This objective assessment could be used, for example, to personalize the rehabilitation treatment or adjust medication.

There are several types of robotic devices for hand treatment, such as exoskeletons and end-effector systems, all dedicated to motor rehabilitation (Calabr et al., 2019; Tyromotion, 2023). Some of these devices, due to the presence of sensors and actuators, include the possibility to assess upper limb kinematics and provide an objective and quantitative evaluation of arm movements after brain damage (Dehem et al., 2017). Some devices such as the REAplan robot (Dehem et al., 2017), Reharob system, HWARD, Reogo (De-la-Torre et al., 2021), MIT Manus (Bosecker et al., 2010), HapticKnob (Lambercy et al., 2010), and Tyromotion Amadeo device (Tyromotion, 2023) aim also to assess and grade the spasticity. We will focus on the Amadeo Tyromotion robotic device due to its ability to provide an automatic spasticity assessment of the hand and the individual fingers in stroke patients.

Amadeo Tyromotion is a robotic device oriented to motor and sensory rehabilitation of the hand that also allows the assessment of spasticity. It contains several programs designed for any stage of a hand affected by a neurological pathology (Butt et al., 2020). It consists of a screen facing the user who can interact with the robot through games, tasks, or more specific programs in an interactive format. The hand and forearm are placed on a platform that is connected to the main unit. The wrist is restrained with a Velcro band to prevent movement of the elbow and shoulder. The fingers are attached through magnets to the unit's rails. The visual feedback on the screen is an added factor for functional motor rehabilitation. Amadeo can be adapted to any type of patient, whether adult or pediatric, offering therapeutic exercises through games aimed at motor control during grip functions (finger flexion) or hand release (finger extension) (Fasoli and Adams-Dexter, 2019). The robot also quantifies the measuring tone, spasticity, strength, and

ROM through games and specific tests, monitoring the status and progress of patients using the device (Germanotta et al., 2020).

The aim of this study is to describe the quality of the spasticity measures provided by Amadeo Tyromotion and compare it with the clinical assessment. We aim to verify the reliability, concurrent and discriminant validity of spasticity measurements offered by the robotic device.

2. Materials and methods

2.1. Material

For this study, we used the Amadeo Tyromotion robotic device (Tyromotion, 2023), a robot for hand rehabilitation that includes both motor and sensory rehabilitative components (see Figure 1). To ensure that the data acquisition was accurate, the hand unit (i.e., a main platform where force and position sensors are located) was sent for calibration to Tyromotion's factory.

To perform the Amadeo Tyromotion therapy, the PT places the forearm of the patient's affected limb on a platform, restraining the arm and wrist with straps to ensure the stability of the limb on the device (see Figure 1). Then, each finger is independently placed on magnetized rails, directly coupling the person with the device, which allows the flexion–extension movement of the fingers. The Amadeo has three operation modes of mobility treatment as follows: passive, active assisted, and active movement. The robot is able to calibrate the full passive range of motion for each finger before the start of a session and provides assistive force to complete the remaining ROM during the exercise. In addition, the maximum flexion and extension force of each finger is recorded to calibrate the exercise when force control is needed. Amadeo also provides automatic measures of ROM, strength, muscle tone, and spasticity (Bishop et al., 2017).

The assessment and quantification of spasticity are based on algorithms that calculate, from raw data, both MAS and Tardieu scale, attributing a score for each finger and the full hand. In the current study, we focus only on the MAS assessment, since it is most often used clinically in the assessment of adults. The robot starts from a position of finger flexion, and it extends the fingers in two different groups as follows: the thumb (finger one) on one side in a separate way and the other fingers (from finger two to finger five) on the other side. The Amadeo selects a time window during finger extension, in which it performs the spasticity measurement (0–100% ROM, individually for each finger). If an unexpected finger flexion reaction is detected during the evaluation and the finger cannot reach the full ROM, the finger slide automatically stops, and the spasticity evaluation finishes, flexing the fingers again to end the assessment, attributing the corresponding degree of spasticity based on the force exerted against that extension. During the Amadeo spasticity assessment, the fingers are extended at three different velocities as follows: slow ($v1 \approx 0.01$ m/s), medium ($v2 \approx 0.05$ m/s), and fast ($v3 \approx 0.1$ m/s). Although the MAS is performed clinically at a single speed, here, we retained the Amadeo spasticity measurements at the three velocities, to test the effect of speed on the assessment.

For data collection, data acquisition software is used. This program records the force and position data of the fingers in real

time, while the subject is performing the therapy with the Amadeo device. After collecting data, these were processed with Matlab (R2021a, The MathWorks Inc.).

Physical therapists used the MAS to assess the patients' hand spasticity at a single high speed, as established by the scale (UAB UA, 2014).

2.2. Participants

In this study, we analyzed data obtained from 40 volunteer participants, recruited through the Hospital Los Madroños (Madrid), divided into two groups:

1. The control group, composed of 20 healthy subjects, was selected based on the inclusion criteria as follows: (1) being aged between 18 and 80 years (2), their age being close to the mean age of the experimental group, and (3) acceptance of informed consent. The exclusion criteria for this group were as follows: (1) having previously suffered neurological pathologies, (2) presenting pathologies affecting the mobility and strength of the upper limb, (3) photosensitive epilepsy, (4) rejection of new technologies, and (5) cognitive deficits preventing them from understanding the program.
2. The experimental group was composed of 20 stroke patients from the advanced neurorehabilitation unit of hospital los madroños. the inclusion criteria for this group were as follows: (1) diagnosis of hemispheric stroke with upper limb involvement; (2) being aged between 18 and 80 years; (3) ability to provide informed consent; (4) sufficient trunk control to maintain prolonged sitting for at least the minimum time necessary to perform the robotic therapy; (5) preserved vision; (6) patient conscious and able to understand verbal commands and instructions; and (7) patients with no other concomitant pathologies affecting motor and/or sensory function. The exclusion criteria were as follows: (1) hemiparesis caused by other diagnoses; (2) pregnancy or lactation; (3) photosensitive epilepsy; (4) severe medical or psychiatric disorder; and (5) refusal of new technologies.

All participants gave their informed consent; the procedures had the approval of the institutional ethics committee (Hospital Universitario Severo Ochoa de Leganés Ethical Committee for clinical research) and were conducted in accordance with the Declaration of Helsinki.

2.3. Experimental design

Each participant was independently assessed on the same day by two physical therapists (PT1 and PT2) who scored the spasticity of the full hand and each finger using the MAS. The therapists were mutually blind to each other's assessment. To minimize the modulation of muscle tone induced by mobilization, the assessors were asked to estimate spasticity in <5 repetitions. Then, the participant was assessed using the Amadeo device. The positioning on the device was carried out according to the indications in the user manual provided by Tyromotion for the correct use



FIGURE 1
Amadeo Assessment of MAS scale with the hand support of the physical therapist while clinical evaluation.

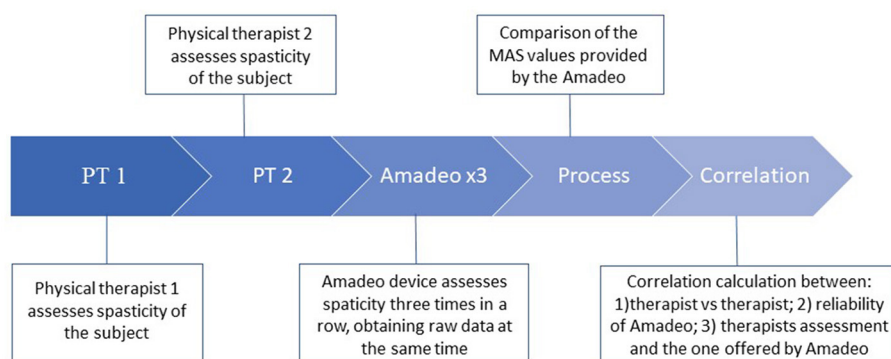


FIGURE 2
Scheme of the protocol used for the data acquisition of spasticity in subjects.

of Amadeo. The subjects were held in a seated position, in a comfortable and relaxed posture, in a chair with backrest and armrests, and with the forearm resting on the device in pronation. The straps were adjusted to the arm and wrist, and the magnets were placed on the distal phalanx of the fingers, leaving the distal interphalangeal joint free. The experimental room was set between 21°C and 23°C, according to regulatory bodies in Spain.

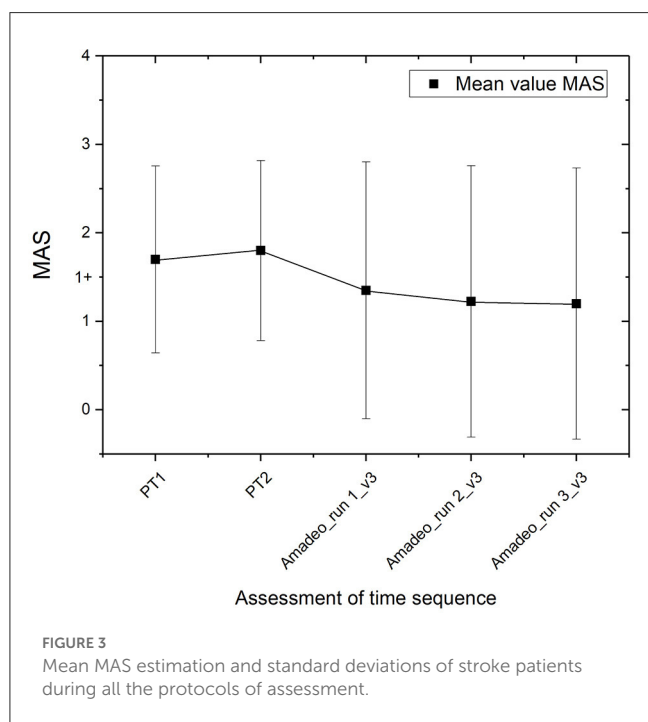
Before starting the assessment, Amadeo needs a reference of the passive ROM of each finger to establish the limits of movement in which the device will move the subject's fingers during the session. The therapist passively opened the participant's hand coupled to the device until reaching the limit of flexion–extension movements. Then, for each velocity, the Amadeo device performs

a cycle consisting of the extension of fingers, maintenance of this extension, and flexion (one cycle for velocity). Amadeo provides spasticity estimation and delivers a score for both the full hand and each finger, that is assumed to be equivalent to the MAS. Raw data of position and force were acquired while spasticity assessment saved in an external device. The result of Amadeo's evaluation for each finger and the full hand was recorded in the data collection notebook at the end of the test, together with relevant observations, if applicable. The time-course of the whole evaluation is presented in Figure 2.

The three velocities mentioned above were measured, starting with the slowest (v1) and ending with the fastest (v3). At each velocity, the group from finger two to finger five was recorded

TABLE 1 Demographic and clinical characteristics of the evaluated individuals.

Subjects	Age (years)	Sex	Type of stroke	Time since stroke (months)	NIHSS
Stroke N = 20	Mean: 62.5 ± 14.5 Range: 48 ± 29	Male = 10 Female = 10	Ischemic = 13 Hemorrhagic = 7	Mean: 6.1 ± 6.7 Range: 16.5 ± 14.5	Median: 10 Range: 15 ± 10
Controls N = 20	Mean: 53 ± 14.8 Range: 50.5 ± 28.5	Male = 7 Female = 13			



first, followed by the evaluation of finger one. This procedure was repeated three times (r1, r2, and r3) (see Figure 2).

The PTs carried out the assessment in succession with ~1-min rest between the two evaluations. 1-min rest was also assured before the assessment by Amadeo.

2.4. Data presentation and analysis

The raw data were recorded by the software with a 200 Hz sampling rate. These were analyzed automatically by MATLAB for their interpretation. To verify whether the number of repetitions of both the PTs and Amadeo affected the evaluation, we analyzed the time-course of the MAS ratings using a Friedman test.

Amadeo's quality of data used for MAS estimation was descriptively reported in the result section. Statistical analysis was made for (1) Amadeo reproducibility assessment, (2) correlation between Amadeo and each PT evaluation, (3) correlation between clinical assessment obtained from the two PTs, and (4) capability of the Amadeo to distinguish between healthy and stroke patients. The Amadeo reproducibility assessment was obtained by correlating each velocity (v1, v2, and v3) over the three runs of evaluation

(run 1, run 2, and run 3) of the whole hand using the weighted kappa coefficient.

Moreover, we also computed the one-way random effect interclass correlation coefficient (ICC), with a 95% confidence interval (Lee et al., 1989; Meseguer-Henarejos et al., 2018), Spearman (Brashear et al., 2002; de Raadt et al., 2021), and Kendall's tau correlation. We decided to use these correlation analyses, in order to compare our results with previous studies (Mokkink et al., 2020). However, we considered the kappa statistics as the more appropriate due to the characteristics of the measured variable (MAS) (McHugh, 2012).

The comparison of spasticity measured by PTs and the Amadeo device was performed using both whole hand spasticity assessment and values for each individual finger. We observed that the total values attributed by the Amadeo device in the MAS correspond to the highest spasticity value found in fingers two, three, four, and five, leaving the spasticity value given to the finger one isolated and without considering it for the MAS total scale (probably due to the bad quality of the results obtained from finger one, see "Results"). For this reason, the position and force curves for the finger one have been excluded from the data analysis.

To evaluate the capability of Amadeo to distinguish between healthy and stroke subjects, we also calculated the percentage of agreement between PTs and between Amadeo and PTs. We considered the value as correct assigned by Amadeo which agrees with the value offered by the therapists. For this purpose, the percentage of success between the Amadeo and PTs for each velocity in each run was calculated. Two variables about the agreement were calculated as follows: (i) the percentage of absolute agreement (only the exact value is considered between the Amadeo and PT); (ii) the percentage of agreement by considering agreement values that oscillate between ± 1 of the MAS (i.e., with a value of MAS 1+, the values 1 and 2 are also taken as a hit, with all the values of the scale).

3. Results

All participants completed the whole examination. Clinical and demographic data are presented in Table 1. Full patients' characteristics and spasticity assessment scores are provided as Supplementary material.

To confirm if the number of repetitions of the PTs and Amadeo affects our evaluation, we analyzed the time-course of the MAS ratings. Figure 3 shows the mean MAS estimation and the standard deviations of all stroke patients evaluated by PTs and Amadeo in time sequence, as shown in Figure 2, including only the highest

velocity, i.e., v3. No statistically significant differences among evaluations were observed (Friedman, $p > 0.05$).

3.1. Amadeo quality of data used for MAS estimation (descriptive)

Figure 4 shows some examples of the finger position data from the Amadeo device during acquisitions at velocities that are assumed constant. Figures 4A, B show examples of data acquisition on the displacement from finger two to finger five. Figure 4A shows the change in the position represented by a constant velocity with corresponding to a linear performance, which we refer to as a good-quality acquisition. However, Figure 4B, shows not perfectly straight lines, for this subject at v3, which we refer to as poor-quality acquisition. Figure 4C shows examples of particularly low-quality finger one displacement. These inconsistencies occur during finger extension, i.e., the motion whose data are used by the device for spasticity assessment and are present in both healthy and stroke subjects. This can lead to errors in data analysis, resulting in incorrect assessment of spasticity. These inconsistencies are mostly found in the finger one, where the occasions, when a curve with straight lines is obtained, are rare.

To confirm the quality of the recorded data and speed-dependency of the spasticity assessment, Amadeo's MAS estimation vs. velocity was performed. As observed in Figure 5A, finger one presents low-quality data as its value does not seem to increase with velocity: it basically presents a value of 4 on the spasticity assessed by Amadeo for any velocity in each run of acquisition for stroke patients. On the other hand, Figures 5B, C show an increase in the spasticity measurements of Amadeo with the velocity for finger two and the whole hand. This behavior was identified for the rest of the fingers.

3.2. Comparisons of spasticity scores obtained by PTs and amadeo

3.2.1. Correlation analysis

The reproducibility of the Amadeo spasticity estimation using weighted kappa was 0.584 for v1, 0.748 for v2, and 0.749 for v3. These scores indicate a substantial agreement at least for data obtained at v2 and v3 (Bohannon and Smith, 1987). These values are presented as mean values of the three runs for each velocity, with errors of 0.064, 0.159, and 0.053, respectively. Similar good agreement was obtained also using ICC, where the results show a correlation of 0.908 for v1, 0.958 for v2, and 0.964 for v3, for the whole hand evaluation.

When correlating the Amadeo data of the whole hand with the PT evaluations, maximum correlation results were obtained at the highest velocities (v3) for both the whole hand and all fingers and ICC and weighted kappa. For example, the ICC was 0.76 with PT1 (run 1 v3, being the best correlation) and 0.72 with PT2 (run2, v3 being the best correlation). On the other hand, the worst correlations were obtained with lower velocity (v1). For example, the ICC was 0.27 with PT1 (run 1 v1 being the worst correlation) and 0.18 with PT2 (run 2, v1 being the worst correlation).

MAS evaluations between therapists (PT1 vs. PT2) showed high correlations for the hand assessment (ICC = 0.911; weighted kappa = 0.586). When individual fingers were evaluated, a satisfactory result was obtained (ICC = 0.961, Spearman's correlation = 0.867, Kendall's tau = 0.847), these data being the highest correlations found in the analysis of each finger. The percentage of agreement between PTs was also very high (see Figure 6B).

As described above, some curves obtained by Amadeo were of poor quality (inconsistencies). However, when the analysis was conducted after removing the curves with inconsistencies, the results were similar. No relationship was observed between the quality of the biomechanical curves and the agreement between the PTs and Amadeo assessment.

3.2.2. Percentage of agreement

In this analysis, we considered as correct the value assigned by Amadeo that agrees with the value offered by the therapists. For this purpose, the percentage of success between the Amadeo and therapists for each velocity in each run was calculated (see Figure 6). In healthy subjects, the Amadeo device has a mean accuracy (i.e., percentage of zero values on the MAS) of 60% in run 1; 68% in run 2, and 76% in run 3, as can be observed in Figure 6A. However, if we also consider as correct MAS values of ± 1 (see methods), the accuracy percentage in healthy subjects rises to 73% in run 1, 78% in run 2, and 82% in run 3 (see Figure 6A). In stroke patients, the percentage of hits between PTs, that is, the number of times that therapists rate stroke subjects with the same MAS value, we obtain a 45% hit rate when they obtain the same score, and it increases to 90% if we consider a ± 1 difference in the scale between them (see Figure 6B).

As for the spasticity assessment in stroke patients, the percentage of agreement between the Amadeo and the PTs scores (i.e., same value for Amadeo and PT) was 26% for run 1, 31% for run 2, and 30% for run 3, when considering PT1 (see Figure 6C), and 25% for run 1, 22% for run 2, and 20% for run 3, when considering PT2 (see Figure 6D). If we include in the percentage of agreement also differences between the Amadeo and the PT MAS score of ± 1 , then this percentage increases, obtaining values between 24% and 30% for PT1, and between 26% and 33% for PT2.

4. Discussion

Our data can be summarized as follows: (1) the reproducibility of the Amadeo grading is high (substantial agreement obtained using weighted kappa calculation); (2) the correlation between Amadeo and PTs is higher when Amadeo evaluates spasticity at high velocity (v3), while it is very low at lower velocities (v1 and v2); (3) the reproducibility of the PT grading is high; and (4) the percentage of agreement between Amadeo and PTs is lower than the agreement between PTs. Moreover, we observed that Amadeo evaluation of the spasticity of finger one is often of very poor quality, with many inconsistencies and the absence of an observed correlation between spasticity scores and velocity. Thus, finger one should be discarded from the Amadeo spasticity assessment. The other fingers also have occasional inconsistencies, but the

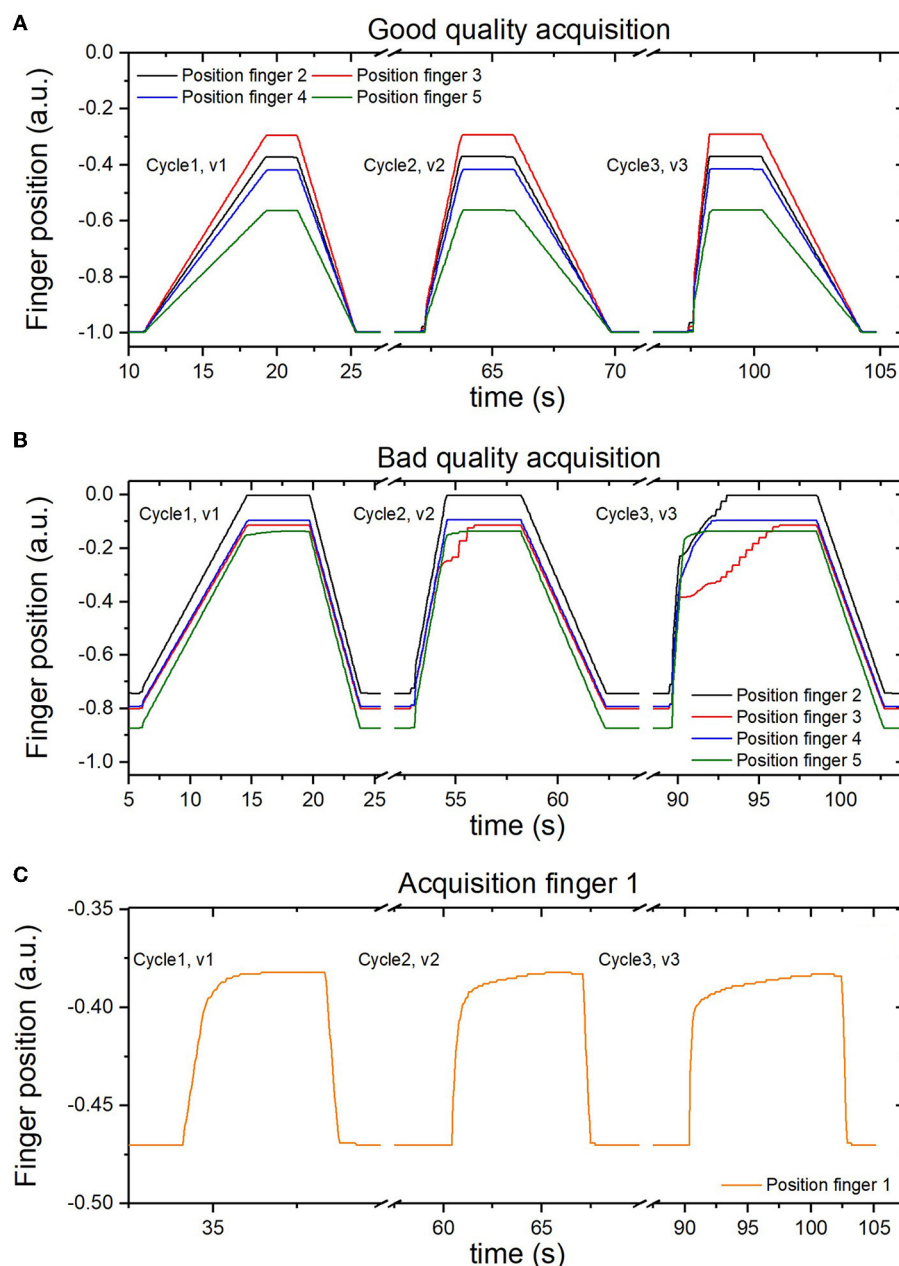


FIGURE 4

Examples of the acquired data of finger position. (A) with a constant velocity of extension from finger two to finger five. (B) with inconsistencies during the extension from finger two to finger five. (C) with inconsistencies found in finger one.

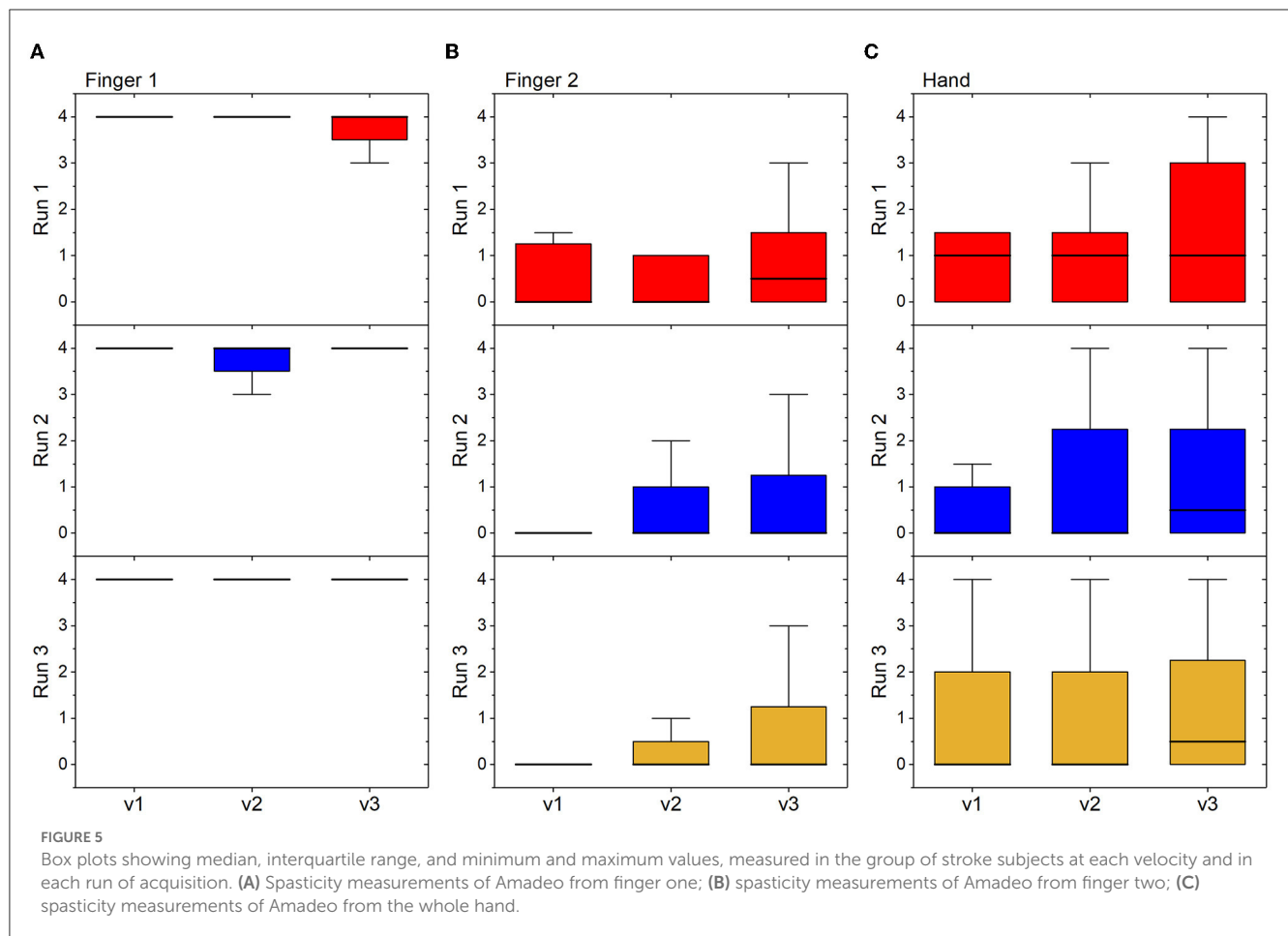
elimination of inconsistencies does not improve the correlation between Amadeo and PTs.

The Amadeo spasticity assessment returned the best results, both in terms of reproducibility and correlation with clinical scores, for v3. This is not surprising since, among the three speeds, v3 (0.1 m/s) is the closest one to the velocity that should be adopted in the clinical test, according to Bohannon and Smith (1987) (full ROM in 1 s) (UAB UA, 2014).

Early finger extension capacity after stroke is a critical motor sign of recovery. This capacity can be used for direct therapy to those who will most benefit from it (Orihuela-Espina et al., 2016). Quantifying spasticity, which directly influences the hand opening

function, may help clinicians to identify the focus of treatment for people affected by stroke. In addition, a reliable assessment of spasticity will provide relevant and objective information about the neurorehabilitation treatment (Balci, 2018).

MAS is a simple and quick method of assessment, which does not require any equipment (Meseguer-Henarejos et al., 2018). Despite this, it is still a controversial tool as it partly depends on the person performing the assessment. Since spasticity depends on the speed of stretching, differences between raters in the velocity of passive motion may contribute to disagreement in MAS scoring (Balci, 2018). Our data confirmed partially that the operator dependency of the MAS as the percentage of the agreement to



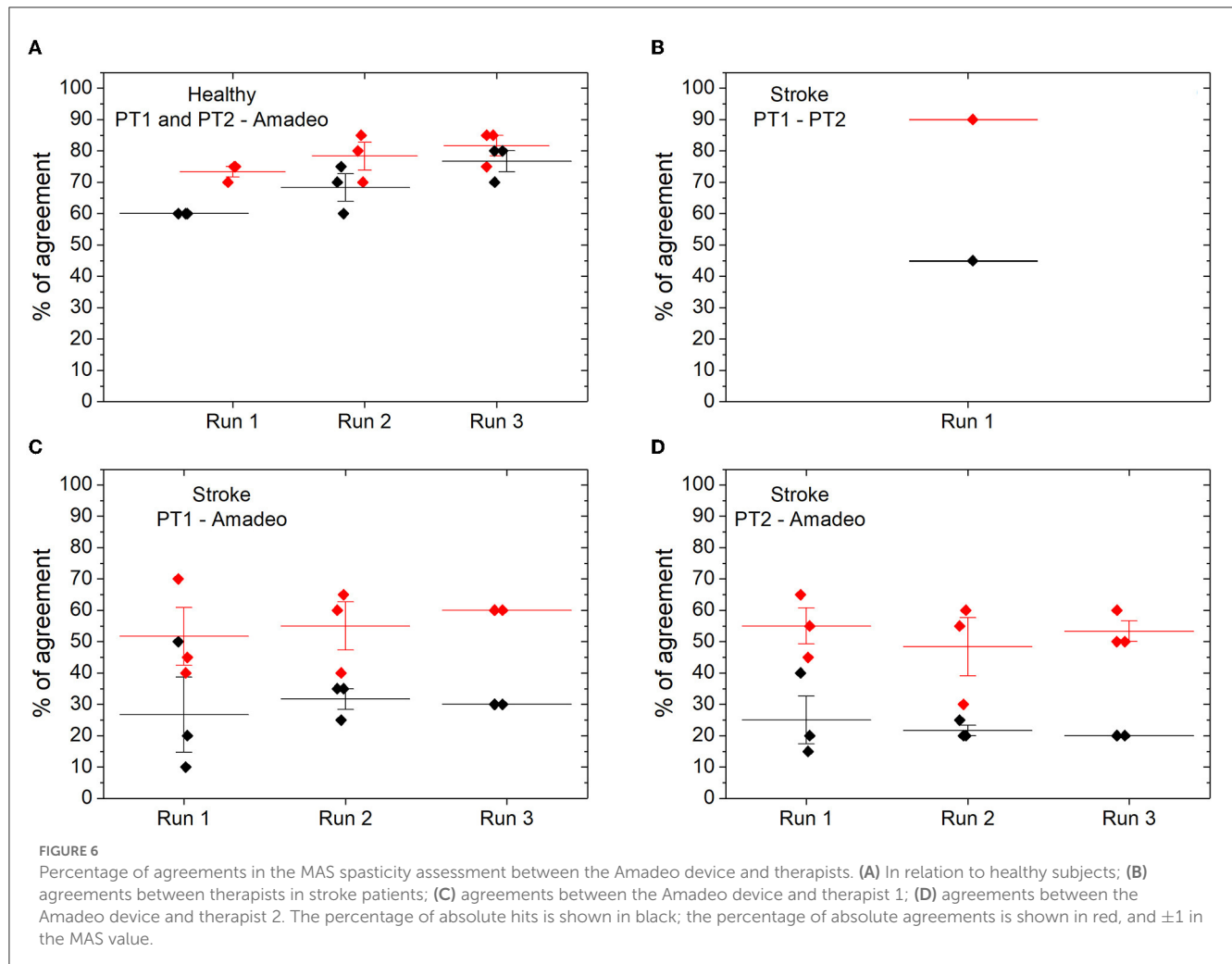
provide the exact values of MAS is low (~50%). On the other hand, when we consider as an acceptable agreement a difference of one point of the MAS, this percentage of agreement is quite high (around 90%).

The MAS inter-rater reliability (PT1 VS PT2) for the hand spasticity assessment reported a moderate-substantial weighted kappa of 0.586, and an ICC of 0.911. According to Hager (2003), ICC scores should be considered poor when they are below 0.4, sufficient if ranging between 0.4 and 0.59, good if ranging between 0.6 and 0.75, and excellent if above 0.75. Based on this, the inter-rater reliability of the two PTs in rating the spasticity of the whole hand was excellent, and even higher than what reported for other joints (Bohannon and Smith, 1987).

We also found good reliability for the robotic device, with ICC > 0.900 at all three velocities and weighted kappa > 0.6 at v2 and v3. These values are much higher than those reported by Germanotta et al. (2020), who found a low reproducibility (ICC < 0.5) of the Amadeo spasticity measurements at v1 and v3. However, the study by Germanotta et al. (2020) has an important difference from the present study because it compared Amadeo evaluations performed on consecutive days, using the passive ROM of the first day. This may greatly influence the measurement, given the characteristics of spasticity and a possible different positioning of the patient on the device. Since patient positioning and passive range of motion setting are part of the Amadeo assessment procedure, the reliability of Amadeo spasticity measurements in the present study might

be partially overestimated. Taking into account the characteristics of spasticity, the MAS value depends on the afferences received by the muscle spindle, so a good position is essential to avoid triggering this neural hyperreactivity and, in turn, get the spasticity assessment (Aloraini et al., 2015). Some articles have elaborated a treatment protocol with the Amadeo in which they specify the modes and times of treatment (Aprile et al., 2020), but there is no clear agreement on how the patient should be placed in the Amadeo. This issue could be very important to improve the measure and the effectiveness of the device, improving the quality of the session (Bevan et al., 2021; Meyer et al., 2021). Indeed, future studies should provide more insight into the usability of this device (Orekhov et al., 2021) in comparison to other devices (Park et al., 2020).

In the study by Esquenazi et al. (2018), the validity of the Amadeo system in measuring spasticity in stroke patients on the MAS was tested in comparison to a physical therapist, and perfect reliability was found between the two measurements (ICC = 1.0). However, the reliability was estimated by computing the average measures of ICC, that is, usually much higher than the single measurements of ICC. This finding has not been confirmed by Germanotta et al. (2020) in a multicenter trial that enrolled both stroke patients and healthy subjects, where the correlation between the MAS measured with Amadeo and the MAS measured clinically was found very low as in the present study. On the other hand, they concluded a good discriminant validity of Amadeo, with all



spasticity measurements obtained from stroke patients who were statistically different from those of healthy controls. Our data do not show that the device always differentiates between these subjects, but it reaches 80% of success in the detection of healthy subjects at v3. It is important to point out that, although we were expecting a zero MAS score for healthy participants, Amadeo returned 33% of values (i.e., 353 out of 1080) above zero. However, since we did not set criteria for the setting of the flexion–extension passive ROM in the Amadeo, it is possible that inconsistent results may at least be partially related to this factor. Indeed, if the range is too wide when approaching the last degrees of movement, the device exerts a longitudinal pull on the fingers rather than a joint extension. Further research should address this issue.

This study has some limitations. First, PTs and Amadeo evaluation were performed sequentially during a single session of assessment. As we know that training may affect spasticity, it is possible that the real evaluation conditions were not the same. To avoid interfering with the reproducibility of the scale, some authors suggest that MAS should not be repeated more than five times in each record (de Raadt et al., 2021). This is because muscle tone can be modulated and has an impact on the subsequent rating of spasticity. Other authors leave some time of rest between evaluations, to avoid this interference (Mokkink

et al., 2020). Our therapists carried out the assessment consecutively with 1-min rest between evaluations, and the repetitions on each finger were always <5 in each patient. The preparation phase for the Amadeo assessment (e.g., placing the magnetized guides on the patient's fingers, positioning, and immobilizing the arm and wrist on the device, setting the passive range of motion for evaluation) started 1 minute after the second PT assessment and lasted several minutes. After that, the Amadeo MAS assessment was conducted. Thus, it is unlikely that the previous evaluations have influenced the Amadeo measurements. Although we cannot exclude the fact that the absence of a longer period of rest among the evaluations may have contributed to some extent to the observed disagreement, the effect should have been minimal, if any (see Figure 3). In our opinion, this limitation cannot explain the very low percentage of agreement between PTs and Amadeo.

Another limitation is that the three acquisitions with the Amadeo device were performed in succession, without repositioning the patient's arm and hand. We chose this procedure because we were interested in studying the reproducibility of the Amadeo measurements during passive finger extension, avoiding the influence of other potential sources of variability. Of course, both arm positioning and ROM setting depend on the rater and

have a great impact on the measurements, so they could greatly increase variability.

Moreover, the whole evaluation was performed on the same day, and no longitudinal study was performed. Considering that assessment of spasticity usually requires multiple longitudinal measurements, future studies should confirm our data in a longitudinal way and possibly on a larger sample of patients. Future studies should also include a more accurate standardization of the position of the hand and fingers and the ROM setting, together with stronger control over parameters such as the temperature of the environment and the time elapsed since the pathological event, to reduce errors during acquisitions. Finally, we chose the MAS as the gold standard, but the validity and reproducibility over time of this scale have been thoroughly questioned. Possibly, the Amadeo scores and the clinical MAS scores should be compared with instrumental measurements of spasticity, providing a more reliable and valid reference standard. Moreover, since the device offers an assessment also on the Tardieu scale, future studies should verify the reliability and the concurrent and discriminant validity of the measurements of spasticity offered by the robotic device for this scale. Indeed, while the MAS focuses on the resistance of the muscle to stretching, the Tardieu scale is based on the velocity exerted during stretching. It is possible that the three speeds of assessment proposed by the Amadeo protocol are therefore specifically designed for the Tardieu-like assessment, possibly returning better results.

5. Conclusion

In conclusion, both the clinical and the Amadeo MAS scores were reproducible, although further studies are needed to test reproducibility over different days. However, the Amadeo MAS scores did not show a strong clinical correlation with the MAS in stroke patients. This may suggest that some aspects of spasticity are engaged by Amadeo and not by the PTs and/or vice versa. It is possible that Amadeo scores related to finger 2–5 at high velocities measure a performance consistent with spasticity, but this should be verified by further research. Future studies, including standardization of the position of the hand and finger in order to reduce errors during acquisitions and adopting an instrumental gold standard for measuring spasticity, may provide more insight into the validity of these measurements.

Data availability statement

The raw data supporting the conclusions of this article will be made available by the authors, without undue reservation.

References

Aloraini, S. M., Gäverth, J., Yeung, E., and MacKay-Lyons, M. (2015). Assessment of spasticity after stroke using clinical measures: a systematic review. *Disabil. Rehabil.* 37, 2313–2323. doi: 10.3109/09638288.2015.1014933

Ethics statement

The studies involving human participants were reviewed and approved by the Comité de Ética de la Investigación con medicamentos del Hospital Universitario Severo Ochoa. The patients/participants provided their written informed consent to participate in this study.

Author contributions

RU, AM, and JT: conceptualization. RU, AM, and CS-M: data curation and formal analysis. RU and AG: methodology. RU, AG, AO, and NL: investigation. JT: project administration. AM: software. AO and JT: supervision. RU, AM, AP, MB, FC, FL, AO, and JT: writing. RU, AG-M, FL, and JT: critical revisions. All authors contributed to the article and approved the submitted version.

Acknowledgments

The authors would like to thank Adrián Álvarez for supporting this research.

Conflict of interest

The authors declare that the research was conducted in the absence of any commercial or financial relationships that could be construed as a potential conflict of interest.

Publisher's note

All claims expressed in this article are solely those of the authors and do not necessarily represent those of their affiliated organizations, or those of the publisher, the editors and the reviewers. Any product that may be evaluated in this article, or claim that may be made by its manufacturer, is not guaranteed or endorsed by the publisher.

Supplementary material

The Supplementary Material for this article can be found online at: <https://www.frontiersin.org/articles/10.3389/fnbot.2023.1172770/full#supplementary-material>

Aprile, I., Germanotta, M., Cruciani, A., Loreti, S., Pecchioli, C., Cecchi, F., et al. (2020). Upper limb robotic rehabilitation after stroke: a multicenter, randomized clinical trial. *J. Neurol. Phys. Ther.* 44, 3–14. doi: 10.1097/NPT.0000000000000295

- Balci, B. P. (2018). Spasticity measurement. *Noro. Psikiyatr. Ars.* 55, S49–S53. doi: 10.29399/npa.23339
- Bevan, N., Carter, J., and Harker, S. I. S. O. (2021). “Revised: What Have We Learnt About Usability Since 1998?” in *Human-Computer Interaction: Design and Evaluation. HCI 2015. Lecture Notes in Computer Science*, ed M. Kurosu. Cham: Springer.
- Bishop, L., Gordon, A. M., and Kim, H. (2017). Hand robotic therapy in children with hemiparesis: a pilot study. *Am. J. Phys. Med. Rehabil.* 96, 1–7. doi: 10.1097/PHM.0000000000000537
- Bohannon, R. W., and Smith, M. B. (1987). Interrater reliability of a modified Ashworth scale of muscle spasticity. *Phys. Ther.* 67, 206–207. doi: 10.1093/ptj/67.2.206
- Bosecker, C., Dipietro, L., Volpe, B., and Krebs, H. I. (2010). Kinematic robot-based evaluation scales and clinical counterparts to measure upper limb motor performance in patients with chronic stroke. *Neurorehabil. Neural. Repair.* 24, 62–9. doi: 10.1177/1545968309343214
- Brashear, A., Zafonte, R., Corcoran, M., Galvez-Jimenez, N., Gracies, J. M., Gordon, M. F., et al. (2002). Inter- and intrarater reliability of the Ashworth Scale and the disability assessment scale in patients with upper-limb poststroke spasticity. *Arch. Phys. Med. Rehabil.* 83, 1349–1354. doi: 10.1053/apmr.2002.35474
- Butt, M., Naghdy, G., Naghdy, F., Murray, G., and Du, H. (2020). Patient-specific robot-assisted stroke rehabilitation guided by EEG - a feasibility study. *Annu. Int. Conf. IEEE. Eng. Med. Biol. Soc.* 2020, 2841–2844. doi: 10.1109/EMBC44109.2020.9175459
- Calabrò, R. S., Accorinti, M., Porcari, B., Carioti, L., Ciatto, L., Billeri, L., et al. (2019). Does hand robotic rehabilitation improve motor function by rebalancing interhemispheric connectivity after chronic stroke? Encouraging data from a randomised-clinical-trial. *Clin. Neurophysiol.* 130, 767–780. doi: 10.1016/j.clinph.2019.02.013
- Chien, W. T., Chong, Y. Y., Tse, M. K., Chien, C. W., and Cheng, H. Y. (2020). Robot-assisted therapy for upper-limb rehabilitation in subacute stroke patients: a systematic review and meta-analysis. *Brain. Behav.* 10, e01742. doi: 10.1002/brb3.1742
- de Raadt, A., Warrens, M. J., Bosker, R. J., and Kiers, H. A. L. A. (2021). Comparison of reliability coefficients for ordinal rating scales. *J. Classif.* 38, 519–543. doi: 10.1007/s00357-021-09386-5
- Dehem, S., Gilliaux, M., Lejeune, T., Detrembleur, C., Galinski, D., Sapin, J., et al. (2017). Assessment of upper limb spasticity in stroke patients using the robotic device REAplan. *J. Rehabil. Med.* 49, 565–571. doi: 10.2340/16501977-2248
- Dehem, S., Gilliaux, M., Stoquart, G., Detrembleur, C., Jacquemin, G., Palumbo, S., et al. (2019). Effectiveness of upper-limb robotic-assisted therapy in the early rehabilitation phase after stroke: a single-blind, randomised, controlled trial. *Ann. Phys. Rehabil. Med.* 62, 313–320. doi: 10.1016/j.rehab.2019.04.002
- De-la-Torre, R., Oña, E. D., Balaguer, C., Jardón, A. (2021). Robot-aided systems for improving the assessment of upper limb spasticity: a systematic review. *Sensors* 20, 5251. doi: 10.3390/s20185251
- Esquenazi, A., Lee, S., Watanabe, T., Nastaskin, A., McKee, C., O'Neill, J., et al. (2021). Comparison of the Armeo to Tabletop-assisted Therapy Exercises as Supplemental Interventions in Acute Stroke Rehabilitation: A Randomized Single Blind Study. *PM. R.* 13, 30–37. doi: 10.1002/pmrj.12397
- Esquenazi, A., Tobin, M., Nastaskin, A., Lee, S., and Wikoff, A. (2018). Robotic assisted assessment of ashworth and tardieu scores for the fingers. *Int. Symp. Wearable. Robot. Rehabil.* 5, 1–1. doi: 10.1109/WEROB.2017.8383880
- Fasoli, S. E., and Adans-Dester, C. P. A. (2019). Paradigm shift: rehabilitation robotics, cognitive skills training, and function after stroke. *Front. Neurol.* 10, 1088. doi: 10.3389/fneur.2019.01088
- Germanotta, M., Gower, V., Papadopoulou, D., Cruciani, A., Pecchioli, C., Mosca, R., et al. (2021). Reliability, validity and discriminant ability of a robotic device for finger training in patients with subacute stroke. *J. Neuroeng. Rehabil.* 17, 1. doi: 10.1186/s12984-019-0634-5
- Hager, K. M. R. (2003). *Reliability of Fatigue Measures in an Overhead Work Task : A Study of Shoulder Muscle Electromyography and Perceived Discomfort Reliability of Fatigue Measures in an Overhead Work Task : A Study of Shoulder Muscle Electromyography and Perceived Discomfort*. Virginia: Virginia Polytech Inst State University.
- Jakob, I., Kollreider, A., Germanotta, M., Benetti, F., Cruciani, A., Padua, L., et al. (2018). Robotic and sensor technology for upper limb rehabilitation. *PM. R.* 10, S189–S197. doi: 10.1016/j.pmrj.2018.07.011
- Johnson, G. R. (2002). Outcome measures of spasticity. *Eur. J. Neurol.* 9, 10–16. doi: 10.1046/j.1468-1331.2002.0090s1010.x
- Keller, U., Schölch, S., Albisser, U., Rudhe, C., Curt, A., Riener, R., et al. (2015). Robot-assisted arm assessments in spinal cord injured patients: a consideration of concept study. *PLoS ONE* 10, e0126948. doi: 10.1371/journal.pone.0126948
- Lamercy, O., Dovat, L., Yun, H., Wee, S. K., Kuah, C., Chua, K., et al. (2010). “Robotic assessment of hand functions with the HapticKnob,” in *Proceedings of the 4th International Convention on Rehabilitation Engineering & Assistive Technology* (Singapore Therapeutic, Assistive & Rehabilitative Technologies (START) Centre), 1–4. doi: 10.5555/1926058.1926091
- Lee, K. C., Carson, L., Kinnin, E., and Patterson, V. (1989). The ashworth scale: a reliable and reproducible method of measuring spasticity. *Neurorehabil. Neural. Repair.* 3, 205–209. doi: 10.1177/136140968900300406
- McHugh, M. L. (2012). Interrater reliability: the kappa statistic. *Biochem. Med.* 22, 276–282. doi: 10.11613/BM.2012.031
- Mehrholz, J., Pohl, M., Platz, T., Kugler, J., and Elsner, B. (2018). Electromechanical and robot-assisted arm training for improving activities of daily living, arm function, and arm muscle strength after stroke. *Cochrane. Datab. Syst. Rev.* 9, CD006876. doi: 10.1002/14651858.CD006876.pub5
- Meseguer-Henarejos, A. B., Sánchez-Meca, J., López-Pina, J. A., and Carles-Hernández, R. (2018). Inter- and intra-rater reliability of the Modified Ashworth Scale: a systematic review and meta-analysis. *Eur. J. Phys. Rehabil. Med.* 54, 576–590. doi: 10.23736/S1973-9087.17.04796-7
- Meyer, J. T., Gassert, R., and Lamercy, O. (2021). An analysis of usability evaluation practices and contexts of use in wearable robotics. *J. Neuroeng. Rehabil.* 18, 170. doi: 10.1186/s12984-021-00963-8
- Mokkink, L. B., Boers, M., van der Vleuten, C. P. M., Bouter, L. M., Alonso, J., Patrick, D. L., et al. (2020). Risk of Bias tool to assess the quality of studies on reliability or measurement error of outcome measurement instruments: a Delphi study. *BMC. Med. Res. Methodol.* 20, 293. doi: 10.1186/s12874-020-01179-5
- Orehov, G., Fang, Y., Cuddeback, C. F., and Lerner, Z. F. (2021). Usability and performance validation of an ultra-lightweight and versatile untethered robotic ankle exoskeleton. *J. Neuroeng. Rehabil.* 18, 163. doi: 10.1186/s12984-021-00954-9
- Orihuela-Espina, F., Roldán, G. F., Sánchez-Villavicencio, I., Palafox, L., Leder, R., Sucar, L. E., et al. (2016). Robot training for hand motor recovery in subacute stroke patients: a randomized controlled trial. *J. Hand. Ther.* 29, 51–57. doi: 10.1016/j.jht.2015.11.006
- Pandyan, A. D., Johnson, G. R., Price, C. I., Curless, R. H., Barnes, M. P., Rodgers, H. A., et al. (1999). review of the properties and limitations of the Ashworth and modified Ashworth Scales as measures of spasticity. *Clin. Rehabil.* 13, 373–383. doi: 10.1191/026921599677595404
- Park, J. H., Park, G., Kim, H. Y., Lee, J. Y., Ham, Y., Hwang, D., et al. (2020). comparison of the effects and usability of two exoskeletal robots with and without robotic actuation for upper extremity rehabilitation among patients with stroke: a single-blinded randomised controlled pilot study. *J. Neuroeng. Rehabil.* 17, 137. doi: 10.1186/s12984-020-00763-6
- Roman, N. A., Miclaus, R. S., Nicolau, C., and Sechel, G. (2022). Customized manual muscle testing for post-stroke upper extremity assessment. *Brain. Sci.* 12, 457. doi: 10.3390/brainsci12040457
- Sáinz-Pelayo, M. P., Albu, S., Murillo, N., and Benito-Penalva, J. (2020). Spasticity in neurological pathologies. An update on the pathophysiological mechanisms, advances in diagnosis and treatment. *Rev. Neurol.* 70, 453–460. doi: 10.33588/rn.7012.2019474
- Serrano-López Terradas, P. A., Criado Ferrer, T., Jakob, I., and Calvo-Arenillas, J. I. (2022). Quo vadis, amadeo hand robot? A randomized study with a hand recovery predictive model in subacute stroke. *Int. J. Environ. Res. Public. Health.* 20, 690. doi: 10.3390/ijerph20010690
- Spasticity, L. (2017). Motor recovery, and neural plasticity after stroke. *Front. Neurol.* 8, 120. doi: 10.3389/fneur.2017.00120
- Sunnerhagen, K. S. (2016). Predictors of spasticity after stroke. *Curr. Phys. Med. Rehabil. Rep.* 4, 182–185. doi: 10.1007/s40141-016-0128-3
- Thibaut, A., Chatelle, C., Ziegler, E., Bruno, M. A., Laureys, S., Gosseries, O., et al. (2013). Spasticity after stroke: physiology, assessment and treatment. *Brain. INJ.* 27, 1093–1105. doi: 10.3109/02699052.2013.804202
- Tyromotion (2023). *Amadeo. AMADEO:® Der Pionier in der Finger-Hand-Rehabilitation | Tyromotion*. Available online at: <https://tyromotion.com/produkte/amadeo/> (accessed January 12, 2023).
- UAB UA (2014). Coeficiente de correlación intraclase. Estud postgrado en Metodol la Investig en Ciencias la Salud. 1–8.
- Wissel, J., Verrier, M., Simpson, D. M., Charles, D., Guinto, P., Papapetropoulos, S., et al. (2015). Post-stroke spasticity: predictors of early development and considerations for therapeutic intervention. *PM. R.* 7, 60–67. doi: 10.1016/j.pmrj.2014.08.946



OPEN ACCESS

EDITED BY

Jonghyun Kim,
Sungkyunkwan University, Republic of Korea

REVIEWED BY

Xinxing Chen,
Southern University of Science and Technology,
China

Usman Ghafoor,
Pusan National University, Republic of Korea
Farong Gao,
Hangzhou Dianzi University, China

*CORRESPONDENCE

Neha Das
✉ neha.das@tum.de

RECEIVED 31 January 2023

ACCEPTED 19 June 2023

PUBLISHED 14 July 2023

CITATION

Das N, Endo S, Patel S, Krewer C and Hirche S
(2023) Online detection of compensatory
strategies in human movement with supervised
classification: a pilot study.
Front. Neurobot. 17:1155826.
doi: 10.3389/fnbot.2023.1155826

COPYRIGHT

© 2023 Das, Endo, Patel, Krewer and Hirche.
This is an open-access article distributed under
the terms of the [Creative Commons Attribution
License \(CC BY\)](#). The use, distribution or
reproduction in other forums is permitted,
provided the original author(s) and the
copyright owner(s) are credited and that the
original publication in this journal is cited, in
accordance with accepted academic practice.
No use, distribution or reproduction is
permitted which does not comply with these
terms.

Online detection of compensatory strategies in human movement with supervised classification: a pilot study

Neha Das^{1*}, Satoshi Endo¹, Sabrina Patel², Carmen Krewer^{2,3} and
Sandra Hirche¹

¹Information-Oriented Control, TUM School of Computation, Information and Technology, Technical
University of Munich, Munich, Germany, ²Human Movement Science, Department of Sports and Health
Sciences, Technical University of Munich, Munich, Germany, ³Department of Neurology, Research
Group, Schoen Clinic Bad Aibling, Bad Aibling, Germany

Introduction: Stroke survivors often compensate for the loss of motor function in their distal joints by altered use of more proximal joints and body segments. Since this can be detrimental to the rehabilitation process in the long-term, it is imperative that such movements are indicated to the patients and their caregiver. This is a difficult task since compensation strategies are varied and multi-faceted. Recent works that have focused on supervised machine learning methods for compensation detection often require a large training dataset of motions with compensation location annotations for each time-step of the recorded motion. In contrast, this study proposed a novel approach that learned a linear classifier from energy-based features to discriminate between healthy and compensatory movements and identify the compensating joints without the need for dense and explicit annotations.

Methods: Six healthy physiotherapists performed five different tasks using healthy movements and acted compensations. The resulting motion capture data was transformed into joint kinematic and dynamic trajectories. Inspired by works in bio-mechanics, energy-based features were extracted from this dataset. Support vector machine (SVM) and logistic regression (LR) algorithms were then applied for detection of compensatory movements. For compensating joint identification, an additional condition enforcing the independence of the feature calculation for each observable degree of freedom was imposed.

Results: Using leave-one-out cross validation, low values of mean brier score (<0.15), mis-classification rate (<0.2) and false discovery rate (<0.2) were obtained for both SVM and LR classifiers. These methods were found to outperform deep learning classifiers that did not use energy-based features. Additionally, online classification performance by our methods were also shown to outperform deep learning baselines. Furthermore, qualitative results obtained from the compensation joint identification experiment indicated that the method could successfully identify compensating joints.

Discussion: Results from this study indicated that including prior bio-mechanical information in the form of energy based features can improve classification performance even when linear classifiers are used, both for offline and online classification. Furthermore, evaluation compensation joint identification algorithm indicated that it could potentially provide a straightforward and interpretable way of identifying compensating joints, as well as the degree of compensation being performed.

KEYWORDS

compensation detection, stroke rehabilitation, machine learning, bio-mechanical features, supervised classification

1. Introduction

Stroke is one of the leading causes for long-term disability worldwide (Murray et al., 2012) and often results in upper-extremity motor impairment in survivors (Kwakkel et al., 2003) that can severely affect their quality of life and health (Franceschini et al., 2010; Morris et al., 2013). Hence, regaining upper-limb function post-stroke is vital for patient recuperation and consequently, is a major target of rehabilitative-therapy. In particular, repetitive and task specific training of the affected limbs have been suggested to be one of the main drivers of rehabilitation (Bütefisch et al., 1995; Dickstein et al., 1997). Training has traditionally been conducted with assistance and feedback from physiotherapists in a clinical setting. However, this requires constant monitoring and guidance by the physiotherapist, a task that becomes difficult with the increasing number of patients (Pollock et al., 2000). While this can be addressed in part by recommending exercises to the patient for in-home rehabilitation at later stages of recovery (Turton and Fraser, 1990), adopting such an approach introduces novel challenges - namely, providing appropriate feedback to the patient regarding their performance.

Recently, efforts have been made to this end, as well as to alleviate the physiotherapists' workload in clinical settings by introducing automation into the rehabilitation pipeline, for instance via robot-assisted therapy (Aprile et al., 2020; Takebayashi et al., 2022) and interactive game-based therapy (Laver et al., 2017; Laffont et al., 2020). These techniques must be equipped with evaluation mechanisms that can automatically assess the quality and success of the ongoing rehabilitation exercise or task performed by patients, ideally in an online manner, in order to provide useful feedback for facilitating improvement in real-time. However, such an automatic quantification of task performance can be challenging. While the success of task or exercise completion is relatively simple to track and quantify automatically—for example by tracking the distance between the end-point of the impaired limb and the goal position, it might not provide an adequate picture of performance, especially with regards to the reappearance of premorbid motor behavior (Cirstea and Levin, 2007). This complication arises in part from the use of compensatory strategies by the patient in the post-stroke period.

Stroke patients often compensate for the impairment caused in one joint by overusing an unimpaired joint for the successful

accomplishment of rehabilitation exercises or activities of daily living (Cirstea and Levin, 2000). Any redundant joint that is relatively underused for a particular motion or task can be recruited when the typically used joint is impaired to ensure successful completion of the task. The degree of compensation provided by the recruited joint can vary from mild to severe (Cirstea and Levin, 2000). It has been noted that the long-term use of compensatory strategies can interfere with rehabilitation goals (Takeuchi and Izumi, 2012). Accurate and automatic identification of compensatory strategies and deviation from healthy motion is therefore an integral part of monitoring exercise/task performance during a therapy session. Moreover, inclusion of this information has been found to be helpful by the patients (Fruchter et al., 2022).

Most of the research toward automatic compensation detection has been geared toward exploiting data-driven supervised learning methods for the task. In general, such methods rely on the availability or acquisition of a dataset of motions which are labeled by experts to be either healthy or compensatory. The acquired dataset of motions is used to train a machine learning model, which can be used afterwards for classifying observed motions at test time. Previous works have explored a variety of machine-learning architectures and models for this task, ranging from decision-trees (Sellmann et al., 2022) and non-parametric methods, such as k-Nearest Neighbor classification (Cai et al., 2019) and Support Vector Machine classifiers (Taati et al., 2012; Zhi et al., 2017) to parametric deep learning methods, such as a Multi-layer Perceptron (MLP) (Lin et al., 2021) or recurrent neural networks with Long Short-Term Memory (LSTM networks) (Zhi et al., 2017). A wide range of measurements including kinematics (Taati et al., 2012; Zhi et al., 2017; Sellmann et al., 2022), applied forces (Cai et al., 2019), and muscle activity (Ma et al., 2019) have been used as an input for these data-driven classifiers.

However, existing learning-based solutions fall short of fully addressing one or more of several common challenges posed by the task of automatic compensation detection. One major challenge is the identification of compensating joints. By leveraging multi-class classification techniques, many approaches are able to detect three common types of compensations in reaching motion—namely torso lean-forward, torso rotation and scapular elevation (Zhi et al., 2017; Cai et al., 2019; Ma et al., 2019). By design, such a classification method is geared toward detecting only one type of compensation per input motion

segment, which can be a shortcoming when the motion segment contains multiple compensation strategies. Kashi et al. (2020) uses multi-label classification to mitigate this issue. However, like the preceding works, this approach relies on explicit annotations of compensation locations. This requirement can pose some limitations on the applicability of the compensation detection mechanism since providing such a detailed descriptor of the compensation strategy can be cumbersome and is subject to labeling error by the expert annotator Hickey et al. (2007). The latter can especially occur when indicators of compensatory movements are subtle and beyond the visual capabilities of physiotherapists (Abbott et al., 2022). This indicates that it is hard to find an objective measure for compensation magnitude and affected location, especially via supervised classification methods that rely on detailed annotations from experts.

Another challenge is discriminating between healthy and compensatory motions in real-time. This is particularly desirable since it can allow for the correction of a compensatory motion as it is being performed either by the means of direct feedback to the patient or through other methods such as alerting the responsible physiotherapist in case of in-clinic rehabilitation. The classification output could also be used by a robotic system to promote more desirable kinematics by means of a force feedback. However, many of the methods discussed above either train their model with pre-segmented motions and assume access to similarly segmented data during test-time (Kashi et al., 2020) or use a sliding window of fixed size for online classification (Zhi et al., 2017; Cai et al., 2019; Ma et al., 2019) which may not be able to capture long-range temporal correlations.

Lastly, most existing works for compensation detection leverage datasets that are quite small in size due to the difficulty of collecting data on a large scale from patients. For example, many works (Zhi et al., 2017; Uy and Abu, 2020; Khoramdel et al., 2021) learn from the Toronto Rehab Stroke Pose Dataset (Dolatbadi et al., 2017) that collects kinematic data from a cohort of 9 stroke survivors and 10 healthy patients, Cai et al. (2019) perform their analysis on data from 8 stroke survivors, and Lin et al. (2021) uses a dataset of motions from 10 stroke survivors. Yet, many works use deep neural networks for learning a model for compensation detection (Zhi et al., 2017; Khoramdel et al., 2021; Lin et al., 2021). This can be counter-productive since deep learning-based architectures typically have a large number of parameters that often outnumber the small training dataset making the model susceptible to overfitting (Bishop and Nasrabadi, 2006) and reduced generalizability. Furthermore, owing to the large parameter size, these models often take longer to train. Thus, there is a growing need for data-driven methods for compensation detection that can learn from small datasets with non-explicit labels in order to decrease the reliance on manual annotation and can be applied online for obtaining predictions in real-time from streaming data.

In this work, we take a step toward closing these gaps by proposing a novel approach that learns a linear classification model that can not only discriminate between compensatory motions and healthy ones, but also identify compensating upper-body

TABLE 1 Demographic information of the participants.

Characteristics	Distribution (Mean \pm Std.)
Number of participants	6
Female	6
Age (years)	26 \pm 2.5
Weight (kg)	59 \pm 11.15
Height (cm)	167 \pm 3.93
Right-hand dominance	6

joints without requiring explicit labels in the training data. To learn an accurate classifier, selection of appropriate features is of utmost importance. In this regard, we take inspiration from bio-mechanical literature pertaining to natural motion generation and design energy-based features that can be used to learn a classifier. These features include joint jerk, power, torque rate and effort, and they are often used as proxies for metabolic energy expenditure which biomechanical models optimize for producing natural movements (Gauthier et al., 2010; Huang et al., 2012). Thus, by including them as features, we propose that they can inform the classifier regarding the degree of atypicality of the motion. We calculate these features independently for each observed degree of freedom (DoF). This allows us to identify compensating joints in a given motion by exploiting the product of its corresponding features and the weights of the learned classifier.

We verify our approach using leave-one-out cross validation on a dataset of healthy and acted compensatory motions by qualified physiotherapists. The present study reports quantitative results that demonstrate the efficacy of our approach toward identification of compensatory motion and the degree to which the upper-body joints are attributed to such motion. Furthermore, we demonstrate that a linear classification model trained on energy-based features shows competitive performance compared to deep learning-based methods including MLP and LSTM that can automatically extract relevant features from raw data (Shaheen et al., 2016) when discriminating healthy motions from compensatory ones.

2. Materials and methods

2.1. Dataset

Six participants with no mobility impairments were recruited for this study. All participants are trained physiotherapists. Informed consent was gathered from all of the participants. Table 1 summarizes the demographic information for all the participants.

2.1.1. Motion primitives

We collected movement data for five different motion primitives, each of which corresponds to a single goal-oriented

motion trajectory. These include (i) a bimanual task where the participant lifts a tray to their chest level with both arms, (ii) a unimanual task to reach and grasp an object at the eye-level, (iii) a unimanual task to reach and grasp an object at the chest-level, (iv) a unimanual task to reach and grasp an object such that it includes pronation and (v) supination. We illustrate these primitive motion patterns in [Figure 1](#).

Repetition of such motions is often part of rehabilitation exercises ([Thielman et al., 2004](#); [Bayona et al., 2005](#); [Rensink et al., 2009](#)) as they comprise major motions used for performing activities of daily living. Each of these primitives display a wide range of joint activity and joint interactions both for healthy and atypical movements. The experimental setup for the bimanual tray lifting task consists of cardboard tray with dimensions 35.5 cms \times 24.8 cms \times 3 cms and weight 0.1 kgs. For the grasping tasks, we use a height-adjustable tripod that is mounted with a cylindrical rod of length 20 cms (the grasp object). We additionally place a side table close to the participant's dominant arm and adjust its height such that they are able to place their elbow flexed naturally at 90 degrees. We controlled for reach length among the participants by placing the tripod holding the grasp object such that it is always within reach. This is done by adjusting the position of the tripod such that its central column touches the participants' wrist when they extend their arm. At the beginning of the bimanual motion, the tray is placed on the participant's lap and grasped by its sides. The starting point for the participant's dominant arm during the reaching motions is on the side-table. [Figure 2](#) illustrates the experimental setup for this work.

2.1.2. Compensation simulation

In addition to generating natural motions corresponding to each of the 5 tasks, the participants also simulated different types of compensatory movements simulating stroke patients for each task. With regards to the latter, the participants, all of whom were physiotherapists, were instructed to enact compensations that were most commonly observed by them during their experience of interacting with stroke patients using their dominant arm. No other restrictions were placed on the type of the compensation strategies the participants could simulate. However, all of the collected motions (including the acted compensatory movement trajectories) begin with the participant sitting in a natural or "healthy" pose, with no visible joint compensations.

[Figure 1](#) illustrates the different motion primitives that comprise the dataset and compares healthy and compensated movement examples for each motion primitive. We additionally plot the distribution of range of motion (RoM) observed throughout the collected trajectories for each joint in [Figure 3](#). RoM has been widely used by physiotherapists to assess motion health ([Mortazavi and Nadian-Ghomsheh, 2019](#)) along with other criteria. The minimum average overlap between healthy and compensatory motions was noted to be around 38 percent. This can be attributed to the fact that RoM in compensatory motion widely distributed according to the task and a person who performed it, highlighting a challenge in identifying compensatory movements using simple classification approaches, such as thresholding on RoM.

2.1.3. Dataset size

We collected 5 repetitions of healthy movements and 5 repetitions of 3 acted compensatory movements for each of the 5 tasks (bimanual task, unimanual reaching to an eye level height, unimanual reaching to a chest level height, unimanual reaching with pronation, and unimanual reaching with supination) from 6 participants. This means that a total of $5 \times (3 + 1) \times 5 \times 6 = 600$ trajectories are collected, 100 trajectories for each individual participant.

For ensuring the variability of the healthy motions in the dataset, we calculated the width of 95% confidence intervals (C.I) for peak motions of the different joints and compared them to the 95% C.I's width obtained by [Gates et al. \(2016\)](#) on a similar task (unimanual reaching). We found these values to be comparable to the previous work for most joints. Furthermore, for most joints, the range of peak motions in compensatory movements was found to be greater than 70% of the 95th percentile of peak motion range across all movements (where this range is given by [0, 95th percentile of peak motion]), indicating high variability of the motions in the acted compensations dataset. The 95th percentile of peak motions is calculated from [McGregor et al. \(1995\)](#) for trunk movements and from [Gates et al. \(2016\)](#) for other joints.

2.2. Data measurement

We used Qualisys Track Manager ([Senior, 2004](#)), a marker-based motion capture system with fifteen cameras to capture the movement data of the participants. A total of 31 markers were placed on each participant. Of these, 10 markers were used purely for scaling an OpenSim ([Delp et al., 2007](#)) upper-body musculoskeletal model used for analysis (discussed below) to the participant and were removed while tracking and recording the actual motion of the participant. [Figure 4](#) summarizes the placement and purpose of the body markers. We collected the 3D positions of the markers with respect to a common global reference frame for each of the movement trajectories generated by the 6 participants at a rate of 100 Hz.

2.3. Automatic motion segmentation

In order to streamline the process of data collection, the healthy repetitions of the distinct tasks by each physiotherapist are collected as one contiguous motion. We adopt the same approach for collecting the 3 different types of acted compensation movements from the participants. Therefore, we essentially have 4 contiguous motion data per task per participant. From these trajectories, we automatically extract the individual motions corresponding to each of the 5 primitives with a simple approach similar to work presented in [Fod et al. \(2002\)](#). The following steps are performed for this purpose: (i) the marker trajectory is first smoothed with a Savitzky-Golay filter ([Savitzky and Golay, 1964](#)) of a window of length 200 milliseconds. Next, (ii) the velocity of the end-effector markers (in our case, the markers on the participants' wrists) is calculated by taking the first derivative of the marker positions. Finally, (iii) zero-crossings vector for the marker velocity

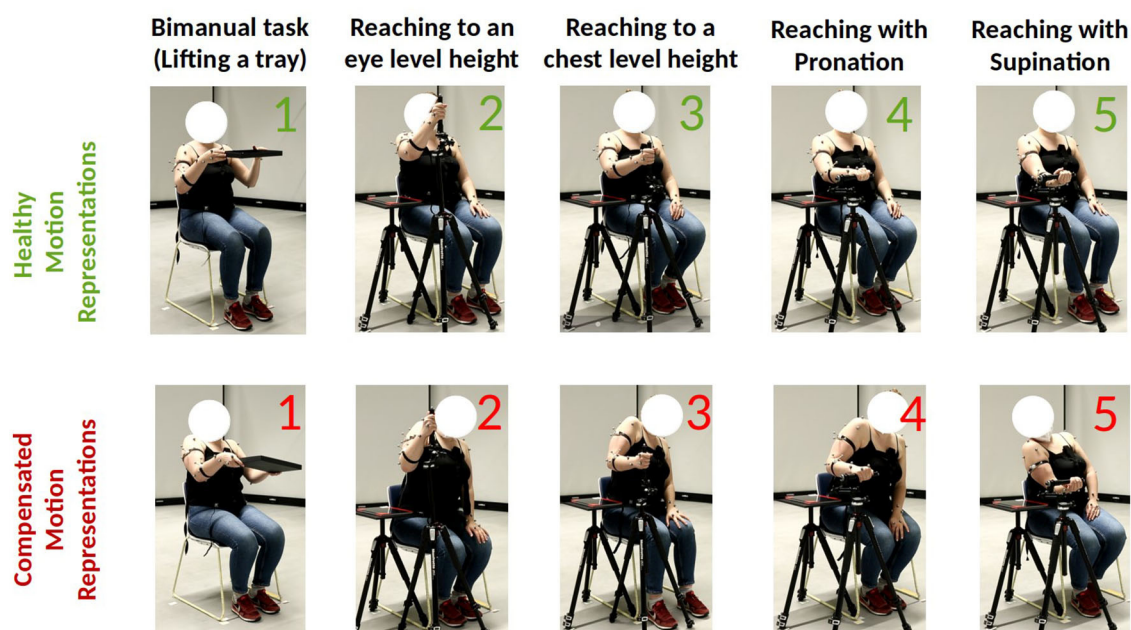


FIGURE 1
Representation of healthy and compensatory motions for the 5 primitives in our dataset.

trajectory are obtained. We pick the locations where velocity is 0 in all three axes. These yield the start and end locations of each individual motion. We illustrate these steps in Figure 5. We modify this approach for extracting non-segmentable motion primitives during online classification at test time as described in Section 2.9 Note that each trajectory consists of multiple repeated motions that begin from the start position, execute the motion primitive, which ends when a target configuration is reached (for example, the tray is lifted to the chest level in the bimanual task, and the cylindrical object is grasped in a particular manner for the reaching task) and return back to the start position. Since participants are not explicitly asked to follow any protocol as they move back to the start position, after executing the motion primitive, we exclude this portion of the trajectory from our analysis.

2.4. Data processing

We used OpenSim (Delp et al., 2007), an open source software package for modeling, simulation and analysis of human biomechanical systems for processing the collected data. For our analysis, we used an OpenSim biomechanical model of a human skeleton with 17 DoFs. The first three of these 17 DoFs are (i) torso flexion, which corresponds to leaning forward (ii) torso tilt, a movement that corresponds to a sideways bend of the torso, and (iii) torso rotation, which corresponds rotation of the torso about its length. The rest of the 14 DoFs correspond to the left and right arms of the participant and mirror each other. For brevity's sake, we list the DoFs for only one arm. These include (iv) elevation plane, (v) elevation angle, (vi) shoulder rotation, (vii) elbow flexion, (viii) forearm rotation, (ix) wrist flexion, and (x) wrist deviation.

For detailed descriptions of these DoFs, we refer the readers to Holzbaaur et al. (2005). The 3 DoFs corresponding to the torso along with the 7 arm DoFs corresponding to the dominant arm of the participants comprise the set that is used for our analysis.

We will now describe our data processing pipeline (illustrated in Figure 6). First, a generic upper-body musculoskeletal model with 17 DoFs was scaled and registered to each of the 6 participants. Following this, the marker trajectories were processed using OpenSim's inverse kinematics tool to infer the corresponding joint angle trajectories of the scaled models associated with each participant. We represent the joint angle trajectories with $\{q_t\}_{t=1}^T$, where q_t denotes the joint configuration of the musculoskeletal system at the discretized time-step t and T denotes the length of the motion trajectory. The joint configuration $q_t = \{q_t^i\}_{i=1}^{N_j}$ is essentially a vector of relative angles corresponding to the N_j rotational DoFs in the musculoskeletal model of the upper body that we are using for this study. We additionally obtain trajectories of joint angle velocity $\{\dot{q}_t\}_{t=1}^T$ and acceleration $\{\ddot{q}_t\}_{t=1}^T$ via automatic differentiation. Finally, we used Opensim's inverse dynamics tool to derive the torques applied at each joint at each time-step (represented in this work as the joint-dynamic trajectory $\{\tau_t\}_{t=1}^T$) for producing the corresponding joint-kinematic trajectory $\{q_t, \dot{q}_t, \ddot{q}_t\}_{t=1}^T$. All collected trajectories are smoothed by using a low-pass filter with a cut off frequency of 6 Hz.

2.5. Feature extraction

Given the kinematic and dynamic trajectories of the motion, we obtain several metrics commonly used for analysis of human motion generation in biomechanics literature. This includes (i)

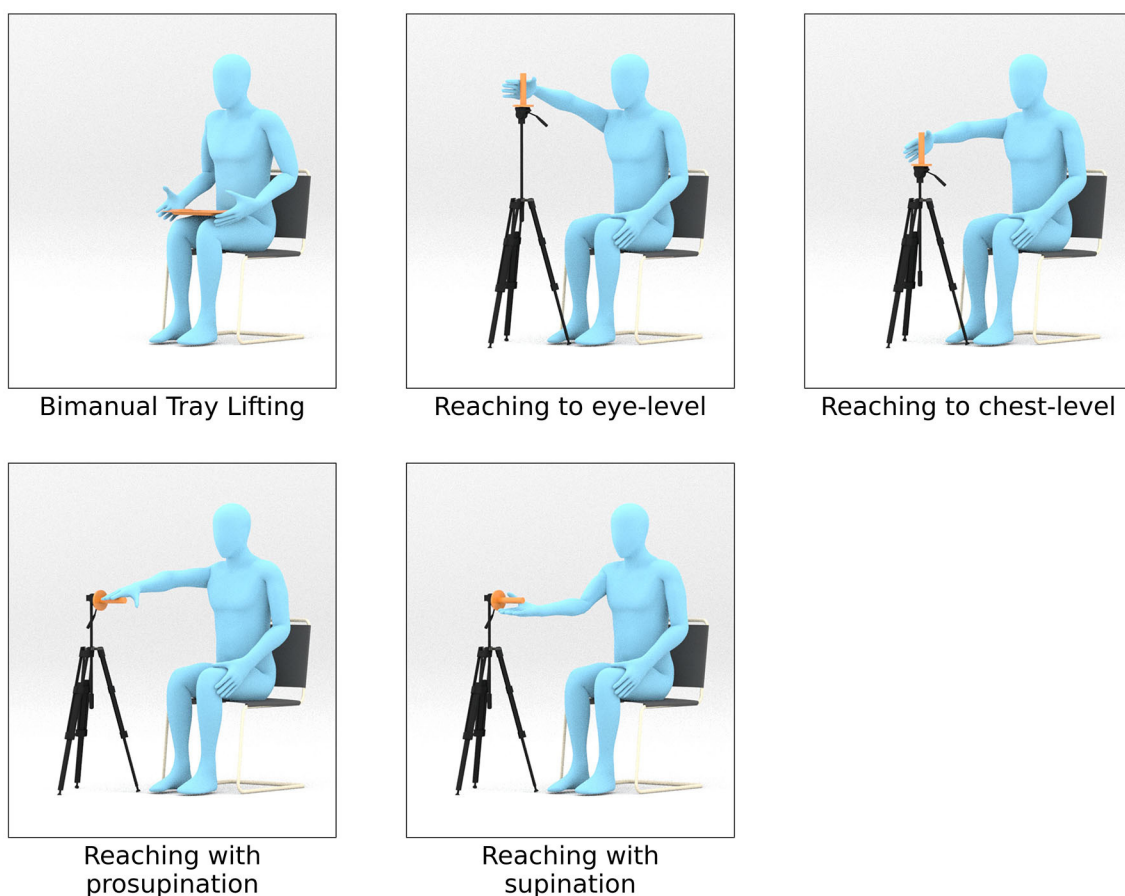


FIGURE 2

Setup for each of the 5 motion primitives. A tray is used for the bimanual lifting task. A cylindrical rod fixed at the top of a tripod is used to mark the target position for the reaching tasks. The participants were asked to grasp the cylindrical rod during the reaching tasks. For reaching to an eye-level and chest-level heights, the rod is aligned vertically. For pronation and supination tasks, the rod was rotated 90 degrees such that it was horizontal.

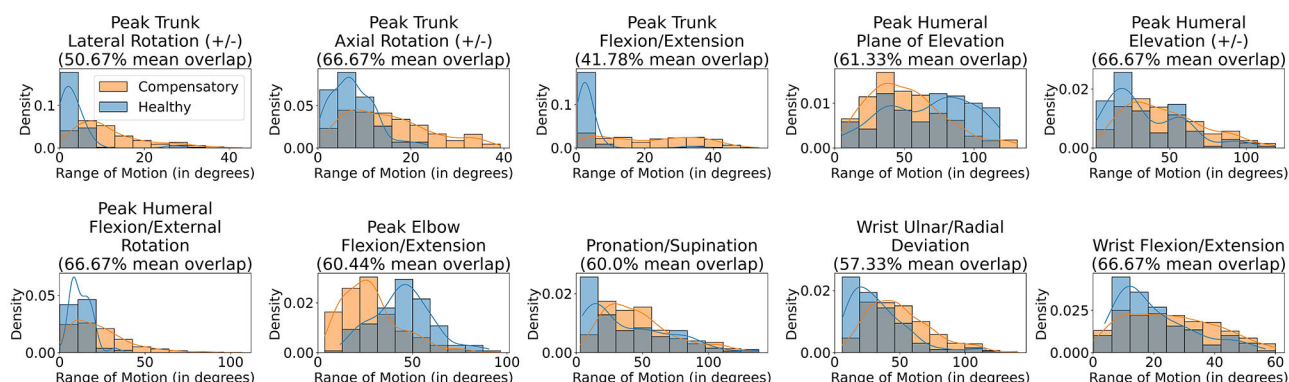
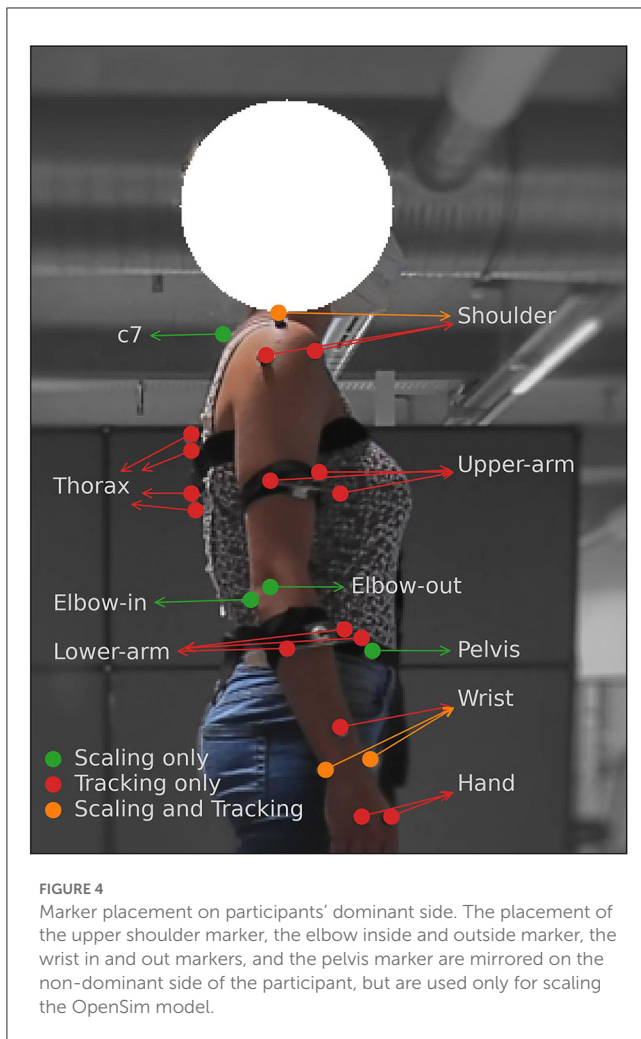


FIGURE 3

Histogram plotting the Range of Motion observed for different joints for healthy and compensatory motions.

angular jerk (\ddot{q}_t^i), an indicator of the degree of movement smoothness in the joint space, maximization of which has been correlated to natural arm movement generation (Wada et al., 2001), (ii) power ($|\dot{q}_t^i \cdot \tau_t^i|$), (iii) effort ($|\ddot{\tau}_t^i|$), and (iv) torque rate ($|\dot{\tau}_t^i|$). The weighted sum of the last three metrics have

been proposed by several previous works to be an indicator of metabolic cost (Zhou et al., 2017; Wong et al., 2021), minimization of which is theorized as one of the biomechanical principles for human motion (Gauthier et al., 2010; Huang et al., 2012).



We create an input feature matrix ϕ_t corresponding to each time-step t of the trajectory. This is done in two steps. First, we calculate the 4 aforementioned metrics for 10 DoFs in the musculoskeletal model separately at each time-step t of the movement trajectory. Next, we update each feature at time-step t by replacing it with cumulative averaging of all the features seen until t to obtain the Cumulative Averaged Energy (CAE) features. This attempts to encode temporal information in the features.

2.5.1. Input normalization

Lastly, all features are normalized using min-max scaling between the values of 0 and 1 across the training dataset in order to remove any bias arising from numerically higher feature values (Singh and Singh, 2020). At test time, the feature values are scaled using the min-max values extracted from the training dataset. Since, we use leave-one-out cross-validation, feature normalization is done independently for each fold of evaluation. The resulting CAE feature matrix (see Figure 7) denoted by $\phi = \{\phi_d\}_{d=1}^{40}$ containing 40 scalar features forms one of the inputs to the classifier discussed in the Section 2.7.

2.6. Generation of the training dataset

For online classification, we generate the training dataset \mathcal{D}_{tr} by calculating the feature matrix for each time-step of each of the $N_{M_{tr}}$ movement trajectories. This corresponds to the input feature vector $\phi_{t,m}$ comprising a single datapoint along with a ground-truth label. The latter is required by supervised learning methods. Since we have access to only sparse binary labels which we denote as y_m corresponding to the full m -th trajectory, we generate ground-truth labels for the intermediate steps of the trajectory by replicating the label corresponding to the full trajectory for all the frames, thus obtaining a label $y_{t,m}$ for the t -th frame of the m -th motion trajectory. Assuming that the m -th trajectory has a length of T_m , the full dataset \mathcal{D} has a total of $\sum_{m=1}^{N_{M_{tr}}} T_m$ data-points. We can therefore succinctly represent our training dataset \mathcal{D}_{tr} as follows:

$$\mathcal{D}_{tr} = \{\phi_{m,t_m}, y_{m,t_m}; \forall t_m \in \{1, \dots, T_m\}, \forall m \in \{1, \dots, N_{M_{tr}}\}\} \quad (1)$$

2.7. Classification algorithm

We train a linear classification model (Bishop and Nasrabadi, 2006) using supervised learning for discriminating between healthy and compensatory motions. More concretely, our goal is to learn a linear hyperplane $\mathbf{w} \cdot \phi + b = 0$, where the learnable parameters \mathbf{w} and b are learnt such that the following conditions:

$$\begin{aligned} \mathbf{w} \cdot \phi + b < 0 &\implies \text{Compensation} \\ \mathbf{w} \cdot \phi + b \geq 0 &\implies \text{No Compensation} \end{aligned} \quad (2)$$

are maximally satisfied over the training dataset \mathcal{D}_{tr} .

Many different methods for learning the parameters \mathbf{w}, b have been described in the literature. We employ two popular approaches, namely linear Support Vector Machine (SVM) classification and Logistic Regression (LR) for learning these parameters. We describe these methods in the following subsections.

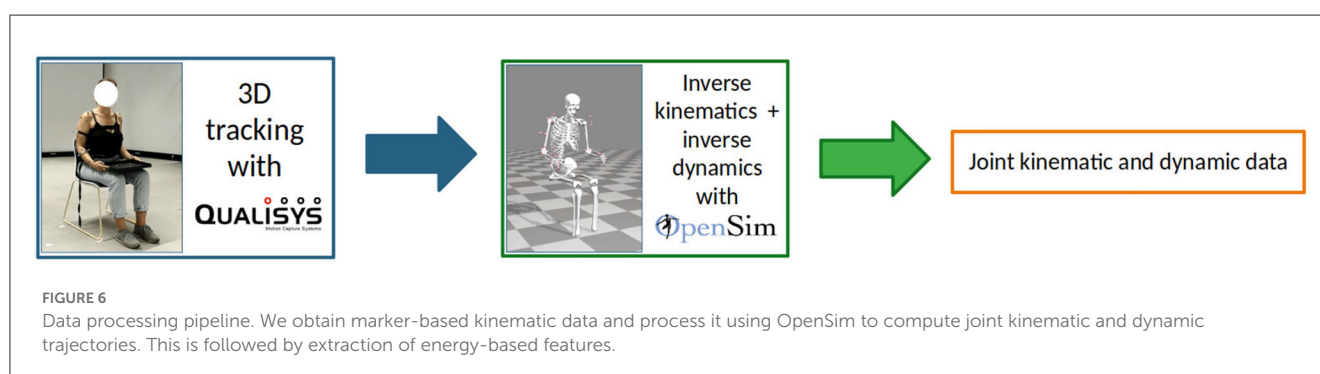
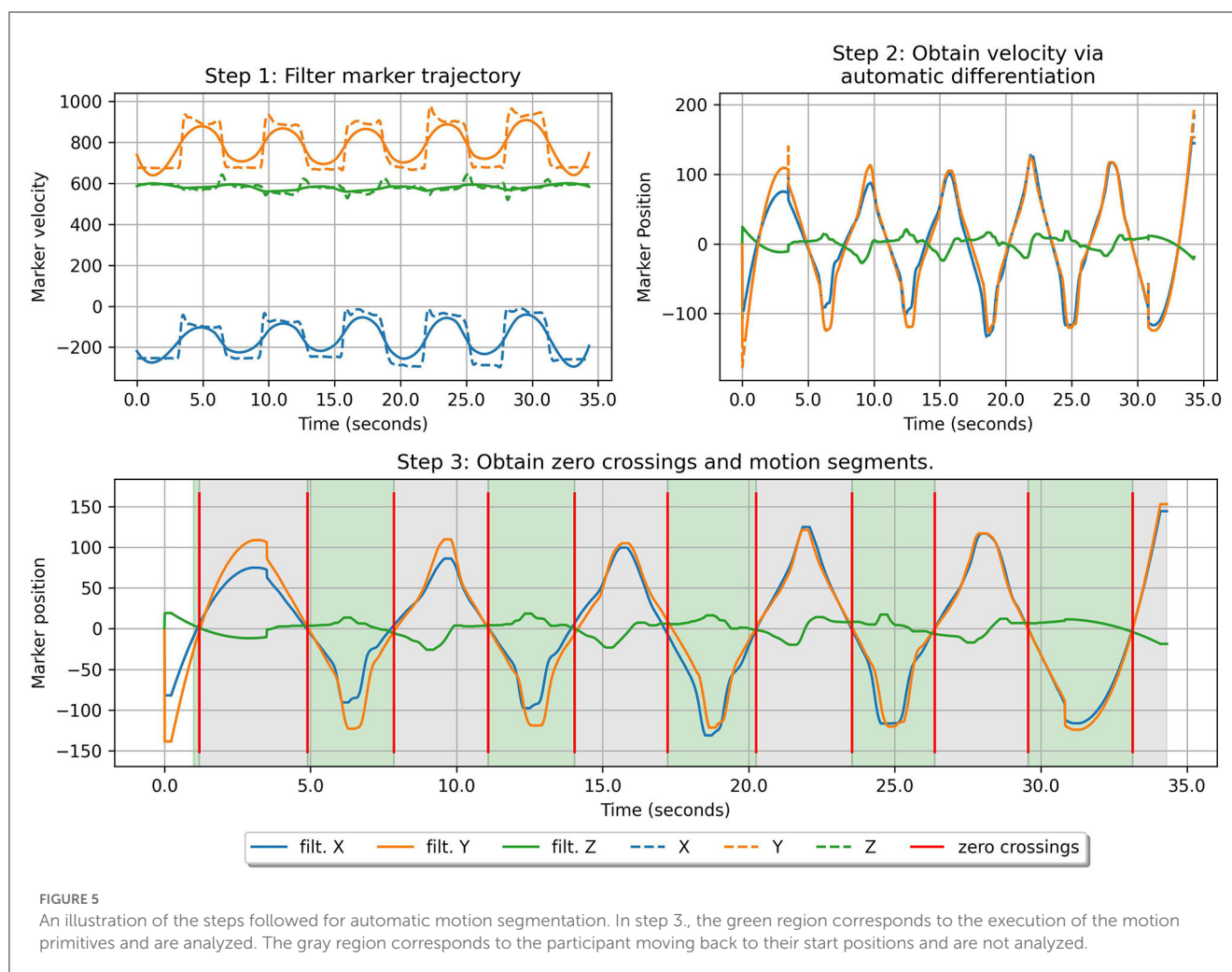
2.7.1. Logistic regression

LR (Bishop and Nasrabadi, 2006) learns the parameters \mathbf{w}, b by minimizing the regularized cross-entropy loss on the training dataset.

$$\begin{aligned} \mathcal{L}(\mathbf{w}, b | \mathcal{D}) = & - \sum_{i=1}^{N_{D_{tr}}} [y_i \log \sigma(\mathbf{w} \cdot \phi_i + b) \\ & + (1 - y_i) \log(1 - \sigma(\mathbf{w} \cdot \phi_i + b)) + \lambda \|\mathbf{w}\|_2^2] \end{aligned} \quad (3)$$

where $\sigma(a) = \frac{1}{1 + \exp(-a)}$ denotes the sigmoid function, $\|\cdot\|$ denotes the Euclidean norm, λ is the regularization constant, and $N_{D_{tr}}$ denotes the size of the training dataset.

This loss has its basis in Maximum Likelihood Estimation (Bishop and Nasrabadi, 2006) which maximizes the probability $p(\phi) = \sigma(\mathbf{w} \cdot \phi + b)$ of the input ϕ that belongs to the true class over the dataset \mathcal{D}_{tr} . Once the classification model has been trained, the output of function $p(\cdot)$ can be interpreted as an indicator of the classification confidence. Thus, a probability value of 0.5 indicates that the classification model is uncertain



regarding its prediction, while values closer to 0 or 1 indicate high model confidence.

2.7.2. Support vector machine with a linear kernel

SVMs learn a linear classification hyperplane that can separate the positive and the negative class such that the margin for separating these two classes has the maximum distance. While SVM is a non-parametric method and typically remaps the input feature space to an infinite dimensional latent space when using

complex kernels (Bishop and Nasrabadi, 2006), in this work, we use a linear kernel, that effectively translates to learning the model parameters \mathbf{w}, b by minimizing the Hinge Loss, that is given as follows:

$$\mathcal{L}(\mathbf{w}, b | \mathcal{D}) = \sum_{i=1}^{N_{Dir}} y_i \frac{1}{2} \mathbf{w}^T \mathbf{w} + \alpha \sum_{i=1}^{N_{Dir}} \max(0, 1 - y_i(\mathbf{w} \cdot \boldsymbol{\phi} + b)) \quad (4)$$

where α is a regularization parameter.

	Jerk	Power	Effort	Torque rate
Torso flexion	$\phi_{1,Jerk}$	$\phi_{1,Pow}$	$\phi_{1,Eff}$	$\phi_{1,TR}$
Torso tilt	$\phi_{2,Jerk}$	$\phi_{2,Pow}$	$\phi_{2,Eff}$	$\phi_{2,TR}$
Torso rotation	$\phi_{3,Jerk}$	$\phi_{3,Pow}$	$\phi_{3,Eff}$	$\phi_{3,TR}$
Elevation plane	$\phi_{4,Jerk}$	$\phi_{4,Pow}$	$\phi_{4,Eff}$	$\phi_{4,TR}$
Elevation angle	$\phi_{5,Jerk}$	$\phi_{5,Pow}$	$\phi_{5,Eff}$	$\phi_{5,TR}$
Shoulder rotation	$\phi_{6,Jerk}$	$\phi_{6,Pow}$	$\phi_{6,Eff}$	$\phi_{6,TR}$
Elbow flexion	$\phi_{7,Jerk}$	$\phi_{7,Pow}$	$\phi_{7,Eff}$	$\phi_{7,TR}$
Forearm rotation	$\phi_{8,Jerk}$	$\phi_{8,Pow}$	$\phi_{8,Eff}$	$\phi_{8,TR}$
Wrist flexion	$\phi_{9,Jerk}$	$\phi_{9,Pow}$	$\phi_{9,Eff}$	$\phi_{9,TR}$
Wrist deviation	$\phi_{10,Jerk}$	$\phi_{10,Pow}$	$\phi_{10,Eff}$	$\phi_{10,TR}$

FIGURE 7
The CAE feature matrix. The rows depict the 10 DoFs and the columns depict the feature types. Each cell in the matrix corresponds to a feature.

2.7.3. Training hyper-parameters

Our proposed models with energy based features are both trained for 5,000 iterations. The SVM model is trained with a squared-hinge loss and L2 penalty, while the LR model is trained with an LBFGS optimizer that minimizes the L2 -penalized cross-entropy loss described in Equation 4.

2.8. Identification of compensating joint

We propose to identify the compensating DoFs by exploiting a feature vector corresponding to each DoF independently. Given the parameters of the Ridge Regression model $\{w, b\}$, where $w = \{w_d\}_{d=1}^{40}$ is the set of weights with a one-to-one correspondence with the elements of the feature matrix ϕ , we sort the list of 10 DoFs based on the corresponding weight-feature product given by:

$$\psi_j = w_{j,Jerk}\phi_{j,Jerk} + w_{j,Pow}\phi_{j,Pow} + w_{j,Eff}\phi_{j,Eff} + w_{j,TR}\phi_{j,TR} \quad (5)$$

for the j -th DoF. If the class predicted by a trained model is “Compensated”, the DoF corresponding to the most negative weight-feature product contributes the most to that classification. This can be seen in Equation 2 which shows the linear combination of the weights and features per DoF determines the classification prediction by the model.

2.9. Online feature extraction and classification

For online classification, we must calculate the CAE features in an online manner from the input stream of joint kinematic and dynamic data. As noted in Section 2.5, creation of CAE features includes an aggregation process that presupposes the availability of segmented motion primitives. Therefore, similar to Section 2.3, we employ automated

motion segmentation using zero-crossings of the end-effector velocity to extract goal-directed motion primitives from the trajectory. However, since for online classification, data is processed as a stream, and the full trajectory is revealed to us frame-by-frame, automatic segmentation is reapplied at regular intervals to update motion-primitive locations. The procedure for online segmentation is given as follows: (i) Maintain a history of T_{hist} previous observations of joint kinematics and dynamics, i.e. $\{q_t, \dot{q}_t, \ddot{q}_t, \tau_t\}_{t=1}^{T_{hist}}$ as well as marker positions $\{m_t\}_{t=1}^{T_{hist}}$. (ii) At regular intervals, recalculate the zero-crossing points from the marker history as well as update the observation history. (iii) Use the last observed zero-crossing point as the beginning of a motion primitive for calculating CAE features at time step t as described in Section 2.5.

2.10. Baseline models for comparison

We compare our approach of training the SVM and LR linear classifiers with energy-based features against 2 other baseline models. The first is an MLP with 2 hidden layers and 10 neurons in each layer. The second baseline is an LSTM with 2 hidden layers with 50 neurons each. Both architectures were employed in recent works for classification of compensatory motion (Zhi et al., 2017; Lin et al., 2021) and have served as baselines for other works that use deep learning architectures for analysing human motion data (Azmi and Sulaiman, 2017; Rustam et al., 2020; Wan et al., 2020; Ahad et al., 2021; Yao et al., 2021; Yu et al., 2021). LSTM, in particular has been considered to be suitable for modeling temporal processes, both in context of compensation detection as well as other domains. Since our objective is to demonstrate that exploiting prior bio-mechanical knowledge via energy-based features has competent performance to automatic feature extraction via deep neural networks, the input to our deep neural network baselines are joint-kinematic and dynamic trajectories [similar to Zhi et al. (2017)]. We use a sliding window of size s and an overlap of $s - 1$ frames to create input vector at time-step t of size $s \times 4 \times N_j$. This is aligned with previous approaches which also look at a fixed-length window of data that slides along the trajectory, both for generating training datapoints and at test-time, for online classification (Zhi et al., 2017; Lin et al., 2021). Window length s was determined to be 100, corresponding to 1.0 seconds for MLP and 20, corresponding to 0.2 seconds for LSTM using grid-based hyper-parameter search. Further, the number of neurons in each layer of MLP and LSTM was also determined by using grid-based hyper-parameter search.

2.10.1. Input normalization

Similar to the CAE features, before the input is accepted by either of the classification models, it is normalized using min-max scaling. Normalization is done independently for each fold of evaluation similar to the feature normalization for our proposed approach (Section 2.5.1).

2.11. Evaluation criteria

2.11.1. Evaluation metrics and cross-validation

We evaluate our proposed approach against other approaches with three performance metrics - mean brier score, mean miss-classification rate and mean false discovery rate. Brier Score (BS) is used to measure the quality of uncertainty estimation of the model and can be formulated as $BS = \frac{1}{N} \sum_{i=1}^N y_i - p(\phi_i)$ where N is the size of the set over which BS is being calculated. A small value for BS indicates that the classification model is well calibrated. Miss-classification rate (MCR) measures the proportion of true class examples miss-classified as the other class. Note that $MCR = 1 - \text{recall}$, which is another popular metric for quantifying classification performance. Finally, false discovery rate (FDR) is calculated as the proportion of true class predictions that are incorrectly classified. We note that $FDR = 1 - \text{precision}$. Smaller values for each of these metrics (BS, MCR, FDR) is indicative of good classification performance.

All performance metrics are calculated for samples belonging to each class separately and take the mean. This is done to counterbalance the class-imbalance in the dataset which occurs since more acted compensation trajectories are collected than healthy trajectories.

Cross-validation for all evaluations is performed with leave-one-out approach (LOOCV), in order to ensure that we do not overfit to the test dataset (Cawley and Talbot, 2003).

2.11.2. Significance testing

We additionally report the significance of classification performance among different methods. While it is common to use McNemar's test for this purpose, we cannot directly apply it on our test datapoints since they constitute different time-steps of the same trajectory and can be highly correlated, thus violating the independent samples assumption of the test. As a result, we instead use voting to aggregate the predictions at trajectory level where possible (model comparison and ablation study) and apply the Bonferroni-Holm correction to adjust the p-values whenever we conduct multiple comparisons. We deem the results to be statistically significant if $p < 0.05$. For each of the comparisons, we report statistics in the following format, $\chi^2(\text{degrees-of-freedom}, N = \text{number of samples}) = \text{value of statistic}, p < 0.05$ or $p > 0.05$.

Unfortunately, when assessing online classification performance, the test outputs always correspond to fractions of the same trajectory since the purpose of the experiment is to test the model performance on streaming data. This violates the independence assumption of McNemar's test. Consequently,

TABLE 2 Comparison of model performance using three metrics whose mean and standard deviation over all the test-folds generated using LOOCV are reported.

Model	Brier score	Mis-classification rate	False discovery rate
MLP	0.191 ± 0.05	0.332 ± 0.092	0.221 ± 0.094
LSTM	0.230 ± 0.109	0.270 ± 0.122	0.281 ± 0.169
SVM	0.119 ± 0.093	0.151 ± 0.124	0.177 ± 0.103
LR	0.119 ± 0.060	0.137 ± 0.072	0.194 ± 0.089

The bold entries indicate the smallest mean and corresponding standard deviation in the column.

3. Results

3.1. Model comparison

We compare the performance of our linear classifiers (SVM and LR) trained with energy-based features on the baseline deep learning models MLP and LSTM trained on raw observations (See Section 2.10 for a detailed description of the baseline models).

As indicated in Section 2.11.2, we use voting to aggregate the predictions at trajectory level to calculate the average performance metrics (Table 2). LR achieves the lowest mean mean BS (0.119) and MCR (0.137) amongst all the models. SVM has the lowest FDR (0.177). The highest mean BS (0.230) and FDR (0.281) is obtained by LSTM and the highest mean MCR (0.332) is obtained by MLP.

Furthermore, we conduct McNemar's test to assess the significance of model performances. LR significantly outperforms MLP, $\chi^2(1, N_k = 600) = 8.51, p < 0.05$, as well as LSTM, $\chi^2(1, N_k = 600) = 5.78, p < 0.05$. No significant differences were found between the classification performance of SVM and LR, $\chi^2(1, N = 600) = 5.54, p > 0.05$. SVM significantly outperforms MLP, $\chi^2(1, N = 600) = 23.36, p < 0.05$, and LSTM, $\chi^2(1, N = 600) = 17.69, p < 0.05$. Finally, the classification performance of MLP was not found to be significantly different from that of LSTM, $\chi^2(1, N = 600) = 0.653, p > 0.05$.

We additionally report averaged balanced accuracy (i.e the mean of "Healthy" and "Compensation" classification accuracies) separately for each temporal inter-quartile-range of the trajectory where the temporal-quartiles describe the fraction of the trajectory covered. These results are categorized by type of motion primitive and illustrated in Figure 8. Balance accuracy (BA) for each bin B with $N_{B_{\text{heal}}}$ healthy datapoints and $N_{B_{\text{comp}}}$ compensatory datapoints is calculated as:

$$BA = \frac{1}{2} \left(\frac{\sum_{i=1}^{N_{B_{\text{heal}}}} \mathbb{I}[\phi_i^{B_{\text{heal}}} \text{ classified as "Healthy"}]}{N_{B_{\text{heal}}}} + \frac{\sum_{i=1}^{N_{B_{\text{comp}}}} \mathbb{I}[\phi_i^{B_{\text{comp}}} \text{ classified as "Compensatory"}]}{N_{B_{\text{comp}}}} \right)$$

significance testing with McNemar's test could not be conducted for this experiment.

3.1.1. Online classification results

We validate our proposed method for online feature extraction and classification in this section. Our test data for each

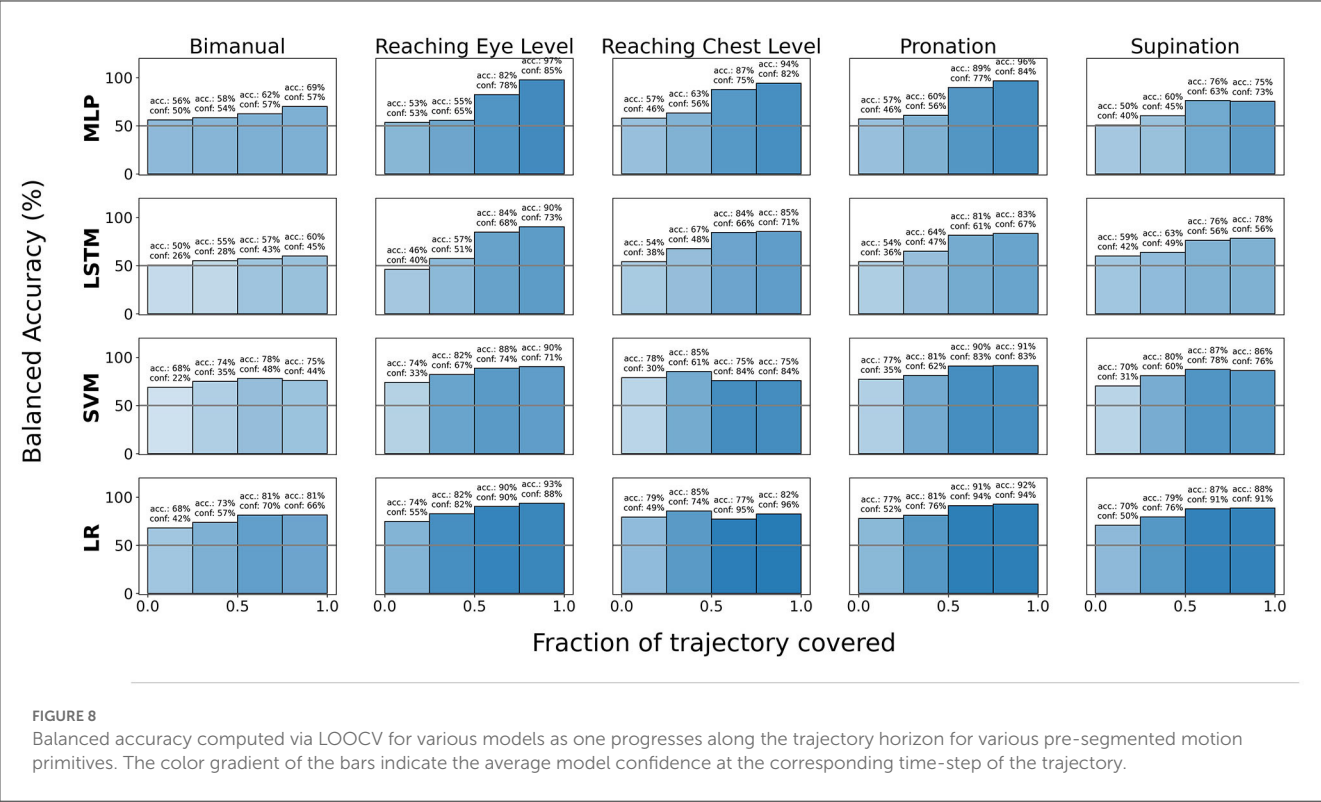


TABLE 3 Comparative performance of different models on online classification tasks.

	Brier score	Misclassification rate	False discovery rate
MLP	0.199 ± 0.047	0.298 ± 0.066	0.299 ± 0.065
LSTM	0.217 ± 0.059	0.328 ± 0.080	0.342 ± 0.068
SVM (fixed-seg)	0.188 ± 0.036	0.233 ± 0.072	0.313 ± 0.036
LR (fixed-seg)	0.169 ± 0.056	0.223 ± 0.075	0.302 ± 0.039
SVM (auto-seg)	0.154 ± 0.05	0.171 ± 0.085	0.237 ± 0.048
LR (auto-seg)	0.134 ± 0.075	0.168 ± 0.085	0.228 ± 0.051

The mean and standard deviation of three evaluation metrics over the folds of LOOCV are reported here. The bold entries indicate the smallest mean and corresponding standard deviation in the column.

fold from LOOCV comprises of the continuous trajectories of repeated motions (healthy or compensatory) collected from the corresponding “Left Out” participant before the data-processing step of automatic segmentation. We process the whole continous trajectory frame-by-frame at the rate of 100 Hz for both our energy-based linear classifiers, as well as the baseline methods (MLP and LSTM). Thus at each time-step t , we have access to only the first t frames. We use the method proposed in Section 2.9 for automatic segmentation and online extraction of the CAE features. We contrast the method proposed for online feature extraction in Section 2.9 with a simple method that assumes that all the non-segmentable motion primitive have a length of 1 second and are contiguous. In the case of the deep learning baselines MLP and LSTM, we use a First In First Out (FIFO) buffer for obtaining the windowed input. These buffers have the same length as the sliding windows used for

training the models. Thus, $s = 100$ (corresponding to 1.0 seconds) for MLP and $s = 20$ (corresponding to 0.2 seconds) for LSTM.

Thus, for all the approaches, we obtain a predicted class for each time-step of the trajectory. However, during the calculation of evaluation metrics, we exclude test datapoints that correspond to the portion of the trajectory where the participant is returning to the start position after executing the motion primitive since participants are not explicitly asked to follow any protocol during this portion of the motion. We report our results in Table 3. Our experiment shows that when automatic segmentation employed, our method (LR (auto-seg) achieves the lowest mean BS (0.134), MCR (0.168), and FDR (0.228). The highest mean BS (0.217), MCR (0.328), and FDR (0.342) is achieved by LSTM.

3.1.2. Uncertainty estimation comparison

In addition to model accuracy, the quality of uncertainty estimation is also an important factor for measuring the performance of classification models. As discussed previously, BS is one approach toward quantifying model uncertainty estimation performance and has been reported for various models in [Tables 2, 3](#). We additionally provide qualitative results in the [Figure 9](#) in the form of calibration plots. We note that while none of the models are perfectly calibrated, SVM and LR, both of which use CAE features, are the closest to the ideal classifier.

3.2. Compensating joint identification

In this section, we show qualitative results for the identification of compensating joints in [Figure 10](#). All the sample trajectories shown in the Figure belong to the “Compensated” class and were randomly sampled from the same class. However, note that despite this, some of the early frames of the motion are classified as “Healthy”. Since all our test trajectories begin with a healthy pose, this result is in accordance with our expectations. We note that the weight-feature product also potentially provides an interpretable way of identifying the compensating joints as well as the relative degree of compensation. The more negative the weight-feature product corresponding to a DoF, the more likely it is that the DoF is contributing to a compensation classification.

3.3. Ablation study of feature aggregation

Lastly, we conduct an ablation study of the feature aggregation step (Section 2.5) for LR models to evaluate the benefit of aggregating the trajectory features until current time step t with an averaging function. We compare our proposed aggregation mechanism against other feature aggregation mechanisms, including no aggregation, where no feature aggregation is performed, and windowed aggregation, where instead of calculating the cumulative average, the final feature at each time step t is calculated as the average of the feature values over a window of size $s \in \{20, 100\}$ centered at time step t , corresponding to 0.2 and 1.0 seconds respectively.

Similar to Section 3.1, we use voting to aggregate the predictions at trajectory level to calculate the average performance metrics ([Table 4](#)). Using CAE features yields the lowest mean MCR (0.137) and lowest mean FDR (0.194). The lowest mean BS (0.110) is achieved by using features averaged over a 1 second long window i.e., “Windowed Avg Feature (1s)”. Models that do not use any feature aggregation yield the highest mean BS (0.168), highest mean MCR (0.229), and highest mean FDR (0.286).

Statistical testing with McNemar’s test reveals that models trained with CAE features significantly outperform models that do not use feature aggregation, i.e., “Without Feature Aggregation”, $\chi^2(1, N = 600) = 65.29, p < 0.05$, as well as models using features averaged over a 0.2 seconds long window i.e., “Windowed Avg Feature (0.2s)”, $\chi^2(1, N = 600) = 65.29, p < 0.05$. However, the McNemar’s test is unable to show a significant difference between

the classification performances of models using CAE features and models with features averaged over a 1 second long window i.e., “Windowed Avg Feature (1s)”, $\chi^2(1, N = 600) = 0.02, p > 0.05$. Among other comparisons, models with “Windowed Avg Feature (1.0s)” significantly outperform models trained on “Windowed Avg Feature (0.2s)”, $\chi^2(1, N = 600) = 34.68, p < 0.05$, as well as models trained without feature aggregation, $\chi^2(1, N = 600) = 69.89, p < 0.05$. Finally, models with “Windowed Avg Feature (0.2s)” significantly outperform models trained without feature aggregation, $\chi^2(1, N = 600) = 30.04, p < 0.05$.

4. Discussion

The aim of this work was to validate a novel approach for automatically detecting compensation strategies with an analytical capability from the kinematic and dynamic trajectory of a motion. For this purpose, we trained a linear classifier on energy-based features. In order to identify the individual joints contributing to compensation, these features were calculated independently for each observable DoF in the distinct segments of the upper body. Temporal information was encoded by aggregating the energy-based features along the input trajectory using cumulative averaging. Two typical methods for learning the linear classifier, namely SVM and LR were investigated.

Our proposed method was validated on a dataset of 5 motion primitives collected from 6 physiotherapists with healthy movements as well as acted compensations. This allowed us to collect a larger variety of compensatory behavior as observed by experienced physiotherapists in contrast to simulating just three types of compensatory behaviors ([Zhi et al., 2017](#)). Furthermore, previous approaches ([Zhi et al., 2017](#); [Cai et al., 2019](#); [Ma et al., 2019](#)) only collected a dataset for uni-manual reaching tasks. In contrast, we record the motions for a bi-manual task (lifting a tray), as well as tasks requiring pronation and supination.

We compared our method against two deep learning baselines MLP and LSTM (Section 2.10) that can perform automatic feature extraction, and have been used in previous approaches for compensation detection ([Zhi et al., 2017](#); [Khoramdel et al., 2021](#); [Lin et al., 2021](#)).

Comparison of evaluation metrics ([Table 2](#)) and statistical testing with McNemar’s test (Section 3.1) showed our methods (LR and SVM) significantly outperformed deep learning baselines, namely MLP and LSTM. In contrast, in [Zhi et al. \(2017\)](#), classification performance of LSTM was noted to be similar for healthy participants and better for stroke patients compared to SVM (without energy-based features). Our results thus indicate that including prior biomechanical information in the form of energy-based features can allow for superior classification performance compared to deep learning approaches, even when simple linear classification methods are used. These results are very promising since both baseline models that exploit deep learning have a larger number of trainable parameters by design and are therefore susceptible to overfitting to the training data ([Bishop and Nasrabadi, 2006](#)).

We additionally validated our proposed online classification mechanism. [Table 3](#) showed that our proposed methods, LR and SVM models yielded lower values of mean BS, MCR and FDR

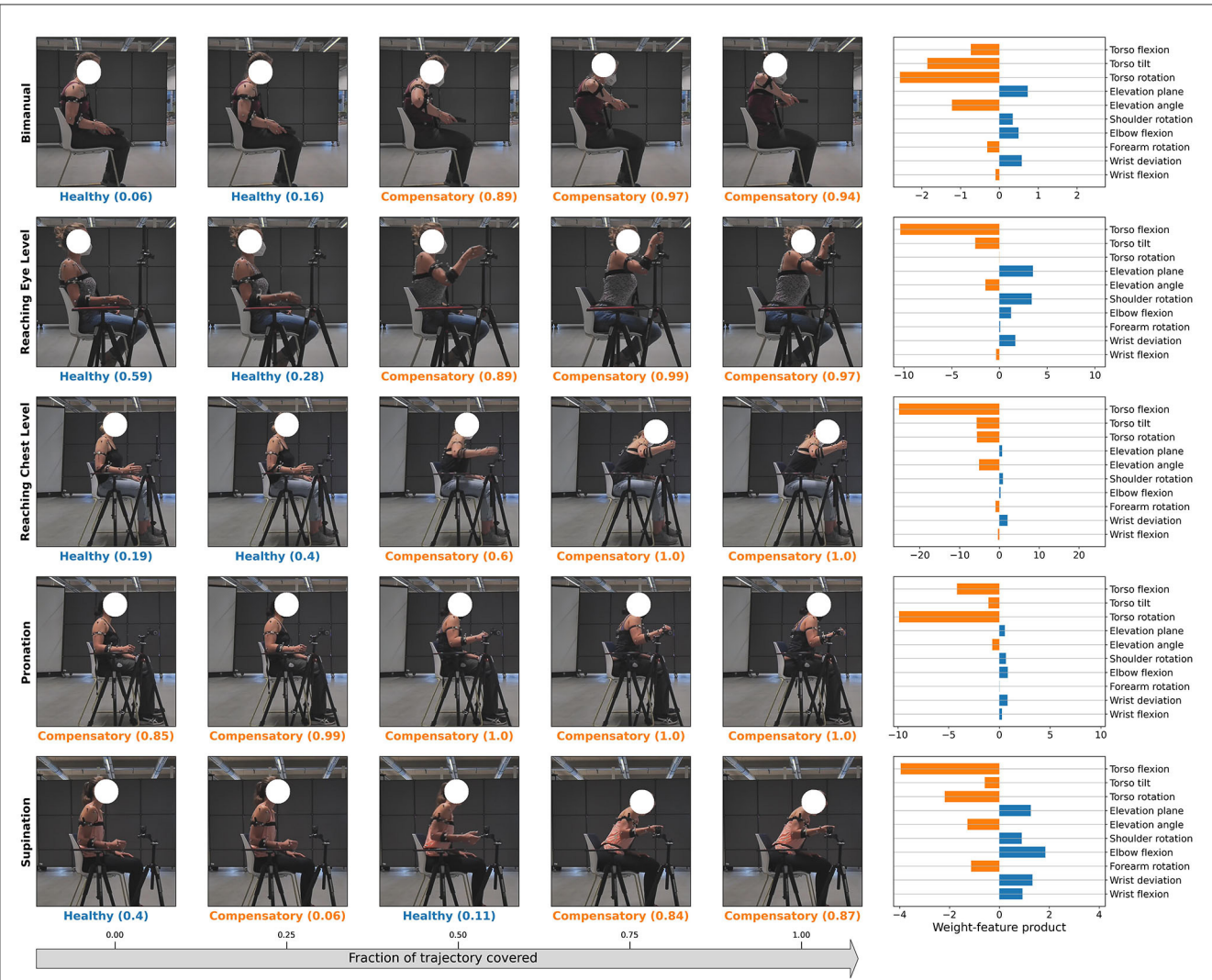
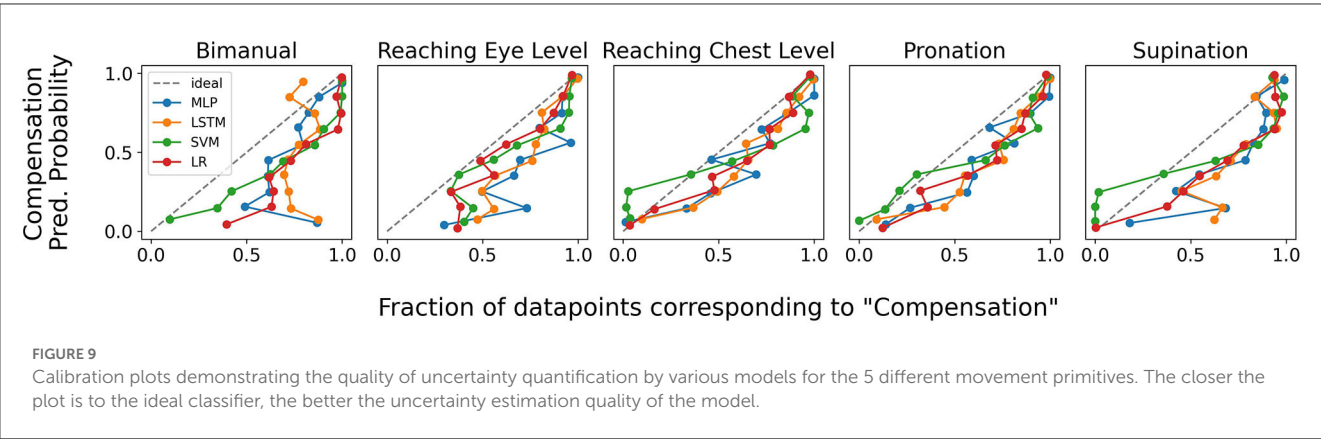


TABLE 4 Results from the ablation study for determining the best aggregation over features.

Feature aggregation mode	Brier score	Mis-classification rate	False discovery rate
Without Feature Aggregation	0.168 \pm 0.034	0.229 \pm 0.059	0.286 \pm 0.03
Windowed Avg Feature (0.2s)	0.140 \pm 0.039	0.188 \pm 0.048	0.260 \pm 0.038
Windowed Avg Feature (1s)	0.110 \pm 0.051	0.138 \pm 0.079	0.202 \pm 0.091
Cumulative Avg Feature	0.119 \pm 0.060	0.137 \pm 0.072	0.194 \pm 0.089

The mean and standard deviation of all three metric values are calculated over LOOCV folds. The bold entries indicate the smallest mean and corresponding standard deviation in the column.

compared to LSTM. Furthermore, these models yielded lower values of mean BS and MCR; and lower or similar values of FDR compared to MLP. In practice, lower values of these metrics corresponds to better classification performance. This indicates that, equipped with energy-based features, models with less trainable parameters such as LR and SVM can perform online classification for compensation detection as well as deep learning-based models that have considerably more parameters. Since training time scales with the size of the model, and can consequently impact online classification computation time in cases where model retraining is needed (such as continual learning Hadsell et al., 2020), this is a promising result.

Within the context of online classification, we studied two different methods for online segmentation of motion primitives for calculating CAE features. Our preferred method, automated motion-primitive segmentation using zero-crossing of velocities (Section 2.3) achieved lower values of BC, MCR, and FDR compared to a method that assumes the full motion to be composed of contiguous segments, each with a fixed length of one second. However, the method that we use for automated motion-primitive segmentation can be limited in its applicability since it strongly depends on how cleanly the movement data is separable into primitives by instances of zero velocity, which is not always possible in real scenarios. In a real-world setting, natural human movements may contain hesitation and noise, and therefore multiple points of zero-crossing velocities can be observed, despite not corresponding to the actual beginning or end of a motion primitive. In such situations, assuming a fixed segmentation-length for the calculation of CAE features can still give acceptable results. Many additional methods exist for primitive motion segmentation in literature. For instance, Barbič et al. (2004) uses probabilistic principal component analysis to track changes in the motion distribution and find segmentation points; Beaudoin et al. (2008) uses k-Nearest Neighbors to cluster individual motion frames, associate different clusters with a unique symbol and subsequently partition the complete movement based on identification of different cluster sub-sequences; Kulić et al. (2012) uses clustering and hidden markov models (HMM) for online segmentation; and Zhou et al. (2022) uses transfer learning to learn a segmentation model from related motion data that already has segmentation labels. We leave the investigation and validation of these methods and their robustness to real-world noisy data for compensation detection to future works.

Our proposed approach for compensation joint identification (Section 2.8 and Figure 10), potentially provides a straightforward and interpretable way of identifying compensating joints, as well

as the degree of compensation being performed without having to rely on detailed-annotations of compensation locations as opposed to previous approaches (Zhi et al., 2017; Cai et al., 2019; Ma et al., 2019; Kashi et al., 2020). Visual verification of the randomly sampled trajectories in the figure indicates the method can successfully identify the compensating joints. However, this result is only a qualitative observation since the ground truth labels for loci of true compensation were not a part of the dataset annotation. Full validation of this technique via collection of annotations for a validation set and comparison of the prediction results with the same is left to future work.

We additionally investigated the impact of trajectory progress toward the final kinematic pose on classification accuracy and model confidence. Our analysis in Figure 10 indicates that model confidence tends to increase as the time step t of the trajectory progresses. This is more clearly observed in Figure 8 at a macro level, where both the model confidence and accuracy tends to increase as the trajectory progresses for all the model architectures we studied. However, we also noted that for most cases, model accuracy reached higher magnitudes earlier for linear classification models (LR and SVM) compared to the deep learning baselines (MLP and LSTM). We believe that this is owed to including prior biomechanical information in the linear classifiers inputs in form of energy-based features, which, as we have already shown in Section 3.1, outperform baseline deep learning methods.

Regarding model performance across various tasks, the analysis presented in Figure 8 indicates that classification accuracy is relatively lower for bimanual tray lifting compared to other tasks. This suggests that the difference between healthy and compensatory behavior in terms of joint kinematics and dynamics during bimanual motions is inherently dissimilar to that during uni-manual motions. If that is the case, ensemble-based models, where each model is trained to identify compensations for individual task types can be used. However, additional data and analysis is required for a thorough investigation of this dissimilarity.

We also studied model confidence more closely in calibration plots shown in Figure 9. Both a qualitative review of these results along with the BS reported in Tables 2, 3 show that LR and SVC models are better calibrated than the deep learning-based MLP and LSTM models. This implies that the uncertainty values estimated by our linear classification models is more reliable than those predicted by the deep learning baselines. This result is consistent with previous literature which link overfitting (more commonly observed in deep neural networks) to uncertainty calibration (Guo et al., 2017; Mukhoti et al., 2020).

Lastly, we conducted an ablation study to determine the best mode of feature aggregation. We found that models trained with CAE features significantly outperform models trained without feature aggregation or with features averaged over a sliding window of size 0.2 seconds. We speculate that the success of CAE features can be attributed cumulative averaging of the features over the seen trajectory, which helps encode the trajectory history in the feature and leads to better classification. We note however, that averaging features over a larger window (with length 1 second) does not lead to a significantly different classification performance than using CAE features. A possible reason could be that a window of length 1 second is able to capture enough temporal information for accurate classification. However, the window size is still an additional hyper-parameter to be optimized when the mode of feature aggregation is chosen to be averaging over a fixed length window. In contrast, using CAE features does not require any such hyper-parameter optimization.

While this study proposes a novel method for compensation detection and compensating joint identification from sparse labels, which, to our knowledge has not been explored before in literature, it also has a few limitations that must be considered during application of this approach, and can be improved upon in future extensions of this work.

Even though all of our participants, being experienced physiotherapists, are familiar with common compensation strategies and drew from experience while simulating compensated motions, variability of compensation strategies in patients can be higher since multiple factors, such the stroke severity (Levin et al., 2016) and fatigue (Zhi et al., 2017) and their combinations can affect the type and degree of compensation employed in different ways. Compensations arising from milder impairments may be only slightly discernible and consequently harder to classify (Zhi et al., 2017). Future work will therefore explore the robustness of the methods established in this approach on motion data collected from patients.

Furthermore, this study comprised of analysing 5 motion primitives, most daily living tasks are much more complex and are composed of different primitive motions. We will therefore verify the robustness of this approach on a dataset of more complex motions in the future.

Additionally, this work strictly imposes the condition of calculating features that are independent for each observable DoF in order to infer compensating joints. However, low coordination between 2 or more DoFs has also been noted to be an indicator of compensation (de Los Reyes-Guzmán et al., 2017). Thus, incorporating features measuring joint-coordination such as movement correlation (de Los Reyes-Guzmán et al., 2017) can be a promising line of investigation for subsequent studies.

Finally, the problem of compensation detection from kinematic data is closely related to other applications for human motion classification such as human activity recognition Vrigkas et al. (2015) and gait analysis Yao et al. (2021). Many of these works therefore deal with similar challenges, such as processing temporal data, online classification and multilabel classification. Consequently, future works can also investigate

novel solutions from these works for compensation detection. For instance, Chamroukhi et al. (2013) proposed a method for automated motion segmentation for human activity recognition using expectation-maximization and HMM which can also be investigated for online classification using our approach; and Yao et al. (2021) combined different temporal features such as time-domain, frequency-domain and wavelet-domain based features for gait analysis which can also be used to extend the CAE feature set proposed in this work for compensation detection.

5. Conclusion

Reliable identification of compensatory strategies in post-stroke patients is crucial for the long-term recovery of the patient. Current methods rely on densely annotated training datasets that can be cumbersome to acquire. To mitigate this, we propose to train a linear classifier with energy-based features that can automatically classify disjointed motion primitives as healthy or compensatory in addition to identifying the compensating joints from sparsely labeled training data. We acquired a dataset of 5 motion primitives including bimanual lifting and uni-manual reaching tasks executed by 5 healthy physiotherapists multiple times, both with and without simulated compensations. The methods proposed in this were validated on the aforementioned dataset using leave-one-out cross validation and outperformed deep learning-based methods that are parameter heavy and are more difficult to train. Future studies will verify the methods proposed in this work on data collected from actual stroke patients.

Data availability statement

The raw data supporting the conclusions of this article will be made available by the authors, without undue reservation.

Ethics statement

The studies involving human participants were reviewed and approved by Ethics Committee of the Medical Faculty of the Technical University of Munich. The patients/participants provided their written informed consent to participate in this study.

Author contributions

Conceptualization: ND, SE, CK, and SH. Software and data processing: ND and SE. Validation, writing—original draft preparation, and visualization: ND. Data acquisition: ND and SP. Writing—review and editing: ND, SE, SP, CK, and SH. Supervision: SE, CK, and SH. Funding acquisition: CK and SH. All authors have read and agreed to the published version of the manuscript.

Funding

This work was supported by the Horizon 2020 research and innovation program of the European Union under Grant Agreement No. 871767 of the project ReHyb and by the European Research Council (ERC) Consolidator Grant Safe data-driven control for human-centric systems (CO-MAN) under Grant Agreement No. 864686.

Acknowledgments

The authors thank all the participants who took part in the study.

References

- Abbott, E., Campbell, A., Wise, E., Tidman, S. J., Lay, B. S., and Kent, P. (2022). Physiotherapists could detect changes of 12 degrees or more in single-plane movement when observing forward bending, squat or hand-over-head: A cross-sectional experiment. *Musculoskeletal Sci. Pract.* 61, 102594. doi: 10.1016/j.msksp.2022.102594
- Ahad, M. A. R., Ahmed, M., Antar, A. D., Makihara, Y., and Yagi, Y. (2021). Action recognition using kinematics posture feature on 3d skeleton joint locations. *Patt. Recogn. Lett.* 145, 216–224. doi: 10.1016/j.patrec.2021.02.013
- Aprile, I., Germanotta, M., Cruciani, A., Loreti, S., Pecchioli, C., Cecchi, F., et al. (2020). Upper limb robotic rehabilitation after stroke: a multicenter, randomized clinical trial. *J. Neurol. Phys. Ther.* 44, 3–14. doi: 10.1097/NPT.0000000000000295
- Azmi, M. M., and Sulaiman, M. N. (2017). Accelerator-based human activity recognition using voting technique with nbtree and mlp classifiers. *Int. J. Adv. Sci. Eng. Inf. Technol.* 7, 146–152. doi: 10.18517/ijaseit.7.1.1790
- Barbič, J., Safonova, A., Pan, J.-Y., Faloutsos, C., Hodgins, J. K., and Pollard, N. S. (2004). "Segmenting motion capture data into distinct behaviors," in *Proceedings of Graphics Interface* (Citeseer) 185–194.
- Bayona, N. A., Bitensky, J., Salter, K., and Teasell, R. (2005). The role of task-specific training in rehabilitation therapies. *Topics Stroke Rehabil.* 12, 58–65. doi: 10.1310/BQM5-6YGB-MVJ5-WVCR
- Beaudoin, P., Coros, S., Van de Panne, M., and Poulin, P. (2008). "Motion-motif graphs" in *Proceedings of the 2008 ACM SIGGRAPH/Eurographics Symposium on Computer Animation* 117–126.
- Bishop, C. M., and Nasrabadi, N. M. (2006). *Pattern Recognition and Machine Learning*, vol 4. New York: Springer.
- Bütefisch, C., Hummelsheim, H., Denzler, P., and Mauritz, K.-H. (1995). Repetitive training of isolated movements improves the outcome of motor rehabilitation of the centrally paretic hand. *J. Neurol. Sci.* 130, 59–68. doi: 10.1016/0022-510X(95)00003-K
- Cai, S., Li, G., Zhang, X., Huang, S., Zheng, H., Ma, K., et al. (2019). Detecting compensatory movements of stroke survivors using pressure distribution data and machine learning algorithms. *J. Neuroeng. Rehabil.* 16, 1–11. doi: 10.1186/s12984-019-0609-6
- Cawley, G. C., and Talbot, N. L. (2003). Efficient leave-one-out cross-validation of kernel fisher discriminant classifiers. *Patt. Recogn.* 36, 2585–2592. doi: 10.1016/S0031-3203(03)00136-5
- Chamroukhi, F., Mohammed, S., Trabelsi, D., Oukhellou, L., and Amirat, Y. (2013). Joint segmentation of multivariate time series with hidden process regression for human activity recognition. *Neurocomputing* 120, 633–644. doi: 10.1016/j.neucom.2013.04.003
- Cirstea, M., and Levin, M. (2007). Improvement of arm movement patterns and endpoint control depends on type of feedback during practice in stroke survivors. *Neurorehabil. Neur. Rep.* 21, 398–411. doi: 10.1177/1545968306298414
- Cirstea, M., and Levin, M. F. (2000). Compensatory strategies for reaching in stroke. *Brain* 123, 940–953. doi: 10.1093/brain/123.5.940
- de Los Reyes-Guzmán, A., Dimbwadyo-Terrer, I., Pérez-Nombela, S., Monasterio-Huelin, F., Torricelli, D., Pons, J. L., et al. (2017). Novel kinematic indices for quantifying upper limb ability and dexterity after cervical spinal cord injury. *Med. Biol. Eng. Comput.* 55, 833–844. doi: 10.1007/s11517-016-1555-0

Conflict of interest

The authors declare that the research was conducted in the absence of any commercial or financial relationships that could be construed as a potential conflict of interest.

Publisher's note

All claims expressed in this article are solely those of the authors and do not necessarily represent those of their affiliated organizations, or those of the publisher, the editors and the reviewers. Any product that may be evaluated in this article, or claim that may be made by its manufacturer, is not guaranteed or endorsed by the publisher.

- Delp, S. L., Anderson, F. C., Arnold, A. S., Loan, P., Habib, A., John, C. T., et al. (2007). Opensim: open-source software to create and analyze dynamic simulations of movement. *IEEE Trans. Biomed. Eng.* 54, 1940–1950. doi: 10.1109/TBME.2007.901024
- Dickstein, R., Heffes, Y., Laufer, Y., Abulaffio, N., and Shabtai, E. L. (1997). Repetitive practice of a single joint movement for enhancing elbow function in hemiparetic patients. *Percept. Motor Skills* 85, 771–785. doi: 10.2466/pms.1997.85.3.771
- Dolatabadi, E., Zhi, Y. X., Ye, B., Coahran, M., Lupinacci, G., Mihailidis, A., et al. (2017). "The toronto rehab stroke pose dataset to detect compensation during stroke rehabilitation therapy," in *Proceedings of the 11th EAI International Conference on Pervasive Computing Technologies for Healthcare* 375–381. doi: 10.1145/3154862.3154925
- Fod, A., Matarić, M. J., and Jenkins, O. C. (2002). Automated derivation of primitives for movement classification. *Auton. Rob.* 12, 39–54. doi: 10.1023/A:1013254724861
- Franceschini, M., La Porta, F., Agosti, M., Massucci, M., et al. (2010). Is health-related-quality of life of stroke patients influenced by neurological impairments at one year after stroke? *Eur. J. Phys. Rehabil. Med.* 46, 389–399.
- Fruchter, D., Polak, R. F., Berman, S., and Levy-Tzedek, S. (2022). Automating provision of feedback to stroke patients with and without information on compensatory movements: A pilot study. *Front. Human Neurosci.* 16, 918804. doi: 10.3389/fnhum.2022.918804
- Gates, D. H., Walters, L. S., Cowley, J., Wilken, J. M., and Resnik, L. (2016). Range of motion requirements for upper-limb activities of daily living. *Am. J. Occup. Ther.* 70, 7001350010p1–7001350010p10. doi: 10.5014/ajot.2016.015487
- Gauthier, J.-P., Berret, B., and Jean, F. (2010). A biomechanical inactivation principle. *Proc. Steklov Inst. Math.* 268, 93–116. doi: 10.1134/S0081543810010098
- Guo, C., Pleiss, G., Sun, Y., and Weinberger, K. Q. (2017). "On calibration of modern neural networks," in *International Conference on Machine Learning* (PMLR) 1321–1330.
- Hadsell, R., Rao, D., Rusu, A. A., and Pascanu, R. (2020). Embracing change: Continual learning in deep neural networks. *Trends Cogn. Sci.* 24, 1028–1040. doi: 10.1016/j.tics.2020.09.004
- Hickey, B. W., Milosavljevic, S., Bell, M. L., and Milburn, P. D. (2007). Accuracy and reliability of observational motion analysis in identifying shoulder symptoms. *Manual Ther.* 12, 263–270. doi: 10.1016/j.math.2006.05.005
- Holzbaur, K. R., Murray, W. M., and Delp, S. L. (2005). A model of the upper extremity for simulating musculoskeletal surgery and analyzing neuromuscular control. *Ann. Biomed. Eng.* 33, 829–840. doi: 10.1007/s10439-005-3320-7
- Huang, H. J., Kram, R., and Ahmed, A. A. (2012). Reduction of metabolic cost during motor learning of arm reaching dynamics. *J. Neurosci.* 32, 2182–2190. doi: 10.1523/JNEUROSCI.4003-11.2012
- Kashi, S., Polak, R. F., Lerner, B., Rokach, L., and Levy-Tzedek, S. (2020). A machine-learning model for automatic detection of movement compensations in stroke patients. *IEEE Trans. Emerg. Topics Comput.* 9, 1234–1247. doi: 10.1109/TETC.2020.2988945
- Khoramdel, J., Moori, A., Moghaddam, M., and Najafi, E. (2021). "Compensatory movement detection in upper limb rehabilitation with deep learning methods," in *2021 9th RSI International Conference on Robotics and Mechatronics (ICRoM)* (IEEE) 465–471. doi: 10.1109/ICRoM54204.2021.9663458

- Kulić, D., Ott, C., Lee, D., Ishikawa, J., and Nakamura, Y. (2012). Incremental learning of full body motion primitives and their sequencing through human motion observation. *Int. J. Robot. Res.* 31, 330–345. doi: 10.1177/0278364911426178
- Kwakkel, G., Kollen, B. J., van der Grond, J., and Prevo, A. J. (2003). Probability of regaining dexterity in the flaccid upper limb: impact of severity of paresis and time since onset in acute stroke. *Stroke* 34, 2181–2186. doi: 10.1161/01.STR.0000087172.16305.CD
- Laffont, I., Froger, J., Jourdan, C., Bakhti, K., van Dokkum, L. E., Gouaich, A., et al. (2020). Rehabilitation of the upper arm early after stroke: video games versus conventional rehabilitation: a randomized controlled trial. *Ann. Phys. Rehabil. Med.* 63, 173–180. doi: 10.1016/j.rehab.2019.10.009
- Laver, K. E., Lange, B., George, S., Deutsch, J. E., Saposnik, G., and Crotty, M. (2017). Virtual reality for stroke rehabilitation. *Cochrane Database Syst. Rev.* 11, CD008349. doi: 10.1002/14651858.CD008349.pub4
- Levin, M. F., Liebermann, D. G., Parmet, Y., and Berman, S. (2016). Compensatory versus noncompensatory shoulder movements used for reaching in stroke. *Neurorehabil. Neur. Rep.* 30, 635–646. doi: 10.1177/1545968315613863
- Lin, G., Wu, W., Lin, C., Song, Y., Cai, S., and Xie, L. (2021). “A vision-based compensation detection approach during robotic stroke rehabilitation therapy,” in *2021 3rd International Academic Exchange Conference on Science and Technology Innovation (IAECST)* 768–771. doi: 10.1109/IAECST54258.2021.9695873
- Ma, K., Chen, Y., Zhang, X., Zheng, H., Yu, S., Cai, S., et al. (2019). semg-based trunk compensation detection in rehabilitation training. *Front. Neurosci.* 13, 1250. doi: 10.3389/fnins.2019.01250
- McGregor, A. H., McCarthy, I. D., and Hughes, S. P. (1995). Motion characteristics of the lumbar spine in the normal population. *Spine* 20, 2421–2428. doi: 10.1097/00007632-199511001-00009
- Morris, J. H., Van Wijck, F., Joice, S., and Donaghy, M. (2013). Predicting health related quality of life 6 months after stroke: the role of anxiety and upper limb dysfunction. *Disab. Rehabil.* 35, 291–299. doi: 10.3109/09638288.2012.691942
- Mortazavi, F., and Nadian-Ghomsheh, A. (2019). Continues online exercise monitoring and assessment system with visual guidance feedback for stroke rehabilitation. *Multim. Tools Applic.* 78, 32055–32085. doi: 10.1007/s11042-019-08020-2
- Mukhoti, J., Kulharia, V., Sanyal, A., Golodetz, S., Torr, P., and Dokania, P. (2020). Calibrating deep neural networks using focal loss. *Adv. Neural Inf. Proces. Syst.* 33, 15288–15299. doi: 10.5555/3495724.3497006
- Murray, C. J., Vos, T., Lozano, R., Naghavi, M., Flaxman, A. D., Michaud, C., et al. (2012). Disability-adjusted life years (dalys) for 291 diseases and injuries in 21 regions, 1990–2010: a systematic analysis for the global burden of disease study 2010. *Lancet* 380, 2197–2223. doi: 10.1016/S0140-6736(12)61689-4
- Pollock, A. S., Legg, L., Langhorne, P., and Sellars, C. (2000). Barriers to achieving evidence-based stroke rehabilitation. *Clin. Rehabil.* 14, 611–617. doi: 10.1191/0269215500cr369oa
- Rensink, M., Schuurmans, M., Lindeman, E., and Hafsteinsdottir, T. (2009). Task-oriented training in rehabilitation after stroke: systematic review. *J. Adv. Nurs.* 65, 737–754. doi: 10.1111/j.1365-2648.2008.04925.x
- Rustam, F., Reshi, A. A., Ashraf, I., Mehmood, A., Ullah, S., Khan, D. M., et al. (2020). Sensor-based human activity recognition using deep stacked multilayered perceptron model. *IEEE Access* 8, 218898–218910. doi: 10.1109/ACCESS.2020.3041822
- Savitzky, A., and Golay, M. J. (1964). Smoothing and differentiation of data by simplified least squares procedures. *Analyt. Chem.* 36, 1627–1639. doi: 10.1021/ac60214a047
- Sellmann, A., Wagner, D., Holtz, L., Eschweiler, J., Diers, C., Williams, S., et al. (2022). Detection of typical compensatory movements during autonomously performed exercises preventing low back pain (lbp). *Sensors* 22, 111. doi: 10.3390/s22010111
- Senior, D. (2004). *Qualisys track manager*. User manual.
- Shaheen, F., Verma, B., and Asafuddoula, M. (2016). “Impact of automatic feature extraction in deep learning architecture,” in *2016 International Conference on Digital Image Computing: Techniques and Applications (DICTA)* 1–8. doi: 10.1109/DICTA.2016.7797053
- Singh, D., and Singh, B. (2020). Investigating the impact of data normalization on classification performance. *Appl. Soft Comput.* 97, 105524. doi: 10.1016/j.asoc.2019.105524
- Taati, B., Wang, R., Huq, R., Snoek, J., and Mihailidis, A. (2012). “Vision-based posture assessment to detect and categorize compensation during robotic rehabilitation therapy,” in *2012 4th IEEE RAS EMBS International Conference on Biomedical Robotics and Biomechanics (BioRob)* (IEEE) 1607–1613. doi: 10.1109/BioRob.2012.6290668
- Takebayashi, T., Takahashi, K., Okita, Y., Kubo, H., Hachisuka, K., and Domen, K. (2022). Impact of the robotic-assistance level on upper extremity function in stroke patients receiving adjunct robotic rehabilitation: sub-analysis of a randomized clinical trial. *J. NeuroEng. Rehabil.* 19, 1–10. doi: 10.1186/s12984-022-00986-9
- Takeuchi, N., and Izumi, S.-I. (2012). Maladaptive plasticity for motor recovery after stroke: mechanisms and approaches. *Neural Plast.* 2012, 359728. doi: 10.1155/2012/359728
- Thielman, G. T., Dean, C. M., and Gentile, A. (2004). Rehabilitation of reaching after stroke: task-related training versus progressive resistive exercise. *Arch. Phys. Med. Rehabil.* 85, 1613–1618. doi: 10.1016/j.apmr.2004.01.028
- Turton, A., and Fraser, C. (1990). The use of home therapy programmes for improving recovery of the upper limb following stroke. *Br. J. Occup. Ther.* 53, 457–462. doi: 10.1177/030802269005301104
- Uy, S. R. U., and Abu, P. A. (2020). “Analysis of detecting compensation for robotic stroke rehabilitation therapy using imbalanced learning and outlier detection,” in *2020 International Conference on Artificial Intelligence in Information and Communication (ICAIIIC)* (IEEE) 432–437.
- Vrigkas, M., Nikou, C., and Kakadiaris, I. A. (2015). A review of human activity recognition methods. *Front. Robot. AI* 2, 28. doi: 10.3389/frobt.2015.00028
- Wada, Y., Kaneko, Y., Nakano, E., Osu, R., and Kawato, M. (2001). Quantitative examinations for multi joint arm trajectory planning—using a robust calculation algorithm of the minimum commanded torque change trajectory. *Neural Netw.* 14, 381–393. doi: 10.1016/S0893-6080(01)00026-0
- Wan, S., Qi, L., Xu, X., Tong, C., and Gu, Z. (2020). Deep learning models for real-time human activity recognition with smartphones. *Mobile Netw. Applic.* 25, 743–755. doi: 10.1007/s11036-019-01445-x
- Wong, J. D., Cluff, T., and Kuo, A. D. (2021). The energetic basis for smooth human arm movements. *Elife* 10, e68013. doi: 10.7554/eLife.68013.sa2
- Yao, T., Gao, F., Zhang, Q., and Ma, Y. (2021). Multi-feature gait recognition with dnn based on semg signals. *Math. Biosci. Eng.* 18, 3521–3542. doi: 10.3934/mbe.2021177
- Yu, X., Xiao, B., Tian, Y., Wu, Z., Liu, Q., Wang, J., et al. (2021). A control and posture recognition strategy for upper-limb rehabilitation of stroke patients. *Wirel. Commun. Mobile Comput.* 2021, 1–12. doi: 10.1155/2021/6630492
- Zhi, Y. X., Lukasik, M., Li, M. H., Dolatabadi, E., Wang, R. H., and Taati, B. (2017). Automatic detection of compensation during robotic stroke rehabilitation therapy. *IEEE J. Transl. Eng. Health Med.* 6, 1–7. doi: 10.1109/JTEHM.2017.2780836
- Zhou, L., Bai, S., and Li, Y. (2017). Energy optimal trajectories in human arm motion aiming for assistive robots. *Model. Identific. Control* 38, 11–19. doi: 10.4173/mic.2017.1.2
- Zhou, T., Fu, H., Gong, C., Shao, L., Porikli, F., Ling, H., et al. (2022). Consistency and diversity induced human motion segmentation. *IEEE Trans. Patt. Anal. Mach. Intell.* 45, 197–210. doi: 10.1109/TPAMI.2022.3147841



OPEN ACCESS

EDITED BY

Kosta Jovanovic,
University of Belgrade, Serbia

REVIEWED BY

Scott A. Beardsley,
Marquette University, United States
Francesco Scotto di Luzio,
Campus Bio-Medico University, Italy

*CORRESPONDENCE

Samuel Tesfazgi
✉ samuel.tesfazgi@tum.de

RECEIVED 16 February 2023

ACCEPTED 17 July 2023

PUBLISHED 24 August 2023

CITATION

Tesfazgi S, Sangouard R, Endo S and Hirche S
(2023) Uncertainty-aware automated
assessment of the arm impedance with
upper-limb exoskeletons.
Front. Neurobot. 17:1167604.
doi: 10.3389/fnbot.2023.1167604

COPYRIGHT

© 2023 Tesfazgi, Sangouard, Endo and Hirche.
This is an open-access article distributed under
the terms of the [Creative Commons Attribution
License \(CC BY\)](#). The use, distribution or
reproduction in other forums is permitted,
provided the original author(s) and the
copyright owner(s) are credited and that the
original publication in this journal is cited, in
accordance with accepted academic practice.
No use, distribution or reproduction is
permitted which does not comply with these
terms.

Uncertainty-aware automated assessment of the arm impedance with upper-limb exoskeletons

Samuel Tesfazgi*, Ronan Sangouard, Satoshi Endo and
Sandra Hirche

Chair of Information-oriented Control (ITR), TUM School of Computation, Information and Technology,
Technical University of Munich, Munich, Germany

Providing high degree of personalization to a specific need of each patient is invaluable to improve the utility of robot-driven neurorehabilitation. For the desired customization of treatment strategies, precise and reliable estimation of the patient's state becomes important, as it can be used to continuously monitor the patient during training and to document the rehabilitation progress. Wearable robotics have emerged as a valuable tool for this quantitative assessment as the actuation and sensing are performed on the joint level. However, upper-limb exoskeletons introduce various sources of uncertainty, which primarily result from the complex interaction dynamics at the physical interface between the patient and the robotic device. These sources of uncertainty must be considered to ensure the correctness of estimation results when performing the clinical assessment of the patient state. In this work, we analyze these sources of uncertainty and quantify their influence on the estimation of the human arm impedance. We argue that this mitigates the risk of relying on overconfident estimates and promotes more precise computational approaches in robot-based neurorehabilitation.

KEYWORDS

reliable automated assessment, sensitivity analysis, human-exoskeleton interaction, uncertainty quantification, neuromechanical state estimation, uncertainty-aware simulation

1. Introduction

Medical robotics have advanced greatly with application in many domains, such as robot-assisted surgery (D'Ettorre et al., 2021), service robots in healthcare (Holland et al., 2021) or rehabilitation robotics (Laut et al., 2016). Particularly in the field of physical rehabilitation, an ever-increasing demand for automation technology is observed. Stroke, for instance, is the second leading cause of death worldwide (Feigin et al., 2014) with an increasing trend due to rising life expectancy in many parts of the world (Boehme et al., 2017; Donkor, 2018). However, while stroke is a highly relevant cause for motor impairment, many other neurological disorders, such as cerebral palsy, multiple sclerosis or Parkinsons disease, require similar treatment strategies during rehabilitation to improve or retain motor functions (Krebs et al., 2008). In particular, high-intensity (Ringleb et al., 2008) and repetition training (Kwakkel et al., 1999) have been shown to produce promising recovery results. Due to these requirements, effective rehabilitation is time- and labor-intensive, therefore, both patients and healthcare professionals can benefit greatly from robot-assisted rehabilitation strategies.

In recent years exoskeletons, also referred to as wearable robotic devices (Lo and Xie, 2012), have emerged as a powerful tool for rehabilitation. Since they are designed in a manner that the kinematic chain aligns with the user, sensing and actuation can be performed at the joint level here. One of the main benefits of rehabilitation robotics lies in their application during robot-aided patient assessment. Here, robotic devices are used to monitor patients before, after, or during training, thereby tracking the recovery progress and informing the treatment strategy. In the case of neurological disorders, there are multiple functional impairments, e.g., arm hemiparesis, limited hand dexterity or over-rigid joints, that inhibit motor functions of affected individuals (Carvalho-Pinto and Faria, 2016). Thus, the quantitative estimation of the dynamic parameters underlying these effects using wearable robotic devices can greatly benefit neurorehabilitation. Particularly relevant in the case of stroke is spasticity, a motor disorder described by hyperactivity in tonic stretch reflexes (McLellan, 1981) which leads muscles to be overly resistive to elongations and thus reduced mobility of the affected limb (Sommerfeld et al., 2004). In current clinical practice, spasticity assessment scales, such as the Modified Ashworth Scale (MAS) are used to evaluate the muscle tone of patients. Here, the clinician induces a passive motion by manually perturbing the target joint of the patient. Concurrently, the muscle tone is assessed by tactually observing the movement resistance. Even though this method has been proven to be useful in clinical practice (Gregson et al., 1999), there are shortcomings that could be alleviated through robotic assessment. Specifically, the coarse and discrete nature of the scales limit the level of precision. Additionally, the evaluation is subjective at its core, which can lead to possibly unreliable and biased estimates that are not consistently reproducible (Blackburn et al., 2002; Raghavan, 2015).

Hence, the deployment of robot-aided assessment is expected to improve the objectivity and repeatability of clinical evaluations (Lamercy et al., 2012). In particular, joint impedance is commonly used as a concise measure for the patient state (Maggioni et al., 2016), since it describes the relationship between joint motion and opposing torque, which is often abnormally increased (Chung et al., 2004). In recent years, a multitude of these assessment approaches based on exoskeletons for upper-limb rehabilitation have emerged. In Ren et al. (2013), an upper-limb exoskeleton quantitatively estimates the joint stiffness of the shoulder, elbow and wrist joints. More recently, a decomposition of the coupled human arm dynamics is proposed to allow the estimation of local and inter-joint stiffness effects following stroke (Zhang et al., 2017). A more extensive impedance estimation is conducted in Wang et al. (2021), where an exoskeleton is used to identify the inertia, viscosity and stiffness components of the elbow joint of patients' with spastic arms using genetic algorithms. Despite the fact that the benefits of robot-aided assessment in comparison to human-administered clinical scales have been demonstrated in studies (Bosecker et al., 2010), exoskeleton applications suffer from the introduction of unintended interaction forces to the user (Jarrassé et al., 2010) with adverse effects on the clinical evaluation. These interaction forces cannot be avoided completely due to uncertainties in the complex physical human-exoskeleton interaction. In particular, sources of uncertainty are known to arise due to kinematic

incompatibilities, soft coupling and inaccuracies in the human dynamics model (Pons, 2008). So far, the influence of these sources of uncertainty on the arm impedance estimation has not been analyzed sufficiently, and a quantitative ranking of their impact is missing. However, since the assessment is used to guide the therapy of patients, it is paramount to make these uncertainties explicit in order to increase precision and ensure that clinicians are not misinformed by overconfident assessment results. Therefore, it is important to investigate how uncertain the obtained impedance parameter estimates are and how to effectively reduce uncertainty for exoskeleton-based automated assessment.

1.1. Related work

The influence of uncertainties on the robot-aided impedance estimation can be quantified by mean of a sensitivity analysis. These methods investigate how uncertainty in the output of a system, e.g., the result of the automated assessment, is influenced by variations in the input of a system (Pianosi et al., 2016), e.g., sources of uncertainty in the complex human-exoskeleton interaction. Thus, by analyzing these sensitivities and ascribing quantitative measures of importance to each source of uncertainty, the robustness of the automated assessment can be quantified (Thabane et al., 2013). Previously, it has been shown how sensitivity analysis methods are used to support efforts in uncertainty reduction (Hamm et al., 2006) and facilitate robust decision making under uncertainty (Nguyen and de Kok, 2007; Singh et al., 2014).

In general, sensitivity analysis can be approached in multiple ways, with three principle classes identified in Christopher Frey and Patil (2002): analytical, statistical and graphical methods. Typically, analytical methods, such as Kohberger et al. (1978) and Ma et al. (2021), require access to a differential equation model of the system and perform analysis by monitoring the partial derivative over the uncertain parameters (Abraham et al., 2007). In Schiele (2008), an analytical 1 DoF model of the interaction forces induced by kinematic incompatibilities on the elbow joint is proposed. While the presented model was validated experimentally, remaining sources of uncertainty are not considered and it limits the utility of the model as interaction effects cannot be captured by it. Due to the complexity of the human-exoskeleton interaction dynamics, a closed-form description that captures all sources of uncertainty concurrently is not available, which makes analytical sensitivity analysis methods impractical. On the other hand, statistical and graphical approaches solely require access to input-output samples of the system (Christopher Frey and Patil, 2002). Here, samples are generated by evaluating the examined system for a factorial combination of all sources of uncertainty to obtain pertinent statistical information and gain rigorous insights, which is infeasible to do experimentally. Thus, simulations are often used instead (Iooss and Saltelli, 2017). However, to the best of the authors' knowledge, no human-exoskeleton simulation environment considers all of the key sources of uncertainty present during the complex, physical interaction. In Agarwal et al. (2010), for instance, the authors analyzed challenges due to kinematic misalignments on the elbow joint to inform the simulation-based design of an arm exoskeleton. On the other hand, the effect of the human musculoskeletal model on lower-limb exoskeleton control

during gait is investigated in Khamar et al. (2019). Lastly, Kühn et al. (2018) present an upper-limb simulation of the human, exoskeleton and their respective coupling where simplified 6 DoF springs are used to model soft-contacts. However, in order to fully understand the effect of uncertainty in exoskeleton-based impedance assessment, all sources of uncertainty and their interaction effects must be considered. Thus, a simulation platform which can systematically express the uncertain human-exoskeleton interaction is required in order to quantify the impact of sources of uncertainty on the estimated impedance parameter.

1.2. Contribution

In this work, we perform a sensitivity analysis that quantitatively investigates the influence of various sources of uncertainty on the exoskeleton-based arm impedance estimation. Through this process, a more precise understanding of the uncertainty composition and their prioritization is achieved, which facilitates effective measures to increase the performance of exoskeleton-based automated assessment and reduces the risk of relying on overconfident results. We propose a two-phase approach, where initially the negligible sources of uncertainty are identified, and then a ranking of the most influential factors is performed in the second phase. Due to the complexity of the human-exoskeleton interaction dynamics, we adopt a sampling-based sensitivity analysis which allows us to quantify the influence of each source of uncertainty independently as well as the interaction effects among them. In order to generate the samples required for the analysis, we develop a high-fidelity simulation environment of the human-exoskeleton system that includes the key sources of uncertainty, which are informed by the physical understanding of the system and identified in the literature.

2. Materials and methods

In this section, the technical problem is formulated and the relevant material and methods are shown. An overview of the proposed uncertainty quantification procedure is shown in Figure 1. From top to bottom the colored blocks illustrate the *phase selection*, the process of obtaining *input parameter samples*, the process of obtaining *output samples* and the evaluation procedure using quantitative *sensitivity analysis* methods. First, during the *phase selection* the sampling strategy is determined, which is chosen in accordance to the objective of the respective sensitivity analysis method. Following this, the *input parameter samples* are generated. Here, the examined sources of uncertainty are sampled depending on the previously selected sampling strategy. Then, the input parameter samples are retrieved in the form of parameterized human-exoskeleton simulation instances, where the varied parameters are associated with different sources of uncertainty. Subsequently, the *output sample* block is applied. Here, the exoskeleton-based automated assessment is run for the sampled simulation parameterizations to obtain impedance parameter estimates for the human arm. Finally, the *sensitivity analysis* is performed. Depending on the sampling strategy chosen beforehand, different sensitivity analysis methods are deployed on

the estimated impedance parameters to investigate the impact of the modeling uncertainties with respect to the observed estimation error. By deploying this sensitivity analysis scheme we are able to derive the most influential sources of uncertainty that influence the exoskeleton-based arm impedance estimation.

The remainder of the section is structured as follows: in Section 2.1, the dynamics governing the human-exoskeleton system are introduced and a qualitative account on uncertainties in the automated assessment is provided. Subsequently, a high-fidelity simulation of the human-exoskeleton interaction is presented in Section 2.2 with particular focus on including the key sources of uncertainty present in the system. In Section 2.3, the proposed assessment procedure is explained and technical details regarding the estimation process are provided. Finally, in Section 2.4, the deployed sampling strategies and sensitivity analysis methods are presented.

2.1. Uncertainty during human-exoskeleton interaction

In order to perform the sensitivity analysis in an interpretable manner it is necessary to have an understanding of the investigated system. To this end, we first formulate the nominal human-exoskeleton interaction model. Subsequently, uncertainties are introduced to the nominal model.

2.1.1. Nominal human-exoskeleton interaction model

The instrumented assessment using an upper-limb exoskeleton is considered in this work. Therefore, we start by establishing the dynamics governing motion of the human arm. We model the dynamics using Euler-Lagrange equations (Featherstone, 2007) of the form,

$$\mathbf{M}_h(\mathbf{q})\ddot{\mathbf{q}} + \mathbf{C}_h(\mathbf{q}, \dot{\mathbf{q}})\dot{\mathbf{q}} + \mathbf{g}_h(\mathbf{q}) = \boldsymbol{\tau}_{\text{hum}} + \boldsymbol{\tau}_{\text{int,h}}. \quad (1)$$

Here, $\mathbf{q} \in \mathbb{R}^d$ is the d -dimensional state vector containing the joint configuration of the human arm, with $\dot{\mathbf{q}} \in \mathbb{R}^d$ describing the angular velocities and $\ddot{\mathbf{q}} \in \mathbb{R}^d$ describing the angular accelerations. On the left side of (1) the matrix $\mathbf{M}_h: \mathbb{R}^d \rightarrow \mathbb{R}^{d \times d}$ denotes the human inertia matrix, $\mathbf{C}_h: \mathbb{R}^d \times \mathbb{R}^d \rightarrow \mathbb{R}^{d \times d}$ the human Coriolis matrix and $\mathbf{g}_h: \mathbb{R}^d \rightarrow \mathbb{R}^d$ the human gravitational component. In addition to the human generated joint torques $\boldsymbol{\tau}_{\text{hum}}$, an interaction torque $\boldsymbol{\tau}_{\text{int,h}}$ acts on the human arm, due to the contact with the robotic system. In (1), $\boldsymbol{\tau}_{\text{hum}}$ represents the projected joint-level torques induced through variations of muscle lengths, muscle activation and the resulting tensions (Shin et al., 2009). Therefore, $\boldsymbol{\tau}_{\text{hum}}$ describes the summed dynamics of internal origin and contains the relevant joint dynamics parameter necessary to quantify the patient's inner state. In the case of stroke, a viscoelastic model of the human-generated torque during passive mobilization tasks is proposed (McCrea et al., 2003). Thus, we can formulate the human-generated torque $\boldsymbol{\tau}_{\text{hum}}$ as

$$\boldsymbol{\tau}_{\text{hum}} = \mathbf{K}_h(\mathbf{q}, \dot{\mathbf{q}})\mathbf{q} + \mathbf{D}_h(\mathbf{q}, \dot{\mathbf{q}})\dot{\mathbf{q}}, \quad (2)$$

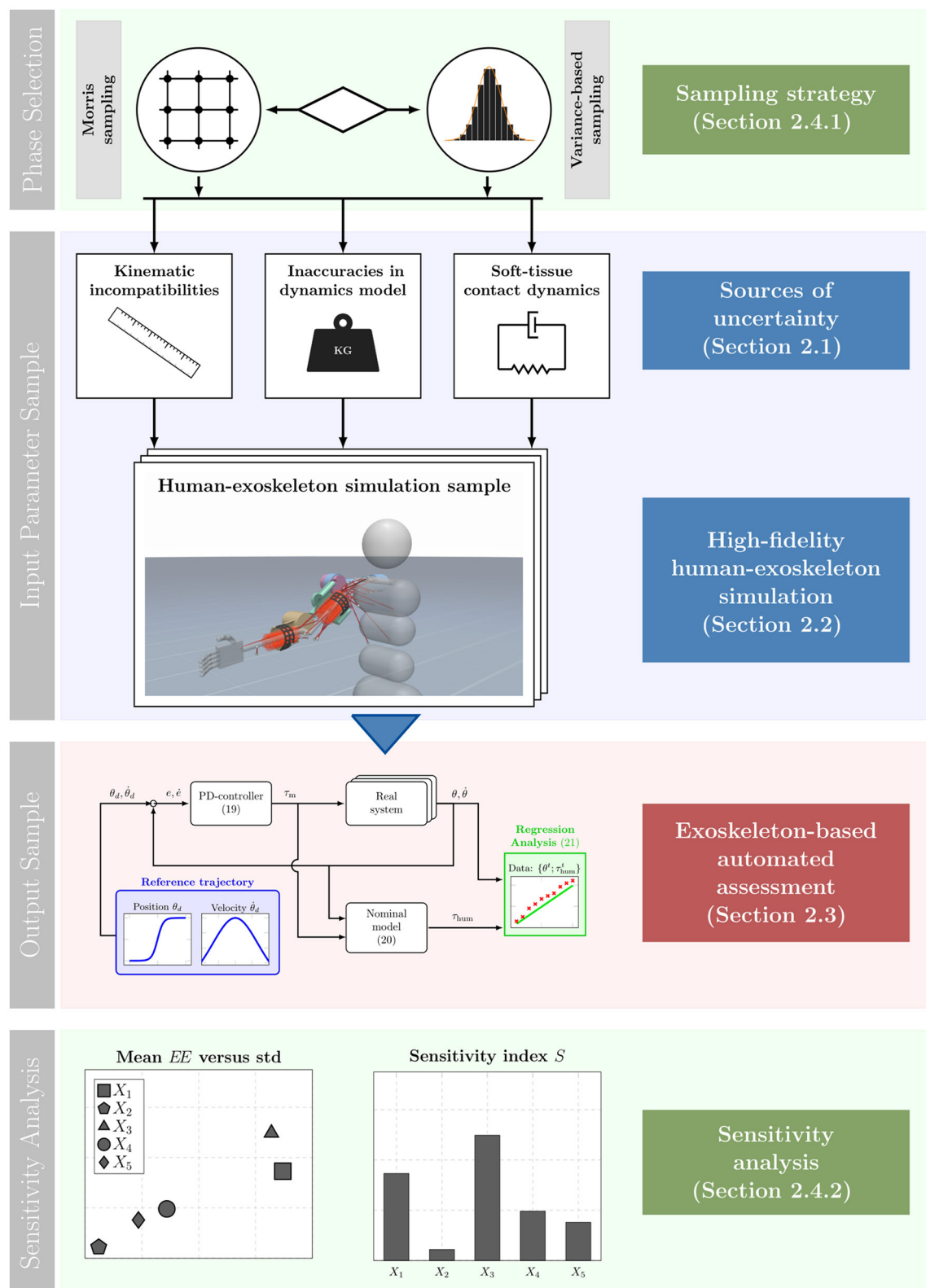


FIGURE 1

Depiction of the complete, proposed sensitivity analysis scheme. From top to bottom the blocks illustrate the different steps taken during the proposed scheme. First, during the *phase selection* the sampling strategy is determined. Subsequently, in the *input parameter sample* block input samples in the form of human-exoskeleton simulation instances are drawn. The *output sample* block illustrates the generation of output samples using the automated assessment process. Lastly, the input-output samples are used to obtain sensitivity measures which is visualized in the *sensitivity analysis*.

where $\mathbf{K}_h: \mathbb{R}^d \times \mathbb{R}^d \rightarrow \mathbb{R}^{d \times d}$ and $\mathbf{D}_h: \mathbb{R}^d \times \mathbb{R}^d \rightarrow \mathbb{R}^{d \times d}$ correspond to the joint stiffness and viscosity matrix, respectively. In [McCrea et al. \(2003\)](#) the validity of linear viscoelasticity parameters for the modeling of resistive torques in personas with chronic stroke is demonstrated. Therefore, it can additionally be assumed that the parameters are independent of the current configuration, which allows the application of standard regression methods. Thus, the instrumented assessment of the patient's state can be reformulated as a linear regression problem using the parametric model

$$\boldsymbol{\tau}_{\text{hum}} = \mathbf{K}_h \mathbf{q} + \mathbf{D}_h \dot{\mathbf{q}}. \quad (3)$$

In order to estimate the impedance parameters \mathbf{K}_h and \mathbf{D}_h , it is first necessary to extract the human generated torque $\boldsymbol{\tau}_{\text{hum}}$ in (1). This is not trivial in general, as the intrinsically generated human muscle torque cannot be measured directly. Hence, $\boldsymbol{\tau}_{\text{hum}}$ has to be inferred using the available measurements and dynamics knowledge. For wearable robots deployed in clinical applications, measurements regarding joint positions and motor torques are typically available (e.g., [Trigili et al., 2020](#)). Unless additional expensive and possibly inconvenient force-torque sensors are mounted at the physical interface between human and exoskeleton ([An and Hollerbach, 1987](#)), the interaction torque $\boldsymbol{\tau}_{\text{int,h}}$ is also unknown. To overcome this issue, knowledge regarding the dynamics model of the robotic system can be exploited to replace the unknown interaction torque $\boldsymbol{\tau}_{\text{int,h}}$. Similar to the human, the exoskeleton is described by its rigid body dynamics

$$\mathbf{M}_e(\boldsymbol{\theta})\ddot{\boldsymbol{\theta}} + \mathbf{C}_e(\boldsymbol{\theta}, \dot{\boldsymbol{\theta}})\dot{\boldsymbol{\theta}} + \mathbf{g}_e(\boldsymbol{\theta}) = \boldsymbol{\tau}_m - \boldsymbol{\tau}_{\text{int,e}}, \quad (4)$$

where $\mathbf{M}_e: \mathbb{R}^n \rightarrow \mathbb{R}^{n \times n}$ is the inertia, $\mathbf{C}_e: \mathbb{R}^n \times \mathbb{R}^n \rightarrow \mathbb{R}^{n \times n}$ the Coriolis matrix and $\mathbf{g}_e: \mathbb{R}^n \rightarrow \mathbb{R}^n$ the gravitational component of the exoskeleton dynamics. The joint positions, velocities and accelerations of the robotic system are given by $\boldsymbol{\theta} \in \mathbb{R}^n$, $\dot{\boldsymbol{\theta}} \in \mathbb{R}^n$ and $\ddot{\boldsymbol{\theta}} \in \mathbb{R}^n$ respectively. In the following, we assume that the kinematic chain of human and exoskeleton align, thereby, resulting in $n = d$. Furthermore, the movement of the joints is driven by the motor torques $\boldsymbol{\tau}_m$ and analogs to (1), an interaction torque $\boldsymbol{\tau}_{\text{int,e}}$ is exerted on the exoskeleton, which acts in the opposing direction in (4).

In the nominal model, three idealized assumptions are made: first, a perfect alignment of the human and exoskeleton kinematic chain is assumed. Second, no displacement of the attachments occurs during movement. Third, a completely rigid interface transmits forces between the human and exoskeleton. If these assumptions hold, both the human's and exoskeleton's joint kinematics match $\mathbf{q} = \boldsymbol{\theta}$ and the interaction torques can be written to

$$\boldsymbol{\tau}_{\text{int,h}} = \boldsymbol{\tau}_{\text{int,e}}. \quad (5)$$

For the sake of the derivation of the nominal model we hypothesize the dynamics of the robotic system and human to be known. Then, it is possible to derive the human generated torque $\boldsymbol{\tau}_{\text{hum}}$ from (1), (4), and (5):

$$\begin{aligned} \boldsymbol{\tau}_{\text{hum}} = & \mathbf{M}_h(\boldsymbol{\theta})\ddot{\boldsymbol{\theta}} + \mathbf{C}_h(\boldsymbol{\theta}, \dot{\boldsymbol{\theta}})\dot{\boldsymbol{\theta}} + \mathbf{g}_h(\boldsymbol{\theta}) \\ & + \underbrace{\mathbf{M}_e(\boldsymbol{\theta})\ddot{\boldsymbol{\theta}} + \mathbf{C}_e(\boldsymbol{\theta}, \dot{\boldsymbol{\theta}})\dot{\boldsymbol{\theta}} + \mathbf{g}_e(\boldsymbol{\theta}) - \boldsymbol{\tau}_m}_{\boldsymbol{\tau}_{\text{int,h}}} \end{aligned} \quad (6)$$

Since the motor torque $\boldsymbol{\tau}_m$ and exoskeleton kinematics $\{\boldsymbol{\theta}, \dot{\boldsymbol{\theta}}, \ddot{\boldsymbol{\theta}}\}$ are measurable and the dynamics are assumed to be known, the human torque $\boldsymbol{\tau}_{\text{hum}}$, as given in (6), is directly computable. Therefore, all the necessary input and output information are available to estimate the human joint viscoelasticity parameters \mathbf{K}_h and \mathbf{D}_h via linear regression using the parametric model (3):

$$\mathbf{y} = \mathbf{X}\boldsymbol{\omega}, \quad (7)$$

where the labels \mathbf{y} follows from the human torque computation according to (6), the input matrix \mathbf{X} contains the human joint measurements under the assumption that $\mathbf{q} = \boldsymbol{\theta}$ and the viscoelasticity parameters of interest are described by $\boldsymbol{\omega}$. Thereby, performing the regression analysis for each joint yields

$$\underbrace{\begin{bmatrix} \tau_{\text{hum},i}^1 \\ \tau_{\text{hum},i}^2 \\ \vdots \\ \tau_{\text{hum},i}^T \end{bmatrix}}_{\mathbf{y}} = \underbrace{\begin{bmatrix} q_i^1 & \dot{q}_i^1 \\ q_i^2 & \dot{q}_i^2 \\ \vdots & \vdots \\ q_i^T & \dot{q}_i^T \end{bmatrix}}_{\mathbf{X}} \underbrace{\begin{bmatrix} k_{h,ii} \\ d_{h,ii} \end{bmatrix}}_{\boldsymbol{\omega}}, \quad (8)$$

with $\{\tau_{\text{hum},i}^t\}_{t=1}^T$ denoting the computed human torques and $\{q_i^t, \dot{q}_i^t\}_{t=1}^T$ representing the kinematics measurements of the i -th joint at discrete time step t over the duration T of the assessment. Here, k_{ii} and d_{ii} are the i -th main diagonal entries of the joint stiffness and viscosity matrices, respectively. The parameter vector $\boldsymbol{\omega}$ can be computed directly given access to inputs \mathbf{X} and labels \mathbf{y} as such:

$$\boldsymbol{\omega} = (\mathbf{X}^T \mathbf{X})^{-1} \mathbf{X}^T \mathbf{y}. \quad (9)$$

However, while the approach is mathematically convenient and can straight forwardly be implemented, it can result in large estimation errors, because it does not account for the uncertainties in the human-exoskeleton interaction dynamics.

2.1.2. Sources of uncertainty

There are multiple factors that introduce uncertainties to the above described nominal model, which stem from variations in the biomechanics of individuals. In particular three key sources of uncertainty that adversely affect the physical interaction are identified in the literature ([Pons, 2008](#)): kinematic incompatibilities, soft contact dynamics and inaccuracies in the nominal dynamics model. In the following these sources of uncertainty and their impact on the nominal dynamics are presented in more detail.

2.1.2.1. Kinematic incompatibilities

First, we consider kinematic incompatibilities between the exoskeleton and human, which are particularly prevalent in wearable robots with kinematic chains mirroring the human kinematics. These kinematic incompatibilities arise due to anatomical variations between users and variations within a user that occur during motion. Therefore, achieving a perfect alignment is infeasible ([Jarrassé and Morel, 2012](#)). Depending on the extent of the mismatch, it is considered a macro-misalignment or a micro-misalignment. Here, macro-misalignments are typically induced by offsets in the center of rotation (CoR) between the human and

exoskeleton joints. These CoR offsets are the result of a multiple factors, such as an imprecise donning procedure or translations that occur in the instantaneous center of rotation of human joints for certain movements (Grant, 1973). In Figure 2A, the macro-misalignment due to CoR offsets is shown conceptually for a simplified two-link human-exoskeleton-system moving in the vertical plane. The top and bottom links represent the upper arm and forearm, respectively, emulating motion in flexion/extension direction. Here, the CoR offsets are visualized by x_{off} and y_{off} using red arrows. While macro-misalignment can be reduced by performing careful donning and including redundant DoFs in the robotic kinematic chain, micro-misalignments still occur despite these mitigation strategies. This is for instance because the human kinematic chain is not comprised of idealized, circular joints. Therefore, misalignments cannot be removed completely in practice and must be explicitly considered for a robust automated assessment.

The main consequence of these kinematic incompatibilities is induced displacements of the attachments between the exoskeleton and human limb during joint motion. Consequently, these displacements result in forces at the physical interface. The resulting impact on the nominal dynamics of the human-exoskeleton interaction can be observed at multiple points. First, the previously assumed joint alignment does not hold anymore, leading to a discrepancy in the joint angles, i.e., $\mathbf{q} \neq \boldsymbol{\theta}$ in general. Moreover, an offset and joint angle dependent displacement of the attachments along the axial direction occurs, which leads to a change in the interaction torque transmission (5):

$$\tilde{\boldsymbol{\tau}}_{\text{int,h}} = \mathbf{B}(\mathbf{x}_{\text{off}}, \mathbf{y}_{\text{off}}, \mathbf{q}, \boldsymbol{\theta}) \boldsymbol{\tau}_{\text{int,e}}, \quad (10)$$

where $\mathbf{B}: \mathbb{R}^{d \times d}$ is a d -dimensional diagonal matrix with the main diagonal entries describing the displaced attachment points. In (10), $\tilde{\boldsymbol{\tau}}_{\text{int,h}}$ represents the uncertain interaction torques which now depends on the CoR offsets denoted by \mathbf{x}_{off} and \mathbf{y}_{off} . Similarly, the induced displacement torques depend on the CoR offsets and joint angles deviations (Schiele, 2008). Therefore, we obtain following uncertain human torque under consideration of kinematic incompatibilities:

$$\tilde{\boldsymbol{\tau}}_{\text{hum}} = \mathbf{M}_h(\mathbf{q})\ddot{\mathbf{q}} + \mathbf{C}_h(\mathbf{q}, \dot{\mathbf{q}}) + \mathbf{g}_h(\mathbf{q}) + \tilde{\boldsymbol{\tau}}_{\text{int,h}}(\mathbf{x}_{\text{off}}, \mathbf{y}_{\text{off}}, \mathbf{q}, \boldsymbol{\theta}) + \tilde{\boldsymbol{\tau}}_d(\mathbf{x}_{\text{off}}, \mathbf{y}_{\text{off}}, \mathbf{q}, \boldsymbol{\theta}), \quad (11)$$

where $\tilde{\boldsymbol{\tau}}_d$ denotes the uncertain displacement torques. In addition to $\tilde{\boldsymbol{\tau}}_{\text{int,h}}$ and $\tilde{\boldsymbol{\tau}}_d$, uncertainty also arises in (11) due to the dependence on \mathbf{q} , since the human joint angle cannot be measured directly and cannot be inferred accurately from $\boldsymbol{\theta}$, since $\mathbf{q} = \boldsymbol{\theta}$ no longer holds. Note that, given completely rigid bodies, these kinematic incompatibilities would theoretically make movements impossible and lead to extremely high interaction forces, due to the kinematic system being hyperstatic (Jarrassé and Morel, 2012). However, in practice deformation occurs at the physical interface, since the human limb is not rigid, which allows to retain mobility. The uncertainty that arises due to this plasticity is addressed in the following.

2.1.2.2. Soft-tissue contact dynamics

The second important aspect that introduces uncertainty to the physical human-exoskeleton interaction are morphological factors at the coupling between the robot and human. Specifically, the robotic system induces the desired movement by transmitting forces through the soft-tissue of the human limb at the attachment straps. Here, the considered soft-tissue primarily includes muscles, fat tissue and skin, but may also include smaller anatomical parts, such as ligaments, tendons or blood vessels. This is in contrast to the nominal dynamics model which assumes a rigid connection (11). Therefore, the dynamic properties of the human soft-tissue impact the description of the physical interaction.

Soft-tissue is most commonly modeled by elastic or viscoelastic components (Maurel, 1999). Viscoelastic dynamic behavior can for instance be represented by Voight-elements as illustrated in Figure 2B. Here, the soft coupling between the human and exoskeleton link is achieved via a Voight-element at the attachment. Hence, the displacement torques $\tilde{\boldsymbol{\tau}}_d$ and the interaction torque $\tilde{\boldsymbol{\tau}}_{\text{int,h}}$ become functions of the viscoelastic parameters, since all interaction forces are transmitted through soft contacts. It leads to

$$\begin{aligned} \tilde{\boldsymbol{\tau}}_{\text{hum}} = & \mathbf{M}_h(\mathbf{q})\ddot{\mathbf{q}} + \mathbf{C}_h(\mathbf{q}, \dot{\mathbf{q}}) + \mathbf{g}_h(\mathbf{q}) \\ & + \tilde{\boldsymbol{\tau}}_{\text{int,h}}(\mathbf{x}_{\text{off}}, \mathbf{y}_{\text{off}}, \mathbf{q}, \boldsymbol{\theta}, \mathbf{K}_{\text{st}}, \mathbf{D}_{\text{st}}) \\ & + \tilde{\boldsymbol{\tau}}_d(\mathbf{x}_{\text{off}}, \mathbf{y}_{\text{off}}, \mathbf{q}, \boldsymbol{\theta}, \mathbf{K}_{\text{st}}, \mathbf{D}_{\text{st}}), \end{aligned} \quad (12)$$

where \mathbf{K}_{st} and \mathbf{D}_{st} denote the lumped viscoelastic properties of the coupling due to soft-tissue. In Schiele (2008) a more detailed analysis of the displacement forces and their transmission through soft-tissue modeled as Voight-elements is presented. However, while linear, uniaxial models as shown in (12) are used for practicality, they describe the complex relationship between applied pressure and resulting deformation of the soft-tissue in a simplified manner. A more rigorous approach is to use discrete finite element to approximate the continuous medium and propagating the evolution of the deformation in simulations (Maurel et al., 2002). However, since this is an iterative procedure, it cannot straightforwardly be translated to an analytical model.

2.1.2.3. Inaccuracies in the human dynamics model

Another source of uncertainty that needs to be considered are inaccuracies in the human dynamics model. This is due to significant variations in the biomechanics of each human. To mitigate this, precise measurements of geometrical and inertial properties of the anatomical links are necessary to compute the personalized model parameters required for the human rigid body dynamics (1). However, gathering the information needed to estimate the human model parameter can be expensive, cumbersome and time-intensive (Zajac et al., 2002). Therefore, in clinical practice most commonly standard tables of anthropometric parameters are used (de Leva, 1996) to infer model parameters by scaling the default dynamics model to the height and weight of a particular individual. However, since the approach only yields an approximate measure, uncertainties are introduced. Thus, the uncertain human torque $\tilde{\boldsymbol{\tau}}_{\text{hum}}$ under additional consideration of

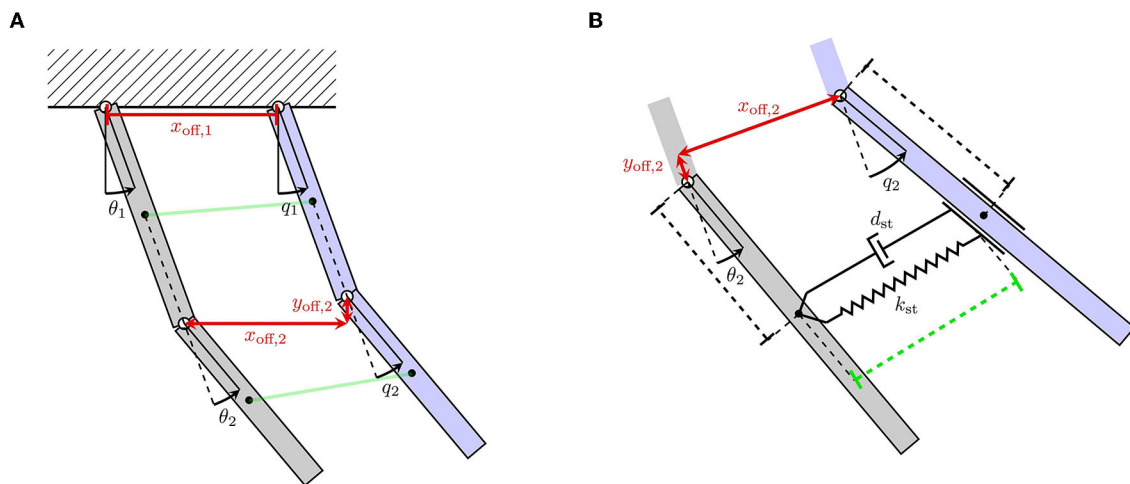


FIGURE 2

Two-link mechanical model of an interaction between a human (blue) and exoskeleton (gray) arm. (A) Illustrates kinematic incompatibilities and the resulting CoR offsets depicted with x_{off} and y_{off} . (B) Visualizes soft coupling between the human and exoskeleton link using a Voigt-element.

the modeling inaccuracies is

$$\begin{aligned} \tilde{\tau}_{hum} = & \tilde{M}_h(q)\ddot{q} + \tilde{C}_h(q, \dot{q}) + \tilde{g}_h(q) \\ & + \tilde{\tau}_{int,h}(x_{off}, y_{off}, q, \theta, K_{st}, D_{st}) \\ & + \tilde{\tau}_d(x_{off}, y_{off}, q, \theta, K_{st}, D_{st}), \end{aligned} \quad (13)$$

where \tilde{M}_h , \tilde{C}_h , and \tilde{g}_h denote the uncertain inertial, Coriolis and gravitational component of the human arm dynamics, which differ from the approximation obtained from the anthropometric tables. We summarize the torque due to the uncertain passive dynamics of the human limb with

$$\tilde{\tau}_{rbd,h} = \tilde{M}_h(q)\ddot{q} + \tilde{C}_h(q, \dot{q}) + \tilde{g}_h(q). \quad (14)$$

Thereby, we can write (13) to a more compact form for improved readability

$$\tilde{\tau}_{hum} = \tilde{\tau}_{rbd,h} + \tilde{\tau}_{int,h} + \tilde{\tau}_d. \quad (15)$$

Here, $\tilde{\tau}_{rbd,h}$ denotes the uncertain rigid body dynamics of the human arm due to unknown parameters in \tilde{M}_h , \tilde{C}_h and \tilde{g}_h . Differently to the human limb, the model parameters governing the dynamics of the exoskeleton (4) can reasonably be assumed to be known or can be obtained accurately using classical identification procedures (Hollerbach et al., 2008). Note that in (15), both $\tilde{\tau}_{int,h}$ and $\tilde{\tau}_d$ are in principle torques that are induced by the interaction with the exoskeleton. However, they differ in the sense that $\tilde{\tau}_{int,h}$ represents the desired loads that should be transmitted to the human limb, while $\tilde{\tau}_d$ are purely undesired torques due to kinematic incompatibilities. Since the human torque under consideration of uncertainties $\tilde{\tau}_{hum}$ (15) differs from the nominal human torque τ_{hum} (6) used in the regression analysis (8), errors are introduced to the estimated impedance parameters. In particular, deploying (6) for the computation of the human torque τ_{hum} implicitly allocates torques that are unaccounted for by the

nominal dynamics model to be generated due to joint spasticity. Thus, solving the regression problem will not result in the true viscoelasticity parameter K_h and D_h . By directly comparing the nominal human torque τ_{hum} to the true, uncertain human torque $\tilde{\tau}_{hum}$, we obtain

$$\underbrace{\tau_{hum}}_y = \underbrace{\tilde{\tau}_{hum}}_{\tilde{y}} - \underbrace{\Delta\tau_{rbd,h} - \Delta\tau_{int,e} - \tilde{\tau}_d}_{\Delta y}. \quad (16)$$

Here, $\Delta\tau_{rbd,h}$ denotes residual torques due to differences in the nominal human dynamics model $\tau_{rbd,h}$ and the unknown, true dynamics model $\tilde{\tau}_{rbd,h}$. Similarly, $\Delta\tau_{int,e}$ represents residual torques due to errors in the interaction torque modeling, while $\tilde{\tau}_d$ are the displacement torques due to kinematic incompatibilities. From (16) it can be seen that the labels y deployed in (8) do not agree with the true output \tilde{y} , i.e., the human torque $\tilde{\tau}_{hum}$ under consideration of uncertainties. The difference is summarized in (16) using Δy . Moreover, the measurements for the desired input matrix X according to (8) are not available, since kinematic incompatibilities result in a mismatch between the human joint angle q and exoskeleton joint angle θ . Hence, it can be seen how the uncertainties qualitatively influence the outcome of the regression analysis and impact the automated assessment negatively. However, it remains unclear exactly how sensitive the assessment is with respect to the different sources of uncertainty, which we propose to quantify with a sampling-based sensitivity analysis in this work.

2.2. High-fidelity human-exoskeleton simulation

In order to perform a sampling-based sensitivity analysis, a highly controlled environment is required. Obtaining the samples experimentally is infeasible, due to the missing ground-truth information and the large sample size that is required. Therefore,

in this work we deploy a high-fidelity simulation environment of the human-exoskeleton system to generate samples. To this end, we develop a novel human-exoskeleton simulation which explicitly accounts for the complex contact dynamics present during physical interaction. Here, an optimization-based physics engine called MuJoCo (Todorov et al., 2012) is deployed which is widely used in the modeling of robotic and biomechanical systems in contact-rich environments (Lowrey et al., 2016; Acosta et al., 2022). In particular, three key features of the proposed simulation enable the realistic emulation of the effects caused by sources of uncertainty and thereby facilitate the sampling-based sensitivity analysis: A musculoskeletal model to simulate the human, the consideration of soft contact dynamics at the attachments and a realistic load transmission via a mechanical interface. The proposed human-exoskeleton simulation is shown in Figure 1 in the *input parameter sample* block. Here, the human skeletal system is depicted in gray, while the muscular system is visualized with red lines. Furthermore, the two red cylindrical shapes on the forearm and upper arm represent the simulated human soft-tissue. Also, it can be seen that the physical interface is realized via cuffs and straps that wrap around the human upper and forearm. The complete human-exoskeleton simulation environment is made publicly available.¹ A brief summary of the key components is presented below. Following this, a more detailed explanation of each of the components of the simulation, their working principles and the performed validations is provided.

Human musculoskeletal model: A musculoskeletal model is implemented for the shoulder and elbow. Deploying a musculoskeletal model of the human arm here is necessary for two reasons. First, the simulated muscular system is used to generate the human torque and emulate spastic behavior. Second, the rigid skeletal system facilitates the introduction of variability in the human kinematics and dynamics. Thereby, it is possible to sample over two of the three sources of uncertainty described in Section 2.1.2.

Soft-tissue simulation: In the proposed simulation, soft-tissue is explicitly implemented by a composition of multiple micro-elements, which together form an object with viscoelastic material properties. The viscoelastic properties of the soft-tissue object can be varied, thereby allowing to sample over viscoelastic properties of the soft-tissue.

Physical human-exoskeleton interface: We simulate the mechanical interface explicitly by implementing cuffs and straps, which enclose the human arm and facilitate a realistic load transmission. Thereby effects that typically arise at the interface, such as attachment displacements, can be emulated.

2.2.1. Simulation of the human musculoskeletal system

A musculoskeletal model is used in the proposed simulation environment. Here, the rigid component of the human arm has

five DoFs, three on the shoulder joint and two at the elbow joint. For the shoulder, the human simulation can rotate along the flexion-extension, abduction-adduction and internal-external axis. Regarding the elbow, the simulation allows movement along the flexion-extension and pronation-supination rotations. While a rigid wrist-hand model is also included in the simulation, in our envisioned interaction scenario with the exoskeleton it is not pertinent. The inertial properties of the rigid skeletal system are designed using statistical anthropometric data (Ramachandran et al., 2016) with a default reference person of height 1.75m weighting 70kg. Thereby resulting in a nominal upper arm length of 36.37cm, a nominal forearm length of 34.9cm, a nominal upper arm mass of 2.25kg and a nominal forearm mass of 1.31kg. However, it is possible to adjust all of the parameters to account for variations in the target population.

In addition to the multi-link rigid body dynamics, the simulation accounts for the dynamics induced by the muscular system. In MuJoCo, biological muscles are modeled by means of muscle-tendon systems which induce dynamics dependent on origin and insertion sited and the forces generated by a muscle actuator. Here, the generated muscle force F_m follows the dynamics

$$F_m(l, v, a) = -F_0 F_{lv}(l, v, a), \quad (17)$$

where l is the scaled length of the muscle, v is the scaled velocity and $a \in [0, 1]$ denotes the muscle activation level. Additionally, F_0 describes the peak active force and F_{lv} , the force-length-velocity function, which are both fitted according to values derived from the experimental findings in Holzbaur et al. (2005). The origin and insertion sites of the muscles are also implemented in accordance with anthropometric data (Ramachandran et al., 2016), thereby ensuring that the dynamics of the simulated musculoskeletal system follow the real-world dynamics closely.

2.2.1.1. Validation of the human musculoskeletal model

In order to check the validity of the simulated human musculoskeletal model, a simulation experiment is performed. Specifically, it is examined whether the moments generated by the muscular system lie in similar ranges as those observed in real experiments. A common clinical procedure to assess the muscle strength is by means of the maximal isometric torque test (Amis et al., 1980; Garcia et al., 2016). Here, we use this procedure to adapt and validate the simulated elbow muscle contraction, which is a useful measure to quantify the neuromuscular properties of spastic muscles (Wang et al., 2019). In the proposed simulation, the dynamics of the elbow are governed by eight muscles. Specifically, four extensor muscles are considered, namely, the long, lateral and median triceps and the anconeus. Moreover, four flexor muscles are regarded, including the long and short biceps, the brachialis and the brachioradialis. The experimental procedure for the isometric torque test in flexion direction is as follows: First, the shoulder is flexed in the sagittal plane at 90deg and mechanically locked in this configuration. While the shoulder is fixed in place, the elbow is flexed in discrete steps of 1deg increments. At each of the discrete

¹ Open-source code of the upper-limb human-exoskeleton simulation environment is available at: https://github.com/stesfazgi/rehyb_mujoco.

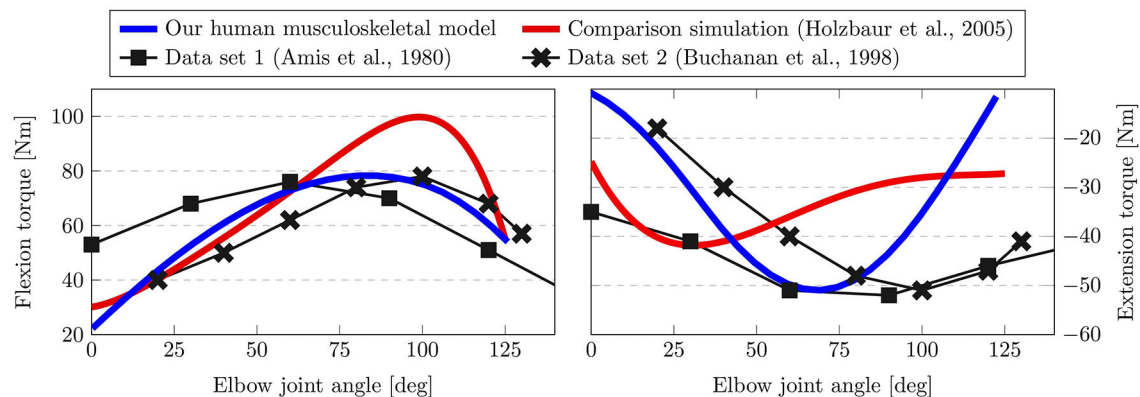


FIGURE 3
Results of the maximum isometric torque test. Here, the torque generated by the elbow flexors (**left**) and extensors (**right**) is shown over different elbow joint angle. Our human musculoskeletal model (blue) is shown to agree more closely with experimental data than the comparison simulation (red).

increments a maximum contraction of the elbow flexor muscles is applied, and the resulting torque is measured.

The results of performing the maximum isometric torque test in the simulation are shown in [Figure 3](#). Here, the left-hand side shows the isometric flexion torque, while the right side depicts the extension torque. We compare our simulation results (blue) against related biomechanical models of the musculoskeletal system ([Holzbaur et al., 2005](#)) (red) and two experimental data sets ([Amis et al., 1980](#); [Buchanan et al., 1998](#)). For the isometric flexion torque on the left, it is possible to see that our simulation results match the observed maximum torque of around 80Nm closely, while the comparison simulation exhibits a higher peak at 100Nm. Analogously, our simulation obtains a similar value for the peak extension torque as the experimental data set at -50Nm, while the simulation in [Holzbaur et al. \(2005\)](#) results in a lower absolute value at -41Nm. With respect to the curve shape both data set 1 ([Amis et al., 1980](#)) and data set 2 ([Buchanan et al., 1998](#)) display different behaviors. This is to be expected due to variability in real experiments and between different subjects, however, the simulation results indicate that our model lies within this range. Particularly, when observing the joint angle at which the peak extension torque is reached for instance, it is clearly visible that our simulation agrees with the experimental data more closely.

2.2.2. Simulation of the upper-limb exoskeleton

In this work, the simulated robotic system is inspired by the specification detailed in [Trigili et al. \(2020\)](#), where an upper-limb exoskeleton with three actuated DoFs on the shoulder level and one actuated DoF for the elbow (flexion-extension) is presented. For the envisioned scenario, we consider all passive and regulatory DoFs to be fixed, therefore, the simulated upper-limb exoskeleton is a four-DoF open chain. Joint friction is implemented via viscous dampers and the inertial properties are designed to roughly match comparable robotic devices. While each joint is associated with an actuator in the simulation, we do not consider elastic actuators here. The actuating motors are

also scaled in accordance with the maximum torques the real system can provide according to [Trigili et al. \(2020\)](#). Note that while the simulated exoskeleton is inspired by [Trigili et al. \(2020\)](#), this represents an exemplary device and may be replaced by a different wearable robotic system of interest. The proposed method for the spasticity assessment and sensitivity analysis constitute a general methodology and are therefore not limited to this specific hardware and could be applied to other exoskeleton designs as well.

2.2.3. Physical interface and complex contact dynamics

In our simulation, the physical interface is composed of two contact areas which represent the exoskeleton attachments on the upper and lower arm of the human. On the human side, complexity of the contact dynamics is primarily caused by soft-tissues and their influence on the force transmission at the linkage between the human arm and exoskeleton. In order to replicate the behavior of human soft-tissue in the simulation, three-dimensional composite objects are used, where one central element is surrounded by multiple external elements. Here, the elements of the three-dimensional composite object are arranged such that the resulting geometry approximates the human limb shape and thus a simplification of the commonly used finite element method ([Maurel et al., 2002](#)) is achieved. [Figures 4A–C](#) depicts the composite object which takes an ellipsoid shape in the simulation environment, where the large sphere at the center of the ellipsoid visualizes the central element of the composite object, while the external elements are illustrated by the smaller spheres. The viscoelastic behavior of the resulting composite object is determined by several soft equality constraints on the relative distance between the different elements, which is illustrated in [Figure 4D](#). Each soft equality constraint generates a force that can be approximately interpreted as a spring-damper link between two elements. Additionally, one constraint acting on all the elements is set to preserve the global volume of the composite object.

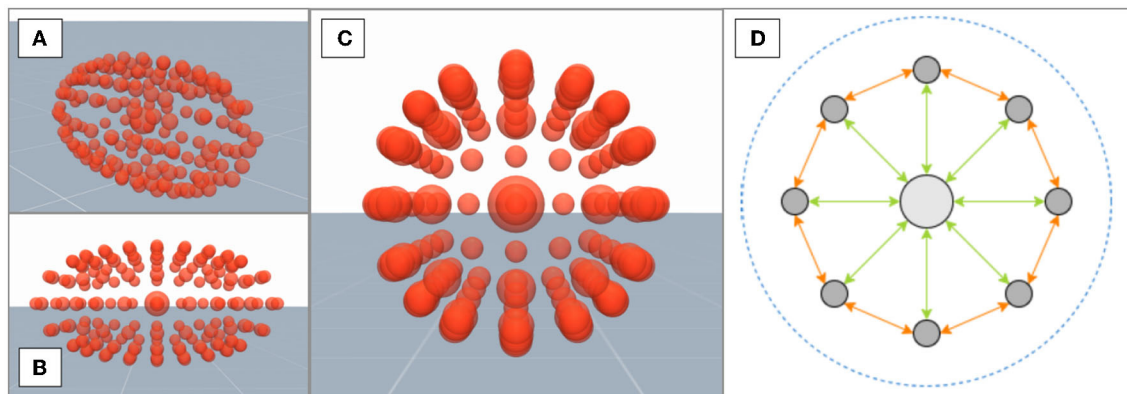


FIGURE 4 (A–C) Depict a composite object with an ellipsoid shape from different viewing angles. (D) A cross-section of the composite object with the central element in light gray and external elements in dark gray. Three types of soft constraints hold the elements together: central-external constraints (green), external neighbors constraints (orange), and a global volume constraint (blue).

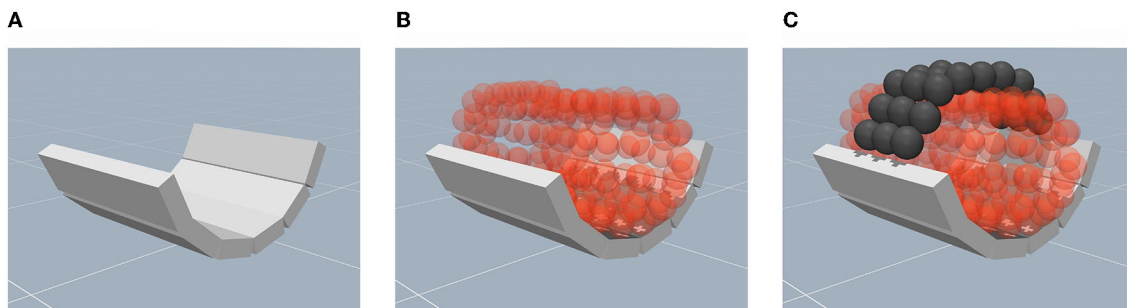


FIGURE 5 Depiction of the mechanical support at the physical interface in the simulation environment. (A) An illustration of the semi-cylindrical cuff composed of welded box primitives. (B) An illustration of the placement of the human limb within the cuff. (C) The implementation of straps using composite objects to fix the limb to the semi-cylinder.

The parameters of all constraints are fitted to approximate the viscoelastic behavior of real human soft-tissue.

On the exoskeleton side, forces are generally transmitted to the human arm via the mechanical supports, e.g., cuffs and straps, which induce movement by pushing or pulling the limb (Pons, 2008). Therefore, we follow the same design principle in the simulation in order to render the contact dynamics in high fidelity. First, the arm supports are implemented using a hollow semi-cylinder shape. Since MuJoCo does not directly handle concave bodies, the desired shape is approximately realized by an arrangement of welded box primitives (Figure 5A). Second, the human arm is placed inside the support (Figure 5B). Third, the implementation of the arm straps is realized using composite objects which are arranged in a two-dimensional grid. By welding two opposing sides of the strap to the arm support, the human limb is fixed to the attachment as illustrated in Figure 5C.

2.2.3.1. Validation of the human-exoskeleton contact dynamics

In order to validate the geometric compliance of the simulated limb, the stress-strain relationship of the composite object is investigated in the form of a compression test. In the validation, a uniaxial tension is applied to a solid material and the

relationship between compressing stress σ and axial strain ε is quantified (Pelleg, 2012). This property is called Young's modulus E and is computed as

$$E = \frac{\sigma}{\varepsilon} = \frac{F/A}{dl/l}, \quad (18)$$

where F is the applied force, A is the unit area and dl/l is the relative, normalized displacement of the composite body. It characterizes the compressive properties of a material, i.e., a higher Young's modulus E describes a stiffer material and a lower E indicates a softer material.

During the compression test, an incrementally increasing compressive stress is applied to the composite body via two rigid objects to opposing sides of the body. Subsequently, at each incremental step, the Young's modulus was computed from the strain, i.e., the relative deformation, of the composite body. The results are compared with experimental data acquired from mammal muscular tissue (Ogneva et al., 2010) to verify the validity of the simulated soft-tissue. The results of this comparison are shown in Figure 6. Here, the green lines visualize the experimentally determined Young's moduli for relaxed (solid line) and contracted (dashed line) muscle fibers (Ogneva et al., 2010) and the green shaded area indicate the resulting range of

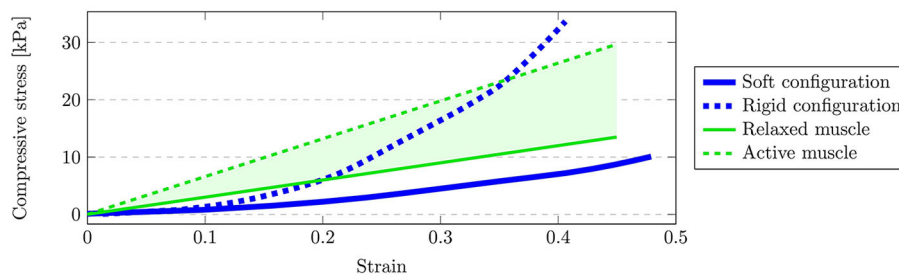


FIGURE 6

Result of the compression test. The green shaded area depicts the potential range of Young's moduli (Ogneva et al., 2010) determined by relaxed muscles (solid green) and active muscles (dashed green) from experimental data. The range of achievable Young's moduli in the simulation is bound by the soft configuration of the composite object (solid blue) and the rigid configuration (dashed blue).

potential Young's moduli. Analogously, the blue lines bound the range of achievable Young's moduli via the simulated composite object. The upper and lower bound are obtained by performing the above-described compression test for different parameterizations of the composite object. Given that the simulated, admissible values enclose the experimental data for higher strains, it is possible to approximate the elastic properties of muscle soft-tissue partially. Note however, that the Young's modulus provided from the experimental data (Ogneva et al., 2010) constitutes a linear fit and therefore does not exhibit the typical nonlinear stress-strain relationship which is normally characterized by a region of increasing modulus (Pons, 2008) as depicted by our simulation in Figure 6. Thus, the slight difference for lower strain levels can be explained due to approximation error caused by the linear fit in Ogneva et al. (2010). Furthermore, the experimental data only considers muscle fibers and is therefore expected to vary from the considered soft-tissue, e.g., due to additional fat tissue at the attachments. The additional flexibility in the simulation environment to parameterize lower Young's moduli is thus favorable, since the expected variation generally leads to softer materials.

2.3. Exoskeleton-based automated assessment

With the nominal and uncertain dynamics model (Section 2.1) and a human-exoskeleton simulation that includes the key sources of uncertainty (Section 2.2) introduced, the required input samples for the sensitivity analysis can be generated. Here, the input samples are instantiations of the simulation with varying parameters for the different sources of uncertainty. Since we investigate how these uncertainties impact the results of an automated assessment, the output samples are in the form of estimated impedance parameter. The procedure by which these output samples are generated is explained in this section.

In order to perform the spasticity assessment in an automated manner, two components are necessary. First, a data generation procedure is required during which the robotic system interacts with the human arm to induce observations from which the impedance parameters can be inferred. Secondly, the captured data needs to be used to estimate the parameters. In this work,

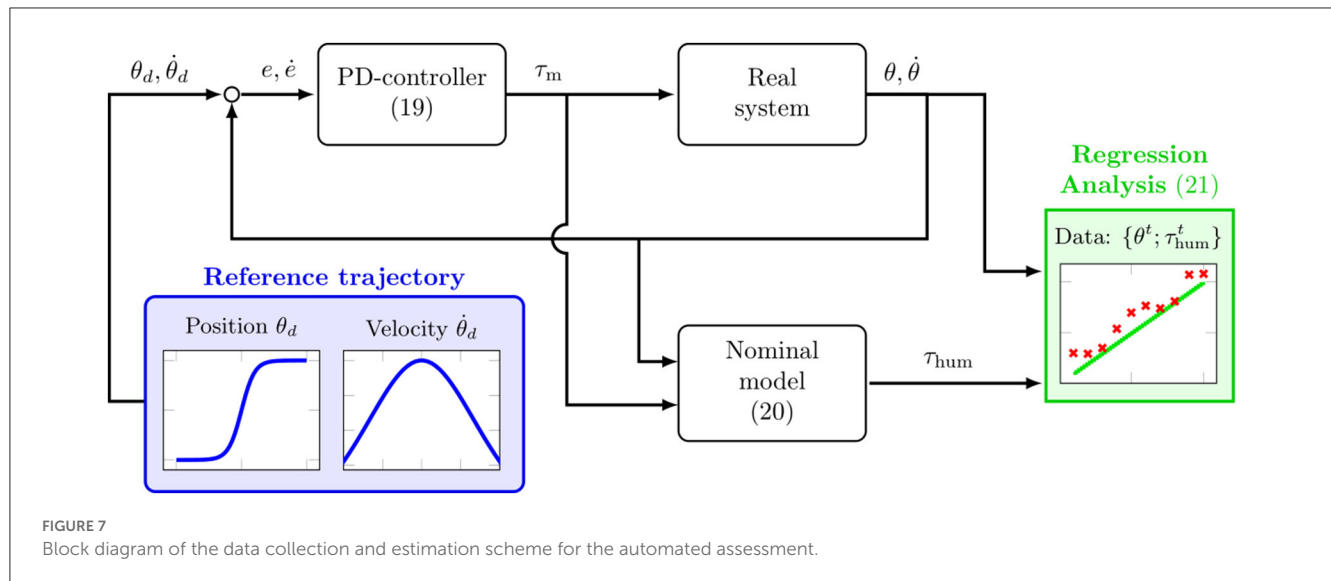
we propose a fully automated scheme for the data generation and estimation that leverages model knowledge to produce the required labels \mathbf{y} . The complete scheme is illustrated with a block diagram in Figure 7. Here, the real system represents the true, uncertain human-exoskeleton system which is reproduced in the simulation environment. On the other hand, the nominal model block describes the idealized dynamics model that can be computed analytically. The reference trajectory $\theta_d, \dot{\theta}_d$ is depicted in the blue block and is used to observe the joint resistance along a predefined movement, similar to the passive mobilization that is typically performed by a clinician. It acts as an input to the PD-controller, which replicates the manual perturbation generated by the clinician using the exoskeleton.

For the reference trajectory a sigmoid function is selected, since it is known to generate a minimum jerk profile on the joint level (Flash and Hogan, 1985), thus, leading to a natural and comfortable motion for the patient. With the reference trajectory being defined, the exoskeleton applies a torque on the human arm to emulate the manual perturbation performed by the clinician. This is achieved by using the feedback provided by the exoskeleton measurements $\theta, \dot{\theta}$ and feeding the current tracking error $\mathbf{e}, \dot{\mathbf{e}}$ into a PD-controller to compute the required motor torque:

$$\tau_m(\mathbf{e}, \dot{\mathbf{e}}) = \mathbf{K}_p \mathbf{e} + \mathbf{K}_d \dot{\mathbf{e}}, \quad (19)$$

where $\mathbf{e} = \theta_d - \theta$ and $\mathbf{K}_p, \mathbf{K}_d$ are the feedback gains of the controller. By applying the motor torque (19), the human-exoskeleton system is moved and, given sufficiently high control gains, the desired trajectory θ_d is tracked. For the gains of the exoskeleton PD-controller $K_p = 50$ and $K_d = 15$ is set. In order to induce spastic behavior in the human simulation, a constant, co-contracting muscle activation of $a = 0.4$ is simulated for the muscles associated with the examined joint. Thereby the human arm will produce a resisting torque opposing the exoskeleton during a change in joint position. The data that is generated during the passive mobilization is used for the regression analysis (8).

For the data generation according to the nominal model, perfect alignment between the human and exoskeleton kinematic chain is assumed. Thus, the measured angles $\theta, \dot{\theta}$ are assumed to match the human joint kinematics $\mathbf{q}, \dot{\mathbf{q}}$, thereby providing the nominal input variables \mathbf{X} for the linear regression (8). Furthermore, the output vector \mathbf{y} is required, which comprises



measurements of the human internal torque τ_{hum} . Since τ_{hum} is not directly measurable, we exploit the nominal model in Figure 7 to overcome this problem. Specifically, using the known motor torque (19) and the nominal dynamics model (6) we can compute the nominal human torque τ_{hum} to be

$$\tau_{\text{hum}}(\theta, \dot{\theta}, e, \dot{e}) = \underbrace{M_h(\theta)\ddot{\theta} + C_h(\theta, \dot{\theta}) + g_h(\theta)}_{\tau_{\text{rbd,h}}} + \underbrace{M_e(\theta)\ddot{\theta} + C_e(\theta, \dot{\theta}) + G_e(\theta) - \tau_m(e, \dot{e})}_{\tau_{\text{int,h}}} \quad (20)$$

Here, the parameters of the nominal human model are chosen according to anthropometric data (Ramachandran et al., 2016) with a nominal reference person of height 1.75m and a weight of 70kg, which results in a nominal upper arm length of 33.37cm, a nominal forearm length of 31.9cm, a nominal upper arm mass of 2.25kg and a nominal forearm mass of 1.31kg. Thus, by measuring the trajectory of the exoskeleton joint kinematics $\theta, \dot{\theta}$ over time and computing the corresponding nominal human torques τ_{hum} according to (20), the regression analysis (8) can be performed for each joint independently.

$$\underbrace{\begin{bmatrix} \tau_{\text{hum},i}^1 \\ \tau_{\text{hum},i}^2 \\ \vdots \\ \tau_{\text{hum},i}^T \end{bmatrix}}_{\gamma} = \underbrace{\begin{bmatrix} \theta_i^1 & \dot{\theta}_i^1 \\ \theta_i^2 & \dot{\theta}_i^2 \\ \vdots & \vdots \\ \theta_i^T & \dot{\theta}_i^T \end{bmatrix}}_{\hat{X}} \underbrace{\begin{bmatrix} k_{h,ii} \\ d_{h,ii} \end{bmatrix}}_{\omega} \quad (21)$$

where, differently to (8), \hat{X} represent the inputs when the exoskeleton kinematic measurements $\theta, \dot{\theta}$ are used as a placeholder for the human joint kinematics q, \dot{q} . Note that deploying (20) for the computation of the human torques implicitly allocates torques that are unaccounted for by the nominal dynamics model to be generated due to spasticity in the patient's joints. Intuitively, this is analog to the principle applied during manual assessment, where the human limb is assumed to be passive and any encountered resistance is allocated to spasticity. However, as

detailed in Section 2.1.2, different sources of uncertainty impact the human-exoskeleton interaction, which result in interaction torques that are not considered in (20). Thus, solving (21) will not result in the true viscoelasticity parameter K_h and D_h , due to the impact of uncertainties on the regression analysis.

2.4. Sensitivity analysis of uncertainties

The goal of this section is to quantify the impact of the uncertainties on the estimated impedance parameters during the exoskeleton-based automated assessment. To this end a sensitivity analysis is performed to examine how variations in the output of a numerical model or simulations can be ascribed to variations of its inputs. We consider uncertainties in the modeling of physical human-exoskeleton interaction as input factors to quantitatively assess their importance. Analogously, the estimated viscoelasticity parameters K_h and D_h represent the output samples of the sensitivity analysis. Therefore, sensitivity is defined as the induced variability in the parameter estimates K_h and D_h due to variability in the uncertain inputs and is quantified by means of so-called sensitivity indices (Saltelli et al., 2004). Intuitively, these sensitivity indices represent importance measures which are allocated to each input parameter of the simulation, i.e., each source of uncertainty (Pianosi et al., 2016). In this section, the methods used for the sampling-based sensitivity analysis procedure are presented. First, the input sample generation is described in Section 2.4.1. Following this, Section 2.4.2 details the deployed methods for the computation of the sensitivity indices.

2.4.1. Sampling sources of uncertainty

For the input sample generation, we draw samples over different parameterization of the human-exoskeleton simulation. Here, each sampled simulation instance represents a distinct patient with the individual variations present in the population. Six biomechanical parameters are chosen as input factors, where

TABLE 1 Sources of uncertainty and associated simulation parameters for the input sample generation.

Uncertainty	Simulation parameter	Value range
Kinematic incompatibilities	Length upper arm	27.28cm–37.78cm
Kinematic incompatibilities	Length forearm	28.27cm–34.55cm
Inaccuracies in dynamics model	Mass upper arm	0.3kg–3.41kg
Inaccuracies in dynamics model	Mass forearm	0.1kg–1.82kg
Soft contact dynamics	Elasticity upper arm	100.5N/m–974.43N/m
Soft contact dynamics	Elasticity forearm	100.5N/m–974.43N/m

each parameter is associated with a different source of uncertainty. An overview of the parameters, their respective uncertainties and the value ranges is depicted in Table 1. Here, kinematic incompatibilities are produced by varying the length of the human limb. In particular, changes in the upper arm length lead to macro-misalignments and a resultant CoR offset, since the exoskeleton link length remains unchanged. In contrast, varying the human forearm length induces micro-misalignments. The second source of uncertainty investigated during the sensitivity analysis are inaccuracies in the dynamics model. By perturbing the mass of the upper and forearm, errors in the nominal model are evoked as the gravitational component and inertia of the human limb are dependent on the mass. Lastly, uncertainties due to soft-tissue contact dynamics are considered by sampling over different elasticities of the human upper arm and forearm at the attachments. The value ranges of the samples shown in Table 1 are derived from statistical information provided by anthropometric data (Ramachandran et al., 2016). Here, a fixed viscosity of 100Ns/m is chosen for the micro-elements comprising the soft-tissue to avoid numerical instabilities.

In addition to defining the input variability space, i.e., the value ranges shown in Table 1, further design choices regarding the sampling strategy have to be made. In general two classes of sampling concepts can be differentiated, One-At-a-Time (OAT) and All-At-a-Time (AAT) methods (Pianosi et al., 2016). While in OAT methods variations are induced by perturbing one input parameter only and keeping all other fixed, AAT methods induce output variations by varying all input parameters concurrently. The main advantage of OAT in comparison to AAT sampling is the reduced computational load due to fewer samples being required. However, because of the concurrent sampling in AAT methods, the joint influence of input factors due to interaction between the parameters can be analyzed, thereby, providing more insights (Pianosi et al., 2016). Depending on the deployed method to estimate the importance measures, both approaches can be beneficial. Therefore, the following section presents sensitivity analysis methods with distinct sampling strategies for different investigation purposes.

2.4.2. Sensitivity analysis methods

Depending on the setting and purpose of the sensitivity analysis, different methods are appropriate. In Saltelli et al. (2008)

two main purposes are introduced. First, the goal of ranking the most relevant input factors which is called *factor prioritization*. Second, identifying input factors with negligible impact which is called *factor fixing*. Beyond these two main settings, other purposes are introduced as well. However, given that the proposed sensitivity analysis is supposed to inform the decision making process in clinical practice and lead to more robust spasticity assessment, our quantitative analysis is mainly focused on factor prioritization and factor fixing, since these information lead to a practical guide to performing more robust automated assessment. Additional information may also be derived by qualitative sensitivity analysis methods, e.g., using scatter plots (Beven, 1993; Kleijnen and Helton, 1999).

Furthermore, potential interactions between the investigated sources of uncertainty should also be considered. Since these interactions may emerge for various parameters and it is a-priori unknown how the interactions behave with respect to the magnitude of the parameters, we ideally want to perform a dense sampling over the input variability space. To this end global sensitivity analysis methods are preferred, which investigate variations over the complete range of admissible inputs. Global sensitivity analysis methods have previously been shown to facilitate tasks such as supporting efforts in uncertainty reduction (Hamm et al., 2006) and facilitating robust decision making (Nguyen and de Kok, 2007; Singh et al., 2014).

2.4.2.1. Elementary effects method

Given these requirements, there are multiple viable sensitivity analysis methods. First, Morris method (Morris, 1991), also referred to as *elementary effects test*, is an efficient and suitable approach to perform factor prioritization and fixing. Here, a perturbation-based design is deployed, where the whole input space is explored by applying perturbations to each input factor separately and computing global sensitivity measures from the probed samples. This is done by computing so-called elementary effects *EE* for each input factor x_i

$$EE_i = \frac{f(x_1, \dots, x_{i-1}, x_i + \Delta_i, x_{i+1}, \dots, x_K) - f(x_1, \dots, x_K)}{\Delta_i}, \quad (22)$$

where $\mathbf{x} = (x_1, x_2, \dots, x_K)$ represents a set of input parameters, $f(\mathbf{x})$ denotes the function that maps inputs to model responses, K is the total amount of examined input parameters and Δ_i is the perturbation applied to the i -th input parameter. In order to achieve a global measure of sensitivity, the input space is sampled with r trajectories, each consisting of $K + 1$ sampling points, where each point differs in just one input factor by a fixed amount Δ (Morris, 1991). Thereby, each trajectory allows for the computation of one *EE* per input factor and the sensitivity measures for each parameter can be computed as such:

$$\mu_i = \frac{1}{r} \sum_{j=1}^r EE_i^j \quad (23)$$

$$= \frac{1}{r} \sum_{j=1}^r \frac{f(x_1^j, \dots, x_i^j + \Delta_i^j, \dots, x_K^j) - f(x_1^j, \dots, x_K^j)}{\Delta_i^j}$$

$$\sigma_i^2 = \frac{1}{r-1} \sum_{j=1}^r (EE_i^j - \mu_i)^2, \quad (24)$$

where Δ_i^j represents the perturbation of the i -th input parameter x_i^j in trajectory j and EE_i^j denotes the computed elementary effect associated with parameter x_i along trajectory j . Here, the mean μ and standard deviation σ of the elementary effects EE are proposed as sensitivity measures (Saltelli et al., 2008). In particular, μ (23) represents how much the input parameter affects the output, while σ (24) is a measure for the induced effects due to interaction with other inputs, i.e., how much EE_i varies when changes in the remaining $i - 1$ parameters occur. Specifically, a small σ_i implies that the effect of parameter x_i on the output, which is shown by μ_i , is independent of the other parameters. Therefore, Morris method is particularly well suited for factor fixing, since a simultaneous consideration of both μ and σ allows the identification of negligible input factors, which have both little interaction with the other inputs (small σ) and do not influence the output strongly (small μ). Moreover, applying this approach requires relatively few samples, which further increases its utility for factor fixing in cases where model evaluations are expensive. However, since it is a perturbation-based OAT method, it may lead to erroneous results if the target system exhibits high-frequencies in its response to variations in the input (Pianosi et al., 2016).

2.4.2.2. Variance-based sensitivity analysis

An alternative approach that facilitates the analysis of output sensitivity with respect to each input factor over their complete value range are variance-based sensitivity analysis methods, also referred to as Sobol method (Sobol, 1993). Here, modeling uncertainty is specifically considered by regarding the input parameters as stochastic variables with a defined probability distribution. Thereby, a conceptual link between sensitivity and uncertainty is exploited and sensitivity is analyzed by investigating how uncertainty in the input propagates to the output variables. Subsequently, the relative contribution of each input is decomposed and used as a measure of sensitivity. To this end variance is used as a measure to quantify uncertainty. The so-called *first-order effect* S_i , which is a measure for the individual contributions of inputs to the output variance, is computed as

$$S_i = \frac{\mathbb{V}(z) - \mathbb{E}_{x_i}[\mathbb{V}_{x_{-i}}(z | x_i)]}{\mathbb{V}(z)}, \quad (25)$$

where $z = f(\mathbf{x})$ is the output variable, \mathbb{E} denotes the expectation and \mathbb{V} the variance. Here, $\mathbb{V}_{x_{-i}}(z | x_i)$ expresses the conditional variance of the output z over x_{-i} , i.e., all inputs except x_i , given that x_i is fixed. Analogously, $\mathbb{E}_{x_i}(z | x_i)$ denotes the conditional expected value. Therefore, the second term in (25) expresses the expected variance in the output given that the i -th input x_i is fixed. A small value for this expectation, and consequently a high value for S_i , implies that a significant reduction in output variance can be achieved by fixing x_i (Saltelli et al., 2008). Thus, the first-order index S_i is a measure for the direct contribution of an input to the output variance, which in turn functions as a place-holder for sensitivity.

On the other hand, the *total-order index* S_{Ti} indicates the total effect of an input x_i on the output variance including interactions with other input factors (Homma and Saltelli, 1996) and is defined as

$$S_{Ti} = \frac{\mathbb{E}_{x_{-i}}[\mathbb{V}_{x_i}(z | x_i)]}{\mathbb{V}(z)}. \quad (26)$$

Moreover, variance-based methods allow for the computation of further, higher-order indices, such as second-order or third-order ones. Thereby, by computing all $2^K - 1$ orders, variance-based sensitivity measures can theoretically capture the sensitivities present in the system completely. However, since this is computationally infeasible in practice, a good approximation can be achieved by computing only the first-order and total-order terms (Saltelli et al., 2004).

Thus, variance-based methods are well equipped to analyze sensitivities in a principled manner by both quantifying the importance of individual inputs and groups of inputs. Moreover, an uncertainty-aware modeling paradigm is supported and, by sampling the input space using probability distributions, the full range of input variations can be investigated. However, due to their sampling-intensive nature, it is impractical to deploy them directly when model evaluations are expensive. Therefore, we propose to use both the elementary effect test and variance-based sensitivity analysis in conjunction. Thereby, non-influential input parameters are detected by the efficient elementary effect method and can be discarded prior to performing a more extensive analysis using variance-based methods.

3. Results

In this section we present the findings of performing the proposed two-phase sensitivity analysis scheme. First, in Section 3.1 the elementary effect test is deployed to screen parameters that do not effect the automated assessment outcome significantly and can therefore be fixed for subsequent investigations. Second, the variance-based sensitivity analysis is performed on the remaining input parameter in Section 3.2 to determine the relative importance of the different model uncertainties. Lastly, a qualitative analysis of the obtained samples is conducted in Section 3.3 to provide further insights. For clarity of presentation the automated assessment is limited to the estimation of the elbow joint stiffness. The presented sensitivity analysis is implemented in Matlab using the SAFE toolbox (Pianosi et al., 2015), while the simulation model is implemented in Python using the MuJoCo physics engine (Todorov et al., 2012).

3.1. Factor fixing using elementary effects

In order to identify non-influential parameters, we deploy the elementary effect method as described in Section 2.4.2. To this end, input parameter samples are drawn for which the human-exoskeleton simulation is instantiated and subsequently the automated assessment is run for each model instance to generate the respective output samples. Here, we use a radial design for sampling the input parameter hyperspace, since it has been shown to achieve superior performance for computing elementary effects (Campolongo et al., 2011). A total of $r = 150$ trajectories is generated for $k = 6$ input parameters, which are listed in Table 1, resulting in 1050 sampling points. For the generation of the random sampling vectors required in the radial design, the well-established Latin hypercube approach (McKay et al., 1979;

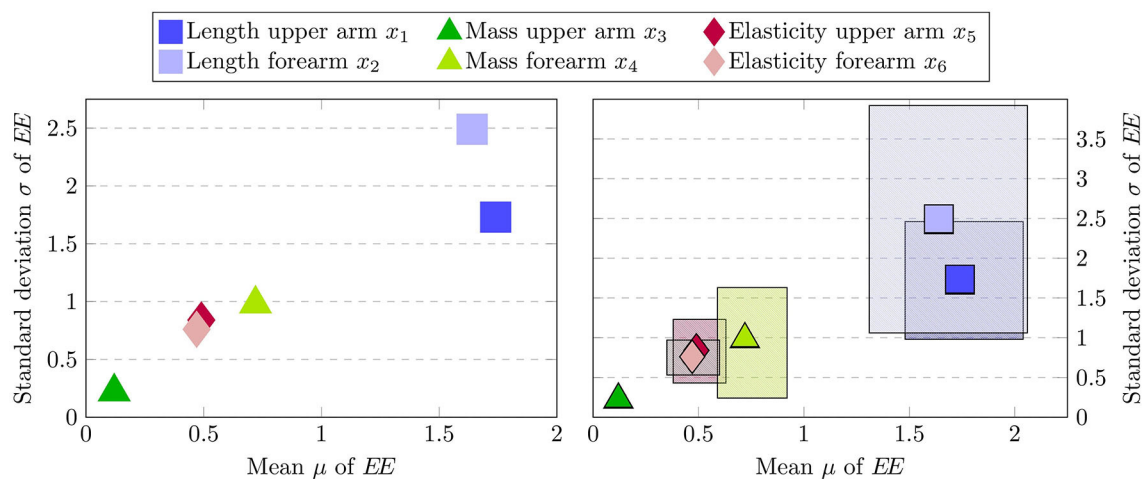


FIGURE 8

Estimated mean μ vs. standard deviation σ of the elementary effects EE (left) and approximated 95% confidence bounds via bootstrapping (right). Here, each input factor is represented by one marker and the confidence bounds are represented by the patterned area associated with each marker.

Helton and Davis, 2003) is used. Moreover, a uniform distribution of the input parameter space is assumed.

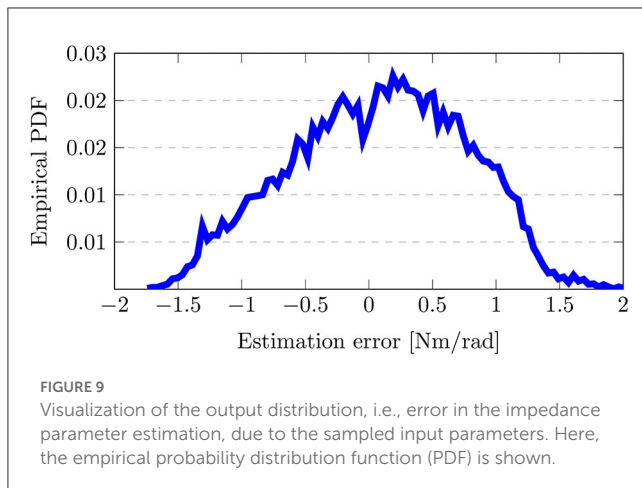
The results of the elementary effect test are depicted in Figure 8. On the left-hand side, it is clearly visible that the estimated sensitivity measures indicate the mass of the upper arm x_3 as the least influential input parameter. The low value estimated for both the mean and standard deviation implies that the input factor has both little direct impact on the estimated joint stiffness during the automated assessment procedure and moreover does not interact strongly with the remaining parameters. This makes sense intuitively since the mass of the upper arm is not expected to influence the estimated torque on the elbow level. However, due to the design of the passive mobilization experiment in Section 2.3, it is first necessary to drive the human arm into the desired initial configuration to start the procedure. Thereby different upper arm mass parameterization could potentially influence the precise starting state, which in turn can lead to slight changes in the estimated stiffness. However, from the results of the elementary effect test it is apparent that these disturbances do not impair the assessment process. Differently, the length of the upper and forearm exhibit the highest sensitivity both with respect to the mean and standard deviations. Therefore, the elementary effect method identifies the parameters associated with uncertainties due to kinematic incompatibilities as the most dominant ones. Lastly, the remaining parameters regarding the soft-tissue contact dynamics and the mass of the forearm are estimated to have a comparable sensitivity measure with the mass having a slightly larger impact in both μ and σ .

Sampling-based sensitivity analysis methods inherently approximate the true sensitivity indices given the observed samples. Therefore, especially when working with small to medium sample sizes, it is pertinent to validate the robustness of the obtained results. In order to investigate this, an additional robustness analysis can be performed (Pianosi et al., 2016) which assesses whether similar sensitivity measures would have been obtained with different input samples. This can be achieved

in a sample-efficient manner by approximately computing the confidence bounds of the estimated similarity measures using bootstrapping (Efron and Tibshirani, 1993). Note that while bootstrapping is an efficient technique, the obtained confidence intervals do not constitute theoretically guaranteed bounds in general and can result in overly optimistic estimates when applied to the Morris method (Yang, 2011; Romano and Shaikh, 2012). However, applying the method still allows to retrieve valuable insights regarding the estimated sensitivity indices. The results of the robustness analysis are displayed in Figure 8 on the right. Here, a total of 300 μ and σ values are computed for each input factor, where each value is generated by drawing 150 samples with replacement from the original 1050 sampling points. Notably, the confidence bounds for the upper arm mass x_3 are very small, thereby indicating that the mass of the upper arm can confidently be regarded as a non-influential input factor that can be fixed for subsequent analysis. In contrast, the upper arm length x_1 and forearm length x_2 , which are identified as the most important ones by the elementary effect test, are associated with large confidence intervals. In particular the forearm length x_2 features the highest uncertainty in the estimated sensitivity measures. Therefore, the results are not conclusive to make reliable statements beyond the screening of the upper arm mass and the deployment of further sensitivity analysis methods is required.

3.2. Factor prioritization using variance-based sensitivity analysis

Following the elementary effect test in the previous evaluation, we perform an additional variance-based sensitivity analysis to obtain a more rigorous understanding of the uncertain sensitivity patterns present in the human-exoskeleton system. To this end we exploit the findings of the prior section to fix the upper arm mass x_3 , as it is identified as a non-influential factor, which leads to a reduction of the computational load of the proposed



variance-based analysis. For the input sample generation of the remaining parameter we use the two-phase sample procedure proposed for the variance-based approximation of the first-order and total-order indices (Saltelli et al., 2010). In the first phase, a total of $2N$ random samples is generated, which are referred to as base samples. Subsequently, KN additional input samples are produced by resampling vectors of the base samples. Thereby, this method requires $N(K + 2)$ model evaluation for the estimation of the first-order and total-order effects and is computationally more efficient than a naive approach (Saltelli et al., 2010). Here, we set $N = 3,000$ and investigate $K=5$ input factors leading to a total of 21,000 simulation runs. The random base samples are again obtained using the Latin hypercube method assuming a uniform distribution over the input parameters.

The resulting output distributions is shown in Figure 9 with the empirical probability distribution function (PDF), which is approximated from the output samples. Here, the output distribution, i.e., the estimation error in K_h , resembles a Normal distribution with a mean estimation error slightly larger than 0 Nm/rad. Thereby, it can be seen how the sampling of uncertainties in the input variability space induces an output distribution and impacts the assessment results. Note that an implicit assumption in variance-based sensitivity analysis is that variance is an appropriate measure to capture uncertainty (Pianosi et al., 2016). Since the empirical PDF in Figure 9 resembles a Normal distribution and is neither multi-modal nor highly-skewed, this assumption holds true, thus strengthening the viability of deploying the approach here.

Figure 10 depicts the resulting first-order indices S_i on the left and total-order indices S_{Ti} on the right. Additionally, the 90% confidence interval are shown by the error bars, which are computed using bootstrapping. From the first-order effects it is clearly visible that the factors x_1 , x_2 and x_3 are the most influential ones, with the length of the forearm x_2 having the highest impact. Moreover, the results indicate that the softness of the upper and forearm x_5 and x_6 are negligible, since their respective total-order indices are close to zero. Note that a total-order index of value zero constitutes a necessary and sufficient condition for an input factor to be non-influential (Pianosi et al.,

2016). The negative signs for the first-order indices of x_5 and x_6 can be attributed to numerical errors, which are known to occur for input factors with negligible sensitivity indices when using the deployed sampling method (Saltelli et al., 2008). Moreover, the sum of the first-order effects computes to 0.78, while the sum of the total-order effects is 1.13. Since both sums are not equal to 1, it can be concluded that there are interaction effects present among the input factors in the system. Additionally, it can be seen in Figure 10 that the total-order indices of each factor are greater than the respective first-order indices. Thus, it can be inferred that all of the studied input parameter participate in the interactions.

Finally, we perform a convergence analysis to affirm the reliability of the obtained results. Since the sensitivity indices are approximated from samples, a convergence analysis assesses whether the evaluated sample size is sufficiently large to make a statement regarding the importance of the input factors. This can be done efficiently by recomputing the results from increasing sets of sub-samples of the original data set and analyzing the convergence of the observed indices (Nossent et al., 2011; Pianosi et al., 2016). The results of the performed convergence analysis are shown in Figure 11. Here it can be seen that both the first and total-order indices converge quickly when increasing the size of the sub-samples with few changes in the indices after sub-samples of half the size of the original set. This indicates that a sufficiently large input sample size is chosen in the evaluation. Since the error bars in Figure 10 are also small when compared to the estimated indices, the obtained results can be deemed robust. Therefore, we can conclude that the length of the forearm is the most influential source of uncertainty, with the upper arm length and the mass of the forearm following as the next most important factors.

3.3. Qualitative sensitivity analysis

In previous sections, we have analyzed the impact of uncertainties on the human-exoskeleton interaction from a quantitative manner, which is a particularly suitable approach when screening for influential and non-influential factors and when ranking those. By applying the elementary effect test and variance-based sensitivity analysis in Sections 3.1 and Section 3.2, input parameters associated with kinematic incompatibilities and erroneous dynamics model are identified as the most relevant uncertainties. However, little information regarding their functional influence on the system is retrieved and, while interaction between the inputs is indicated, their exact nature remains unclear. Therefore, we perform an additional qualitative sensitivity analysis to gain further insights into the most influential sources of uncertainty.

Figure 12 visualizes the relationship between input and output samples for x_1 , x_2 , and x_4 . Each black dot in the scatter plot indicates an input-output sample pair, while the larger red dots depict the average output values over an interval range of the respective input. Here, equidistant intervals that split the input value ranges into 10 bins are used, which result in a width of 0.02 for x_1 and x_2 , and 0.17 for x_4 . For the evaluation, a total of 1,500 input samples are generated assuming a uniform distribution

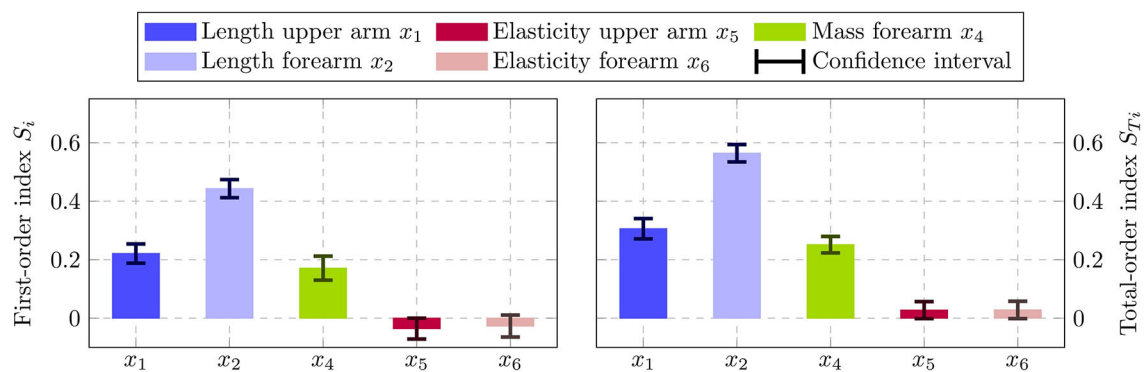


FIGURE 10

Estimated first-order indices S_i (left) and total-order indices S_{Ti} (right) with 90% confidence intervals using the variance-based sensitivity analysis. The left figure shows the most influential factor is x_2 followed by x_1 and x_4 . The total-order effects on the right identify both x_5 and x_6 to have no impact, since $S_{Ti} = 0$ constitutes a necessary and sufficient condition.

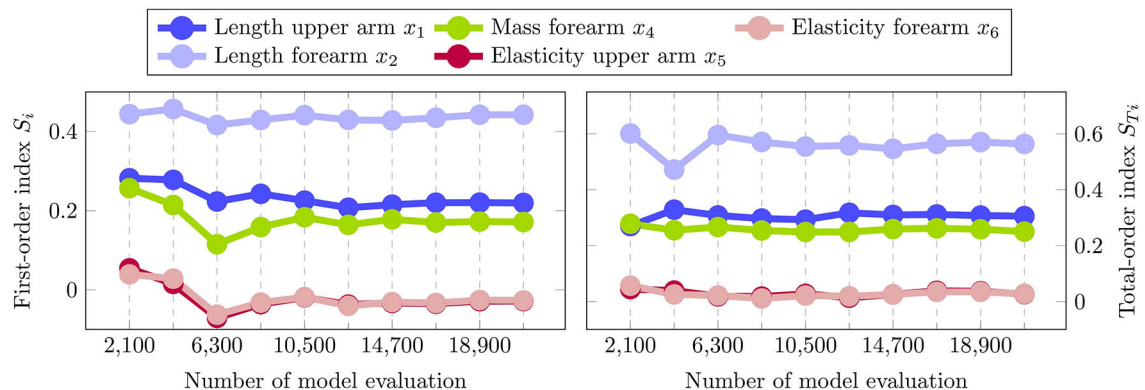


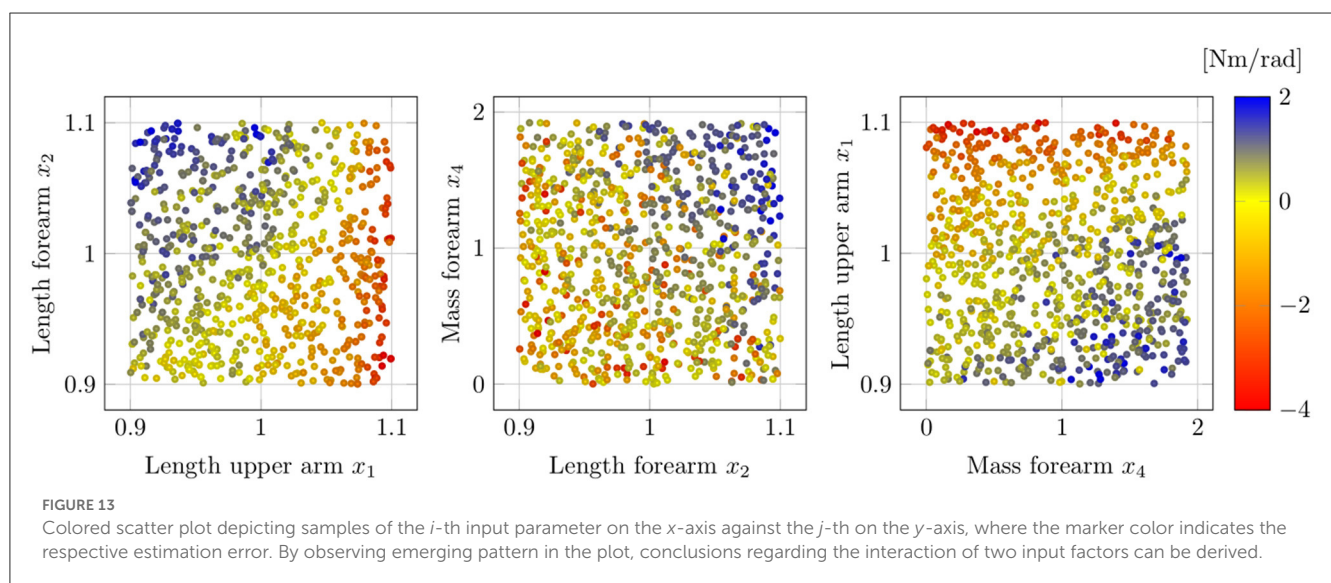
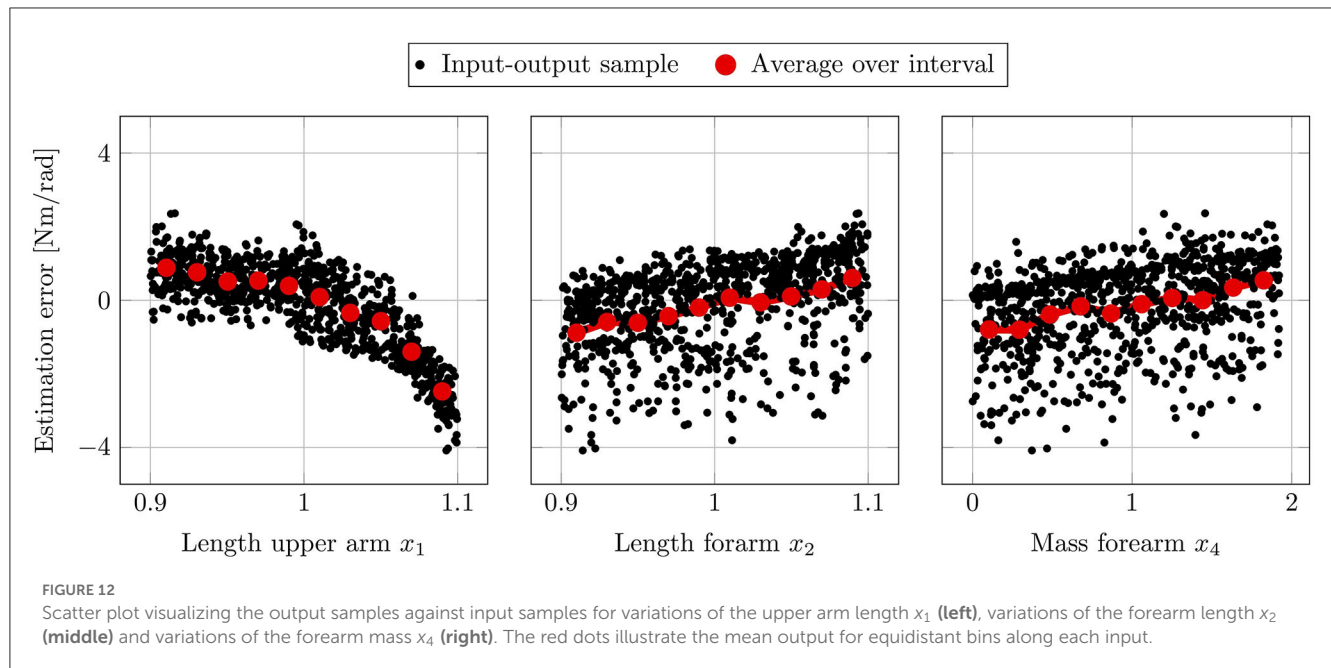
FIGURE 11

Convergence plot illustrating the estimated sensitivity indices using an increasing amount of sub-samples. Both the first-order and total-order indices converge quickly, which implies that a sufficient sample size is chosen for the variance-based sensitivity analysis.

for each parameter. Note that here the x_2 sample range is slightly larger compared to the previous evaluation, since the sampling strategy of the qualitative sensitivity analysis is more robust to erroneous model responses, which can occur due to simulation failures caused by unreasonable input parameter combinations. In Figure 12 it is clearly visible that variation in the length of the upper arm x_1 induce a nonlinear change in the output, while both forearm length changes x_2 and forearm mass changes x_4 have a linear influence. The linear relationship in x_2 and x_4 is consistent with the physical intuition for the examined system, since the gravitational component of the human arm dynamics in (1) is a linear function in the link length and the mass. Thus, it is indicated that the forearm length x_2 has to be considered as a source of uncertainty with respect to both kinematic incompatibilities and modeling errors, which leads to a better understanding of the high sensitivity ranking of x_2 in the variance-based analysis. Differently, the output exhibits a nonlinear behavior in x_1 with a continuous decrease in the slope for larger upper arm lengths. Thereby, it can be derived that beyond a certain threshold the misalignment in the

center of rotations due to variations in x_1 , lead to extreme errors in the output value and may cause catastrophic failures. Thus, despite the relative lower prioritization in Section 3.2, the upper arm length remains a significant uncertainty and it needs to be ensured that the mismatch to its nominal values is below certain runaway boundary conditions.

Finally, we visualize the interaction between the input parameters using colored scatter plots in Figure 13, where one input factor is depicted on the x -axis against another one on the y -axis with the marker color indicating the output value. Here, the emergence of patterns provides an indication for the interaction between two factors. From Figure 13 on the far right it can be seen that little interaction is taking place between upper arm length x_1 and forearm mass x_4 , since the output values do not change significantly with concurrent changes in the input parameters. However, it can be detected that the upper arm length x_1 is dominant for very large values, since the markers along the maximal y -axis values are all colored in red. On the other hand, a slight interaction between the forearm length x_2 and mass x_4



can be inferred from the middle plot, where the estimation error appears to grow strongly, if both input parameters are increased jointly. Intuitively, this can be ascribed to the fact that an increase in the forearm length also shifts the center of mass of the link, which in turn increases the influence of the forearm mass. Lastly, in Figure 13 on the left it can clearly be seen that for very high values of x_1 the upper arm length dominates the output, which is indicated by the red marker coloring along maximal x -axis values.

4. Discussion

The present study performed a quantitative sensitivity analysis of the major sources of uncertainty present in an upper-limb human-exoskeleton system, and their impacts on the arm impedance parameter estimation was investigated. The performed

analysis indicates kinematic incompatibilities and errors in the nominal dynamics model as the most influential sources of uncertainty. Specifically, variations in the assumed forearm length belong to both classes of uncertainty and appear to be the most significant factor according to the results in Figure 10. However, given a wider input variability space, the influence due to variations in the upper arm length dominates, as shown in the qualitative analysis in Figures 12, 13. Here, the results indicate that for slight kinematic misalignments within a 5% range of the nominal upper arm length, the resulting estimation error only grows approximately linearly. However, when the upper arm misalignment increases beyond the approximately linear range, the nonlinear functional behavior results in a blow up of the estimation error. While qualitative sensitivity analysis approaches are more ambiguous, this finding makes sense intuitively, as the upper arm

length is associated with offsets in the center of rotation, which is typically considered a significant source of uncertainty (Schiele, 2008; Jarrassé and Morel, 2012). In addition to the above-described link lengths, the mass of the forearm is the third-most relevant source of uncertainty according to both the elementary effect test and the variance-based sensitivity analysis. Here, the forearm mass has implications regarding the nominal dynamics model, since it is relevant for both the gravitational and inertial properties of the human arm. In contrast, the contact dynamics due to soft-tissue at the attachment are the least relevant as the results in Figure 10 indicate them to be non-influential.

Given the results, it can be seen that uncertainty has a significant effect on the exoskeleton-based arm impedance estimation. In order to help reduce overconfidence in assessment results, the estimation procedure may benefit from employing uncertainty-aware regression techniques, e.g., Gaussian Processes, which model uncertainty explicitly, and thus make it transparent for the clinician (Rasmussen and Williams, 2005). Besides modeling the uncertainty, practical steps can be taken to increase the precision of the assessment by exploiting insights provided by our sensitivity analysis. In particular, reducing the effect of kinematic incompatibilities should be prioritized here. More specifically, a close alignment of the center of rotations has to be ensured. Inclusion of passive DoFs on the shoulder as well as the elbow level can mitigate the influence of kinematic incompatibilities (e.g., Vitiello et al., 2013). Additionally, special care should be taken during the donning procedure to ensure an ideal alignment before and during the usage. Second, our sensitivity analysis shows that errors in the nominal dynamics model, due to inaccuracies in the modeling of gravitational and inertial properties of the human arm, adversely affect the impedance estimation result. Therefore, measures should be taken to reduce these effects. This can be achieved by performing more extensive identification procedures for the human arm model instead of relying on standardized models derived from anthropometric data. The benefits of deploying more personalized models has been demonstrated recently in rehabilitation scenarios (Just et al., 2020). While modeling inaccuracies are expected to be less prevalent for the robotic system, they may also adversely affect the assessment. For example in scenarios where unknown and nonlinear friction components influence the robot joints (Chang et al., 2009), the device dynamics may differ from the original identification. Therefore, ensuring the accuracy of the robot model also needs to be considered in practice when performing automated assessment.

The simulation environment proposed in the presented study emulates realistic load transmissions between the human and exoskeleton via a mechanical interface composed of supporting cuffs and straps. In addition, we facilitate soft contacts by augmenting the human musculoskeletal model by simulated soft-tissue at the attachment areas. To the best of the authors' knowledge, it is the first upper-limb human-exoskeleton simulation that acknowledges the contact dynamics at the mechanical interface between human and robot by implementing both the interface and the human soft-tissue explicitly. Therefore we believe that the developed high-fidelity simulation platform lends itself well for exploitation in diverse use cases and is particularly suitable to investigate safety and ergonomics in control development. The consideration of ergonomics in physical

human-robot interaction is a field that has recently gained growing attention and is considered crucial for driving advances in human-robot collaboration (Gualtieri et al., 2021; Sunesson et al., 2023). Having an explicit implementation of the physical interface is particularly relevant here, in order to accurately represent loads arising at the human limb during interaction with an exoskeleton. Moreover, our proposed simulation platform also provides utility in assisting simulation-based hardware development of wearable robotics, as the consideration of safety and ergonomics is desirable here (Agarwal et al., 2010).

While the present study quantitatively analyzed how uncertainties in the human-exoskeleton interaction impact the arm impedance estimation, some simplifying assumptions were made. First, an idealized, fully known robotic system is assumed. Despite the fact that inertial and gravitational components can reasonably be derived for the exoskeleton, commonly, unknown friction dynamics remain. However, we do not expect this to be a significant issue, since a multitude of friction compensation strategies exist (Huang et al., 2019), which can straight-forwardly be applied in the considered scenario. Another assumption was made with respect to the simulation of spastic behavior of the human arm. In particular, we did not consider joint synergies or phase-dependent descriptions of spasticity. Since in this work the focus lied on isolating the influence of uncertainties on the mechanical interaction and consequently on the assessment, the consideration of a more complex spasticity model would provide limited additional benefit to the objective of the study. Still the presented human musculoskeletal simulation allows for the inclusion of different spasticity behaviors in principle. Thus, despite these limitations, the presented results enable us to derive the most relevant sources of uncertainty that impact the physical human-exoskeleton interaction, and thereby help increase the precision of exoskeleton-based arm impedance estimation.

5. Conclusion

We conclude that this work presents a novel framework to analyze the influence of sources of uncertainty in the human-exoskeleton interaction and their impact on the exoskeleton-based impedance estimation. Due to an increasing demand for robot-based neurorehabilitation and assessment, we argue that the explicit consideration and quantification of uncertainties is paramount, as this allows for more robust and trustworthy estimates. To this end, a human-exoskeleton simulation environment is developed to facilitate the use of sampling-based sensitivity analysis methods. The performed sensitivity analysis indicates that uncertainties significantly impact the impedance estimation, and are primarily caused due to kinematic incompatibilities and inaccuracies in the nominal rigid body dynamics model of the human arm. Therefore, the findings of the study may also be used to increase the precision of exoskeleton-based automated assessment, i.e., by extending model calibrations of the human arm, more careful donning procedures or by deploying uncertainty-aware regression techniques. In the future, we plan to exploit this framework to develop approaches for uncertainty reduction during exoskeleton-based impedance estimation, in order to reduce the estimation

uncertainty below pre-defined tolerances. Thus, providing a constructive approach for improving exoskeleton-based automated assessment.

Data availability statement

The original contributions presented in the study are included in the article, further inquiries can be directed to the corresponding author.

Author contributions

ST and RS implemented the simulation, validated the components with experimental data, and wrote the first draft of the manuscript. ST performed the sensitivity analysis. SE and SH provided the critical revisions. All authors contributed to the conceptualization, methodology, read, and approved the manuscript.

References

- Abraham, A., Krzyzanski, W., and Mager, D. (2007). Partial derivative based sensitivity analysis of models describing target-mediated drug disposition. *AAPS J.* 9, 181–189. doi: 10.1208/aapsj0902020
- Acosta, B., Yang, W., and Posa, M. (2022). Validating robotics simulators on real-world impacts. *IEEE Robot. Autom. Lett.* 7, 6471–6478. doi: 10.1109/LRA.2022.3174367
- Agarwal, P., Narayanan, M. S., Lee, L.-F., Mendel, F., and Krovi, V. N. (2010). "Simulation-based design of exoskeletons using musculoskeletal analysis," in *Proceedings of the ASME Design Engineering Technical Conference* (Montreal, Quebec, QC: ASME), Vol. 3, 1357–1364. doi: 10.1115/DETC2010-28572
- Amis, A., Dowson, D., and Wright, V. (1980). Analysis of elbow forces due to high-speed forearm movements. *J. Biomech.* 13, 825–831. doi: 10.1016/0021-9290(80)90170-0
- An, C., and Hollerbach, J. (1987). "Dynamic stability issues in force control of manipulators," in *In Proceedings. 1987 IEEE International Conference on Robotics and Automation* (Raleigh, NC: IEEE), Vol. 4, 890–896.
- Beven, K. (1993). Prophecy, reality and uncertainty in distributed hydrological modelling. *Adv. Water Resour.* 16, 41–51. doi: 10.1016/0309-1708(93)90028-E
- Blackburn, M., Van Vliet, P., and Mockett, S. P. (2002). Reliability of measurements obtained with the Modified Ashworth Scale in the lower extremities of people with stroke. *Phys. Ther.* 82, 25–34. doi: 10.1093/ptj/82.1.25
- Boehme, A. K., Esenwa, C., and Elkind, M. S. (2017). Stroke risk factors, genetics, and prevention. *Circ. Res.* 120, 472–495. doi: 10.1161/CIRCRESAHA.116.308398
- Bosecker, C., Dipietro, L., Volpe, B., and Krebs, H. I. (2010). Kinematic robot-based evaluation scales and clinical counterparts to measure upper limb motor performance in patients with chronic stroke. *Neurorehabil. Neural Repair* 24, 62–69. doi: 10.1177/1545968309343214
- Buchanan, T. S., Delp, S. L., and Solbeck, J. A. (1998). Muscular resistance to varus and valgus loads at the elbow. *J. Biomech. Eng.* 120, 634–639. doi: 10.1115/1.2834755
- Campolongo, F., Saltelli, A., and Cariboni, J. (2011). From screening to quantitative sensitivity analysis. a unified approach. *Comput. Phys. Commun.* 182, 978–988. doi: 10.1016/j.cpc.2010.12.039
- Carvalho-Pinto, B. P., and Faria, C. D. C. M. (2016). Health, function and disability in stroke patients in the community. *Braz. J. Phys. Ther.* 20, 355–366. doi: 10.1590/bjpt-rbf.2014.0171
- Chang, P. H., Kang, S. H., and Park, K. B. (2009). "Stochastic estimation of human arm impedance under nonlinear friction in robot joints: a model study," in *2009 IEEE International Conference on Rehabilitation Robotics* (IEEE: Kyoto), 147–154. doi: 10.1109/ICORR.2009.5209566
- Christopher Frey, H., and Patil, S. R. (2002). Identification and review of sensitivity analysis methods. *Risk Anal.* 22, 553–578. doi: 10.1111/0272-4332.00039
- Chung, S. G., van Rey, E., Bai, Z., Roth, E. J., and Zhang, L.-Q. (2004). Biomechanical changes in passive properties of hemiplegic ankles with spastic hypertonia¹. *Arch. Phys. Med. Rehabil.* 85, 1638–1646. doi: 10.1016/j.apmr.2003.11.041
- de Leva, P. (1996). Adjustments to zatsiorsky-seluyanov's segment inertia parameters. *J. Biomech.* 29, 1223–1230. doi: 10.1016/0021-9290(95)00178-6
- D'Ettorre, C., Mariani, A., Stilli, A., Rodriguez y Baena, F., Valdastrì, P., Deguet, A., et al. (2021). Accelerating surgical robotics research: a review of 10 years with the da vinci research kit. *IEEE Robot. Autom. Mag.* 28, 56–78. doi: 10.1109/MRA.2021.3101646
- Donkor, E. (2018). Stroke in the 21st century: a snapshot of the burden, epidemiology, and quality of life. *Stroke Res. Treat.* 2018, 1–10. doi: 10.1155/2018/3238165
- Efron, B., and Tibshirani, R. J. (1993). *An Introduction to the Bootstrap. Number 57 in Monographs on Statistics and Applied Probability*. Boca Raton, FL: Chapman and Hall/CRC. doi: 10.1007/978-1-4899-4541-9
- Featherstone, R. (2007). *Rigid Body Dynamics Algorithms*. Berlin: Springer-Verlag. doi: 10.1007/978-1-4899-7560-7
- Feigin, V. L., Forouzanfar, M. H., Krishnamurthi, R., Mensah, G. A., Connor, M., Bennett, D. A., et al. (2014). Global and regional burden of stroke during 1990–2010: findings from the Global Burden of Disease Study 2010. *Lancet* 383, 245–255. doi: 10.1016/S0140-6736(13)61953-4
- Flash, T., and Hogan, N. (1985). The coordination of arm movements: an experimentally confirmed mathematical model. *J. Neurosci.* 5, 1688–1703. doi: 10.1523/JNEUROSCI.05-07-01688.1985
- Garcia, S. C., Dueweke, J. J., and Mendias, C. L. (2016). Optimal joint positions for manual isometric muscle testing. *J. Sport Rehabil.* 25, 1–13. doi: 10.1123/jsr.2015-0118
- Grant, P. G. (1973). Biomechanical significance of the instantaneous center of rotation: the human temporomandibular joint. *J. Biomech.* 6, 109–113. doi: 10.1016/0021-9290(73)90080-8
- Gregson, J. M., Leathley, M., Moore, A. P., Sharma, A. K., Smith, T. L., Watkins, C. L., et al. (1999). Reliability of the tone assessment scale and the modified Ashworth scale as clinical tools for assessing poststroke spasticity. *Arch. Phys. Med. Rehabil.* 80, 1013–1016. doi: 10.1016/S0003-9993(99)90053-9
- Gualtieri, L., Rauch, E., and Vidoni, R. (2021). Emerging research fields in safety and ergonomics in industrial collaborative robotics: a systematic literature review. *Robot. Comput. Integr. Manuf.* 67, 101998. doi: 10.1016/j.rcim.2020.101998

Funding

This work was supported by the Horizon 2020 research and innovation program of the European Union under grant agreement no. 871767 of the project ReHyb.

Conflict of interest

The authors declare that the research was conducted in the absence of any commercial or financial relationships that could be construed as a potential conflict of interest.

Publisher's note

All claims expressed in this article are solely those of the authors and do not necessarily represent those of their affiliated organizations, or those of the publisher, the editors and the reviewers. Any product that may be evaluated in this article, or claim that may be made by its manufacturer, is not guaranteed or endorsed by the publisher.

- Hamm, N., Hall, J., and Anderson, M. (2006). Variance-based sensitivity analysis of the probability of hydrologically induced slope instability. *Comput. Geosci.* 32, 803–817. doi: 10.1016/j.cageo.2005.10.007
- Helton, J., and Davis, F. (2003). Latin hypercube sampling and the propagation of uncertainty in analyses of complex systems. *Reliab. Eng. Syst. Saf.* 81, 23–69. doi: 10.1016/S0951-8320(03)00058-9
- Holland, J., Kingston, L., McCarthy, C., Armstrong, E., O'Dwyer, P., Merz, F., et al. (2021). Service robots in the healthcare sector. *Robotics* 10, 47. doi: 10.3390/robotics10010047
- Hollerbach, J., Khalil, W., and Gautier, M. (2008). *Model Identification*. Berlin: Springer Berlin Heidelberg. doi: 10.1007/978-3-540-30301-5_15
- Holzbaur, K., Murray, W. M., and Delp, S. L. (2005). A model of the upper extremity for simulating musculoskeletal surgery and analyzing neuromuscular control. *Ann. Biomed. Eng.* 33, 829–840. doi: 10.1007/s10439-005-3320-7
- Homma, T., and Saltelli, A. (1996). Importance measures in global sensitivity analysis of nonlinear models. *Reliab. Eng. Syst. Saf.* 52, 1–17. doi: 10.1016/0951-8320(96)00002-6
- Huang, S., Liang, W., and Tan, K. K. (2019). Intelligent friction compensation: a review. *IEEE/ASME Trans. Mechatron.* 24, 1763–1774. doi: 10.1109/TMECH.2019.2916665
- Iooss, B., and Saltelli, A. (2017). *Introduction to Sensitivity Analysis*. Cham: Springer International Publishing, 1103–1122. doi: 10.1007/978-3-319-12385-1_31
- Jarrassé, N., and Morel, G. (2012). Connecting a human limb to an exoskeleton. *IEEE Trans. Robot.* 28, 697–709. doi: 10.1109/TRO.2011.2178151
- Jarrassé, N., Tagliabue, M., Robertson, J. V. G., Maiza, A., Crocher, V., Roby-Brami, A., et al. (2010). A methodology to quantify alterations in human upper limb movement during co-manipulation with an exoskeleton. *IEEE Trans. Neural Syst. Rehabil. Eng.* 18, 389–397. doi: 10.1109/TNSRE.2010.2056388
- Just, F., Özen, Ö., Tortora, S., Klamroth-Marganska, V., Riener, R., and Rauter, G. (2020). Human arm weight compensation in rehabilitation robotics: efficacy of three distinct methods. *J. Neuroeng. Rehabil.* 17, 13. doi: 10.1186/s12984-020-0644-3
- Khamar, M., Edrisi, M., and Zahiri, M. (2019). Human-exoskeleton control simulation, kinetic and kinematic modeling and parameters extraction. *MethodsX* 6, 1838–1846. doi: 10.1016/j.mex.2019.08.014
- Kleijnen, J., and Helton, J. (1999). Statistical analyses of scatterplots to identify important factors in large-scale simulations, 2: robustness of techniques. *Reliab. Eng. Syst. Saf.* 65, 187–197. doi: 10.1016/S0951-8320(98)00090-8
- Kohberger, R. C., Scavia, D., and Wilkinson, J. W. (1978). A method for parameter sensitivity analysis in differential equation models. *Water Resour. Res.* 14, 25–29. doi: 10.1029/WR014i001p00025
- Krebs, H. I., Dipietro, L., Levy-Tzedek, S., Fasoli, S. E., Rykman-Berland, A., Zipse, J., et al. (2008). A paradigm shift for rehabilitation robotics. *IEEE Eng. Med. Biol. Mag.* 27, 61–70. doi: 10.1109/MEMB.2008.919498
- Kühn, J., Hu, T., Schappler, M., and Haddadin, S. (2018). "Dynamics simulation for an upper-limb human-exoskeleton assistance system in a latent-space controlled tool manipulation task," in *2018 IEEE International Conference on Simulation, Modeling, and Programming for Autonomous Robots (SIMPAR)* (Brisbane, QLD: IEEE), 158–165. doi: 10.1109/SIMPAR.2018.8376286
- Kwakkel, G., Wagenaar, R. C., Twisk, J. W., Lankhorst, G. J., and Koetsier, J. C. (1999). Intensity of leg and arm training after primary middle-cerebral-artery stroke: a randomised trial. *Lancet* 354, 191–196. doi: 10.1016/S0140-6736(98)09477-X
- Lamercy, O., Lünenburger, L., Gassert, R., and Bolliger, M. (2012). *Robots for Measurement/Clinical Assessment*. London: Springer London, 443–456. doi: 10.1007/978-1-4471-2277-7_24
- Laut, J., Porfiri, M., and Raghavan, P. (2016). The present and future of robotic technology in rehabilitation. *Curr. Phys. Med. Rehabil. Rep.* 4, 312–319. doi: 10.1007/s40141-016-0139-0
- Lo, H. S., and Xie, S. Q. (2012). Exoskeleton robots for upper-limb rehabilitation: state of the art and future prospects. *Med. Eng. Phys.* 34, 261–268. doi: 10.1016/j.medengphy.2011.10.004
- Lowrey, K., Dao, J., and Todorov, E. (2016). "Real-time state estimation with whole-body multi-contact dynamics: a modified ukf approach," in *2016 IEEE-RAS 16th International Conference on Humanoid Robots (Humanoids)* (Cancun: IEEE), 1225–1232. doi: 10.1109/HUMANOIDS.2016.7803426
- Ma, Y., Dixit, V., Innes, M. J., Guo, X., and Rackauckas, C. (2021). "A comparison of automatic differentiation and continuous sensitivity analysis for derivatives of differential equation solutions," in *2021 IEEE High Performance Extreme Computing Conference (HPEC)* (Waltham, MA: IEEE), 1–9. doi: 10.1109/HPEC49654.2021.9622796
- Maggioni, S., Melendez-Calderon, A., van Asseldonk, E. H. F., Klamroth-Marganska, V., Lünenburger, L., Riener, R., et al. (2016). Robot-aided assessment of lower extremity functions: a review. *J. Neuroeng. Rehabil.* 13, 72. doi: 10.1186/s12984-016-0180-3
- Maurel, W. (1999). *3D Modeling of the Human Upper Limb Including the Biomechanics of Joints, Muscles and Soft Tissues*. Lausanne: EPFL. 204. doi: 10.5075/epfl-thesis-1906
- Maurel, W., Thalmann, D., Hoffmeyer, P., Beylot, P., Gingins, P., Kalra, P., et al. (2002). "A biomechanical musculoskeletal model of human upper limb for dynamic simulation," in *5th IEEE EMBS International Summer School on Biomedical Imaging, 2002* (Berder Island: IEEE), 16. doi: 10.1109/SSBI.2002.1233995
- McCrea, P. H., Eng, J. J., and Hodgson, A. J. (2003). Linear spring-damper model of the hypertonic elbow: reliability and validity. *J. Neurosci. Methods* 128, 121–128. doi: 10.1016/S0165-0270(03)00169-9
- McKay, M. D., Beckman, R. J., and Conover, W. J. (1979). A comparison of three methods for selecting values of input variables in the analysis of output from a computer code. *Technometrics* 21, 239–245. doi: 10.1080/00401706.1979.10489755
- McLellan, D. (1981). Spasticity: disorder motor control. *J. Neurol. Neurosurg. Psychiatr.* 44, 961. doi: 10.1136/jnnp.44.10.961
- Morris, M. D. (1991). Factorial sampling plans for preliminary computational experiments. *Technometrics* 33, 161–174. doi: 10.1080/00401706.1991.10484804
- Nguyen, T., and de Kok, J. (2007). Systematic testing of an integrated systems model for coastal zone management using sensitivity and uncertainty analyses. *Environ. Modell. Softw.* 22, 1572–1587. doi: 10.1016/j.envsoft.2006.08.008
- Nossent, J., Elsen, P., and Bauwens, W. (2011). Sobol sensitivity analysis of a complex environmental model. *Environ. Modell. Softw.* 26, 1515–1525. doi: 10.1016/j.envsoft.2011.08.010
- Ogneva, I. V., Lebedev, D. V., and Shenkman, B. S. (2010). Transversal stiffness and young's modulus of single fibers from rat soleus muscle probed by atomic force microscopy. *Biophys. J.* 98, 418–424. doi: 10.1016/j.bpj.2009.10.028
- Pelleg, J. (2012). *Mechanical Properties of Materials*. Solid Mechanics and Its Applications. Springer Netherlands. doi: 10.1007/978-94-007-4342-7
- Pianosi, F., Beven, K., Freer, J., Hall, J. W., Rougier, J., Stephenson, D. B., et al. (2016). Sensitivity analysis of environmental models: a systematic review with practical workflow. *Environ. Modell. Softw.* 79, 214–232. doi: 10.1016/j.envsoft.2016.02.008
- Pianosi, F., Sarrazin, F., and Wagener, T. (2015). A matlab toolbox for global sensitivity analysis. *Environ. Modell. Softw.* 70, 80–85. doi: 10.1016/j.envsoft.2015.04.009
- Pons, J. L. (2008). *Wearable Robots: Biomechatronic Exoskeletons*. Hoboken, NJ: John Wiley and Sons, Ltd. doi: 10.1002/9780470987667
- Raghavan, P. (2015). Upper limb motor impairment after stroke. *Phys. Med. Rehabil. Clin. N. Am.* 26, 599–610. doi: 10.1016/j.pmr.2015.06.008
- Ramachandran, H., Vasudevan, D., Brahma, A., and Pugazhenth, S. (2016). Estimation of mass moment of inertia of human body, when bending forward, for the design of a self-transfer robotic facility. *J. Eng. Sci. Technol.* 11, 166–176.
- Rasmussen, C. E., and Williams, C. K. I. (2005). *Gaussian Processes for Machine Learning*. Cambridge, MA: The MIT Press. doi: 10.7551/mitpress/3206.001.0001
- Ren, Y., Kang, S. H., Park, H.-S., Wu, Y.-N., and Zhang, L.-Q. (2013). Developing a multi-joint upper limb exoskeleton robot for diagnosis, therapy, and outcome evaluation in neurorehabilitation. *IEEE Trans. Neural Syst. Rehabil. Eng.* 21, 490–499. doi: 10.1109/TNSRE.2012.2225073
- Ringleb, P. A., Bousser, M.-G., Ford, G., Bath, P. M., Brainin, M., Caso, V., et al. (2008). Guidelines for management of ischaemic stroke and transient ischaemic attack 2008. *Cerebrovasc. Dis.* 25, 457–507. doi: 10.1159/000131083
- Romano, J. P., and Shaikh, A. M. (2012). On the uniform asymptotic validity of subsampling and the bootstrap. *Ann. Stat.* 40, 2798–2822. doi: 10.1214/12-AOS1051
- Saltelli, A., Annoni, P., Azzini, I., Campolongo, F., Ratto, M., Tarantola, S., et al. (2010). Variance based sensitivity analysis of model output. design and estimator for the total sensitivity index. *Comput. Phys. Commun.* 181, 259–270. doi: 10.1016/j.cpc.2009.09.018
- Saltelli, A., Ratto, M., Andres, T., Campolongo, F., Cariboni, J., Gatelli, D., et al. (2008). *Global Sensitivity Analysis: The Primer*. Chichester: Wiley. doi: 10.1002/9780470725184
- Saltelli, A., Tarantola, S., Campolongo, F., and Ratto, M. (2004). *Sensitivity Analysis in Practice: A Guide to Assessing Scientific Models*. Chicago, IL: Halsted Press, USA.
- Schiele, A. (2008). "An explicit model to predict and interpret constraint force creation in phri with exoskeletons," in *Proceedings - IEEE International Conference on Robotics and Automation* (Pasadena, CA: IEEE), 1324–1330. doi: 10.1109/ROBOT.2008.4543387
- Shin, D., Kim, J., and Koike, Y. (2009). A myokinetic arm model for estimating joint torque and stiffness from EMG signals during maintained posture. *J. Neurophysiol.* 101, 387–401. doi: 10.1152/jn.00584.2007

- Singh, R., Wagener, T., Crane, R., Mann, M. E., and Ning, L. (2014). A vulnerability driven approach to identify adverse climate and land use change combinations for critical hydrologic indicator thresholds: application to a watershed in pennsylvania, usa. *Water Resour. Res.* 50, 3409–3427. doi: 10.1002/2013WR014988
- Sobol, I. (1993). Sensitivity estimates for nonlinear mathematical models. *Math. Modell. Comput. Exp.* 1, 407–414.
- Sommerfeld, D. K., Eek, E. U., Svensson, A. K., Holmqvist, L. W., and Von Arbin, M. H. (2004). Spasticity after stroke: its occurrence and association with motor impairments and activity limitations. *Stroke* 35, 134–139. doi: 10.1161/01.STR.0000105386.05173.5E
- Sunesson, C. E., Schön, D. T., Hassø, C. N. P., Chinello, F., and Fang, C. (2023). Predictor: a physical emulator enabling safety and ergonomics evaluation and training of physical human-robot collaboration. *Front. Neurobot.* 17, 1080038. doi: 10.3389/fnbot.2023.1080038
- Thabane, L., Mbuagbaw, L., Zhang, S., Samaan, Z., Marcucci, M., Ye, C., et al. (2013). A tutorial on sensitivity analyses in clinical trials: the what, why, when and how. *BMC Med. Res. Methodol.* 13, 92. doi: 10.1186/1471-2288-13-92
- Todorov, E., Erez, T., and Tassa, Y. (2012). “MuJoCo: a physics engine for model-based control,” in *2012 IEEE/RSJ International Conference on Intelligent Robots and Systems* (Vilamoura-Algarve: IEEE), 5026–5033. doi: 10.1109/IROS.2012.6386109
- Trigili, E., Crea, S., Moisé, M., Baldoni, A., Cempini, M., Ercolini, G., et al. (2020). Design and experimental characterization of a shoulder-elbow exoskeleton with compliant joints for post-stroke rehabilitation. *IEEE/ASME Trans. Mechatron.* 24, 1485–1496. doi: 10.1109/TMECH.2019.2907465
- Vitiello, N., Lenzi, T., Roccella, S., De Rossi, S. M. M., Cattin, E., Giovacchini, M. C., et al. (2013). Neuroexos: a powered elbow exoskeleton for physical rehabilitation. *IEEE Trans. Robot.* 29, 220–235. doi: 10.1109/TRO.2012.2211492
- Wang, C., Peng, L., Hou, Z.-G., and Zhang, P. (2021). The assessment of upper-limb spasticity based on a multi-layer process using a portable measurement system. *IEEE Trans. Neural Syst. Rehabil. Eng.* 29, 2242–2251. doi: 10.1109/TNSRE.2021.3121780
- Wang, H., Huang, P., Li, X., Samuel, O., Xiang, Y., Li, P., et al. (2019). Spasticity assessment based on the maximum isometrics voluntary contraction of arm muscles in post-stroke hemiplegic paralyses. *Front. Neurol.* 10, 465. doi: 10.3389/fneur.2019.00465
- Yang, J. (2011). Convergence and uncertainty analyses in monte-carlo based sensitivity analysis. *Environ. Modell. Softw.* 26, 444–457. doi: 10.1016/j.envsoft.2010.10.007
- Zajac, F. E., Neptune, R. R., and Kautz, S. A. (2002). Biomechanics and muscle coordination of human walking: part I: introduction to concepts, power transfer, dynamics and simulations. *Gait Posture* 16, 215–232. doi: 10.1016/S0966-6362(02)00068-1
- Zhang, L.-Q., Son, J., Park, H.-S., Kang, S. H., Lee, Y., Ren, Y., et al. (2017). Changes of shoulder, elbow, and wrist stiffness matrix post stroke. *IEEE Trans. Neural Syst. Rehabil. Eng.* 25, 844–851. doi: 10.1109/TNSRE.2017.2707238

Frontiers in Neurorobotics

Investigates embodied autonomous neural systems and their impact on our lives

Part of the most cited neuroscience series, this journal advances understanding of neurorobotics - from prosthetic devices to brain machine interfaces, and wearable systems to home appliances.

Discover the latest Research Topics

[See more →](#)

Frontiers

Avenue du Tribunal-Fédéral 34
1005 Lausanne, Switzerland
frontiersin.org

Contact us

+41 (0)21 510 17 00
frontiersin.org/about/contact

